A UNITED STATES DEPARTMENT OF COMMERCE PUBLICATION

SECTION C

JOURNAL OF RESEARCH

of the NATIONAL BUREAU OF STANDARDS

JNBCAX 76C (1&2) 1-84, Jan.-June 1972

Engineering and Instrumentation

U.S. DEPARTMENT OF COMMERCE
National Bureau of Standards

Journal of Research

of the

National Bureau of Standards

C. Engineering and Instrumentation

Jan.–June • 1972

VOLUME • 76C

NUMBERS • 1 & 2

Editor: Martin Greenspan

Associate Editors: G. F. Montgomery, A. F. Schmidt

Publication dates:
Feb. 15, May 15, Aug. 15, Nov. 15, 1972

J. Res. Nat. Bur. Stand. (U.S.), C

JOURNAL OF RESEARCH

The National Bureau of Standards Journal of Research reports research and development in the fields of activity shown at right. Also included from time to time are survey articles on topics closely related to the Bureau's scientific and technical program.

The Journal is published in three separate sections as follows:

A. Physics and Chemistry

Contains papers of interest primarily to scientists working in these fields. Issued six times a year. Annual subscription: domestic, $9.50; foreign, $11.75. Single copy, varies.

B. Mathematical Sciences

Presents studies and compilations designed mainly for the mathematician and the theoretical physicist. Issued quarterly. Annual subscription: domestic, $5.00; foreign, $6.25. Single copy, $1.25.

C. Engineering and Instrumentation

Reports research and development results of interest chiefly to the engineer and the applied scientist. Issued quarterly. Annual subscription: domestic, $5.00; foreign, $6.25. Single copy, $1.25.

U.S. DEPARTMENT OF COMMERCE
Peter G. Peterson, Secretary
NATIONAL BUREAU OF STANDARDS
Lawrence M. Kushner, Acting Director

The National Bureau of Standards[1] was established by an act of Congress March 3, 1901. The Bureau's overall goal is to strengthen and advance the Nation's science and technology and facilitate their effective application for public benefit. To this end, the Bureau conducts research and provides: (1) a basis for the Nation's physical measurement system, (2) scientific and technological services for industry and government, (3) a technical basis for equity in trade, and (4) technical services to promote public safety. The Bureau consists of the Institute for Basic Standards, the Institute for Materials Research, the Institute for Applied Technology, the Center for Computer Sciences and Technology, and the Office for Information Programs.

THE INSTITUTE FOR BASIC STANDARDS provides the central basis within the United States of a complete and consistent system of physical measurement; coordinates that system with measurement systems of other nations; and furnishes essential services leading to accurate and uniform physical measurements throughout the Nation's scientific community, industry, and commerce. The Institute consists of a Center for Radiation Research, an Office of Measurement Services and the following divisions:

Applied Mathematics—Electricity—Heat—Mechanics—Optical Physics—Linac Radiation[2]—Nuclear Radiation[2]—Applied Radiation[2]—Quantum Electronics[3]—Electromagnetics[3]—Time and Frequency[3]—Laboratory Astrophysics[3]—Cryogenics[3].

THE INSTITUTE FOR MATERIALS RESEARCH conducts materials research leading to improved methods of measurement, standards, and data on the properties of well-characterized materials needed by industry, commerce, educational institutions, and Government; provides advisory and research services to other Government agencies; and develops, produces, and distributes standard reference materials. The Institute consists of the Office of Standard Reference Materials and the following divisions:

Analytical Chemistry—Polymers—Metallurgy—Inorganic Materials—Reactor Radiation—Physical Chemistry.

THE INSTITUTE FOR APPLIED TECHNOLOGY provides technical services to promote the use of available technology and to facilitate technological innovation in industry and Government; cooperates with public and private organizations leading to the development of technological standards (including mandatory safety standards), codes and methods of test; and provides technical advice and services to Government agencies upon request. The Institute also monitors NBS engineering standards activities and provides liaison between NBS and national and international engineering standards bodies. The Institute consists of a Center for Building Technology and the following divisions and offices:

Engineering Standards Services—Weights and Measures—Invention and Innovation—Product Evaluation Technology—Electronic Technology—Technical Analysis—Measurement Engineering—Fire Technology—Housing Technology[4]—Federal Building Technology[4]—Building Standards and Codes Services[4]—Building Environment[4]—Structures, Materials and Life Safety[4]—Technical Evaluation and Application[4].

THE CENTER FOR COMPUTER SCIENCES AND TECHNOLOGY conducts research and provides technical services designed to aid Government agencies in improving cost effectiveness in the conduct of their programs through the selection, acquisition, and effective utilization of automatic data processing equipment; and serves as the principal focus within the executive branch for the development of Federal standards for automatic data processing equipment, techniques, and computer languages. The Center consists of the following offices and divisions:

Information Processing Standards—Computer Information—Computer Services—Systems Development—Information Processing Technology.

THE OFFICE FOR INFORMATION PROGRAMS promotes optimum dissemination and accessibility of scientific information generated within NBS and other agencies of the Federal Government; promotes the development of the National Standard Reference Data System and a system of information analysis centers dealing with the broader aspects of the National Measurement System; provides appropriate services to ensure that the NBS staff has optimum accessibility to the scientific information of the world, and directs the public information activities of the Bureau. The Office consists of the following organizational units:

Office of Standard Reference Data—Office of Technical Information and Publications—Library—Office of International Relations.

[1] Headquarters and Laboratories at Gaithersburg, Maryland, unless otherwise noted; mailing address Washington, D.C. 20234.
[2] Part of the Center for Radiation Research.
[3] Located at Boulder, Colorado 80302.
[4] Part of the Center for Building Technology.

Order all publications from the Superintendent of Documents
U.S. Government Printing Office, Washington, D.C. 20402.

The Secretary of Commerce has determined that the publication of this periodical is necessary in the transaction of the public business required by law of this Department. Use of funds for printing this periodical has been approved by the Director of the Office of Management and Budget through June 30, 1976.

JOURNAL OF RESEARCH of the National Bureau of Standards—C. Engineering and Instrumentation
Vol. 76C, Nos. 1 and 2, January–June 1972

National Bureau of Standards One Kilogram Balance NBS No. 2

H. E. Almer

Institute for Basic Standards, National Bureau of Standards, Washington, D.C. 20234

(January 17, 1972)

The balance described is a one-pan, two-knife, short arm, 1 kg balance. The fulcrum flat and the suspension support elements are mounted on a bed plate supported by three posts attached to the base. The weight handling mechanism is mounted on a center column attached to the base. The balance has two modes of arrestment, the constant load mode and the full arrest mode. A double case encloses the structure.

There are positions for six weights inside the balance. These weights can be compared with each other, according to an appropriate weighing design, without opening the balance case. The operation of the balance and the weight changing are through control elements outside the balance case. The indicating elements for the instruments measuring the pressure, temperature, and relative humidity within the balance are located inside the balance.

The standard deviation of the balance developed by a series of measurements in the National Bureau of Standards Experimental Mass Laboratory was approximately 4 μg.

Key words: Arrestment; balance; beam; buoyant; case; constant-load; equilibrium; knife; one-pan; short arm; two-knife.

1. Introduction

In a continuing program to improve mass measurements, the Mass Section of the National Bureau of Standards designed and constructed a high precision one kilogram capacity balance. After a detailed consideration of the two-knife single pan balance and the three-knife equal arm two-pan balance, a short arm (2 in) two-knife one-pan balance design was chosen principally because [1, 2]: [1]

(1) The geometry associated with the two knife design simplifies adjustments.

(2) This design lends itself to the use of a constant load type of arrestment; that is, the knives are not separated from their cooperating planes during the weighing operation, nor is the mechanical load carried by the knife-plane combination significantly changed between the loaded and unloaded condition.

(3) Versatility of weight handling and weight changing is achieved.

(4) A stiff beam is practical.

Several features were incorporated in the balance design.

(1) The arrestment was designed so that during a series of weighings the knives are always under load, and the knives and their cooperating planes are not separated when weights are interchanged.

(2) The load is applied and removed smoothly by mechanical means.

(3) All operations are controlled from outside the balance case, so that it is not necessary to open the balance during a weighing.

(4) The beam with its short arm is as rigid as practicable, nearly homogeneous, and has good thermal qualities. Cylindrical wedges are used to adjust and retain the knives. This adjusting method was used with permission of Voland Corporation.[2]

(5) The suspension includes a ball bearing gimbal between the cross-knife and the pan.

(6) The upper part of the suspension includes a Thiesen compensator consisting of a knife whose edge was nominally in the same plane as the load knife of the beam.

A test instrument embodying these concepts was built and tested.[3] Results of mass measurements with this test instrument were encouraging and had standard deviations varying from 3 μg to 8 μg [3]. These results led to the conclusion that a practical balance embodying these principles and concepts with at least as good if not better precision was possible.

The present balance, designated NBS No 2, may be described as a one-pan, two-knife beam, constant load

[1] Figures in brackets indicate the literature reference at the end of this paper.

[2] The Voland Corporation holds a patent on the use of cylindrical wedges for adjusting knives in a balance.

[3] This prototype was designated NBS No. 1 for working purposes only. Prototypes NBS Nos. 3, 4, and 5 are being built.

balance. It embodies the above features and others deemed desirable from experience gained with the test instrument and during the development of the present balance. These include:

(1) The beam, suspension system and load are in buoyant and mass equilibrium [2, 4].

(2) A beam brake is provided to prevent excessive movement of the oscillating system during release and arrest. The brake may also be used to limit the amplitude of the oscillation.

(3) A heat source above the balance is provided to maintain a positive vertical gradient (warmer at top) [5].

(4) The case was designed to minimize the horizontal gradient, optimize the vertical gradient within, and insulate the balance from the room environment.

2. Description

The base of the balance sits on a base plate. Mounted in the base is a center column supporting the weight changing and storage members. The fulcrum bearing stand and various other components are mounted on a bed plate supported on three posts attached to the base; the plate is otherwise independent of the weight changing mechanism.

The short-arm two-knife beam and the suspension were designed so that the oscillating system is in buoyant equilibrium when the load is on the pan [4]. Two modes of arrestment are provided [3]. In one, denoted the full-arrestment mode, the knives and the bearing planes are separated. This mode of arrestment is used when the balance is not in use. In the other mode, denoted the constant-load arrestment mode, the knives with bearing planes are not separated. This mode of arrestment is used during weighing operations.

The balance mechanism is enclosed in a double case with windows for the optical lever of the readout and for viewing the position of the weight carrier. The reading scale is reflected through a series of mirrors from the mirror mounted on the beam to the telescope.

The controls are brought out through the base. Instrumentation for reading the pressure, temperature and relative humidity within the balance case is provided.

2.1. Base and Supporting Structure

The base of the balance is a shallow cup-like component made from heavy aluminum, which sits on a base plate supported by three leveling screws.

The center column, which is attached to the base by brackets through a column base plate (see fig. 1), supports the weight changing mechanism and the weight carrier. Three posts support the bed plate upon which are mounted the fulcrum bearing stand, the arrestment-alinement pins, the full-arrest beam lifter, the tit-stop for the constant-load arrestment, the fixed elements of the optical read-out, the beam brake bracket, and the sensitivity weight support. The bed plate is a 1 inch brass plate 11½ inches in

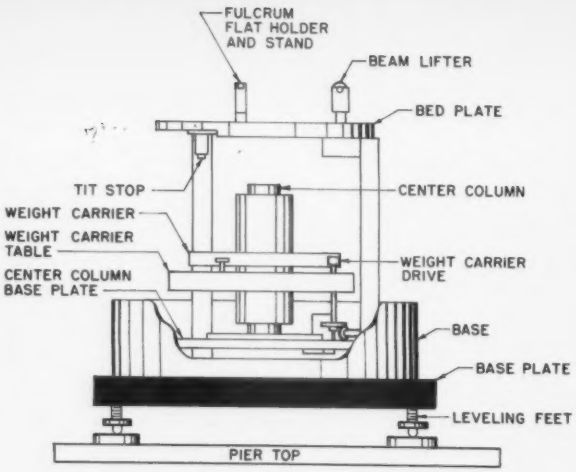

FIGURE 1. *Schematic sketch of balance structure.*

diameter. All the components except the beam lifter and the tit stop are mounted on the top of the bed plate. The beam lifter extends above the bed plate, but its drive gears are below the bed plate and are enclosed in a gear box. The beam lifter moves vertically to arrest or release the beam. The roller which engages the beam has a ball bushing so it can move laterally on its shaft, which has ball bearings for rotational motion. The tit-stop mounted on the underside of the bed plate is adjustable as to height. The fulcrum bearing flat is a piece of boron carbide 2½-in long with a ⅜-in square cross section.

2.2. Weight Changing Mechanism

The weight changing mechanism's vertical travel, of ⅜ in, on the center column is guided by an upper and a lower bearing spaced 5¾ in apart, and actuated by a cam. A horizontal plate forming a table has three sets of ball bearings supporting the weight carrier, which has positions for six weights. The weight carrier is positioned on the weight table by two ball bearing guide rollers and one drive roller (see fig. 2). The drive roller rotates the weight carrier by a friction drive and is itself driven by a friction gear attached to the control rod. This friction gear is designed so that when the weight table is lowered to the weighing position it is disengaged.

2.3. The Beam

The beam of the balance is T-shaped, two knife type, consisting of a beam body to which are attached two bosses, a mirror, two out riggers, and the two knives. A pair of counter-weights are attached to the bosses. The equilibrium and sensitivity adjusting pieces complete the beam. Figure 3 shows an exploded view of the beam.

The beam body is gold-plated brass. The knife seats are spaced so that the nominal arm length is 2 in. The

FIGURE 2. *Photograph of balance structure showing weight table, weight carrier and pan.*

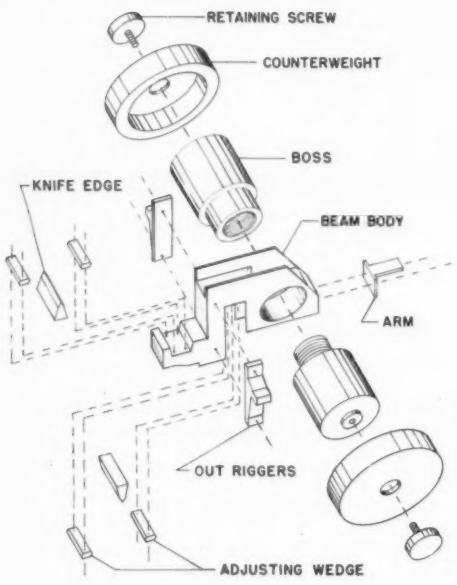

FIGURE 3. *An exploded sketch of the beam.*

knive seats were scraped to provide a flat seat for the knives, which are attached to the beam with cylindrical wedges. These cylindrical wedges serve both as a means of adjusting the knives and as a means of retaining the knives in position. The knife material is Tantung G and the included angle between the knife-edge facets is 120°. At the back of the beam 2 in from the design position of the fulcrum knife is a transverse hole 1¼ inch in diameter to receive the two bosses, to which the two counter-weights are attached by means of gold plated brass retaining screws. The face of the retaining screws that meets the counter-weight is conical and holds the counter-weight securely in position. The bosses are two aluminum cylinders, one with a threaded male portion and the other with a mating threaded female portion. The bosses together with the retaining screws are designed to have the same mass and volume as the suspension system.

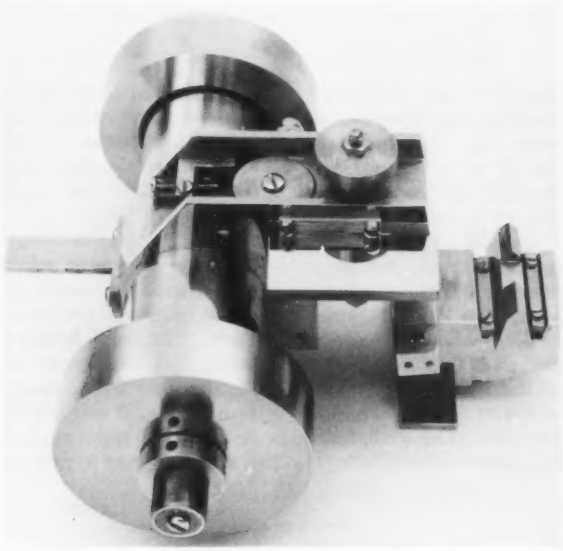

FIGURE 4. *View of the beam from the mirror side.*

The balance was designed so that the counter-weights and the load on the pan be of materials having the same or nearly the same densities. Therefore, the counter-weights are interchangeable. When stainless steel weights are compared stainless steel counter-weights are used and when platinum-iridium weights are compared platinum-iridium counter-weights are used. This minimizes the drift of the balance with changing conditions, because the oscillating system of the balance is near buoyant equilibrium. In figure 4, the beam is shown with stainless steel counter-weights.

2.4. The Suspension System

The suspension system (fig. 5) consists of the pan including risers which attach the pan to the ball bearing gimbal, a part of the suspension, the yoke in which is

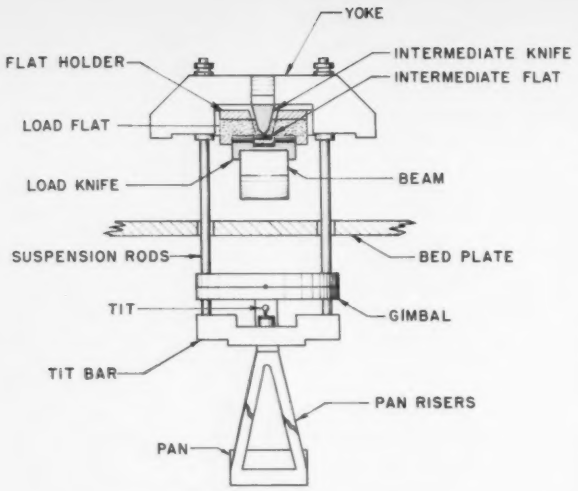

FIGURE 5. *Schematic sketch of the suspension system.*

mounted the intermediate or cross-knife, an intermediate flat holder, and the necessary connecting elements. Also included is the tit and tit-bar on which the tit is mounted. The tit is attached to the yoke through the rods connecting the gimbal to the yoke. The tit is below the gimbal.

Except for the cross-knife, the flats, the ball bearings in the gimbal, the tit, and various screws and other fasteners, the suspension components are made of aluminum. The intermediate knife, which is mounted in the yoke, is made of Tantung. The load bearing flat and the intermediate bearing flat are mounted in the intermediate flat holder. The load flat is made of boron carbide while the intermediate flat is made of Tantung. The ball bearings in the ring type gimbal are made of beryllium. The pan was designed to permit the circular weight carrier to place the weight on the pan or remove it from the pan (see fig. 2) with a minimum disturbance.

The vertical ribs of the pan mesh with the ribs of the weight carrier. Means for separating the pan from the rest of the suspension, without other disassembly, are provided.

2.5. The Indicating System

The indicating system (fig. 6) consists of an illuminated scale located about three meters from the balance; a moving mirror mounted on the beam; three fixed mirrors, two mounted on the bed-plate and one attached to pier outside the balance case; and a reading telescope.

The first of the fixed mirrors mounted on the bed plate directs the image of the reading scale to the moving mirror, attached to the beam, from which it is reflected to the second fixed mirror, which is mounted above the beam mirror at an angle of about 30°. The path of the image between the second fixed mirror and the beam mirror has three reflections from the beam mirror. The last reflection directs the image to the first fixed mirror which then reflects the image to the fixed mirror outside the balance. The image is then reflected to the reading telescope, which has a reticle with a horizontal hair line, where the balance indication is read.

2.6. The Case

The balance has a double case. Both the inner and outer cases are in the form of right circular cylinders. The inner case consists of the three parts; an upper part, which encloses the beam compartment; a lower part which encloses the weight and pan compartment, and can be raised up over the upper part; and the cover. The lower part is fitted with handles for lifting

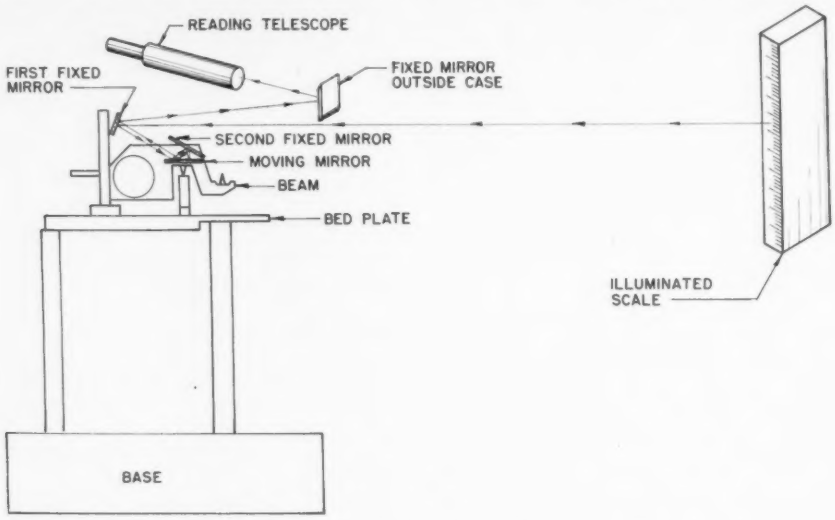

FIGURE 6. *Schematic sketch of the balance indicating system.*

and latches to hold it up when weights are being positioned on the weight carrier. The cover is an aluminum disk $\frac{5}{8}$-in thick equipped with lifting handles. Both the upper and lower parts are built-up of alternating rings of insulating material and aluminum. The insulating rings are 1-in high and $\frac{3}{4}$-in thick. The aluminum rings were cut from D'ds-in stock and are 1-in wide. The inside of the inner case was lined with 0.005-in stainless steel sheets fitted between the aluminum rings. The outside is covered with pressed fiber board.

The outer case is also a built-up case of alternating rings of hard board and insulating material, with an outside skin of sheet aluminum. The hardboard rings were cut from $\frac{1}{4}$-in stock. The insulating rings are 5-in high and $\frac{3}{4}$-in thick (fig. 7). The cover is also of hardboard.

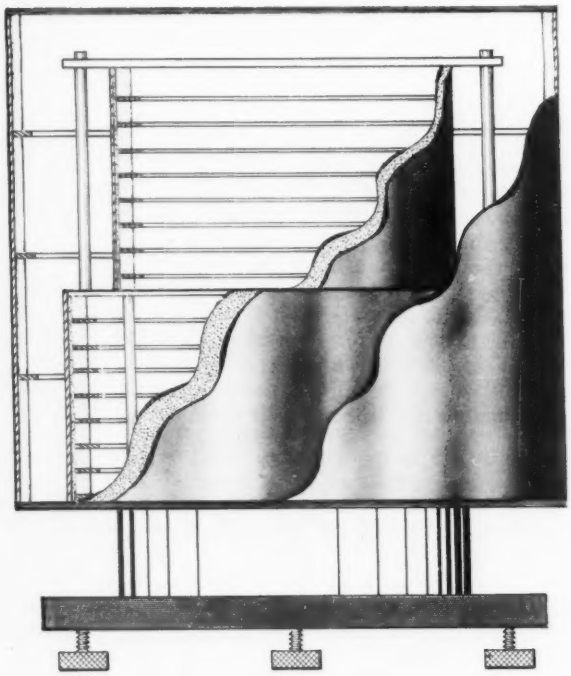

FIGURE 7. *Cut-away view of the balance case.*

In both the inner and the outer case, the insulating rings were made from corrugated paper rolled to form rings, $\frac{3}{4}$-in thick.

The aluminum rings in the inner case form fins to maintain a nearly isothermal horizontal gradient inside the balance.

2.7. The Controls

There are six controls and all but the full arrest control extend to a control panel at the side of the balance convenient to the operator at the reading telescope. The control rod for raising and lowering the weight table is driven by a variable speed electric motor. The motor control box is connected to the motor by a cable so that it can be located in a convenient position. The sensitivity weight, the beam brake, the weight changing, and the full arrest controls are all manually operated. Even though a pan brake was not installed, a control for one was included if it is desired in the future (see fig. 8).

Provision was made for measuring the pressure, relative humidity and temperature within the balance case.

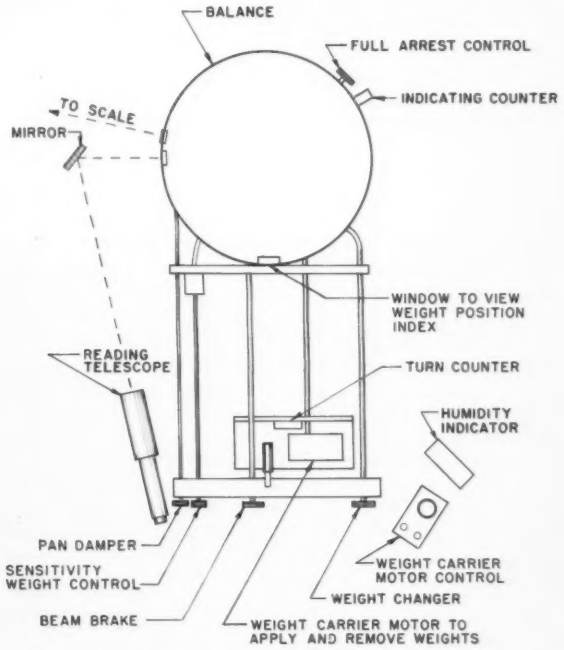

FIGURE 8. *Schematic sketch of the balance controls.*

2.8. The Arresting System

The balance has two arrestment modes or arresting systems. In one, designated the full arrest mode, the knife edges and their cooperating flats are separated when the balance is arrested. The other mode, designated the "constant load" mode, the knives are not separated from their cooperating flats. The contact forces between the knives and flats, when arrested in the "constant load" mode and during the arresting operation varies only slightly from their operating levels. The parts of the arresting systems responsible for the alinement of the beam and the suspension do not move, further minimizing arrestment errors. [3]

The essential features of the full arrest mode are shown in figure 9. In the top view, the balance is shown in the weighing position. In the second view, the beam lifter raised the counterweight end of the beam and lowered the load end until the load flat and the rest of suspension is supported by the alinement-arrestment pins. This is termed the partial arrest.

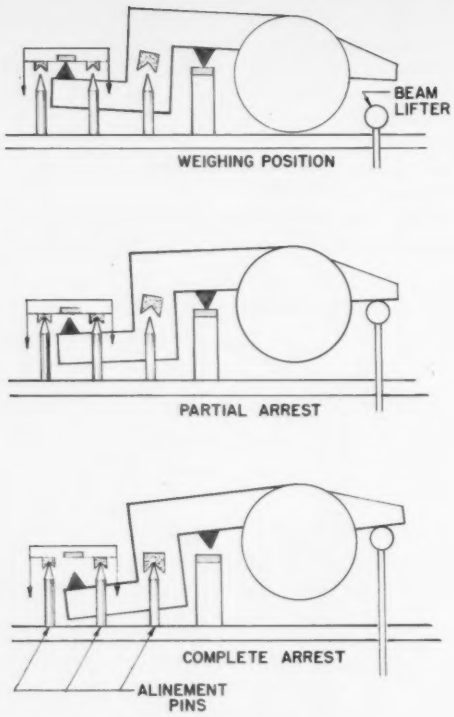

FIGURE 9. *The full arrest mode of arrestment.*

In the bottom view, the beam lifter has raised the counterweight end of the beam until the beam is supported by its alinement-arrestment pins and the beam lifter and the fulcrum knife is separated from its flat. The beam lifter does not contribute to the alinement in the arresting operation because it was fabricated from a roller with a ball bushing riding on shaft with ball bearings. Thus, any horizontal component is taken up by the ball members.

The essential features of the constant load mode of arrestment are shown in figure 10. In the first view (left), the balance is shown in the weighing or released position. In the second view (middle), the weight carrier has been raised so that it is in contact with the weight on the pan. As the weight carrier gradually moves upward lifting the weight, the suspension follows the weight until the tit comes into contact with the tit stop, preventing further upward movement of the suspension. The weight carrier continues to move upward until the weight is free and clear of the pan. When the pan is empty, the force between the tit and the tit stop is about 1 kg. The balance is now arrested in the constant load mode. This condition is shown in the third view (right). The next weight may now be brought to the pan and lowered onto it.

3. Adjustment

Basic to the proper adjustment of the balance is that the balance be level. Specifically this means that the fulcrum flat is level (fig. 11). With the fulcrum flat level the height of the alinement-arrestment pins was adjusted so that when the load and the fulcrum knives lie in the same horizontal plane, the beam is at the midpoint of its travel. The weight carrier table is adjusted so that the weight carrier surface on which the weights rest is level. With the balance mechanism assembled the alinement-arrestment pins are further adjusted so that the knife edges meet their cooperating flats simultaneously along their entire length.

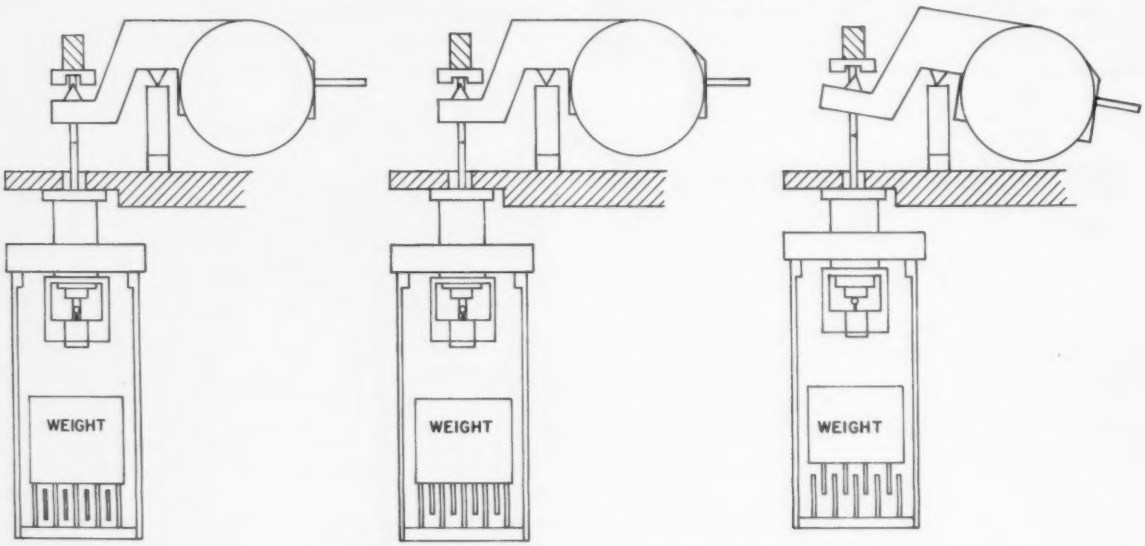

FIGURE 10. *The constant load mode of arrestment.*

For simplicity, the assembly of flats between the load and intermediate knives is not shown. The important point is that these two knives remain in contact with their associated flats in both the released condition (right view) and during the arresting procedure.

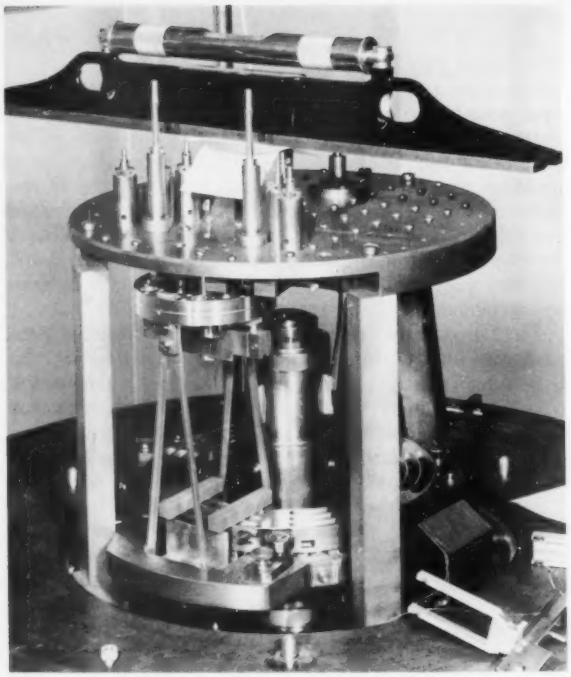

FIGURE 11. *View of balance being leveled.*

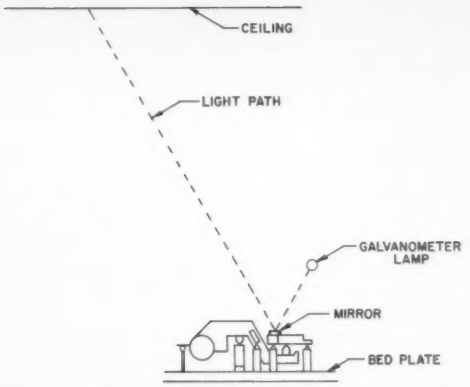

FIGURE 12. *Schematic of optical system used in adjusting the arresting-alinement pins.*

An optical device (fig. 12) was used to indicate when the adjustment was satisfactory. This device consisted of a light source (a galvanometer lamp) positioned above the balance and a small mirror placed on the part whose arrestment pins were being adjusted. The image of the filament of the galvanometer lamp was reflected onto the room ceiling, which served as a viewing screen. Lack of motion of image when the balance was released or arrested indicated proper adjustment.

The pan was leveled (fig. 11) by adding weights to either side, front, or back as required. The height of the weight carrier table was adjusted so that the weight carrier would clear the pan with the weight changing mechanism in the weight changing position, as the weight carrier is rotated during the weight changing operation.

Tests after the final beam adjustment indicated that the knife edges were parallel within about one part in 10^7 and coplanar within about two parts in 10^8.

4. Operation

The operation of the balance is straight forward, but in some aspects, indicated below, its operation differs from that of a conventional one pan balance. The balance is free swinging, therefore, the indication is obtained by taking turning points. The built-in sensitivity weight is controlled from outside the balance case. There are places for six weights on the balance's weight carrier any of which can be brought to the pan and placed on or removed from the pan by means of controls outside the balance. Thus after the weights have been placed in position, the weight on the pan may be changed and a whole series of measurements made without opening the balance case.

When the balance is opened for loading or any other reason, it should always be arrested in the full arrest mode and the weight carrier in the weight changing position. To open the balance the outer case is lifted off, set aside, and the lower part of the inner case raised (fig. 13). The weights are put in position on the weight carrier and successively brought into posi-

FIGURE 13. *View of the balance case being opened.*

tion over the pan for centering. As each weight is brought into position over the pan, it is mechanically centered by alternately placing it on and removing it from the pan, as the weight carrier and table are raised and lowered, until there is no movement of the pan when the weight is put on or removed from the pan.

As the balance is loaded, the position of each weight on the weight carrier is noted and the weights are trimmed to within a milligram of each other, by adding small known weights as required. The balance may now be closed, and the conditions within the balance case allowed to come into equilibrium before the weighings are commenced.

For optimum results, the balance should be exercised before the actual weighing operation is begun. With the selected weight in position over the pan, as indicated by the weight position indicator, and the beam brake applied, the full arrest control is turned to the released position. The weight carrier is then lowered to the weighing position, placing the weight on the pan. The brake is released, and as the balance approaches the equilibrium position the brake may be used to control the amplitude of the swing. After the indication has been noted, the balance is arrested in the constant load mode of arrestment, by raising the weight carrier to the weight changing position, thus removing the weight from the pan. The weight is placed on the pan as before, and the indication noted. The exercising is continued until the balance begins to repeat its indication, within its reproducibility.

When the balance has been exercised sufficiently, the actual measurements are begun. Since this is a one pan balance, all of the measurements are made by the substitution method weighing, preferably by the double substitution method according to an appropriate weighing design. The balance is always arrested in the constant load mode between the readings, even if it is only to apply or remove the sensitivity weight. The beam brake is always applied when arresting or releasing the balance to prevent large uncontrolled oscillation of the balance. The full arrest mode is used only at the beginning and end of a series of measurements, at the beginning to release the balance, at the end to arrest the balance. If the balance is to be left unused for any length of time, such as overnight, it is always left arrested in the full arrest mode of arrestment. If for some reason the balance has been arrested in the full arrest mode before the series of measurements has been completed, it is necessary to reexercise it before again making any measurements.

5. Performance

The balance's performance was evaluated through 13 series of measurements made over a period of a week. Three of these series involved four stainless steel 1 kg weights, designated SI, SII, SIII, and SIV. The SI, 1 kg, served as the restraint. Another three of the series involved two platinum-iridium 1 kg weights designated PI and PII, and two stainless steel 1 kg weights designated SI, and SV. The remaining seven series involved three platinum-iridium 1 kg weights, designated PI, PII, and PIII and one platinum weight, designated PIV.

All of the series of comparisons were made according to a weighing design, designated the 4–1's weighing design, in which four masses are compared in all possible combinations. In this design three degrees of freedom are available for estimating the error of the measurements. A pooled estimate of the standard deviation of one weighing was computed from the data developed during the thirteen series of comparisons. For this work, a double substitution weighing is defined as one weighing.

The barometric pressure, relative humidity, and temperature inside the balance were recorded at the beginning and end of each double substitution weighing. From this data, the average air density was computed for each weighing. Each measured mass difference was individually corrected for the buoyant effect of the atmosphere.

An analysis of the data indicates that in all instances the measurement process was operating in a state of statistical control.

The results of the thirteen series of measurements are shown in table 1. The random portion of the uncertainty of each value, where all of the weights in a given series were of the same material, using 3σ as the limit, is 7.8 μg.

It was noted that the sensitivity of the balance decreased during the course of a series of measurements. Since it took from about 25 to 30 min to complete one comparison between two weights by the double substitution method of weighing, from $2\frac{1}{2}$ to 3 hours were required to complete a series of measurements according to the 4–1's weighing design—the design usually used. This means the knife edges were subject to the full load, continuously, for that period of time. The results shown in table 2 are typical.

After another series of similar measurements, which showed a similar decrease in sensitivity with time, the balance was arrested in the full arrest mode. That is, the knives were separated from their cooperating planes and completely relieved of any load. After about 4 hours, another sensitivity measurement was made. This measurement indicated that the balance had nearly recovered the sensitivity it had at the beginning of the series of measurements. Unfortunately, this data has been lost. The decrease in sensitivity was attributed to elastic deformation of the knife edges while they were loaded. The phenomenon was not investigated further.

The author wishes to express appreciation for the generous assistance and guidance received from many members of the NBS staff during the development of this balance. H. A. Bowman and P. E. Pontious contributed both practical and theoretical assistance and gave continuing support and encouragement throughout the development. The author is indebted to A. G. McNish and Karl G. Kessler for continued support and encouragement through the work, also to H. S. Peiser for encouragement throughout the development.

TABLE 1. *Summary of results of performance test*

Weight/ series	True Mass Corrections								
	P II (mg)	P III (mg)	P IV (mg)	S I (mg)	S V (mg)	S II (mg)	S III (mg)	S IV (mg)	s μg
1						11.0288	11.9110	17.4250	4.8
2						11.0237	11.9087	17.4131	2.4
3						11.0195	11.8981	17.4145	3.0
4	−0.0736	−0.7818	−4.8394						2.3
5	−0.0722	−0.7836	−4.8321						3.4
6	−0.0782			11.6534	13.5051				5.3
7	−0.0708	−0.7818	−4.8390						2.1
8	−0.0674	−0.7806	−4.8347						6.6
9	−0.0718	−0.7832	−4.8396						4.0
10	−0.0711	−0.7806	−4.8304						3.7
11	−0.0797			11.6677	13.5136				7.8
12	−0.0719	−0.7830	−4.8313						2.2
13	−0.0780			11.6611	13.5150				3.4
						Pooled estimate of the standard deviation of all these measurements.			4.3
						Pooled estimate of the standard deviation of the measurements where all the weights in a given series were of the same material.			3.7

Series 1, 2, and 3—All weights are stainless steel
Series 4, 5, 7, 8, 9, 10, and 12—All weights are platinum or platinum-iridium
Series 6, 11, and 13—Two weights are stainless steel and two weights are platinum-iridium

TABLE 2. *Change in value of the division with time*

Intercomparison	Value of the Division
a_1	0.1517 mg
a_2	.1519 mg
a_3	.1524 mg
a_4	.1523 mg
a_5	.1525 mg
a_n	.1527 mg

L. B. Macurdy contributed studies that aided in the development of the design. Randall M. Schoonover contributed design suggestions and assisted in testing the balance during the various stages of its development.

6. Appendix

The balance was loaned to the International Bureau of Weights and Measures for use in the International Bureau's Program of Mass Measurements, including the intercomparison of National Prototype Kilograms with the International Prototype Kilogram.

Prior to shipping the balance, representatives of the International Bureau of Weights and Measures spent from a week to a month at the National Bureau of Standards familiarizing themselves with the balance—its construction and operation. After they had become thoroughly familiar with the balance they oversaw the packing of the balance for shipment to the International Bureau at Sevres, France. The balance beam was hand carried, but the other parts of the balance were shipped by commercial air freight.

Because the International Bureau of Weights and Measures had not completed its new mass laboratory when the balance arrived the balance was temporarily installed in another laboratory. The International Bureau does not consider the weighing conditions in this laboratory to be good. After the balance had been set up in this temporary location, Georges Girard made several series of measurements, using four stainless steel kilograms, according to the 4–1's weighing design. The results of these measurements, in summary form, are shown in the graph below. There are 21

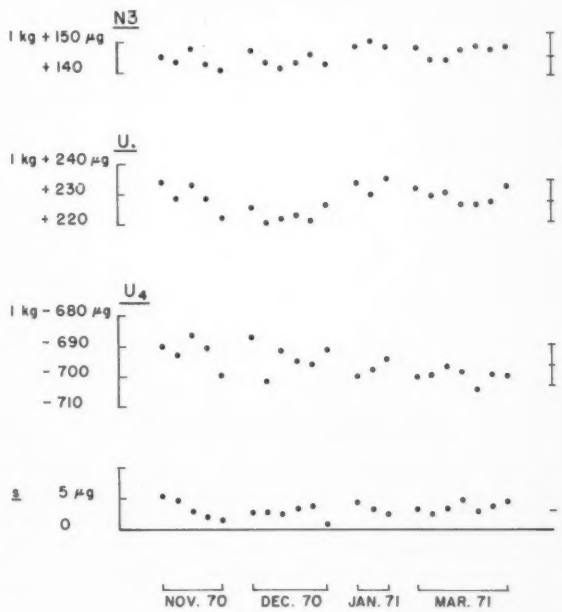

series of measurements and each series has three degrees of freedom available for estimating the error of measurement. The mean standard deviation on the basis of 63 degrees of freedom is 3.2 μg, and the measurement uncertainty of any individual value found is 6.8 μg.

7. References

[1] Peiser, H. S., State Mass Standards, Report of the 45th National Conference of Weights and Measures, June 8, 1960; p. 45.

[2] Almer, H. E., Bowman, H. A., Jensen, M. W., Macurdy, L. B., Peiser, H. S., and Wasko, B., A Direct-Reading Two-Knife 50-Pound Balance of High Precision Suitable for State Weights and Measures Laboratories., J. Res. Nat. Bur. Stand (U.S.), **68C** (Eng. and Instr.) No. 3, 141–154 (July-Sept. 1964).

[3] Bowman, H. A., and Almer, H. E., Minimization of the Arrestment Error in One-pan, Two-knife Balance Systems, J. Res. Nat. Bur. Stand (U.S.)., **67C** (Eng. and Instr.), No. 3, 227–235 (July-Sept. 1963).

[4] Bowman, H. A., and Schoonover, R. M., Procedure for High Precision Density Determinations by Hydrostatic Weighing, J. Res. Nat. Bur. Stand (U.S.), **71C** (Eng. and Instr.), No. 3 179–198 (July-Sept. 1967).

[5] Macurdy, L. B., Response of Highly Precise Balances to Thermal Gradients, J. Res. Nat. Bur. Stand (U.S.), **68C** (Eng. and Instr.) 135–140 (July-Sept. 1964).

(Paper 76C1&2–326)

JOURNAL OF RESEARCH of the National Bureau of Standards—C. Engineering and Instrumentation
Vol. 76C, Nos. 1 and 2, January–June 1972

Ball and Cylinder Interferometer

J. B. Saunders, Sr.

Institute for Basic Standards, National Bureau of Standards, Washington, D.C. 20234

(March 24, 1972)

An interferometer is described that permits the comparison of diameters of balls and cylinders with an etalon. The specimen is located in the cavity of the etalon. Interference is produced by light reflected from each surface of the etalon and the adjacent surface of the specimen. The two pairs of interfering beams of light (one pair from each side of the etalon) are received by the same eyepiece or camera. A shutter permits alternate viewing of the two interferograms. Magnification and contrast of the fringes are obtained by a suitable choice of power and separations of components of the system. After the prime dimension of the etalon is determined, it can be subsequently rechecked with the single mode (stabilized) laser, used with this interferometer, without removing the etalon from the assembly. A method is provided for analyzing the results of this interferometer.

Key words: Density standards; interferometer; volume of spheres.

1. Introduction

This interferometer was designed primarily for measuring the volumes of near perfect spheres that are intended to represent standards for density. The spherical form was chosen because it is believed to permit the highest accuracy for volumetric determination.

Measurement of the geometry of balls and cylinders has usually been made with electrical and mechanical probes. The interferometer method, described below, is believed to provide greater accuracy than can be obtained by other methods. It also eliminates the necessity of physical contact between the surface and other elements, except for gravitational support.

This interferometer permits the measurement of the minimum separation (d_1 and d_2, fig. 1) of the specimen from each of the etalon faces, E_1 and E_2. If the cross section of the specimen approximates a circle, the average of several diameters (whose directions are uniformly spaced) approximates the diameter of a circle whose area equals that of the section. Likewise, if the shape of the specimen approximates a sphere, the average of many equally spaced (angularwise) diameters approximates the diameter of a sphere whose volume equals that of the specimen.

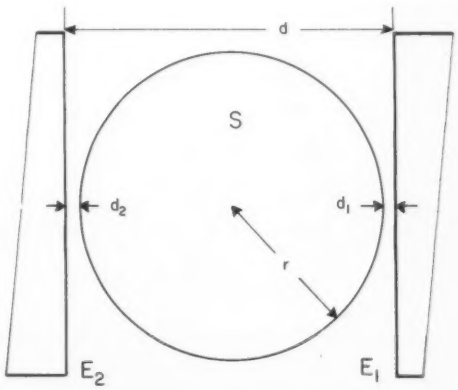

FIGURE 1. *Relative position of etalon and sphere.*

2. Optics of the Interferometer

Figure 2 shows the optical arrangement of the interferometer. A beam of light from the stabilized laser is focused to a small area, f_1, by the microscope objective, L_3, and subsequently collimated by the lens L_1. The collimated beam is divided in the beam splitting prism, BS, which provides a transmitted beam

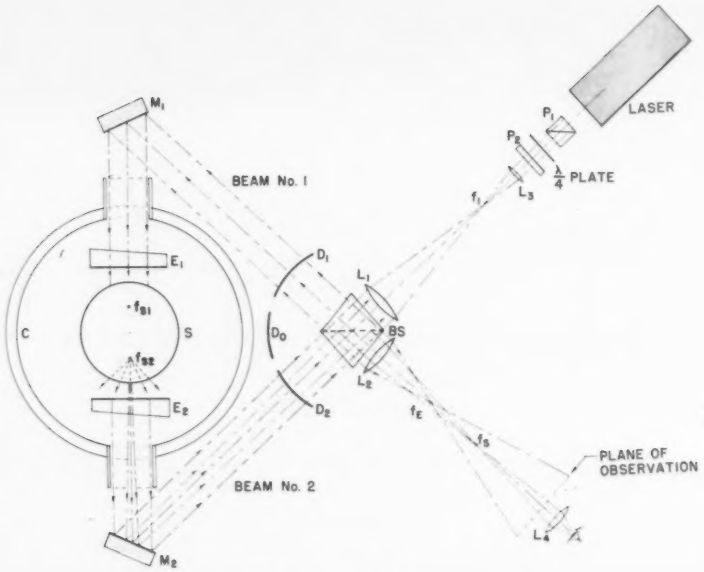

FIGURE 2. *The ball and cylinder interferometer.*

(No. 2) and a reflected beam (No. 1). These two beams are reflected by mirrors M_1 and M_2 toward opposite sides of the ball, S, that is to be measured. Surfaces E_1 and E_2 form a Fabry-Perot etalon when the ball is removed. Light reflected from the two etalon surfaces returns (collimated) to BS and then to lens L_2, which converges it to a small point, f_E, at its focus. The two beams of light then diverge from this point as concentric wave fronts, with their radii increasing and intensity (per unit area) decreasing with increasing distances beyond f_E.

The center of the ball, S, is located on the virtual, coinciding axes of lenses L_1 and L_2. The ball is equally distant from BS by way of the two beams. The collimated beams of light that pass through E_1 and E_2, which are uncoated, are then reflected from the ball and return to BS as divergent beams, one of which is indicated by the 3 central rays shown in beam No. 2. These two beams (one from each side of the ball) are converged, by lens L_2, to f_S from which point they again diverge as spherical wave fronts, very similar to those from f_E.

A movable screen D_ν ($\nu=0,1,2$), pivoted about the center of BS, permits the interception of beam No. 1, or No. 2 or neither beam when in positions D_1, D_2, or D_0, respectively. When either beam is intercepted nonlocalized interference fringes may be observed at any point beyond f_s. The observed interferograms, shown in figure 3, are sets of concentric, circular fringes. The order of interference at the center of the interferogram is a measure of d_1 (fig. 1), when the shutter is at D_2, and d_2 when it is in position D_1.

The magnification (or size) of the fringes are proportional to the distance from f_S to the plane in which they are observed. This plane of observation is the plane of the photographic emulsion when photographing the fringes and is conjugate to the retina of the observer's eye when he is observing them. A collector lens, L_4, permits focusing of the fringes by the eye.

The contrast (visibility) of the fringes depends upon

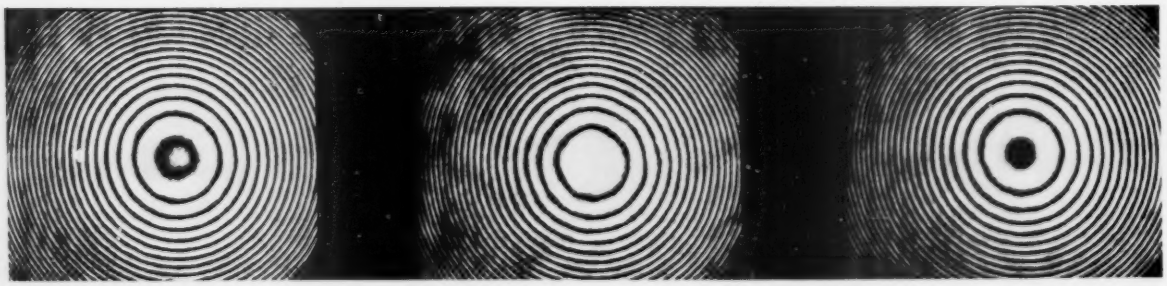

FIGURE 3. *Interference fringes produced by light reflected from the etalon and a spherical surface.*

the relative intensity (per unit area) of the two beams. An optimum contrast and magnification is obtained by a suitable choice of reflection, transmission, spacings and powers of the optical elements. Excellent fringes were obtained for measuring steel balls (reflectivity equal 0.6) with the following dimensions and parameters:

L_3 was a 4× microscope objective
L_1 was a 17 cm.f.l., 2 cm diameter lens
L_2 was a 25 cm.f.l., 2 cm diameter lens
BS was an imbedded aluminum film, having equal transmission and reflection
M_1 and M_2 were highly reflecting, plane mirrors
E_1 and E_2 were uncoated glass surfaces.

Distances:

Laser to L_3 (not critical) is sufficient to allow spaces for the polarizing prism, P_1, the quarter wave plate and the parallel plate, P_2, which is used to facilitate lateral adjustment of the beam;

L_3 to L_1 equals focal length of L_1 plus focal length L_3
L_1 to BS = L_2 to BS = 2 cm
BS to M_1 = BS to M_2 = 24 cm
M_1 to E_1 = M_2 to E_2 = 10 cm
L_2 to plane of observation = 250 cm
E_1 to E_2 = 6.75 cm
diameter of S = 6.35 cm.

3. The Etalon

The cavity of the etalon was chosen to provide two gaps, d_1 and d_2, between the plates and ball of approximately 2 mm each. The etalon plates are 5 cm high, 5 cm wide, 1.3 cm thick, made of fused quartz and cemented to fused quartz plates E_3 and E_4 (see fig. 4) which serve as spacers. The annular shaped spacers have an inside diameter of 7.3 cm to permit insertion of the ball and an outside diameter of 11.4 cm for its insertion in water jacketed, brass cylinder, shown in figure 5. The temperature of the cylinder was thermostatically controlled.

The etalon is shown upside down in figure 4. The three buttons, cemented to its base plate, are contact points that rest on three leveling screws. These screws permit vertical displacements and tilting of the etalon.

The 40′ wedge, between the two surfaces of each etalon place permit the elimination of light reflected from the outer surfaces. These plates were cut from a common plate to insure equality of angles and thickness. They are mounted so that when the inner surfaces are parallel the outer surfaces are also parallel to each other. Thus, when beams No. 1 and No. 2, between the etalon and mirrors M_1 and M_2, respectively, are parallel to each other the two beams, inside the etalon and before their incidence on the ball, are also parallel to each other. This insures that the rays (one of each beam), which are incident normal to the ball, will be incident at opposite ends of a common diameter. This is an essential requirement for the test and insures that

$$d_1 + d_2 + 2r = d, \tag{1}$$

where r is the radius of the ball and d is the length of etalon cavity.

The alinement method, described by Bergman and Thompson [1],[1] was used for paralleling the plates dur-

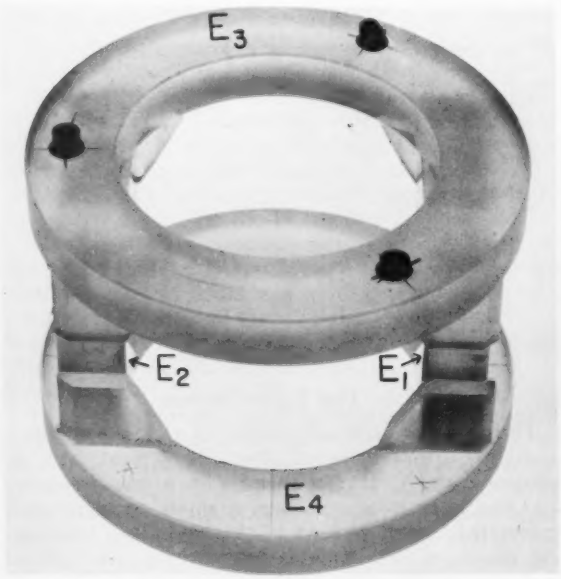

FIGURE 4. *Photograph of the etalon.*

E_1 and E_2 are surfaces. E_3 and E_4 are annular plates.

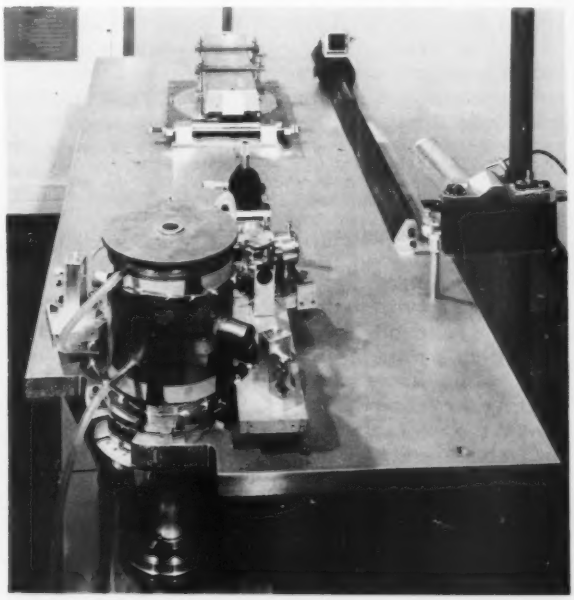

FIGURE 5. *View of interferometer and accessories.*

[1] Figures in brackets indicate the literature references at the end of this paper.

ing the cementing of same. The resultant angle between surfaces E_1 and E_2 at the centers of the plates, was 0.3 seconds of arc. This misalinement is too small to produce any significant error in any of the measurements for which the etalon is to be used.

The conventional method for measuring etalon cavities is to determine the maximum order of interference produced by it when used (in collimated light) as a Fabry-Perot interferometer. This interferometer (see fig. 6A) does not measure the separation of the plates at any one point. The resultant cavity measurement is the average separation of the plates over the illuminated part of the aperture. This, of course, assumes the illuminating beam to be uniform in intensity. Because of imperfections [2] in polished surfaces, the difficulty (approaching the impossible) of paralleling the plates at a chosen point and the need for knowing the separation at a chosen point, the optical arrangement shown in figure 6B was used to evaluate the etalon spacing, d, at the point that is to be used for testing balls. The width of the fringes is controlled by adjusting the distance between the source, lens and etalon.

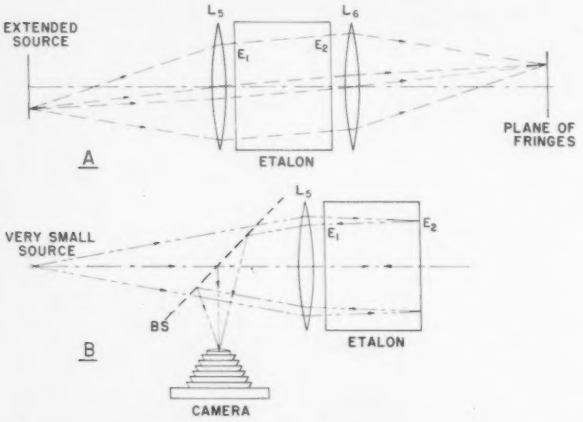

FIGURE 6. *A. Conventional Fabry-Perot interferometer. B. Modified Fabry-Perot interferometer for measuring the cavity at a chosen point in its aperature.*

The fringes produced by the two interferometers shown in figure 6 are quite similar. Consequently, the conventional method of analyzing Fabry-Perot fringes can also be applied to those obtained from the interferometer of figure 6B. The camera, shown in figure 6B, is focused on a plane near the center of the etalon. The center of the fringe pattern is adjusted to the desired point, at the center of the plates. The order of interference at the conjugate of this point is then a measure of the etalon spacing at the point. Interference fringes, produced by four spectral lines of Hg 198, were photographed and analyzed. Because of the low illumination available with the interferometer of figure 6B (with uncoated surfaces) and differences in intensity of the spectral lines used, the several lines were photographed separately. This means that the temperature of the specimen and refractive index of the air (in the etalon cavity) could be different for the several photographs. However, the accuracy of correction to standard conditions is no less than if all lines were photographed simultaneously. Repeated measurements yielded a value for the integral part of the etalon length (at standard conditions) that is believed to be absolutely correct. The fractional part of the order is believed to be accurate to within one tenth of an order. Even though the etalon was previously baked for stabilization, previous to the above mentioned measurements, provisions are made for remeasuring it without removing it from the temperature controlled cylinder.

If the ball, S, and lens, L_1, is removed from figure 2 and beam No. 1 is obstructed by the shutter in position D_1, we have the arrangements shown in figure 7, with the dimensions altered to conserve space. As in figure 2, we have two wave fronts diverging from points f_{E1} and f_{E2} which represent light reflected from E_1 and E_2, respectively. These wave fronts produce a set of concentric, circular, nonlocalized fringes centered on the extension of a straight line through the two points of divergence. The optical path difference between the two beams, on this line, is a measure of the length of the etalon cavity. Thus, by removing L_1 the interferometer of figure 1 permits retesting the etalon with the same source used for measuring the ball—assuming the cavity changes are less than one quarter wavelength between successive measurements. Since the etalon was baked for approximately 3 days (after its assembly) at a temperature of 150 °C, we do not expect much change in its dimensions.

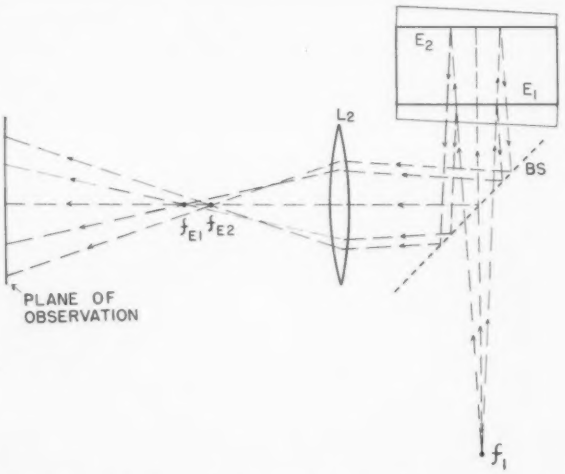

FIGURE 7. *Modification of ball and cylinder interferometer for measuring the etalon in situ.*

4. The Light Source

The gas laser used with this interferometer produces a slightly divergent beam of stabilized light. This divergence was further reduced with a lens, recessed into the laser housing. Thus, a small, approximately collimated, beam of light is obtained. This improves the effects of the elements between the laser and L_1 and permits L_1 to receive the entire beam.

It is not necessary to use a stabilized laser except for retesting the etalon cavity in situ. Any gas laser is suit-

able for measuring balls and cylinders if the etalon cavity is known and the sum (d_1+d_2), does not exceed 1 cm. To permit stabilization, however, little or no light can be allowed to return into the laser. This is readily accomplished by slightly tilting the quarter wave plate (fig. 2), the faces of prism, P_1, the parallel plate, P_2, and adjusting the azimuth of the polarizing prism relative to that of the quarter wave plate to eliminate all light transmitted through and returned (by reflections) to them. The polarizing prism, P_1, insures that the light transmitted by it is plane polarized. The quarter wave plate changes it to circularly polarized light. The light that returns, from the interferometer, to the quarter wave plate remains approximately circularly polarized having been affected slightly by BS, M_1 and M_2. The quarter wave plate converts the return light to approximately plane polarized light, with its plane of polarization normal to that previously transmitted by P_1, so that it is not retransmitted by P_1 and little or no light is returned into the laser.

Further reduction of light, returning to the laser, is obtained by adjusting a screen with a 25 μm hole (a spacial filter) so that the center of the hole coincides with f_1.

The high intensity of the laser source is important, both for obtaining short exposures of the interferograms and for adjusting the instrument. All critical adjustments are performed by observing interference fringes that are produced in various ways and with various combinations of elements. It appears practically impossible to design the hardware of this instrument so that it can be adjusted permanently to the precision which the adjustments allow and for which its operation require. Details for making adjustments are given in Appendix A, at the end of this paper.

5. Direction of Increasing Orders

The analysis of interferograms requires a knowledge of the direction of increasing orders of interference. The analysis of cylinder interferograms is identical to that for sphere interferograms. Consequently, this discussion will be limited to interferograms produced by spherical wave fronts.

The two sets of coherent wave fronts, W_1 and W_2 (fig. 8), combine to produce interference and the resultant interferogram is a set of concentric, circular fringes. The center of these circles ("bull's eye") is on the straight line (defined as the "axis") that passes through the centers of curvature of the two sets of wave fronts.

Let P (fig. 8) be any point in the plane of observation, at a distance y from the bull's eye; W_1 and W_2, the wave fronts that pass through P, with W_2 selected as the one that has traveled the greater distance from the common source to P; R_1 and R_2, the radii of curvature, points f_1 and f_2, the centers of curvature, and Φ_1 and Φ_2, the phases of W_1 and W_2 at f_1 and f_2, respectively. Points f_1 and f_2 correspond, respectively, to f_E and f_S of figure 2.

R_1 and R_2 are positive if the respective wave fronts

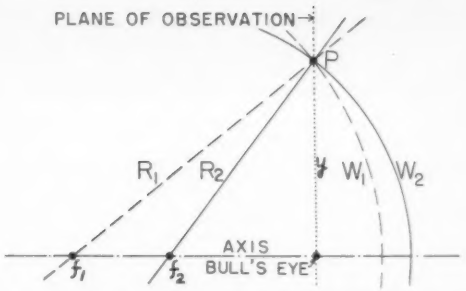

FIGURE 8. *Diagram for determination of direction of increasing orders of interference.*

are concave toward the incident light (diverging) and negative if convex toward it (converging).

The optical paths from the source to P is $[\Phi_1\gamma/(2\pi)+R_1]$ for W_1 and $[\Phi_2\lambda/(2\pi)+R_2]$ for W_2, where λ is the wavelength of the light. Consequently, the order of interference N, at P is

$$N=(\Phi_2-\Phi_1)/(2\pi)+(R_2-R_1)/\lambda.$$

Since $(\Phi_2-\Phi_1)$ is constant for any interferogram, it is apparent from this equation that the order of interference increases if (R_2-R_1) increases and decreases if it decreases. For all interferometers described in this paper, the plane of observation is never chosen between f_1 and f_2. Consequently, the algebraic sign of R_1 and R_2 are always the same.

It is apparent, from figure 8, that $|R_2-R_1|$ always decreases with increasing values of $|y|$. Therefore, the algebraic sign of (R_2-R_1) determines the direction of increasing orders of interference. If $(R_2-R_1)<0$ the order increases with increasing diameters $(=2y)$ of the fringes and decreases if $(R_2-R_1)>0$.

For the analysis of interferograms produced by the interferometer shown in figure 6B, it is apparent that the direction of increasing order will be unchanged if the plane of observations is chosen anywhere between lens L_5 and the first conjugate of the source at f, shown also in figure 9. It is, therefore, chosen on or to the left of E_2 to avoid virtual imagery. Since the light is converging (R_1 and R_2, negative) and $|R_2|$ is larger than $|R_1|$, $(R_2-R_1)>0$. Therefore, for this interferometer, the order of interference decreases with increasing diameters of the fringes.

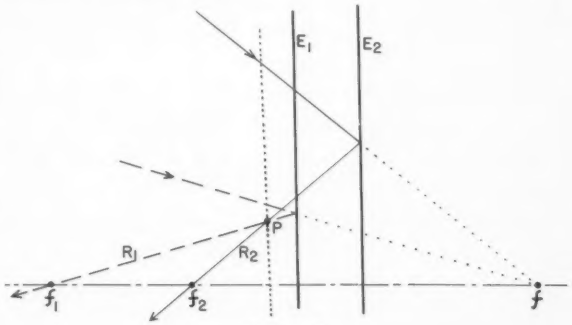

FIGURE 9.

For the interferometer of figure 7, the wave fronts are diverging at the plane of observation (R_1 and R_2, positive) and $R_1 < R_2$. Therefore, $(R_2 - R_1) < 0$ and the order decreases with increasing diameter of the fringes.

In the interferometer of figure 2, the wave fronts are diverging at the plane of observation as in figure 9 (R_1 and R_2, are positive) and R_2 (the distance from f_s to P) is smaller than R_1. Therefore $(R_2 - R_1) < 0$, and the order increases with increasing diameters of the fringes.

6. Analysis of Interferograms

If photoelectric methods of reading the fringes are used, whether at integral orders (centers of bright fringes), integral-plus-half orders (centers of dark fringes), or at other points of equal intensity, the computed value for N at the bull's eye will be practically free from the procedural errors described below. If visual or photographic methods are used and readings are made either for integral or integral-plus-half orders, the observed diameters are usually in error because of variations in fringe width. This error can approximate one tenth of an order.

The solid curve in figure 10 shows the intensity distribution in a set of two-beam fringes such as the one used to produce figure 3. The broken line curve represents the photographed density distribution and/or apparent intensity distribution when observed visually. The apparent centers of the fringes (dark or bright) are not located at maxima and minima of the intensity curve. Consequently, if the apparent centers of bright and dark fringes are considered to be at integral and integral-plus-half orders an error is introduced in the computed order at the bull's eye.

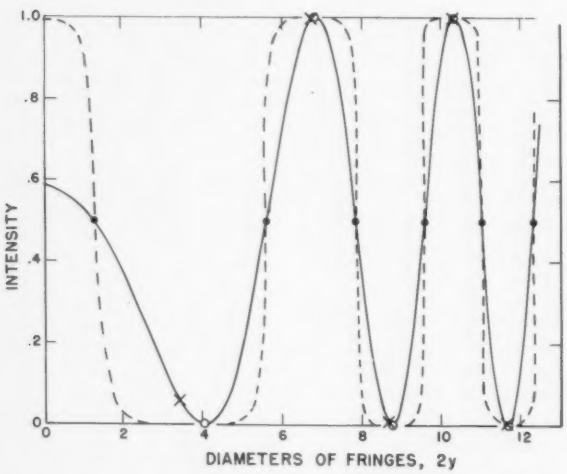

FIGURE 10. *Intensity distribution of light in two-beam, Fabry-Perot type interferograms.*

The small circles represent points of maximum and minimum intensity, which correspond to integral and integral-plus one-half orders of interference, respectively; the solid dots represent apparent edges of fringes, which have equal ordinates; and the X's represent apparent centers of the fringes.

The apparent edge and, consequently, also the width of a fringe, differs from one observer to another. The apparent edges of fringes in a photograph depend on the exposure and contrast of the photographic emulsion used. In general, the bright fringes will be narrower than adjacent dark fringes in an under-exposed interferogram and wider than adjacent dark fringes if the interferogram is overexposed. The relative width of the bright and dark fringes may be varied over a broad range by a choice of exposure and contrast in the photographic emulsions. However, if the aperture of the optical system is uniformly illuminated and the fringes are photographed or visually observed by any one observer, the points which he selects for edges of fringes will differ in phase from adjacent minina (or maxima) by a constant, except for accidental errors. Thus, this phase difference can be introduced into the mathematical model used for computing the orders at the bull's eye.

It can be shown that the relationship between the orders of interference, N, at any point, P, (fig. 8) and the distance, Y, from the bull's eye to P, is given, to a close approximation, by

$$N = A + BY^2 + CY^4. \tag{2}$$

The quantity Y may be replaced by $2Y$, which is the diameter of the circle through P and centered at the bull's eye. Obviously, the value of N at the bull's eye, where $Y = 0$, is A; which is the only information desired from each interferogram.

When observing for values of Y in an interferogram, or a photograph of it, values of N are not known at any chosen reference point. However, if the observer chooses points which he considers to be at the edges of the fringes (fig. 10), he will select points on the intensity curve where the order differs from adjacent integral orders by a constant. This constant, E, may be introduced into eq (2) for the statistical evaluation of A.

For practical reasons, the interference fringes are photographed and the negatives are used for evaluating the Y's. The dark (denser areas) fringes correspond to integral orders.

The procedure, described below for evaluating A, applies to all interferograms produced with this interferometer. It also applies to interferograms produced with conventional Fabry-Perot interferometers.

Observations will be made along a straight line through the bull's eye and at all edges of the first four dark fringes that have inner edges. Reference points are chosen at both outer and inner edges. When the inner edge of the innermost fringe can be read (figs. 3A and 3B), the number of reference points is 16, as shown in figure 11A; when the inner edge of the innermost dark fringe can not be read (fig. 3C), the number of reference points is 18, as shown in figure 11B. The orders of interference, N_ν, at the chosen reference points (edges of fringes, fig. 10) are,

$$N_\nu = \nu/2 + [1 - (-1)^\nu]/4 + (-1)^\nu E. \tag{3}$$

Where ν is the order of reading points (beginning with

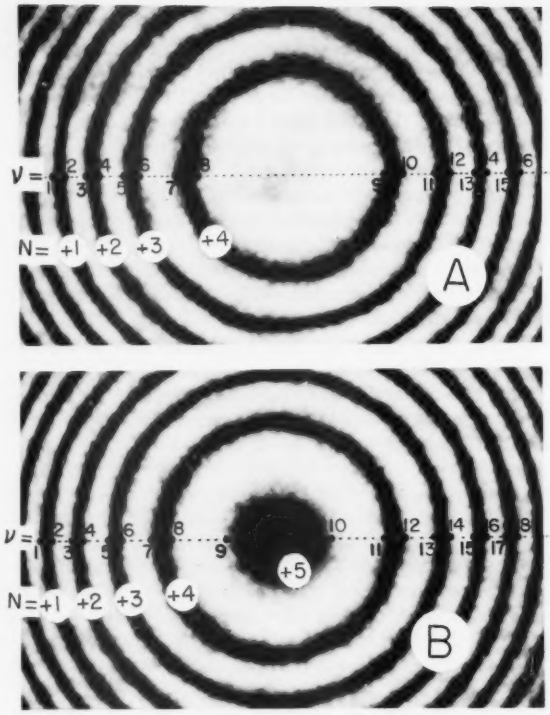

FIGURE 11. *Enlarged portions of figures 3B and 3C.*

The numbers, in the smaller print, represent the order of reading and position of the reference points. The numbers, in the larger print, represent orders of interference.

unity at the left-hand end of the line of points) and E is the unknown difference between N_ν and the integer closest to it.

On eliminating $N(=N_\nu)$ from eqs (2) and (3) we obtain,

$$\nu/2+[1-(-1)^\nu]/4+(-1)^\nu E=A+BY^2+CY^4,$$

where $\nu=1, 2, 3 \ldots 8$ or 9, respectively, for interferograms represented by figure 11A or 11B. By writing the above set of observational equations in the form,

$$A+BY_\nu^2+CY_\nu^4-(-1)^\nu E=[1+2\nu-(-1)^\nu]/4 \quad (4)$$

one can use the computational procedures of standard least squares to arrive at satisfactory values for A, B, C, and E.

The above procedure applies to interferograms in which the order of interference decreases with increasing values of Y. For interferograms in which N increases with increasing values of Y, the plus signs before the integral values of N, shown in figure 11, should be replaced by negative signs. Consequently, the value of A ($\equiv A_i+A_f=$integral plus fractional parts of A) will always be negative and the desired fractional part of the order will be the complement $(1-A_f)$, of A.

It should be noted that the spaces d_1 and d_2 can not be measured individually. Neither of these quantities are known to a sufficient approximation for applying the method of exact fractions [3]. However, the sum (d_1+d_2) can be obtained sufficiently precise by measuring the quantities d and $(2r)$ in eq (1) with micrometers. The theory of exact fractions can then be applied by using the fractional parts of the orders obtained from pairs of interferograms. One interferogram, of each pair, is photographed with the shutter in position D_1 and the other with the shutter in position D_2. The sum of the fractional part of the order that represents d_1 plus the fractional part for d_2 is the sum of the fraction part of the order that represents (d_1+d_2). When the corrections for phase shifts are applied, the absolute value of $2r$ can be computed fron eq (1).

7. Summary

The mean diameter, and consequently also the volume, of nearly spherical balls is obtained by measuring the difference between an etalon cavity and the diameters of the ball. The etalon cavity is measured by the conventional method described in the literature—with slight modifications to obtain the separation of the plates at a known point instead of the average separation which is usually measured. The ball is placed in the cavity and the two spaces (gaps) between the ball and the etalon plates, which form two Fizeau interferometers, are obtained by the conventional methods of absolute measurement of length by interferometry. The difference between the cavity space and the sum of the two Fizeau interferometer spaces is the length of that diameter of the ball which is normal to the etalon plates. The average of many uniformly distributed diameters is a mean diameter that represents the measured volume of the ball.

The accuracy of results of measurement with this instrument is comparable to that of other precision interferometers. Its almost complete freedom from vibration, good temperature control and measurement practically confines the errors to that of determining the orders of interference. There remains in this, as in many other interferometric measurements, the question of phase shift of light when reflected from optical surfaces. If fused quartz or some other dielectric ball is used, which is recommended by this author, the resultant phase shift is the difference between internal and external reflections from dielectrics in air. If this is known the dominant error is in reading the interferograms. The spread of several values, found experimentally for a single ball diameter, did not exceed 0.05 of an order.

8. Appendix A. A Procedure for Adjusting the Ball and Cylinder Interferometer

This instrument is a combination of several interferometers. These are: the triangular interferometer, BS − M_1 − M_2 (fig. 2), by Sagnac [4], a Fabry-Perot interferometer [5], E_1-E_2; and two Fizeau interferometers [6], E_1-S and E_2-S. It is essential that the two beams of light, No. 1 and No. 2, be parallel to each other in the etalon cavity. Only then can E_1 and E_2 be simultaneously adjusted normal to the two

468-108 OL - 72 - 2

beams of light. Also, it is important to have each pair of component rays (one in each beam, No. 1 and No. 2) of the Sagnac interferometer return to a common point in BS and pass through a common point f_E. Fortunately, this interferometer permits adjustments that insure this performance.

When two or more interferometers are compounded, the adjustments of either one effect the resultant output. Consequently, precision adjustment of the combination requires successive approximations. This requires that the adjuster become acquainted with all of the adjustments. For instance, when adjusting beams No. 1 and No. 2 into coincidence, a rotation of BS has relatively little effect on beam No. 2 and the displacement of beam No. 1 is proportional to the distance from BS. A rotation of M_1 changes the relative position of the two beams more at D_2 than at D_1. The elements BS, L_1, L_2, L_3, and M_1, and M_2 are mounted on and fastened to a flat, rigid base. A line is engraved on this base to indicate the normal projection of the center of the light beams. The centers of the elements are mounted two inches vertically above the horizontal base plate and fine adjustments are performed by relatively large screws that permit flexing the bases of the mountings of each element.

A lucite triangle, shown in figure 12, is used for locating the position of the two light beams over any point at which the indexing point of the triangle is located. Two lines are engraved on the triangle. One line is approximately 3 in long, parallel to one leg of the triangle and extending to the other leg. This line, when indexed with the engraved line on the base plate, serves to place the line vertically above the base plate line. A second short line is engraved on the triangle, 2 in from the indexing end of the 1st mentioned line and normal to it. When the triangle is indexed with the base plate line and standing vertically, the intersection of its two lines indicates the desired position of the centers of the light beams. The surfaces of lucite, when slight abraded, will scatter enough light to show the positions of the two beams from either side.

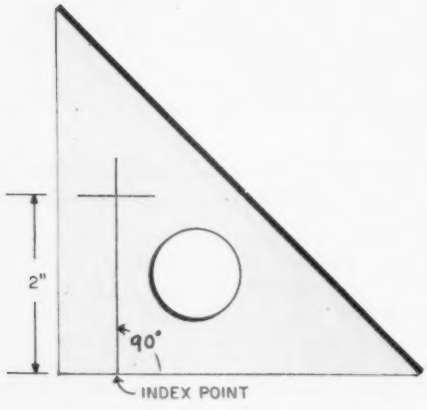

FIGURE 12. *Interferometer beam locator.*

To aid in making adjustments, it will be convenient to cement to the laser housing (fig. 5) an opaque screen black on the inner side and white on the outer side, with a circular aperture (or hole) at its center that is slightly larger than the light beam. This screen should be normal to the beam and adjusted laterally to center the light beam in the aperture.

The following is a recommended procedure for adjusting the ball and cylinder interferometer:

Step 1. The laser is placed approximately 70 cm from BS, to allow adequate space for other elements shown in figure 2, with the center of the laser beam coinciding with the centers of BS and M_2.

Step 2. Remove L_1, L_3, and S from the interferometer and place the etalon as shown in figure 2. The surfaces, E_1 and E_2 should be approximately normal to the line joining the centers of M_1 and M_2, with this line passing near the centers of E_1 and E_2. Adjust the shutter to position D_0. Adjust BS to direct beam No. 1 to the center of M_1. Adjust M_1 to direct beam No. 1 to the center of M_2. Adjust M_2 to direct beam No. 2 to the center of M_1. The two beams will each return to BS where each is again divided, so that two components return toward the laser and two components are transmitted toward the observer. Each pair of these component beams will emerge from BS accurately parallel to each other but, in general, not coincident.

Step 3. The four emerging component beams are adjusted to coincide in pairs by the following procedure:

Place an extended, brightly illuminated screen between BS and the laser, with a small black spot (or an x) on it near the optic axis of the interferometer. On looking at the black spot through BS, from the eye position (shown in fig. 2), with L_2 and L_4 removed, one sees two images of it. The observed separation of these images indicate the magnitude and direction of separation of each pair of component rays from each and every point on the source. These images are formed by light (beams No. 1 and No. 2) traversing the triangle, BS, M_1, M_2, in opposite directions. The two images can be adjusted into coincidence by either BS, M_1 or M_2. These adjustments also affect the position of the beams relative to each other and to the elements of the interferometer. Usually an adjustment (turning of one screw) can be found that improves both the position of the two beams (as revealed by the triangle of fig. 12) and the two source images. When the two images are adjusted to near coincidence, white light fringes of interference can be seen in the source. The width of these fringes indicates the magnitude and the direction of the fringes indicates the direction of separation of the two images of the source. Further adjustment of M_1 or M_2, while observing the white light fringes, will produce one broad, fluffed out fringe which indicates exact coincidence of the images. When the two images of the source are adjusted to coincide, all pairs of components (one from each of beams No. 1 and No. 2) will emerge from BS in coincidence.

At this stage of the adjustment procedure, the etalon surfaces E_1 and E_2 can be adjusted normal to any one component ray but in general not to any pair of com-

ponents because component pairs, although parallel and coincident after emerging from the interferometer, are neither parallel or coincident in the etalon cavity.

Step 4. The telescopic combination, L_1, L_3, is now placed in position, with L_1 close to BS (for conservation of space) and adjusted to pass collimated light into BS. If the axes of L_1 and L_3 are coincident, the unit can be adjusted to leave the paraxial ray unchanged in direction and position. The expansion of the beam, by this unit, must be large enough to provide adequate uniformity of illumination in the fringe patterns, over the area that will be used for measurements. Excessive expansion of the beam results in unnecessary loss of light.

The adjustment of E_1 and E_2 normal to the two component beams is affected in two steps (steps 5 and 6). First, the etalon is adjusted to reflect the two component beams parallel (but in opposite direction) to each other and, secondly, they are adjusted (simultaneously) normal to E_1 and E_2 by changing the direction of the incident beams.

Step 5. The two beams are obstructed by placing an opaque screen between E_1 and E_2. Also, a white screen should be located between the indicated positions of L_2 and L_4, for receiving the four component beams reflected from the four surfaces of the two etalon plates. There will also be four similar beams that return toward the laser. The screen, described above, through whose aperture the light leaves the laser, serves to indicate the position of these returning beams relative to the source. On rotating the etalon the four beams (on each screen) move together in pairs. Each pair represents light reflected from the two surfaces of one etalon plate. The two pairs move in opposite directions on both screens. Each beam must be identified with the surface from which it is reflected. The shutter D permits identification of the plate and wetting the etalon surface (E_1 or E_2) permits identification of the individual surfaces.

Step 6. The two beams from E_1 and E_2 are adjusted to coincide with each other by rotation of the etalon. Rotation of the etalon about a horizontal axis, normal to the beam, causes the four images to move vertically on the screen near f_E. When the two beams from the two inner surfaces are adjusted to near coincidence, interference fringes will appear on the screen in the area illuminated by them. The direction and width of these fringes indicates what direction of rotation of the etalon is required to broaden the fringes. When the fringes are broadened to portray a single fringe on the screen, the etalon is adjusted to the desired condition. It can be shown, when the above adjustment is completed, that the two component beams are incident at equal angles on E_1 and E_2. This angle of incident can now be reduced to zero by changing the direction of the collimated beam from the laser. This is effected by moving the laser beam toward the two coinciding images, that are reflected from E_1 and E_2 and return to the screen cemented to the laser housing. If this movement is effected while maintaining the beam directed toward the center of L_1, the beams from E_1 and E_2 will approach the aperture in the screen. When the two beams return to the source, they are each normal to E_1 and E_2. Because of the magnification of the telescopic system, L_1, L_3, and the relatively large distance from L_3 to the screen on the laser, the movement of images on this screen is very sensitive to rotational adjustments of the etalon. The beams will be sufficiently near normal to E_1 and E_2 when the beams return to within one millimeter of the center of the aperture in the laser screen.

Step 7. If the obstructing screen, between E_1 and E_2 is removed, the two beams transmitted by the etalon, may now be used to recheck the degree of coincidence of component rays that emerge from the interferometer. If the above described adjustments, for making all rays normal to E_1 and E_2, were appreciable, the resultant rotation of the etalon will have displaced the two transmitted beams laterally and in opposite directions so that they no longer coincide after returning to BS. A repetition of step 3 will restore the coincidence of all emerging component rays. This may be done without removing L_1 and L_3 from the system. The extended screen should be located close to L_1 for best visibility of the white light fringes (assuming the screen to be illuminated with white light).

Step 8. Repeat step 5. Usually, the magnitude of this adjustment will be much less than was required previously.

Step 9. Repeat step 3 if the white light fringes have been narrowed too much.

A few alternating repetitions of steps 3 and 5 should bring these adjustments to satisfactory approximation.

With collimated light from the laser traversing the etalon, the ball can then be adjusted to its proper position. This consists of locating the center of the ball on the axis (center of the collimated beam) and at a point equally distant from BS by way of M_1 and M_2.

Step 10. Place the ball at its approximate proper position. If E_1 and E_2 have been located equally distant from BS by way of M_1 and M_2, respectively, the ball should be centered in the etalon. A test for the lateral position of the ball is to place a sheet of white paper, having a circular hole in it whose diameter equals that of the light beam, between the etalon and M_1 (or M_2) so that the beam of collimated light coincides with the hole. If the ball is not centered in the beam, the light reflected from the ball will not illuminate the paper screen symmetrically about the hole. When this illumination is symmetrical about the hole, the ball is on axis. The two beams of light, returning to BS from opposite sides of the ball, will also illuminate the screen near f_S, producing a set of concentric, circular fringes of interference. The width or frequency of these fringes is a measure of the difference between the two distances, S, M_1, BS and S, M_2, BS. Moving the ball parallel to the axis (line through the centers of M_1 and M_2) changes the width of the fringes. When the fringes become very broad, the two distances are very near equal.

Step 11. Lens L_2 is mounted, with its axis coinciding with the center of the beams of light from BS. With D in the position D_1 (fig. 2) the collimated light from E_1

will be focused at f_E and the divergent light from the ball will be focused at f_S. The two beams diverge from these two points, producing interference on a screen located at any place beyond f_S. These fringes may be observed in any plane with a collector lens L_4 or photographically recorded by allowing the two beams to fall on a sheet of photographic emulsion, placed normal to the line through f_E and f_S, at any point beyond f_S. The order of interference at the center of this interferogram is a measure of the distance d_1, shown in figure 4. On shifting the shutter to position D_2, a similar interferogram is obtained which represents the distance d_2.

Since the beams of light from S, E_1 and E_2 are comparable in brightness with those beams reflected from the outer surfaces of the etalon and the outer surfaces of BS, the two beams that produce the desired interference must be isolated from the others. This is effected by constructing the two etalon plates and the two prisms that form BS, with angles between their respective surfaces sufficiently large to cause the undesirable beams to diverge sufficient for easy elimination. An opaque screen, located between f_S and f_E, with an aperture just large enough to transmit the two desired beams, will eliminate all the other beams.

In practice, a small reflecting prism, located between f_S and f_E, reflects the two beams (eliminating others by its small size) parallel to an optical bench (shown in fig. 5), onto a mirror that returns them to a camera box. The optical bench serves to reduce space by folding the light in such a manner that the path can be varied from 0.5 to 2.5 meters and yet be limited to the top of a 2 x 6-foot table.

9. References

[1] Bergman, T. G., and J. L. Thompson, Applied Optics, **7**, p. 923 (1968).

[2] Saunders, James B., J. Res. Nat. Bur. Stand (U.S.), **47**, No. 3, 148–155 (Sept. 1951) RP2239.

[3] Perot, A., and Ch. Fabry, Ann. Chem. Phys. **16**, p. 289 (1899).

[4] Sagnax, M. G., Acasmie des Sciences, Seance du 23 Mai, 1910, p. 1302.

[5] Fabry, C., and A. Perot, Ann. Chem. Phys. (7) **16** (1899), p. 115.

[6] Fizeau, H., Ann. Chem. Phys. (3) **66** (1862), p. 429.

(Paper 76C1&2-327)

JOURNAL OF RESEARCH of the National Bureau of Standards—C. Engineering and Instrumentation
Vol. 76C, Nos. 1 and 2, January–June 1972

Precision Reference Specimens of Surface Roughness: Some Characteristics of the Cali-Block*

Russell D. Young and Fredric E. Scire

Institute for Basic Standards, National Bureau of Standards, Washington, D.C. 20234

(March 27, 1972)

The distribution of Arithmetic Average values of surface roughness across the 120 and 20 microinch patches of NBS Cali-Block "B" have been measured. It is shown that each distribution can be described in terms of its mean value and standard deviation. The observed systematic distribution of *AA* values strongly suggests that the user select several widely spaced regions at random on the patch when calibrating a roughness measuring instrument.

Key words: Arithmetic Average roughness; Cali-Block; calibration; roughness.

1. Introduction

The American Standard for surface finish measurement (ANSI B46.1–1962) specifies the precision reference specimen for calibrating surface finish instrumentation as follows (in part): "The normal surface profile of Precision Reference Specimens of roughness height shall consist of a series of isosceles triangles having included angle of 150°"—"Roughness values shall not vary from the designated value by more than 1 microinch or 3 percent, whichever is larger."

The Natonal Bureau of Standards (NBS) maintains several carefully calibrated precision reference specimens which are employed as calibration masters in the comparison procedure used in surface finish calibration services. Most of the calibration load involves a U.S. manufactured specimen called the Cali-Block, which consists of two patches, one with a nominal Arithmetic Average (*AA*) roughness of 125 microinches and another with 20 microinches. The corresponding standard maintained by NBS consists of a Cali-Block whose *AA* roughness was determined by: (1) calculating the area under a carefully measured profile of the surface, and (2) calibrating the surface profile measuring instrument with an interferometrically measured step. The groove shape employed in the Cali-Block conforms to ANSI B46.1. The NBS standard Cali-Block was calibrated, as described above, by three laboratories in a blind round robin. Each of the three values fell well within the 3σ limit of the other two laboratories. The average of these three measurements is defined as the roughness of the maintained standard. NBS continually examines and reevaluates the measurement process associated with its many calibration services. As a part of this program, we have investigated the distribution of *AA* values over the surface of the two Cali-Block patches on NBS Cali-Block "B", whose history is well known. Briefly, Cali-Block "B" was calibrated several years ago and was then set aside as a "spare" and was essentially unused. It was kept in a protective container in the intervening period. After assuring the cleanliness of the patches, the following measurements were carried out on this block. Since the results obtained were similar to those encountered in previous Cali-Block measurements, it is assumed that the following results are typical for Cali-Blocks. This conclusion is supported by the fact that Cali-Blocks are manufactured by an electrodeposition replicating process which should produce a family of almost identical members.

2. Procedure

The Cali-Block was mounted on an X–Y table in a stylus instrument. The first measurement of surface roughness was carried out in one corner of the 125 microinch patch by making two standard 30 mil scans. The reproducibility of the measurement was such that these two readings were either identical or well within 1 percent of each other. The block was then advanced

*Certain commercial equipment, instruments, or materials are identified in this paper in order to adequately specify the experimental procedure. In no case does such identification imply recommendation or endorsement by the National Bureau of Standards, nor does it imply that the material or equipment identified is necessarily the best available for the purpose.

approximately 3 mm and the process repeated. In this fashion each 3 mm by 2 mm square area on the patch surface was measured. A total of 180 areas were thus measured on each of the two patches. The results are displayed on the *AA* profile map in figure 1. A similar map for the 20 microinch patch is shown in figure 2.

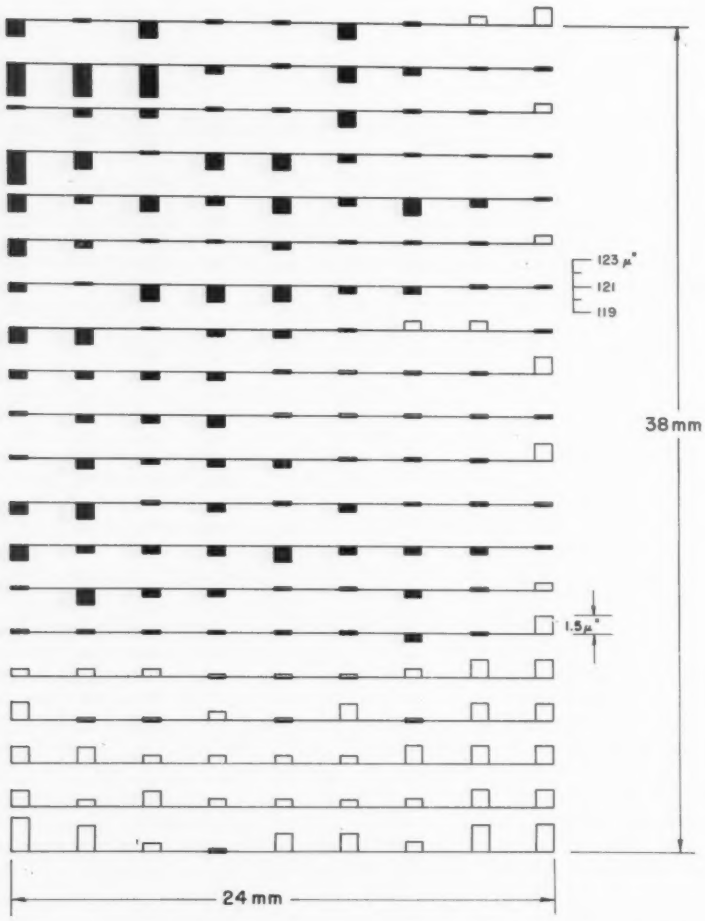

FIGURE 1. *Distribution of Arithmetic Average* (AA) *roughness values over the surface of the 120 microinch patch of Cali-Block.*

Each of the 88 black (or white) boxes represents the amount by which the *AA* value deviated from the mean of the *AA* values for all 88 measurements. Locations where the *AA* value exceeded the mean value are depicted by white bars while smaller values are depicted by black bars.

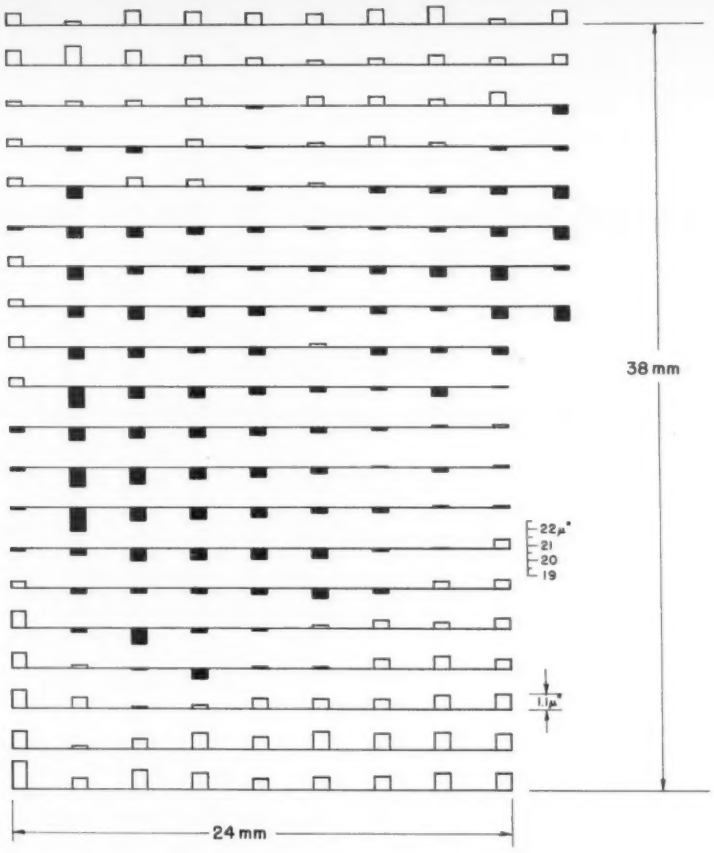

FIGURE 2. *Distribution of* AA *values over the surface of the 20 microinch patch of Cali-Block B, as in figure 1.*

3. Discussion of Results

It would be particularly useful to find a way in which the results in figures 1 and 2 can be succinctly characterized. If the deviations of the *AA* values from the mean value are random, then the mean value, standard deviation and 3σ values should provide a valuable description of the *AA* roughness distribution over the patches.

It is clear from figures 1 and 2 that there is a systematic variation in *AA* values over the surface of each patch. However, about 68 percent of the measurements were within one σ of the mean and only one value (0.5%) exceeded the mean by 3σ. It is anticipated (and recommended) that the user will select several widely spaced regions at random on the patch when calibrating his roughness measuring instrument. This reduces patch wear and serves to minimize the effect of the systematic variation in *AA* values on the accuracy of the calibration. Assuming such a random selection of regions, the standard deviation should provide a useful description of the measurement process. Such a characterization is particularly useful since the techniques for combining σ values with other uncertainties, such as random human errors and instrumental errors, are well known. The results are reported in table 1.

TABLE 1. *Mean roughness, standard deviation* (σ) *and* 3σ *values for each of the patches on NBS Cali-Block "B"*

Patch	Mean value *AA* roughness	σ	3σ
125 microinches	120.9	0.70	2.1 microinches.
20 microinches	20.8	0.66	2.0 microinches.

4. Conclusion

It is evident from this study that one important limiting factor in the accuracy and precision with which surface roughness standards can be transmitted through the use of the Cali-Block is the variation in *AA* value across the surface of the patch. Furthermore, the importance of a random selection of several widely spaced regions on the patch during calibration is very evident.

(Paper 76C1&2-328)

JOURNAL OF RESEARCH of the National Bureau of Standards—C. Engineering and Instrumentation
Vol. 76C, Nos. 1 and 2, January–June 1972

Absorption of Sound in Liquids by the Resonator-Decay Technique: A Critique

Martin Greenspan

Institute for Basic Standards, National Bureau of Standards, Washington, D.C. 20234

(March 13, 1972)

(1) The resonator-decay and the reverberation methods for measurement of the absorption of sound in liquids are in wide use, but their theoretical foundation has not hitherto been investigated. The basic assumptions are in fact invalid, but under most practical conditions the errors are tolerable, at least for three common geometries. (2) The very large excess losses always observed at the lower-order modes are identified with anelastic effects in the envelope, for the most part, and with viscous boundary-layer effects to a lesser, but very substantial extent. For modes of sufficiently high order these become negligible.

Key words: Acoustics; acoustic impedance; acoustic materials; acoustic parameters.

1. Introduction

There is little doubt that many of the best measurements of the absorption of sound in liquids, especially at the lower frequencies, have been made by "decay" or "reverberation" methods. In the first case, a resonator formed by the sample liquid and a suitable container is excited in a single mode; the attenuation coefficient, α, is calculated from the decay rate after the excitation is cut off. The second case is much the same, except that the excitation is over a band of frequencies.

It is curious that it has always been tacitly assumed that α as measured on a resonator is the same as that for a plane running wave in free space. That this cannot be true in general is evident from an obvious counter-example—in the case of uniform expansion (wavelength large *re* dimensions) the losses are governed by the congressional viscosity, $\lambda+2\mu/3$, whereas in free space the losses are governed by $\lambda+2\mu$.

In section 2 we analyze the decay for a single mode in general and apply the results to three common cases: radially symmetric vibrations of a sphere, first used by Leonard [1946][1] and in wide use ever since; radially symmetric vibrations of a cylinder, apparently first suggested by Meyer and Tamm [Mudlers, 1948] and the general vibrations of a rectangular parallelepiped (box). It is found that for the geometries analyzed the assumption in question is in general false, although for suitable configurations the errors in measured values of α may well be small. But even if so, it seems that a method in such wide use, and upon which so much reliance is placed, should rest on a firmer foundation than it has hitherto.

Once precautions are taken to minimize radiation of sound from the resonator into the air and conduction of sound in the supports, the most important sources of error are probably dissipation in the envelope and dissipation in the boundary layer. Both Leonard [1950] and Wilson [1951] tried to calculate envelope losses in a sphere without much success. New calculations are presented in section 3. Boundary layer losses occur whenever the motion of the liquid near the wall has a component parallel to it. This was first pointed out to Leonard by R. J. Christensen, and it is on this account that radial modes of a sphere, for which losses are smaller than for any other configuration, were employed by Leonard and by so many others since. Elementary calculations of boundary layer losses, for which no great originality is claimed, are presented in section 4 for comparison purposes.

2. Theory

The rationale of the resonator decay method can be summarized as follows. In a plane running wave, the energy density is

$$E = E_0 e^{-2\alpha x}$$

in which α is the amplitude attenuation coefficient. The variation with time, for an observer moving with the wave at speed c, is

$$E = E_0 e^{-2\alpha c t}.$$

[1] Figures in brackets indicate the literature references at the end of this paper.

Logarithmic differentiation gives for the instantaneous fraction of E lost per unit time

$$\frac{1}{E}\frac{dE}{dt} = +2\alpha c. \tag{1}$$

This notion is now applied to a resonator. The total energy density is $T + W$, i.e., the sum of the kinetic and potential energy densities. The viscous energy loss per unit volume (heat conduction is here neglected for simplicity; for most liquids it is minor) is twice the dissipation function, $2F$. The ratio $-2F/(T+W)$ corresponds to the left side of eq (1), hence

$$\alpha = \frac{1}{2c}\frac{2\int F dV}{\int (T+W)dV} \simeq \frac{1}{2c}\frac{\int F dV}{\int W dV}, \tag{2}$$

the integrations being taken over the whole volume of liquid. The second expression on the right in eq (2) is not exact; its use will be justified shortly. The assumption we wish to test is that α in eq (2) is the same as that in eq (1).

In the foregoing, and in the sequel as well, all first-order quantities, such as pressure, are supposed to vary as cos ωt. Second-order quantities, such as T, W, and F, will have terms which vary as $\cos^2\omega t$, $\sin^2\omega t$, or sin ωt cos ωt. We are interested in time averages of T, W, and F only—integration over t will yield coefficients of $\frac{1}{2}$ or zero, as the cause may be. We bear this in mind, suppress the factors which indicate time variation, and take all first-order quantities as root-mean-square.

The problem reduces to finding expressions for T, W, and F. These are gotten from the pressure and velocity fields, supposed known. Although these can be determined in principle (for simple shapes) the solutions are too cumbersome to be useful. Instead we make the approximation that the field is the resultant of two others, the first appropriate to an inviscid fluid (i.e., one having a potential) and the second, appreciable only in a relatively thin boundary layer, that of a locally plane shear wave launched at the boundary along the inward normal, the magnitudes of the two being adjusted so that the net tangential velocity on the liquid-solid interface is zero [Morse and Ingard, 1968]. The functions T, W, and F are calculated from the potential-solution only.

The assumed velocity potential, ψ, satisfies the wave equation

$$\nabla^2\psi = -k^2\psi = -(\omega^2/c^2)\psi. \tag{3}$$

The pressure is

$$p = \rho\frac{d\psi}{dt} = i\omega\rho\psi, \tag{4}$$

in which ρ is the undisturbed density, and the velocity is

$$u_i = -\psi_{,i}\ (i = 1,2,3). \tag{5}$$

The comma indicates differentiation. We need also the strain rate

$$\dot{S}_{ij} = \tfrac{1}{2}(u_{i,j} + u_{i,j}) = -\psi_{,ij} \tag{6}$$

and the dilatation rate

$$\dot{\Delta} = \dot{S}_{ii} = -\psi_{,ii} = -\nabla^2\psi = k^2\psi. \tag{7}$$

The summation convention is used throughout.

We are now in a position to calculate T, W, and F. First we note the constitutive equation

$$T_{ij} = (-p + \lambda\dot{\Delta})\delta_{ij} + 2\mu\dot{S}_{ij} \tag{8}$$

in which T_{ij} is the stress, λ and μ the second and first viscosity coefficients respectively, and δ_{ij} the unit tensor. The strain energy density is given by

$$2W = T_{ij}S_{ij} = (-p + \lambda\dot{\Delta})\delta_{ij}S_{ij} + 2\mu\dot{S}_{ij}S_{ij}. \tag{9}$$

In eq (9) S_{ij} is in quadrature with $\dot{S}_{ij}$ and with $\dot{\Delta}$; the only surviving term is that in $p\delta_{ij}S_{ij}$ which equals $p\Delta$, and as $\Delta = \dot{\Delta}/i\omega$, we have from eqs (3) and (4)

$$2W = \rho k^{-2}\psi^2. \tag{10}$$

The kinetic energy density is $\rho u_i u_i/2 = \rho\psi_{,i}\psi_{,i}/2$, from eq (5). A special case of Green's theorem,

$$\int_V \psi_{,i}\psi_{,i}dV + \int_V \psi\nabla^2\psi dV = -\int_S \psi\frac{d\psi}{dn}dS\ , \tag{11}$$

leads to the condition of resonance. It is easily seen that it is equivalent to

$$\int_V (T - W)dV = -\frac{\rho}{2}\int_S \psi\frac{d\psi}{dn}dS\ . \tag{12}$$

At resonance, the total kinetic and potential energies are equal so that the right-hand side of eq (12) vanishes. A sufficient condition is that everywhere on the outer surface (of the container, which we treat as a fluid without too much error because it is relatively thin) either the pressure (proportional to ψ) or the normal velocity (proportional to $d\psi/dn$) is zero. In practice, the resonator is operated at frequencies much above resonance (breathing mode) of the empty envelope. Hence the energy in the envelope is mostly kinetic and therefore most of the potential energy is in the liquid. A good approximation to the total energy is therefore $2\int_v W dV$, the integration being taken over the volume of the liquid. This explains the substitution of $2W$ for $T + W$ in eq (2).

The dissipation function is given by

$$2F = T_{ij}\dot{S}_{ij} = (-p + \lambda\dot{\Delta})\delta_j\dot{S}_{ij} + 2\mu\dot{S}_{ij}\dot{S}_{ij}. \tag{13}$$

Here p is in quadrature with S_{ij} and eq (13) reduces to

$$2F=(\lambda+2\mu)\dot{\Delta}^2+4\mu(\dot{S}_{12}^2+\dot{S}_{23}^2+\dot{S}_{31}^2-\dot{S}_{11}\dot{S}_{22}$$
$$-\dot{S}_{22}\dot{S}_{33}-\dot{S}_{33}\dot{S}_{11})=(\lambda+2\mu)k^4\psi^2+4\mu I_2 \qquad (14)$$

in which I_2 is the quadratic strain-rate invariant. Equation (14) together with eqs (2) and (10) gives finally,

$$\alpha=\frac{\int F dV}{2c\int W dV}=\frac{(\lambda+2\mu)\omega^2}{2\rho c^3}+\frac{2\mu\int I_2 dV}{\rho c k^2\int\psi^2 dV}. \qquad (15)$$

We recognize the first term on the right-hand side of eq (15) as the plane-wave value of α; therefore the condition that the resonator-decay experiment yield the plane-wave value of α is that

$$\int I_2 dV=0. \qquad (16)$$

For reference we repeat

$$I_2=\dot{S}_{12}^2+\dot{S}_{23}^2+\dot{S}_{31}^2-\dot{S}_{11}\dot{S}_{22}-\dot{S}_{22}\dot{S}_{33}-\dot{S}_{33}\dot{S}_{11}. \qquad (17)$$

We note two special cases. In the case of a plane wave, running or standing along x_1, only $\dot{S}_{11}$ in eq (17) is not zero, so $I_2=0$ and eq (15) gives the known result. In the case of uniform expansion, the shear rates in eq (17) are zero and $\dot{S}_{11}=\dot{S}_{22}=\dot{S}_{33}=\dot{S}$ (say), uniform in space. Then $\dot{\Delta}=3\dot{S}$ and $I_2=-3\dot{S}^2=-\frac{1}{3}\dot{\Delta}^2$. With this substitution, eq (15) becomes

$$\alpha=\frac{(\lambda+2\mu/3)\omega^2}{2\rho c^3},$$

which is the correct result, $\lambda+2\mu/3$ being the compressional viscosity.

2.1. Sphere, Radial Mode

Here we use spherical coordinates, r, θ, ϕ, and suppose that the potential, ψ, depends on r only. Then the velocities are

$$u_r=-\frac{d\psi}{dr},\quad u_\theta=u_\phi=0.$$

The nonzero strain rates are

$$\dot{S}_{rr}=-\frac{d^2\psi}{dr^2},\ \dot{S}_{\theta\theta}=\dot{S}_{\phi\phi}=\frac{u_r}{r}=-\frac{1}{r}\frac{d\psi}{dr},$$

so that, from eq (17)

$$I_2=-\frac{2}{r^2}\frac{d\psi}{dr}\left(\frac{d\psi}{dr}+2r\frac{d^2\psi}{dr^2}\right),$$

and with $dV=4\pi r^2 dr$,

$$\int I_2 dV=-4\pi\left[r\left(\frac{d\psi}{dr}\right)^2\right]_0^a=-4\pi a u_a^2, \qquad (18)$$

in which a is the radius of the sphere and $u_a=(u_r)_{r=a}$.

Equations (18) and (15) together show that for this case the resonator-decay result underestimates α except only for $u_a=0$, corresponding to a rigid container.

According to eq (14) for $2F$ the excess in α, $\Delta\alpha$, can be estimated from

$$\frac{\Delta\alpha}{\alpha}=\frac{4\mu\int_V I_2 dV}{(\lambda+2\mu)k^4\int_V\psi^2 dV}. \qquad (19)$$

For the radial mode of a sphere the velocity potential for unit amplitude is

$$\psi=\frac{\sin kr}{r}. \qquad (20)$$

Equations (18), (19) and (20) yield

$$\frac{\Delta\alpha}{\alpha}=-\frac{6}{ka}\frac{\alpha_{c1}}{\alpha}\frac{\left(\cos ka-\frac{\sin ka}{ka}\right)^2}{ka-\sin ka\cos ka}. \qquad (21)$$

In eq (21) we have written α_{c1}/α for $4\mu/3(\lambda+2\mu)$ where α_{c1} corresponds to the "classical" relationship $3\lambda+2\mu=0$. To use eq (21) for a particular case we need the values of k corresponding to the various resonances. Although these are readily calculated, we content ourselves with an examination of the worst case, i.e., the pressure-release case, $p_a=0$. Then in eq (21) $\sin ka=0$, $ka=n\pi$, $\cos ka=\pm 1$. We have

$$\frac{\Delta\alpha}{\alpha}=-6\frac{\alpha_{c1}}{\alpha}\frac{1}{n^2\pi^2}. \qquad (22)$$

In the case of water, for which α_{c1}/α is about $\frac{1}{3}$, the "error" is large for the very low-order modes; about 20 percent for $n=1$, five percent for $n=2$, etc., but is less than one percent for $n\geq 5$. For most other liquids $\Delta\alpha/\alpha$ is even smaller. As we shall see, there are other, more compelling, reasons to operate at the high-order modes, so that for practical purposes the spherical resonator, other things aside, has a reasonably firm theoretical basis.

As a check on eq (21) we note that for $k=0$ (uniform expansion) eq (21) yields the known result.[2]

2.2. Cylinder, Radial-Axial Mode

This case is not so simple, and the explicit expression for ψ is required. If the mid-point of the axis is the origin of cylindrical coordinates, r, θ, z, the potential is, for amplitude unity,

$$\psi=J_0(k_r r)\cos(k_z z+\epsilon), \qquad (23)$$

with the radial and axial wave numbers k_r and k_z subject to

$$k_r^2+k_z^2=k^2=\omega^2/c^2. \qquad (24)$$

[2] The indeterminate form in eq (21) is easily evaluated by expansion of the sine and cosine functions about $ka=0$.

The velocities are

$$u_r = -\frac{\partial \psi}{\partial r} = k_r J_1 c,\ u_\theta = 0,\ u_z = -\frac{\partial \psi}{\partial z} = k_z J_0 s.$$

Here and in the sequel we use abbreviations like J_1 for $J_1(k_r r)$ and c for $\cos(k_z z + \epsilon)$. The strain rates are

$$\dot{S}_{rr} = \frac{\partial u_r}{\partial r} = k_r^2 \left(J_0 - \frac{J_1}{k_r r}\right) c,$$

$$\dot{S}_{\theta\theta} = \frac{u_r}{r} = k_r^2 \frac{J_1}{k_r r} c,$$

$$\dot{S}_{zz} = \frac{\partial u_z}{\partial z} = k_z^2 J_0 s,$$

$$\dot{S}_{rz} = \frac{1}{2}\left(\frac{\partial u_z}{\partial r} + \frac{\partial u_r}{\partial z}\right) = -k_r k_z J_1 s,$$

$$\dot{S}_{r\theta} = \dot{S}_{\theta z} = 0.$$

These, together with $dV = 2\pi r dr dz$ and the limits 0 to a for r and $-L$ to L for z, give after some reduction

$$-\frac{1}{\pi k_r}\int I_2 dV = A + B\,[\sin(k_z L+\epsilon)\cos(k_z L+\epsilon) - \sin(-k_z L+\epsilon)\cos(-k_z L+\epsilon)]$$

where

$$A = 2L J_1(k_r a)\left[k_z^2 a J_0(k_r a) + \frac{k_r}{2} J_1(k_r a)\right]$$

and

$$B = k_z a\{k_r a[J_0^2(k_r a) + J_1^2(k_r a)] - J_0(k_r a) J_1(k_r a)\} + \frac{k_r}{2k_z} J_1^2(k_r a). \qquad (25)$$

For the integral in eq (25) to be zero it is sufficient that $J_1(k_r a) = 0$, that either $\sin(k_z L+\epsilon)$ or $\cos(k_z L+\epsilon)$ be zero, and that either $\sin(-k_z L+\epsilon)$ or $\cos(-k_z L+\epsilon)$ be zero. This follows from the independence of k_r and k_z. Restated, a sufficient condition that the experiment measure the free-space value of α is that the cylindrical wall be rigid and that each end be either rigid or pressure-release. (Another condition is $k_r = 0$, corresponding to a plane wave.)

We can calculate the error, $\Delta\alpha/a$, in the same way as for the sphere. In the special case of pressure-release ends, we get

$$\frac{\Delta\alpha}{\alpha} = -6\,\frac{\alpha_{c1}}{\alpha}\,\frac{k_r}{k^4 a^2}\,\frac{J_1(k_r a)\left[k_z a J_0(k_r a) + \frac{k_r}{2} J_1(k_r a)\right]}{J_0^2(k_r a) + J_1^2(k_r a)}. \qquad (26)$$

Again, the worst case is for a pressure-release cylindrical surface $[J_1(k_r a) = 0]$ for which eq (26) becomes

$$\frac{\Delta\alpha}{\alpha} = -3\,\frac{\alpha_{c1}}{\alpha}\,\frac{\lambda_{0,m}^2}{\left[\lambda_{0,m}^2 + \left(\frac{n\pi a}{2L}\right)^2\right]^2}, \qquad (27)$$

in which $\lambda_{0,m}$ is the mth zero of $J_0(x)$. Thus high mode numbers m or n (or both) insure a small "error." The conclusion is the same as for the sphere—the method is valid in practical cases.

2.3. Rectangular Tank

In rectangular coordinates, x_1, the potential, for amplitude unity, is

$$\psi = c_1 c_2 c_3. \qquad (28)$$

Again, we use abbreviations like $c_1 = \cos(k_1 x_1 + \epsilon_1)$. In eq (28) the k_i are subject to

$$k_1^2 + k_2^2 + k_3^2 = k^2 = (\omega/c)^2.$$

We have

$$u_1 = -\frac{\partial \psi}{\partial x_1} = k_1 s_1 c_2 c_3,\ u_2 = -\frac{\partial \psi}{\partial x_2} = k_2 c_1 s_2 c_3,$$

$$u_3 = -\frac{\partial \psi}{\partial x_3} = k_3 c_1 c_2 s_3,$$

and

$$\dot{S}_{11} = \frac{\partial u_1}{\partial x_1} = k_1^2 c_1 c_2 c_3, \text{ etc.}$$

$$\dot{S}_{12} = \frac{1}{2}\left(\frac{\partial u_2}{\partial x_1} + \frac{\partial u_1}{\partial x_2}\right) = k_1 k_2 s_1 s_2 c_3, \text{ etc.}$$

The invariant I_2 of eq (17) will have three terms. The first is

$$-\frac{1}{2} k_1^2 k_2^2 c_3^2\,[\cos 2(k_1 x_1 + \epsilon_1) + \cos 2(k_2 x_2 + \epsilon_2)];$$

the other two are got by cyclic permutation of the subscripts. Integration over the range $-L_i$ to L_i for x_i yields an expression for $\int I_2 dV$ containing terms of the form

$$\sin(k_i L_i + \epsilon_i)\cos(k_i L_i + \epsilon_i) - \sin(-k_i L_i + \epsilon_i)\cos(-k_i L_i + \epsilon_i)$$

together with cross-products of these taken two at a time. The coefficients of these are various products of L_i and powers of k_i. An account of the independence of these coefficients a sufficient condition that

$$\int_V I_2 = 0$$

is that each face be either rigid (sine term = 0) or pressure-release (cosine term = 0). There are, of

course, other special conditions. For instance if any two k_i are zero the integrand I_2 vanishes—we are back to a plane standing wave.

The actual "errors" for any particular case could be calculated with some labor, but it seems hardly worthwhile in consideration of what we have already learned in the other cases.

3. Losses in the Envelope

3.1. Sphere, Radial Modes

The loss in a spherical shell oscillating in the radial (breathing) mode is not difficult to calculate if a simple expression is obtained for the real component of the impedance of the shell. It is the fraction $1/Q_E$ of the stiffness reactance (not the mass reactance; the losses are associated with strain rates, not with inertia). The stiffness reactance is $M_E\omega_0^2/\omega$, M_E being the mass of the envelope and ω_0 its resonance angular frequency when empty. Hence the dissipation rate is

$$D_E = \frac{M_E\omega_0^2}{Q_E\omega}u_a^2, \tag{29}$$

in which u_a is the radial velocity at $r=a$, the interface. The approximation is here made that the radial velocity is constant throughout the thickness of the envelope. This expression is of use only if the variation of Q_E with ω is known. For many solid materials, including glass, the Q at frequencies of interest here is independent of frequency (elastic hysteresis) [Mason, 1950] and we shall take it as such. We seek the ratio of D_E, the dissipation rate in the envelope, to D_L; that in the liquid. For the latter we use, without significant error only the part $(\lambda+2\mu)k^4\int_V\psi^2dV$ [eq (14)]. This and the value of u_a in eq (29) are gotten from the potential in eq (20). The result is

$$\frac{D_E}{D_L} = \frac{2\rho_E c_L t\sin^2 ka}{(\lambda+2\mu)Q_E(ka)^2}\left(\frac{\omega_0}{\omega}\right)^2\frac{(1-ka\cot ka)^2}{ka-\sin ka\cos ka}, \tag{30}$$

in which ρ_E and t are the density and thickness of the envelope and c_L is the speed of sound in the liquid. Equation (30) is meaningful in our context only for those values of ω (and $k=\omega/c$) which correspond to actual resonances.

One expression of the condition of resonance is that on the boundary between the liquid and the envelope the point admittance of the liquid equals that of the envelope. The former is

$$\frac{u_a}{p_a} = \frac{-\partial\psi/\partial a}{i\omega\rho_L\psi_a} = \frac{1-ka\cot ka}{i\omega\rho_L a},$$

ρ_L being the density of the liquid, and the latter is

$$y_E = 1/i\omega\rho_E t\left[1-\left(\frac{\omega_0}{\omega}\right)^2\right]. \tag{31}$$

Equating these gives as the condition of resonance

$$1-ka\cot ka = \frac{\rho_L a}{\rho_E t\left[1-\left(\frac{\omega_0}{\omega}\right)^2\right]}. \tag{32}$$

This together with eq (30) gives, after much reduction

$$\frac{D_E}{D_L} = \frac{1}{c_L Q_E\omega(\alpha/\omega^2)}\left(\frac{\omega_0}{\omega}\right)^2 \frac{R}{R^2-R[1-(\omega_0/\omega)^2]+(ka)^2[1-(\omega_0/\omega)^2]^2}, \tag{33}$$

in which we have written R for $\rho_L a/\rho_E t$, and have eliminated $\lambda+2\mu$ in favor of α/ω^2 from eq (15). We shall see that in most practical cases $\omega_0 \ll \omega$ so that the bracketed expressions in eq (33) are nearly unity. Equation (33) is still not free of ω (or $k=\omega/c$), but the right-hand side is seen to be a monotonic function of ω, so that the equation is usable as it stands; it is not necessary to solve the frequency equation, eq (31) explicitly.

It seems clear that, everything else being equal, there is no optimum thickness, t, of the envelope wall, because the wall loss would vanish at both extremes—no wall and rigid wall. This notation is verified by eq (33) according to which D_E/D_L has a maximum for $R=ka[1-(\omega_0/\omega)^2]$. ($R$ varies as $1/t$). The variation of the error, D_E/D_L with frequency is very rapid. For a given set-up, and for liquids for which α/ω^2 is independent of frequency, eq (33) predicts that for low-order modes, such that $R \gg ka$, D_E/D_L varies as $1/\omega^3$, and for high-order modes, such that $R \ll ka$, it varies as $1/\omega^5$. Thus we might expect, for a given experimental arrangement, very large errors at low frequencies and negligible errors for sufficiently high frequencies.

These conclusions can be checked against the results obtained by Wilson [1951] whose report contains all of the necessary details. The circles in figure 1 show α_{obs}/α, the ratio of the observed to the known attenuation in water[3] at 4 °C, as measured in a 12-liter borosilicate boiling flask. The errors at the low-order modes are seen to be enormous; the observed attenuation is too high by a factor of more than 100 at 16 kHz (mode 3). Even at the ninth mode, about 46 kHz, the factor is about 4. At the higher-order modes the factor remains constant at about 1.4.

Wilson's report [1951] gives all the data needed to calculate the error from eq (33). There is some question about the Q of borosilicate however. The value most often cited, 1200, is taken from Mason [1950]. Wilson [1951] measured it as 2200 for longitudinal vibrations. Measurements made in our laboratory on two spherical flasks vibrating in a vacuum in the breathing mode give about 2700 at 4 °C.

The full lines in figure 1 show $1+(D_E/D_L)$ from eq (33) for Q_E's of 1000 and 3000. It is clear that eq (33) explains the low-frequency errors fairly well at least

[3] The "known values" are those extrapolated from high-frequency measurements on the supposition that α/ω^2 is independent of frequency.

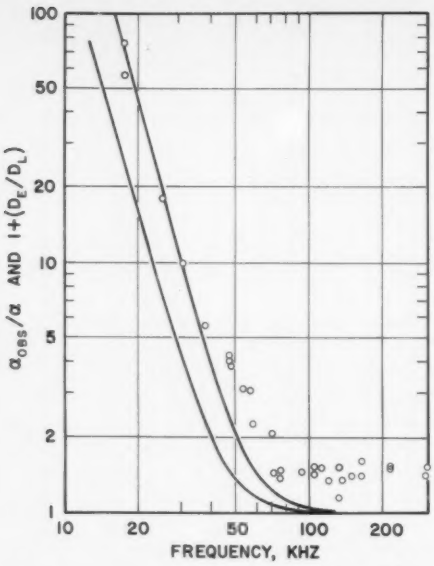

FIGURE 1. *Losses in water at 4 °C, 12-liter spherical Pyrex flask.*

The circles show the ratios of the measured to the known values of the attenuation according to Wilson [1951]. The curves show $1+(D_E/D_L)$ from eq (33); the upper curve is for $Q_E=1000$ and the lower for $Q_E=3000$.

in a qualitative way. It must be remembered that there are other sources of error. Some of these will be discussed later. The constant error at high frequencies, which remains unexplained, is discussed in section 5.

3.2. Cylinder, Radial Axial Modes

The calculation is carried out much as for the sphere. In the case of pressure-release ends, the result is

$$\frac{D_E}{D_L}=\frac{1}{c_L Q_E \omega(\alpha/\omega^2)}\left(\frac{\omega_0}{\omega}\right)^2\left(\frac{k_r}{k}\right)^2\frac{R}{R^2+(k_r a)^2[1-(\omega_0/\omega)^2]^2}. \tag{34}$$

In deriving eq (34) the point admittance of the envelope was calculated in a manner similar to that for a sphere [eq (31)]. This is probably good enough for the $(l, 0, 1)$ modes, but dubious for the $(l, 0, n>1)$ modes. A more ambitious attack was made by Lambert [1953], but his results are not applicable here. The point admittance of the liquid, at the interface, is

$$\frac{u_a}{p_a}=\frac{-\partial\psi/\partial a}{i\omega\rho_L\psi_a}=\frac{k_r J_1(k_r a)}{i\omega\rho_L J_0(k_r a)},$$

so that the condition of resonance is

$$\frac{k_r a J_1(k_r a)}{J_0(k_r a)}=\frac{R}{1-(\omega_0/\omega)^2} \tag{35}$$

in which again, $R=\rho_L a/\rho_E t$.

The main point of eq (34) is that the envelope losses for a cylinder behave like those for a sphere, that is, they can be very large or very small for a given setup, depending on whether the mode numbers are very low or very high.

4. Losses in the Viscous Boundary Layer

The viscous boundary-layer losses are calculated on the assumption that the boundary layer thickness, $d_v=(2\mu/\rho_L\omega)^{1/2}$, is small relative to the interior dimensions of the resonator. The method is very old; a good simple account is given by Lambert [1953]. The viscous loss per unit area at the interface is given by

$$\frac{dD_B}{dS}=\sqrt{\omega\rho_L\mu/2}\,u_t^2, \tag{36}$$

in which u_t is the tangential component of the fluid velocity at the interface as calculated from the potential.

It follows from eq (36) that if $u_t=0$ everywhere at the interface, the boundary-layer losses are zero. This is the case for the radial vibrations of an ideal sphere. In practice, the filling hole prevents the motion from being radially symmetrical, but the resultant field is too complicated to work with analytically.

More generally, the boundary-layer losses vanish if the pressure is uniform, and in particular, zero, on the interface. For then the tangential component of the pressure-gradient, which is proportional to $|\omega u_t|$, is zero. It would appear then that other things being equal, the boundary-layer losses are smaller the thinner and lighter the envelope, that is, the nearer the fluid boundary is to pressure release.

For the radially symmetrical modes of a cylinder having pressure release ends, the potential is

$$\psi=J_0(k_r r)\cos\frac{n\pi}{2L}z \tag{37}$$

in which n is an odd integer. The only nonvanishing component of u_t is $(u_z)_{z=a}=-\partial\psi/\partial a$. This is calculated from eq (37) and substituted into eq (36). Integration over the lateral area gives

$$D_B=\frac{n^2\pi^3 a}{2L}(\omega\rho_L\mu/2)^{1/2}J_0^2(k_r a). \tag{38}$$

As expected, $D_v=0$ if the pressure, proportional to $J_0(k_r r)$, is zero at $r=a$. We compare this to the loss in the liquid itself, which according to eq (14) is given with sufficient accuracy by

$$(\lambda+2\mu)k^4\int_V\psi^2 dV$$

and get

$$\frac{D_B}{D_L}=\frac{3n^2\pi^2}{4(2L)^2}\frac{(2\omega\rho_L/\mu)^{1/2}}{k^4 a}\frac{\alpha_{c1}}{\alpha}\frac{(k_r a)^2[1-(\omega_0/\omega)^2]^2}{R^2+(k_r a)^2[1-(\omega_0/\omega)^2]^2} \tag{39}$$

In obtaining eq (39) we have again made use of the resonance equation, eq (35) and written α_{c1}/α for $4\mu/3(\lambda+2\mu)$.

Comparison of eq (39) with eq (34) shows that the ratio of the boundary-layer loss to the anelastic loss in the envelope varies as $\omega^{3/2}$. Thus we might expect that the loss in the envelope predominates at low, and that in the boundary layer at high, frequencies, and that both are eventually negligible.

Computation shows that in a practical case the mode number may be high enough so that although the loss in the envelope is negligible, the viscous boundary layer loss is still considerable. This viscous loss might then be calculated by the method outlined above and the results corrected accordingly. Mulders [1950] made some interesting measurements on water in a cylinder 28 cm O.D. by 10 cm high. The reverberation method (excitation over a band of frequencies) was used at mean frequencies of 750, 1010, and 1500 kHz, corresponding to very high-order, densely packed modes. Mulders calculated the viscous boundary loss on an "equipartion" basis for a rigid wall and obtained good results even at the lowest frequency of 750 kHz, for which the boundary layer loss was almost half the total.

5. Discussion

The resonator-decay method for the measurement of sound absorption in liquids is known from experience to have serious drawbacks. Our analysis, rough though it is, elucidates the mechanism of some of the losses hitherto considered adventitious, and thus provides a rationale for the design of experiments.

We have shown that the basic theory of the method, usually taken for granted, is in fact only approximate for realistic boundary conditions, but that the errors resulting from its application are small for sufficiently high mode numbers. Much more serious are the anelastic losses in the envelope. These are relatively enormous for low-order modes, but become negligible for modes of sufficiently high order. The same is true for losses in the viscous boundary layer. Although we cannot calculate these in the case of a sphere, for which the boundary condition is not uniform owing to the presence of the filling hole, we get a fair idea of the nature of the effect from the analysis of a cylinder. In any case, this loss can be minimized by minimization of the mass of the envelope relative to that of the liquid.

In our example we have chosen water as a test liquid. Water, having relatively low values of α and of α/α_{c1}, gives a "worst-case" type of example, and the unwanted losses are relatively much less in complex liquids having high viscosities and high ratios of compressional to shear viscosity. The envelope material used in the example, Pyrex, having a Q in the range 2000 to 3000, is typical. A higher Q is of course better, but for a given setup, a large increase in this Q results in a disappointingly small reduction in the lowest frequency at which the losses are acceptable.

The major problems of the method are inherent. The experiments are easier to perform at the lower-order modes because the modes are well separated and easier to identify, and because the demands on the accuracy of the geometry are tolerable, but the lower the mode number, the greater the unwanted losses. Even when the method is used differentially, using a "standard" liquid for which the losses are supposedly known, most workers have had to avoid the lower-order modes.

Another matter of concern is that in the experiment we have used as an example [Wilson, 1951], there is a residual loss of about 40 percent at the high-order modes. It is doubtful that this is due to conduction of sound by the supports and the discrepancy remains unexplained. Moen [1951] in an experiment similar to Wilson's (water, 12-l spherical flask) also found a residual loss of about 40 percent. However, he found greater losses in smaller flasks, and by plotting the decay rate against reciprocal radius and extrapolating the resulting straight line to $1/a=0$, obtained values of α/f^2 in agreement with those measured in the tens of megahertz range even at 150 kHz, the lowest frequency he worked with. Similar results, namely that the residual loss is proportional to the surface-to-volume "ratio" of the resonator, were obtained by Moen for several other liquids. Thus it appears that this loss is a boundary effect not accounted for by our analysis.

Mulders' [1950] results, described in section 4, are of great interest. He considered that the good accuracy of his calculations of viscous boundary layer loss, based partly on the supposition of a rigid wall, furnished empirical proof that the walls behaved as though rigid, and called this an "amazing fact". According to our analysis (sec. 3.) this behavior is to be expected under the conditions of Mulders' experiment.[4]

The lively interest in possible laboratory measurements of absorption at low frequencies, say down to 1 kHz, has recently intensified. The results of our analysis make us pessimistic about this possibility, especially for low loss liquids, except perhaps by methods as yet undreamt of. Mulders' [1950] experiment, properly scaled to 1 kHz, would require a tank having dimensions of tens of meters. To keep such a volume clean, free of air bubbles, and at uniform temperature would tax the resources of even a laboratory which could afford to build the tank.

The Q-values of several empty flasks vibrating in the breathing mode were measured by Carl E. Tschiegg. He also made numerous measurements, not extensive enough to report here, on the vibrations of a liquid filled barium-titanate cylinder. These served to verify the general nature of the variation of the losses with mode number as developed in the text.

The work was supported in part by the Office of Naval Research.

[4] However, we have considered only axisymmetric modes. An unsymmetrical mode of the liquid, such as occurs in Mulders' experiment, drives a flexural mode of the envelope at a frequency much higher than its natural frequency. Hence its impedance is very high and its motion very low. Of course this is only an informed conjecture.

6. References

Lambert, Robert F. (1953), J. Acoust. Soc. Am. **25**, 1068–1083

Leonard, R. W. (1946), J. Acoust. Soc. Am. **18**, 252.

Leonard, R. W. (1950), Technical Report No. 1, UCLA Physics Department.

Mason, W. P. (1950), Piezoelectric Crystals and their Application to Ultrasonics (Van Nostrand, New York) pp. 393–395, 482.

Moen, C. J. (1951), J. Acoust. Soc. Am. **23**, 62–70.

Morse, P. M. and Ingard, K. U. (1968), Theoretical Acoustics (McGraw-Hill, New York) p. 286.

Mulders, C. E. (1948), Appl. Sci. Res. **B1**, 149–167.

Mulders, C. E. (1950), Appl. Sci. Res. **B1**, 341–357.

Wilson, Jr., O. B. (1951), Technical Report No. 4, UCLA Physics Department.

(Paper 76C1&2-329)

JOURNAL OF RESEARCH of the National Bureau of Standards—C. Engineering and Instrumentation
Vol. 76C, Nos. 1 and 2, January-June 1972

Ductile Fracture by Development of Surfaces of Unstable Cavity Expansion

C. A. Berg *

Institute for Basic Standards, National Bureau of Standards, Washington, D.C. 20234

(March 31, 1972)

A model of fracture of a ductile metal in which surfaces of unstable microcavity expansion occur is proposed. It is shown that such surfaces can occur only in locally plane incremental strain. The hardening conditions required for the development of these surfaces are considered. It is shown that in a material possessing an equivalent yield stress (Y) which depends upon the total plastic dilatation (Δ) and equivalent distortional strain (ϵ), the minimum ratio of dilatational softening ($\gamma/\ \Delta < 0$) to distortional hardening ($\gamma/\epsilon > 0$) under which an unstable surface of a dilatation may form is $-\ 2/3$. A possible explanation, based upon the model, for the lack of correlation between plane strain ductility and ductility as measured in a tensile test is offered. Also, the pertinence of the model to fracture of glassy polymers and environmental stress cracking of crystalline polymers is discussed.

Key words: Ductile fracture; plasticity; void growth.

1. Introduction

The chief mechanism of ductile fracture in metals is the expansion, interaction and eventual coalescense of microvoids in regions of large plastic strain and high triaxial stress, (see e.g., Puttick 1959 [1][1], Bluhm and Morrissey, 1966 [2]). The cavity growth which produces fracture appears to take place only on the fracture surface itself, with little or no cavity expansion having taken place to either side of the fracture surface (Hayden and Floreen, 1959 [3]). This indicates that the fracture surface is the locus of instability of plastic cavity dilatation, rather than being merely a surface upon which local accidents of e.g., cavity spacing and hardness leads to fracture extension through a field of uniformly dilating cavities. In the following a theoretical model of fracture by the formation of surfaces of unstable cavity growth is considered, and certain elementary but fundamental considerations concerning the orientation of these surfaces and the requirements of hardening to produce such surfaces are discussed.

It is also pointed out that the mechanism of unstable cavity expansion, which is examined here in connection with fracture of metals, may govern the mechanics of environmental stress cracking of polymers.

2. Material Behavior

The material under consideration is a ductile metal or polymer which contains numerous microcavities. Some of these cavities may have been produced during forming processes. Other cavities may be continuously generated in the metal by e.g., cracking of inclusions or separation of phase boundaries in regions of high triaxial stress (near notch tips, or in necks of tensile specimens). The mechanism of fracture under consideration here entails two stages. First, the density and size of microcavities are assumed to increase as deformation of the material proceeds. The cavity growth in this stage is assumed to take place approximately uniformly throughout material elements which are large compared with the mean spacing between cavities but which are still small compared with the size of the specimen under consideration or the scale of length over which gradients of e.g., strain in the specimen are measured. This stage of deformation may

* Professor and Chairman, Department of Mechanical Engineering, The University of Pittsburgh. Presently visiting scientist, Institute for Basic Standards, National Bureau of Standards, Gaithersburg, Maryland.

[1] Figures in brackets indicate literature references at the end of this paper.

468-108 OL - 72 - 3

be called diffuse cavity growth. The second stage of deformation entails the development of an instability in which cavity dilatation localizes in a preferred thin zone, and all deformation ceases to either side of this zone. This stage of deformation, which may be called localization, is tantamount to fracture. The object of the present writing is to clarify the conditions under which transition from diffuse cavity growth to localization may occur.

The actual material in between microcavities is a metal which undergoes large plastic strain by dislocation motion and therefore deforms according to a local yield locus and an associated flow rule (Bishop and Hill, 1951) [4]. An element of microporous material is shown in figure 1. Provided that diffuse cavity growth takes place throughout the element, and provided that the displacement increment (δu) and the local tractions (t) acting on the material surfaces of the element are statistically uncorrelated, then (Bishop and Hill, 1951 [4]) the element may be treated as a point in a continuum, subject to stress components (σ_{ij}) equal to appropriate averages of the local tractions acting at the surface of the element, and strain increments ($\delta\epsilon_{ij}$) equal to appropriate averages of the incremental displacements (δu) at the surface of the element.[2] In particular, Bishop and Hill [4] demonstrated that because on a local scale the material obeys a yield locus and an associated flow rule, the material element of figure 1 will also obey a yield locus and an associated flow rule.

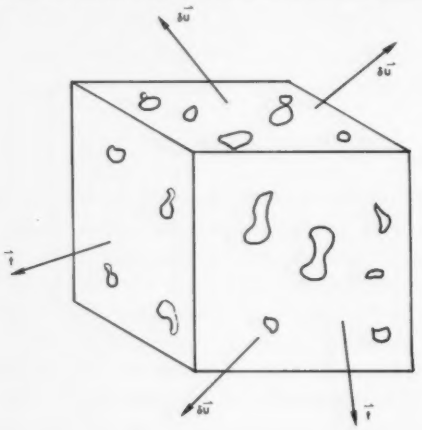

Figure 1: An element of microporous material; local incremental displacements ($\vec{\delta u}$) and tractions ($\vec{t}$) at the surface of the element are shown.

The condition for yielding of the microporous element may be given as

$$f(\sigma_{ij})=0, \tag{1}$$

where the σ_{ij} are obtained by averaging the local tractions. The plastic strain increments $\delta\epsilon_{ij}^{p}$ obtained by averaging the local surface displacement increments (δu) on the element, are given by the associated flow rule

$$\delta\epsilon_{ij}^{p}=\delta\lambda\,\frac{\partial f}{\partial\sigma_{ij}}, \tag{2}$$

where $\delta\lambda$ is a scalar multiplier. Since the present writing concerns elements of microporous metal which undergo substantial plastic strain it is assumed that the distinction between the plastic and the elastic strain increment need not be retained. Thus eq (2) may be used to represent the total strain increment.

Since the cavities in the microporous metal element will expand when sufficient triaxial loading is applied to the surface of the element the yield locus of the element will depend upon the mean triaxial stress. The element will exhibit plastic dilational strain which will be represented by the associated flow rule, eq (2).

It is likely that the array of cavities in the element may have some preferred orientation, deriving both from the history of forming of the part and from the history of plastic strain to which the part has been subjected. The primary concern in this writing is the processes of crack nucleation and extension in ductile materials. One must bear in mind that the large plastic strain which occurs in the vicinity of a notch tip will in all likelihood produce strongly oriented arrays of microcavities. The character of anisotropy which should be attributed to the microporous element in order to reflect preferred orientation of the microcavity array is currently under investigation by several workers in the field of fracture. For the present we shall neither assume any special form for the strain history dependent anisotropy or dilatational properties of the microporous ductile element, nor shall we attempt to employ any of the tentative results of present theoretical studies of this problem (e.g., Subudhi, 1970 [5]). For present purposes it will be sufficient to write the yield condition of the element as in eq (1), with the understanding that all six stress components (σ_{ij}) may appear independently in the yield function, and that the plastic dilatation is given by

$$\delta\epsilon_{kk}=\delta\lambda\,\frac{\partial f}{\partial\sigma_{kk}}, \tag{3}$$

and that in general $\delta\epsilon_{kk}$ does not vanish.[3]

3. Kinematics

Suppose that diffuse cavity growth in a microporous element is to cease, and is to be replaced by localized

[2] The averages employed by Bishop and Hill are given in the appendix.

[3] Conventional cartesion tensor notation, with the summation convention, is used here.

cavity growth on a given surface. If deformation is to cease, except in a thin band of rapidly dilating material represented by this surface, then preservation of continuity of the material between the microcavities requires that the strain increments measured in the surface vanish. Figure 2 shows a band of localized dilation occurring according to the process contemplated here. The surface S, which represents the dilating band in a continuum theory of fracture, is shown on the figure. The actual boundary between the material in the dilating band and the nondeforming regions to either side is indicated by the dashed lines. Since the material

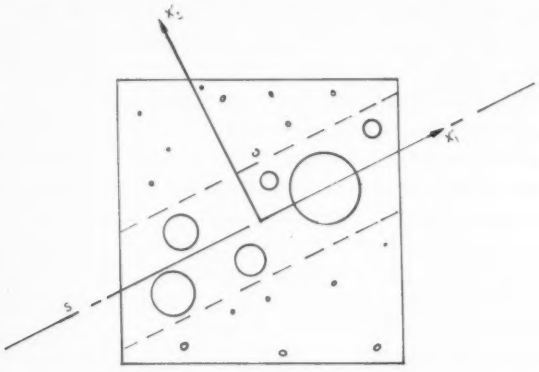

Figure 2 A band of localized cavity expansion along the surface S

in the band may not slip with respect to the nondeforming material to either side of the band, the strain components (e.g., $\delta\epsilon_{1.1.}$, $\delta\epsilon_{1.2.}$, $\delta\epsilon_{2.2.}$ in figure 2) measured in the surface S must vanish. For the sake of brevity a surface satisfying this requirement may be called a rigid surface. The main point to be recognized here is that the formation of a localized band of cavity dilatation may occur only along a rigid surface.

We now consider the general states of (local) strain increment which permit the rigid surfaces on which localized cavity growth may occur. In general, rigid surfaces may be found only in state of plane incremental strain; while it is obvious that plane deformation may permit rigid surface formation it may be somewhat less than obvious, at least at first inspection, that plane deformation is required for rigid surface formation. To demonstrate this, one may consider the general state of strain increment ($\delta\epsilon_{ij}$) which occurs as a rigid surface is formed. Using cartesian coordinates (x_1, x_2, x_3) with the x_1 and x_2 axes lying tangent to the rigid surface, the strain components are

$$\delta\epsilon_{ij}=\begin{pmatrix}0 & 0 & \delta\epsilon_{13}\\ 0 & 0 & \delta\epsilon_{23}\\ \delta\epsilon_{13} & \delta\epsilon_{23} & \delta\epsilon_{33}\end{pmatrix}. \qquad (4)$$

Thus, the (local) state of incremental strain at the site of a rigid surface consists of longitudinal shear ($\delta\epsilon_{13}$, $\delta\epsilon_{23}$) along the direction (x_3) normal to the rigid surface, superposed upon a simple uniaxial strain ($\delta\epsilon_{33}$) along the same axis. By a suitable rotation of the x_1, x_2 axes about the x_3 axis (i.e. $x_1'=\cos\theta x_1+\sin\theta x_2$; $x_2''\sigma\iota\nu\,\theta x_1+\cos\theta.\chi_2$; $x_3'=x_3$, with $-\theta=\tan^{-1}(\delta\epsilon_{13}/\delta\epsilon_{23})$) one obtains a set of coordinates x_1', x_2', x_3' with the x_3' direction still normal to the (local) rigid surface, and in which the components of the strain increments are

$$\delta\epsilon_{ij}'=\begin{pmatrix}0 & 0 & 0\\ 0 & 0 & \delta\gamma\\ 0 & \delta\gamma & \delta\epsilon_{33}\end{pmatrix}, \qquad (5)$$

where $(\delta\gamma)^2=(\delta\epsilon_{13})^2+(\delta\epsilon_{23})^2$. The strain increments state of (5) represent a state of plane incremental deformation in the x_2', x_3' plane; the (x_1', x_2') plane, which is the same as the (x_1, x_2) plane, lies tangent to the rigid surface.

The conclusion of the above is that in order to nucleate fracture by localization of cavity dilatation at a given point in a specimen, a surface which will permit large scale localized deformation on the surface while deformation to either side of the surface ceases must exist, and this requires that the local mode of deformation be incremental plane strain, with uniaxial strain ($\delta\gamma=0$) being a special, but, as will be seen, an important case of plane strain.

Additional conditions to complete the kinematic requirements necessary for nucleation of a band of localized dilatation may now be considered. If a band of localized cavity expansion is to form through a field of diffuse cavity expansion in an element under fixed stress, the yield locus of the material in the band will, at the initial instant of localization, be the same as the yield locus of material outside the band. The associated flow rule requires that the strain increments measured at the boundary of the element preserve the same ratios at the instant of localization as obtained at the previous instant, or as would have obtained had localization not occurred.[4] Since cavity expansion is to occur, the strain increment field immediately prior to localization must contain at least one principal direction along which extension occurs. Recall that a rigid surface can occur only in incremental plane strain. The rigid surface on which localization may nucleate lies perpendicular to the plane of strain , and since the intersection of the rigid surface and the plane of strain must be a line of vanishing extension rate, and the principal strain increments ($\delta\epsilon_1$, $\delta\epsilon_2$) in the plane of strain represent ex-

[4] In brief, we assume that the yield locus changes continuously, has no sharp corners, and that the strain increment remains normal to the yield locus in an appropriate space.

trema of extension rates, the two principal strain increments in the plane of strain must be of opposite sign:

$$\delta\epsilon_1 \cdot \delta\epsilon_2 \leq 0. \tag{6}$$

The equality in eq (6) would hold for incremental uniaxial strain, in which case one must add the additional requirement that one nonvanishing principal strain increment be greater than zero (e.g., $\delta\epsilon_1 > 0$) so that localization of deformation results in cavity expansion rather than compression. For all other cases, eq (9) is sufficient to guarantee the presence of a rigid surface on which localized microcavity expansion is kinematically admissible. It is emphasized that the above pertains to the local kinematic requirements for nucleation of a localized band of cavity expansion, and the requirements stated above are stated in terms of the strain components of the diffuse field of deformation at the inception of the localization instability. The global kinematic requirements for extension of a surface of localization through a field of strain in which all the principal directions of strain are sharply curved, or the strain increment components have strong gradients, have not yet been considered. The requirements given above represent the necessary kinematic conditions for nucleation of fracture by localized cavity growth It is expected that these conditions will be useful in examining both nucleation and progressive extension of fracture, examples of which will be discussed below.

4. Hardening Requirements

In order for a band of localized cavity expansion to form in a field of diffuse cavity growth, the stresses in the element must be stationary with respect to the strain increment at the instant of band localization. Otherwise, the material in the incipient band would harden, requiring that further deformation of the band be accompanied by higher stress levels in the band. Since the band formation considered here can occur only in plane strain, the stress in the band and in the surrounding nondeforming material are compatible.[5] An increase of stress in the band will, at any stage of deformation, require a corresponding increase of stress in the surrounding region. At the inception of banding, when the material in the incipient band has the same yield locus as the surrounding material, hardening of the material in the band would cause deformation of the surrounding material, thus eliminating the band. If the yield locus of the microporous material were represented by

$$f(\sigma_{ij}, I_1, I_2, \ldots I_n), \tag{7}$$

where $I_1, I_2 \ldots I_n$ are parameters describing the strain history of the material,[6] the necessary condition for localization of cavity growth in an element presently being subjected to the kinematically admissible strain increment $\delta\epsilon_{ij}$ would be

$$\delta f = \frac{\partial f}{\partial I_r}\frac{\partial I_r}{\partial \epsilon_{ij}}\delta\epsilon_{ij} = 0. \tag{8}$$

For the practical purposes of estimating, e.g., the mean cavity spacing required in a given material to permit localization under a prescribed strain history and strain increment, eq (8) is of little value unless one has at hand an explicit yield locus and a set of explicit strain history parameters (I_n). Nevertheless, the simple statements of eqs (7) and (8) may prove useful in testing a hypothetical yield locus with respect to internal stability.

It is emphasized that the yield locus need show the stationarity of eq (8) only at the inception of localization. Once localization has developed it would be permissible for the material in the localized band to harden during some later stage of its deformation, provided that the yield locus of the material in the localized band did not increase sufficiently to cause deformation of the material adjacent to the band.

For the purpose of obtaining some concrete estimates of the hardening requirements of localized cavity growth, one may assume that the yield locus does not change shape during deformation and that the hardening of the material may be represented through the net plastic dilatation ($\Delta \cong \int \delta\epsilon_{kk}$) and the equivalent distortional strain

$$\left(\epsilon = \int \sqrt{\frac{2}{3}\left(\delta\epsilon_{ij} - \frac{1}{3}\delta\epsilon_{kk}\delta_{ij}\right)\left(\delta\epsilon_{ij} - \frac{1}{3}\delta_{rr}\delta_{ij}\right)}\right)$$

which serves as the measure of strain hardening in most practical calculations of conventional plasticity theory. Then the yield co dition may be written as

$$f(\sigma_{ij}) - Y(\epsilon, \Delta) = 0. \tag{9}$$

The hardening requirement for localization eq (8) is then simply

$$\delta Y = \frac{\partial Y}{\partial \epsilon}\delta\epsilon + \frac{\partial Y}{\partial \Delta}\delta\Delta = 0. \tag{10}$$

The assumptions leading to eq (9) certainly do not represent the most general material behavior which one might expect to observe in a microporous element at the point of fracture nucleation. Nevertheless these assumptions do include the basic elements of a theory of dilatational plasticity of microporous material, and

[5] The term compatible is used here in the sense of the limit analysis. The stress in the band is always continuable into the surrounding region because the area of the band does not change.

[6] This representation would appear to be sufficiently general.

should therefore yield estimates of material behavior which are not entirely unfaithful representations of actual behavior. From eq (10) the condition for localization is

$$\frac{\partial Y}{\partial \epsilon} \Big/ \frac{\partial Y}{\partial \Delta} \cdot = -\frac{\delta \Delta}{\delta \epsilon}. \tag{11}$$

This expression gives the ratio of the change of yield stress with distortion to the change of yield stress with dilatation, required to permit localization when a given strain increment, having a given ratio of dilatation to distortion is imposed. Dilational strain may either harden or soften the material, depending upon the microcavity density and the rate of hardening of the material between the cavities. Distortional strain, on the other hand, might be expected always to harden the material.[7] In this case the ratio of *distortional hardening* to *dilational softening* required to permit localization of cavity growth in a microporous element subjected to a strain increment having a given ratio of dilation to distortion, is given by eq (11). The strain increment which will permit localization, with the greatest ratio of distortional hardening to dilational softening (i.e., the mode of straining which requires the least softening to permit a localization) is the strain increment which, in addition to meeting the kinematic requirements given previously, provides the maximum ratio of dilatation to distortion; this is just uniaxial extensional strain. Thus, if one wishes to test a given calculational scheme for representing ductile fracture by hole growth in a given array of cavities, it would be useful to consider uniaxial strain, which is the mode of deformation in which fracture by localization of cavity growth may occur earliest. In fact, evaluation of eq (11) for the case of uniaxial incremental strain gives the following estimate of the *minimum* ratio of dilatational softening ($\partial Y/\partial \Delta < 0$) to distortional hardening hardening ($\partial Y/\partial \epsilon > 0$) which will permit localized cavity dilation.

$$\left(\frac{\partial Y}{\partial \Delta} \Big/ \frac{\partial Y}{\partial \epsilon} \right) \leqq -\frac{2}{3}. \tag{12}$$

This estimate was also obtained in an earlier writing (Berg, 1969 [6]) in which a special form of the yield locus was assumed.

5. Orientation of Bands of Localized Cavity Growth

Since localization of cavity growth can occur only in plane incremental deformation, it is especially convenient to use the conventional Mohr circle representation of the strain increment in the plane of deformation to show the orientation of surfaces of localization relative to the principal axes of strain increment. Figure 3 shows Mohr circles of (plane) strain increment for several possible cases. Mohr circle I represents a mode of plane strain increment in which the development of localized cavity growth is kinematically possible on either of the planes represented by a or b (since both a and b represent lines of vanishing extension rate in the plane of strain). Circle II represents a state of uniaxial strain increment; in this case the two planes a and b have coalesced at the origin, and thus formation of a single plane of localization is kinematically possible transverse to the axis of incremental strain. The states of incremental strain represented by Circles IV and V contain no directions of vanishing extension rate and therefore do not permit localized cavity growth.

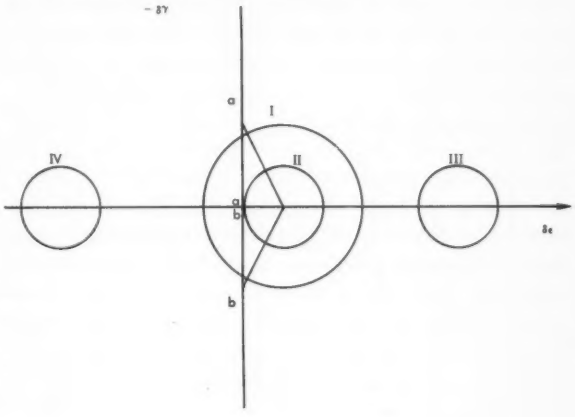

Figure 3: Mohr Circles of incremental strain states; points a and b in circles I and II represent kinematically admissable rigid surfaces.

6. Discussion

The model for ductile fracture by localized cavity growth on rigid surfaces may be helpful in explaining some curious phenomena observed in fracture. For example, R. Brook [7] has observed that fracture extending from a notch tip in high strength steels follows a wavy, zig-zag path. Brook's electron micrographs show a fracture surface made up of hillsides and waves, with cavity dimple markings covering the slopes; the average cavity spacing appears to be approximately 1/10 of the length of the slope, or less, so that the present continuum model of fracture by localized cvavity expansion may be applicable. The surfaces on which localization is admissible will, in general, be

[7] Exceptions to this generalization may exist in materials with strongly anisotropic microcavity arrays.

found in conjugate pairs (e.g., the surfaces represented by a and b in figure 3). It appears plausible that the zigzag surfaces observed by Brook were the result of fracture nucleation by localization of cavity growth on one of the two admissible surfaces which occurred in front of the notch, followed or accompanied by nucleation on another surface ahead of the first and lying at the conjugate inclination. This possibility has been discussed earlier (Berg, 1969 [6]).

One of the more striking implications of the model of fracture discussed above is a possible explanation for the general lack of correlation between ductility as measured in uniaxial tension, and ductility as measured in plane strain (Clausing [8]). In the initial stages of deformation of, e.g., a plane strain fracture toughness specimen, the material in the neighborhood of the notch tip will be virtually incompressible, and thus there will be two sets of rigid (kinematically admissible fracture) surfaces at any point. These surfaces will of course be the planes of principal shear strain rate. The deformation at this stage is incompressible, or virtually so; cavity dilation will not be significant, and will not localize. As deformation proceeds microcavity density will increase due both to expansion of cavities initially present and to generation of new cavities through inclusion cracking, phase separation, etc. Throughout this process, as the ratio of dilatation to distortion of each strain increment increases, there will always be two conjugant surfaces, at the notch tip, on which dilatational banding is kinematically admissible. One merely has to wait for that point in the deformation process at which the requirements of hardening (e.g., eq (11)) for localization are met, in order for a band of localized dilatation— and fracture—to occur.

On the other hand, the material in the neck of a tensile specimen undergoes symmetric deformation, with extension occurring along the specimen axis and biaxial contraction occurring transverse to that axis. In this mode of deformation no kinematically admissible surfaces for localized cavity expansion will occur until the material at the center of the neck has suffered sufficient cavity expansion to permit a uniaxial strain increment. If, at this point in the process the requirements of hardening for localization (e.g., eq (12)) have been met, fracture will occur. However, if these requirements have not yet been met, localization will not occur, and the element at the center of the neck may begin to deform with symmetric biaxial extension occurring transverse to the specimen axis (depending upon the rate of cavity growth and nucleation in the material). In this case, the center of the neck will no longer be able to serve as a nucleation site for the localization, and some other point in the neck must serve that purpose.

Thus, with respect to fracture by localization of cavity growth, the plane strain fracture toughness specimen (or any other plane strain specimen) and the uniaxial tension specimen start from different points and arrive at the necessary conditions for fracture by different routes. In plane strain, the kinematic conditions for localization are satisfied from the outset of deformation; one need only wait for the hardening conditions to be met for localization—and fracture—to occur. In the neck of a tensile specimen, the kinematic conditions for nucleation of fracture by localization of cavity growth cannot be satisfied until substantial cavity growth (sufficient to permit uniaxial strain) has occurred at the center of the neck. If the hardening requirements for localized cavity growth are not met at that juncture, the material in the neck may proceed to deform and might possibly begin to undergo biaxial expansion, eliminating the center of the neck as a potential nucleation cite for fracture by localized cavity growth. The apparent lack of correlation between plane strain ductility and uniaxial tensile ductility is therefore not entirely surprising.

7. Fracture of Polymers

Cracking in glassy polymers (Orowan and Doyle, 1971 [9]) and stress cracking in certain crystalline polymers is preceded by crazing, which itself is a form of localized cold drawing (plastic deformation) entailing dilatation attributable on the microscopic scale to void formation and expansion. The general conditions given above for fracture of du tile metals by formation of surfaces of unstable void growth should apply as well (with perhaps some suitable modification to the description of the yield locus) to those modes of fracture of polymers which are preceded by crazing. In particular, the mechanical properties, such as yield drop and hardening rate, which determine the sensitivity of given crystalline polymers to environmental stress cracking might be better understood if considered in relation to the model of fracture proposed above.

The author is pleased to acknowledge helpful comments of Professor F. A. McClintock (MIT). In addition the assistance of Mr. H. H. Cheng whose careful reading of an early version of this paper led to simplification of certain of the arguments, is gratefully acknowledged.

8. References

[1] Puttick, K. E., Ductile Fracture in Metals, Phil. Mag. **4**, pp. 964-969 (1959).

[2] Bluhm, J. I. and Morrissey, R. J. , Fracture in a Tensile Specimen, Proc. First Internat'l Cong. Fracture Sendai **3**, pp. 17-39 (1966).
[3] Hayden, H. W. and Floreen, S., Observations of Localized Deformation During Ductile Fracture, Acta Met **17**, pp. 213-224 (1969).
[4] Bishop, J. F. W. and Hill, R., A Theory of Plastic Distortion of a Polycrystalline Aggregate Under Combined Stresses, Phil. Mag. **42**, pp. 414-427 (1951).
[5] Subudhi, M., M.S. Thesis, Dept. of Mech. Eng. MIT (1970).
[6] erg, C. A., Plastic Dilatation and Void Interaction, Inelastic Behavior of Solids, McGraw Hill, N. Y. (1970).
[7] Brook, R., Proc. Internat'l Cong. on Mech. Prop. Solids, Kyoto, Japan, (in press 1971
[8] Clausing, D. P., Effect of Plastic Strain State on Ductility and Toughness, Internat'l. J. Fracture Mech. **1**, pp. 71-85 (1970).
[9] Orowan, E. and Doyle, M., Striations on Polymer Fracture Surfaces Caused by Rapid Oscillations of the Fracture Mechanism, MIT Industrial Liason Report, MIT, Cambridge, Mass. (1971).
[10] Subudhi, M., Plasticity of Anisotropic Porous Metals, M.S. Thesis, Mech. Engr. Dept., MIT, Cambridge, Mass. (1970).

Appendix

The method of averaging local (micro) tractions and incremental displacements over the surface of a material element, to provide average stresses (σ_{ij}) and strain increments ($\delta\epsilon_{ij}$), which was employed by Bishop and Hill (1951) is as follows.

The local tractions on a small area (S_j) normal to the x_j axis are used to obtain the average stress component via

$$\sigma_{ij}=\frac{1}{S_j}\int t_i ds_j$$

The local displacement increments (δu_i) acting over the *entire* surface of a *unit* volume of material bounded by the surface S on which the outward normal vector is denoted by n_j are used to obtain the components of average strain increment ($\delta\epsilon_{ij}$) via

$$\delta\epsilon_{ij}=\frac{1}{2}\int_s (n_i\delta u_j+n_j\delta u_i)ds$$

(Paper 76Cl&2–330)

JOURNAL OF RESEARCH of the National Bureau of Standards—C. Engineering and Instrumentation
Vol. 76C, Nos. 1 and 2, January–June 1972

Friction and Wear of Graphite Fiber Composites

C. A. Berg,* S. Batra, and J. Tirosh*****

Institute for Basic Standards, National Bureau of Standards, Washington, D.C. 20234

(May 16, 1972)

Friction and wear of two different types of graphite fiber composites were studied in a pin-disk sliding contact wear machine. Composites reinforced (62% by volume) with low modulus, high strength circular fiber (Modmor II) exhibited very high resistance to wear [a threshold wear load of ~ 20 N, a maximum bearing load of ~ 50 N, and a wear coefficient of ~ 10^{-6}] when worn by hardened steel pins. However, the composite produced extreme abrasion on the steel counterface. Composites reinforced (62% by volume) with high modulus, lower strength, noncircular fiber (GY70) also exhibited high resistance to wear (a threshold wear load of ~ 25 N, a maximum bearing capacity of ~ 20 N, and a wear coefficient of ~ 10^{-6}) when worn by hardened steel, but these composites developed a surface film which prevented abrasional damage to the steel counterface.

Potential applications of the two different types of composites in bearings are discussed. The advantages of these composites in bearings subject to corrosion, vibration, loss of lubrication, or impact damage are noted.

Key words: Composites; friction; graphite fiber; wear.

1. Introduction

In recent years a number of different types of graphite fiber have been developed for use in advanced composite materials. Used in combination with polymeric matrices (epoxy, polyimid, etc.) these fibers produce very light (density, $\rho \sim 1800$ kg/m^3) stiff (Young's modulus, $E \sim 2.8 \cdot 10^{11}$ Pa $\sim 4 \cdot 10^7$ psi) and strong (tensile strength, $\sim 7 \cdot 10^8$ Pa $\sim 10^5$ psi)[1] materials which have attracted wide attention for possible application in lightweight high-performance structures such as airframes and space vehicle frames. However, in addition to their well-recognized potential in aerospace structures, graphite fiber-reinforced plastic composites appear to possess the low friction and high resistance to wear and corrosion required in certain bearing applications. In particular, bearings in which low density and high stiffness are required (e.g., rotating seals or bearings subject to vibration) appear to offer a promising area of application for graphite fiber composites.

The study of friction and wear of graphite fiber-reinforced plastics has attracted less attention than the study of stiffness, strength, and other mechanical properties related to structural requirements. There are several different fiber-making processes, using different precursor fibers and different conditions of graphitization, and yielding fibers of different intimate structure and different mechanical properties. The differences in intimate structure—and resultant mechanical properties—of these fibers strongly influence the friction and wear behavior of their composites.

Broadly speaking, graphite fibers may be classified as having either high strength ($\sim 2.8 \cdot 10^9$ Pa $\sim 4 \cdot 10^5$ psi) and low modulus ($E \sim 2.1 \times 10^{11}$ Pa $\sim 3 \cdot 10^7$ psi) or low strength ($\sim$ ≪ $\cdot 10^9$ Pa $\sim 3 \cdot 10^5$ psi) and high modulus ($E \geq 4.2 \cdot 10^{11}$ Pa $\sim 6 \cdot 10^7$ psi). The various fibers being manufactured commercially, via the

* Professor and Chairman, Department of Mechanical Engineering, The University of Pittsburgh. Presently visiting scientist, Institute for Basic Standards, National Bureau of Standards, Gaithersburg, Md.

** Department of Mechanical Engineering, MIT, Cambridge, Mass.

*** Department of Mechanical Engineering, The Technion, Haifa, Israel.

[1] Properties quoted here are measured parallel to the fiber direction in unidirectional composites.

original R.A.E.[2] process, can be produced with either high modulus and low strength or low modulus and high strength. Typical examples of such fibers are Whittaker Corporation's Modmor I[3] (high modulus, low strength) and Modmor II (low modulus, high strength). In addition to the variations of modulus and strength which may be obtained through suitable alterations of a given graphitization process, one may obtain substantial variations of the intimate structure of graphite fibers by using different precursor materials. Graphite fibers with very high modulus ($E \sim 6.9 \cdot 10^{11}$ Pa) can be produced with radically noncircular cross sections (e.g., Thornel 75 with its crenellated cross section and Celanese GY70 with its "dog bone" cross section). The noncircular cross section of these fibers reflects certain aspects of their intimate structure, and the friction and wear behavior of composites made from these fibers is radically different from that of fibers produced via the original R.A.E. process and having the characteristic circular cross section which results from that process.

Previous reports of friction and wear of graphite fiber-reinforced composites have concerned fibers produced by the original R.A.E. process, or a variant thereof. These reports include the work of Lancaster [1],[4] Giltrow and Lancaster [2, 3], Harris and Wyn-Roberts [4], and Scott et al. [5]. In the following we wish to report and to compare the observed friction and wear behavior of composites made from two widely different types of fibers. Experiments were conducted using Whittaker 5206 epoxy resin reinforced with Whittaker Modmor Type II fiber which is circular with an elastic modulus of $2 \cdot 10^{11}$ Pa, and a tensile strength of $2.4 \cdot 10^9$ Pa. In addition, experiments with composites made of Celanese GY70 fiber in Celanese R350A epoxy were conducted. This fiber has very high modulus ($E \geq 5.2 \cdot 10^{11}$ Pa), lower strength (tensile strength $\sim 2.1 \cdot 10^9$ Pa) and exhibits the most radical departure from circularity, having a "dog bone" shaped cross section. These two fibers represent the extremes in mechanical properties and intimate structure to be found among currently available graphite fibers. These materials are described more fully in a later section.

2. Experimental Procedure

Friction and wear was studied with a pin-disk apparatus, using a fully hardened (yield stress $\sim 2.4 \cdot 10^9$ Pa) 5.04 mm diameter AISI No. 52100 [6] steel pin with a hemispherical head to provide the sliding counterface on a unidirectional GFRP[5] disk. The pin-disk apparatus permits simultaneous measurement of both friction and wear. A schematic diagram of the apparatus is shown in figure 1a, and a photograph of the apparatus actually used is shown in figure 1b. The circular wear track produced by this apparatus was approximately 8.5 mm in radius. A strip chart recorder (fig. 1b) was used to record the signal from the strain ring which measures the frictional force opposing sliding of the pin. The gearbox (fig. 1b) allows variation of the speed of the turntable from 0 to 1.3 rev/s.

The experiments were conducted at controlled room temperature (70 °F ~ 21 °C) and relative humidity (65%). The amount of material worn from the specimens was determined by periodic weighings. Since the weight loss during an experiment was typically of the order of tenths of a milligram, the specimens were permitted to rest undisturbed at ambient temperature and humidity for approximately 24 hours after being removed from the test apparatus in order that any moisture removed by frictional heating

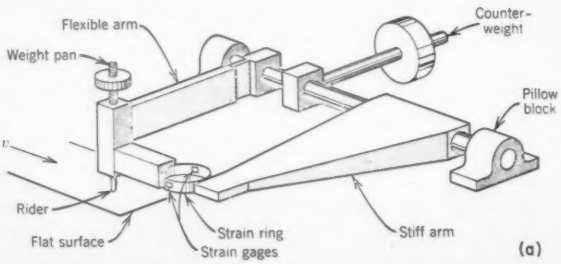

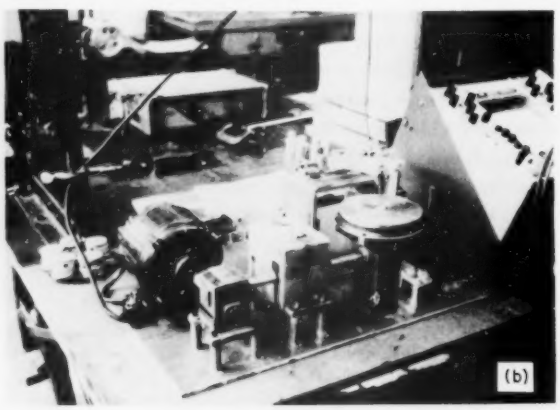

FIGURE 1. *(a) Drawing of the pin-disk wear testing apparatus; (b) photograph of the apparatus used in this study.*

[2] R.A.E. represents the British Royal Aircraft Establishment; see British Patent 1 110 791 (Apr. 24, 1968) "The Production of Carbon Fibers," W. Johnson, L. Philips, and W. Watt.

[3] Graphite fibers are produced by several different proprietary processes with resulting differences in properties. The fibers produced by the various methods can best be identified by their trade names. The trade names are used here for purposes of identification only, and this use does not constitute an endorsement or recommendation of the product.

[4] Figures in brackets indicate literature references at the end of this paper.

[5] The conventional abbreviation GFRP is used here for Graphite Fiber Reinforced Plastic.

of the specimen would not introduce intolerable inaccuracies in the determination of the weight loss.[6] In addition, og some specimens, wear rates were determined from the microsurface profiles of the wear tracks.[7] The wear rates determined by the two methods agreed, in general, to within 10 percent. The wearing load *(P)* was applied by placing calibrated masses on the pedestal of the testing machine (fig. 1). The gearbox was set to provide the desired sliding speed, and then the turntable was set in motion. The frictional force opposing sliding was recorded on the strip chart as the specimen turned. The wear of the specimen was determined via periodic weighings; specimens were allowed to equilibrate with ambient humidity and temperature prior to weighing. After wearing, the surfaces of the specimens were examined with both optical microscopes and a scanning electron microscope to determine the character of wear mechanisms.

3. Materials Studied

Two different types of GFRP were studied:

Composite A: (Whittaker Modmor Type II, graphite fiber in Modulite 5206 epoxy resin.) The modulus of the Type II fiber is $2.4 \cdot 10^{11}$ Pa (35×10^6 psi) and the tensile strength is $2.4 \cdot 10^9$ Pa (350 ksi).[8] The fiber content of the system was approximately 62 percent by volume. Flat plaques of the material with the fibers aligned unidirectionally were prepared by hot pressing several plies of prepreg tape, using the curing procedure (177 °C at 0.7 m Pa for 120 min) recommended by the supplier. The fiber is circular.

Composite B: (Celanese GY70 graphite fiber in R350A epoxy resin.) The fiber modulus is $5.2 \cdot 10^{11}$ Pa (75×10^6 psi), and the tens le strength is $2.1 \cdot 10^9$ Pa (300 ksi). The fiber content of the system was approximately 62 percent by volume. The specimens were formed as flat plaques on caul plates in an autoclave at the Celanese Research Laboratories. The fiber has a flat "dog bone" cross section.

4. Specimens

Specimens of both types of composite were formed as flat plaques $25 \times 25 \times 4$ mm with unidirectional fiber reinforcement running parallel to the plane of the plaque. Each specimen was lightly abraded by hand to remove the resin surface film remaining after hot forming. The specimen was then placed in the wear testing machine.

5. Representation of Wear Data

In dealing with the wear of metals in sliding contact it is possible to characterize wear by a dimensionless wear coefficient, K. The wear coefficient is dimensionless, is a useful design parameter, and offers a convenient means of comparing the wear behavior of different materials in specified ranges of operating conditions. For both the adhesive and abrasive wear of metals and plastics the wear coefficient, K, is given by

$$K = \frac{\Delta V}{L} \cdot \frac{H}{P}, t + 6 \tag{1}$$

where ΔV is the volume of the material removed, L is the sliding distance, P is the total contact load, and H the hardness of the material being worn [7]. Experimental evidence indicates that the wear coefficient may depend upon the surface roughness, humidity, temperature, surface adsorbed layers and other environmental factors. Under a wide range of conditions encountered in practice the wear coefficient *(K)* is constant and serves as a useful measure of wear for a given pair of materials.

Since it is not possible to assign an unambiguous hardness to the surface of a composite material the wear equation (1) cannot be directly applied. The authors would like, if possible, to retain the simple and useful notion of a wear constant to characterize GFRP wear; for this purpose some measure of effective hardness of the surface must be identified. The hardness of a metal surface may be regarded as the average stress required to produce large plastic strain under an indentor. A suitable generalization of hardness for a composite might be the local stress required to cause large irrecoverable strain of that phase of the composite which supports the wearing load. Since the graphite fiber itself appears to support the wear load (see descriptions of the wear surface below), the tensile strength (σ_u) of the reinforcing fiber is proposed here as a measure of the hardness of the composite. The modified wear equation used here is

$$\frac{\Delta V}{L} = K \frac{P}{\sigma_u} \cdot t + 6. \tag{2}$$

One of the questions to be resolved in this study is whether (2) provides a meaningful characterization of

[6] The authors are grateful to Prof. E. Rabinowicz for pointing out this potential source of error at the outset of this investigation.

[7] The talysurf, an instrument which measures surface profiles, was used.

[8] Values supplied by the manufacturer.

wear of graphite fiber composites. For reasons discussed below it is concluded that (2) is useful for this purpose, within the range of bearing loads usually found in practice.

6. Observations of Friction and Wear of Low Modulus, High Strength, Graphite Fiber Composites

In a sequence of tests in which the wearing load (P) varied from 9.8 to 49.0 N, composites reinforced with low modulus, high strength fiber of circular cross section exhibited extremely high resistance to wear, and low friction. At a contact load of 29.4 N the wear coefficient (K of eq 2) was found to be $2.1 \cdot 10^{-7}$, while at a contact load of 49.0 N the wear coefficient was $2.1 \cdot 10^{-6}$. Table 1 gives a summary of data obtained from these experiments.

At contact loads of 9.8 and 19.6 N the wear of the low modulus composite specimens was undetectable by weighing. Many metals exhibit a threshold wear load below which wear actually ceases. In the case of gold wearing on gold at room temperature this threshold load is of the order of 10^{-2} N, while for steel on steel the threshold load is of the order of 10^{-3} N (see, e.g., Rabinowitz [7]). It is somewhat surprising to encounter a threshold wear load as large as 19.6 N. However, the records of the sliding frictional force obtained during wear experiments at 9.8 N load show a highly repetitive pattern, which indicates that the fine structure of the surface does not change during the sliding process.

Figure 2 shows a set of records of sliding frictional force on the low modulus fiber composite, as a function of the angle of rotation of the specimen. The mark $\perp$ indicates that the direction of sliding is perpendicular to the fiber axis, and the mark $\parallel$ indicates sliding parallel to the fiber. The bottom record in figure 2 was taken after 26.5 hours of wearing ($9.5 \cdot 10^4$ passes of the rider over the surface) the middle record was taken at 45.0 hours of wearing ($16.2 \cdot 10^4$ passes) and the top record at 96.0 hours ($34.6 \cdot 10^4$ passes, and a total sliding distance of 24 km). Note that the patterns of frictional force are not merely similar, but are congruent. Repetitive patterns

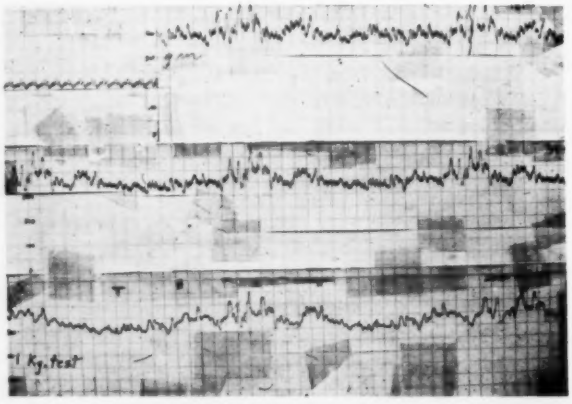

FIGURE 2. *Records of tangential frictional force opposing sliding on the low-modulus circular, fiber-reinforced surface; $\perp$ indicates the sliding direction was transverse to the fiber and $\parallel$ indicates sliding parallel to the fiber.*

Table 1 - Measured wear data for the two types of carbon fiber composites
Composite A - Low modulus fiber composite
Composite B - High modulus fiber composite

No.	Composite	Contact load N	Fiber tensile strength Pa · 10^9	Av distance of sliding km	Sliding speed mm/s	Wear coefficient K x 10^{-6} by weighing	Wear coefficient K x 10^{-6} by talysurf	Wear of rider
1	B	2.45	2.1 (300 ksi)	83.3(1)*	9.5	wear could not be detected		
2	B	4.90	2.1 (300 ksi)	61.6(3)	7.1	1.0 (0.7 - 1.4)**	0.92	not measurable
3	B	9.80	2.1 (300 ksi)	55.4(3)	7.1	0.94 (0.3 - 1.8)	1.1 (0.3 - 2.3)	not measurable
4	B	19.6	2.1 (300 ksi)	0.8(2)	7.1	1.0 (0.8 - 1.2)	-	not measurable
5	A	9.80	2.4 (350 ksi)	24.0(1)	7.1	wear could not be detected		severe
6	A	19.6	2.4 (350 ksi)	32.9(2)	9.7	wear could not be detected		severe
7	A	29.4	2.4 (350 ksi)	39.0(1)	7.1	0.2	-	severe
8	A	49.0	2.4 (350 ksi)	5.0(1)	7.1	2.1	-	severe

*Number in ( ) indicates number of tests.

**Numbers in ( ) indicate range of measured values.

of sliding frictional force are commonly observed over short periods during sliding wear tests of metals. However, these patterns change gradually as wear of the specimen alters the fine structure of the wear surface. Evidently, the surface structure of the wear specimen from which the data of figure 2 are taken was not substantially altered by being subjected to $34.6 \cdot 10^4$ passes of a 52100 steel pin carrying a 9.8 N load. Thus, the surprisingly high threshold wear load of 9.8 N, for low modulus, high strength, graphite fiber-epoxy composite by fully hardened 52100 steel, is indicated both by weighing and by indirect observation of surface detail.

High magnification micrographs of the wear surfaces produced on low modulus, high strength, graphite fiber composites reveal some of the reasons for the high wear threshold load and high resistance to wear of these materials. Figure 3 shows a typical view of the wear track on a specimen, at a point where the direction of sliding was perpendicular to the fiber direction. The specimen carried 9.8 N load for 24 km. Note that the

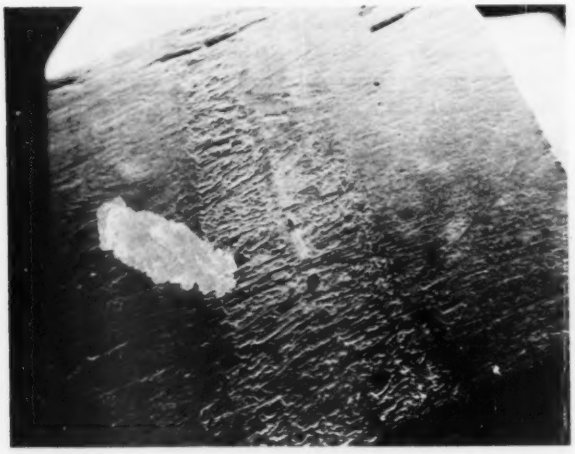

FIGURE 3. *The wear surface of the low-modulus circular fiber-reinforced surface.*

fibers crossing the wear track are substantially intact, and that resin has been removed so that the fibers stand out in relief more boldly than on the unworn surface. Figure 4a shows a high magnification (SEM) micrograph of the wear surface on a specimen of the same material worn at 49.0 N load. Here, the fibers themselves still appear to be intact, but the matrix contains a number of cracks running both at the fiber-matrix interface and through the interfibrile matrix cells. Figure 4b shows several fibers on the same specimen (49.0 N load), which have been polished by the wear process, but which otherwise appear unaffected. In general, the wear surfaces produced on low modulus fiber reinforced specimens showed little, if any, evidence of adhesional wear—or of any other type of wear—occurring on individual fibers. Where wear was produced (at loads exceeding 19.6 N) the chief mechanism of material removal appears to have been extension of systems of fatigue cracks in the matrix (fig. 4a), which eventually undercut whole groups of fibers and allowed bundles of fibers to be broken out of the surface of the specimen. The typical wear particles gathered from wear experiments with this material consist of large fragments of broken fibers, or a few fiber fragments still bonded together. Figure 4c shows one such fragment still situated on the wear surface of the specimen.

During the wear process the graphite fibers apparently support the wearing load. The graphite fibers presently under consideration are circular in cross section, and, according to the few reported studies of fiber intimate structure, the graphite basal plane is believed to be wrapped around the fiber axis. This being the case, whichever way one might rub a circular graphite fiber with a rider (along the fiber direction or transverse to it) the rider would slide on the graphite basal plane. Because of the high energy of bonding in the basal plane there would be little chance for the rider to remove a wear particle from an individual fiber by, e.g., adhesion. Thus, the fibers themselves would be highly wear resistant, and wear, if it is to take place, would occur on some scale comparable to or larger than the individual fiber diameter (e.g., whole fibers or fiber bundles must be broken out of the surface). Apparently the extremely high threshold wear load (19.6 N) found for the low modulus graphite fiber-reinforced material comes about because loads in excess of 19.6 N are required to extend the local fatigue cracking of the matrix over suificiently large areas to produce the loosening and underc tting of fibers and fiber bundles.

Although the high wear resistance of the low modulus, high strength fibers of circular cross section offers encouraging indications of their potential as bearing materials, the effect of these materials on the 52100 steel sliding pin is severe. In fact, during the wear experiment at 9.8 N load, in which the composite underwent no measurable wear, the tip of the steel rider was worn flat. Figure 5 shows the worn tip of the rider in this experiment. In another experiment the clamps which hold the graphite fiber-reinforced specimen to the turntable came loose and the specimen fell off of the turntable. The 52100 steel rider, carrying 9.8 N load, then ran on the mild steel turntable for approximately 4 hours before the situation was discovered. During a previous run in excess of 4 hours under the same conditions the composite specimen exhibited no

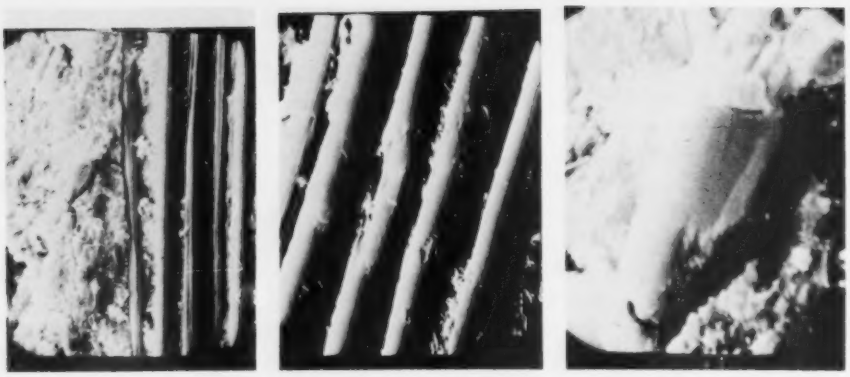

FIGURE 4. *(a) Electron micrograph of wear surface on low-modulus fiber-reinforced material showing fatigue racks in resin; (b) electron micrograph of same surface showing polished fibers; (c) electron micrograph showing a typical "wear particle," i.e., a broken fiber.*

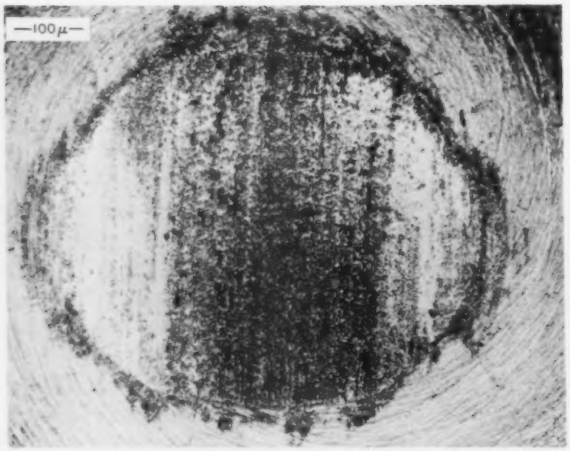

FIGURE 5. *The worn 52100 steel rider tip after wearing on low-modulus circular fiber-reinforced surface.*

measurable wear; however, the steel turntable was severely worn by the 52100 steel rider in the (approximately 4-hour) period during which the specimen was missing. Figure 6 shows the groove which was worn in the turntable. While mild steel wearing against fully hardened 52100 steel is hardly a promising bearing combination, the fact that the composite material experienced no measurable wear under the same conditions which produced the severe wear shown in figure 6 does illustrate the extremely high wear resistance of the graphite fiber-reinforced epoxy composite. On the other hand, the severe wear which the 52100 steel rider experienced (fig. 5) while in contact with the low modulus, circular, graphite fiber-reinforced epoxy illustrates the extreme abrasiveness of this composite. Indeed, in order to take advantag of the high wear resistance of these composites one would have to select counterface materials with great care. The low modulus, circular, graphite fibers, since they exhibit little if any wear themselves, serve as extremely hard, abrasive, rod-shaped particles of approximately 7μm diameter.

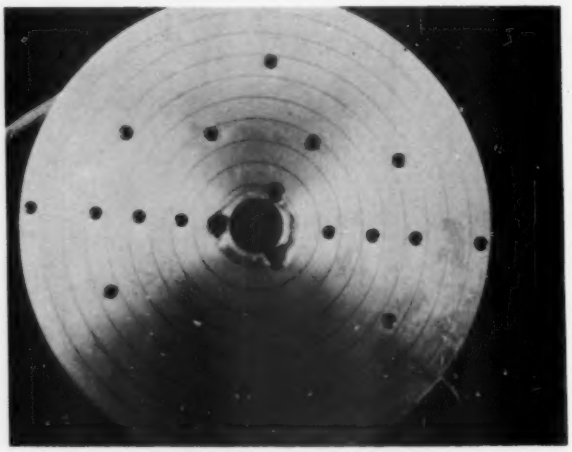

FIGURE 6. *Groove which was worn into steel turntable after composite specimen fell off.*

Survey experiments in which boron carbide tipped riders were used in place of the 52100 steel were carried out. Insofar as the wear of the composite itself was concerned the results were indistinguishable from those obtained with the steel riders. However, the boron carbide riders were sufficiently hard that they did not exhibit wear at loads up to 19.6 N. Experiments with boron carbide riders at loads greater than 19.6 N

have not yet been carried out. In addition, some survey experiments in which both the rider and the plaque were made of composite material were carried out. The general tendency of the composite, both in the rider and the plaque, to resist wear at loads up to 19.6 N, was seen also in these experiments. However, at present the total data from these experiments is sufficient for more than a preliminary report. The coefficient of sliding friction of the low modulus fiber composite sliding against 52100 steel was measured at sliding speeds of 45 mm/s and 1065 mm/s, at 19.6 N load (table 2). The average coefficient of friction for the first condition was found to be 0.135, with the range of data taken from several specimens extending from 0.13 to 0.14. At the higher sliding speed the average coefficient of friction was found to be 0.145, with the range of data extending from 0.13 to 0.16. Thus a slight dependence of friction upon sliding speed is indicated, but has not been investigated further.

7. Observations of Friction and Wear of High Modulus, Intermediate Strength, Graphite Fiber Composites

The wear testing procedures described above were applied to specimens of high modulus, fiber-reinforced epoxy composites. These composites also exhibited high resistance to wear ($0.7 < K \cdot 10^6 < 1.8$) at contact loads ranging from 4.9 to 19.6 N, when worn in contact with 52100 steel riders. At contact loads of 2.45 N and less, the high modulus material exhibited no measurable wear, as determined by periodic weighing. Figure 7 shows records of tangential friction force on the surface of the high modulus composite material under a wearing load (P) of 2.45 N. As in figure 2, the congruency of these records during a wearing process extending from $9.4 \cdot 10^4$ passes to $74.7 \cdot 10^4$ passes of the rider over the surface indicates that the fine structure of the composite surface was not altered by the passage of the rider, and thus provides an indirect confirmation that 2.45 N is below the threshold wear load for the high modulus, graphite fiber-reinforced material.

During all of the wear experiments the wear rider itself exhibited *no* measurable wear. The surface of the tip of the rider showed a slight polishing, and under the

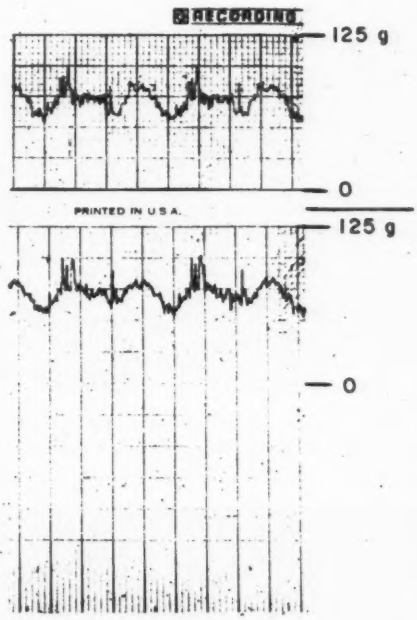

FIGURE 7. *Records of frictional force on high-modulus noncircular (GY 70) fiber-reinforced surface.*

Table 2 - Measured values of the coefficient of friction.
Composite A - Low modulus fiber composite
Composite B - High modulus fiber composite

No.	Composite	Contact load N	Sliding speed 2.9 mm/s	Sliding speed 70 mm/s	Sliding speed 94 mm/s	Sliding speed 4.5 mm/s	Sliding speed 109 mm/s
1	B	2.45			0.14 - 0.19		
2	B	4.90	0.13 - 0.17 0.10 - 0.19	0.16 - 0.20 0.16 - 0.28			
3	B	9.80	0.14 - 0.24 0.12 - 0.15 0.11 - 1.15	0.17 - 0.28 0.15 - 0.18 0.15 - 0.17			
4	B	19.6	0.12 - 0.18 0.13 - 0.19	0.12 - 0.18 0.14 - 0.21			
5	A	19.6				0.13 - 0.14	0.13 - 0.16

optical microscope tentative evidence of a transferred graphite film could be seen (fig. 8).[9]

It is important in judging the potential of the composite material in a bearing application, to bear in mind that the high modulus fiber reinforcement does not cause severe wear on the steel counterface. Figure 9 shows two steel riders, one worn flat after sliding on a low modulus graphite fiber-reinforced surface, and the other merely lightly polished by sliding on a high modulus graphite fiber-reinforced surface; both riders carried loads of 9.8 N for comparable distances of sliding (25 km).[10] When it was attempted to apply wearing loads of 29.4 N or more to the high modulus fiber-reinforced composite specimens, destruction of the surface of the specimen occurred at such a rapid rate that the "wear" of the material was too great to be of practical interest, and certainly could not be represented via the proposed wear constant of (2).

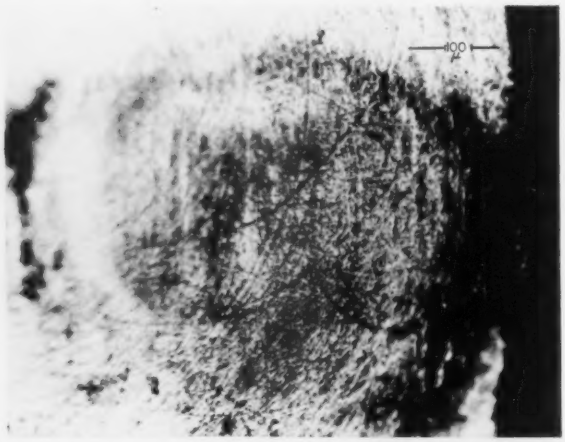

FIGURE 8. *The tip of the 52100 steel rider after wearing against high-modulus noncircular fiber-reinforced surface.*

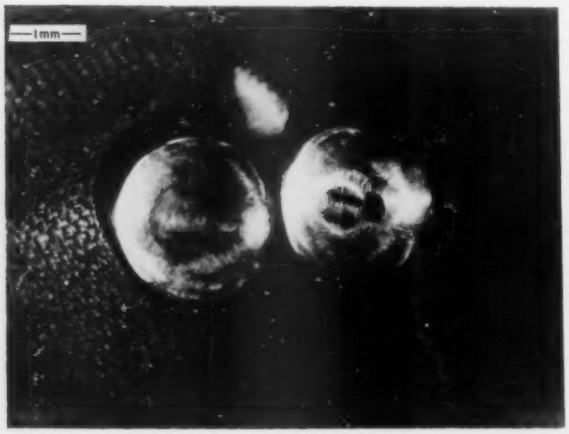

FIGURE 9. *Two riders used in experiments. One worn flat by wearing against circular low-modulus fiber, the other only lightly polished by wearing against high-modulus noncircular fiber.*

In summary, the high modulus, graphite fiber-reinforced material exhibited approximately the same high resistance to wear ($0.7 < K.10^6 < 1.8$) as low modulus fiber-reinforced materials, but has a somewhat lower bearing capacity ($P_{(threshold} \sim 2.45$ N, $P_{(max)} \sim 19.6$ N). On the other hand, the high modulus fiber-reinforced material caused much less severe wear on the 52100 steel wear riders than did the low modulus fiber-reinforced material. Although the threshold wear load of the high modulus material is lower than that of the low modulus material, a threshold wear load of 2.45 N is still remarkably high as compared with threshold wear loads determined for metal-to-metal contact. With a permissible bearing load range of 0 to 19.6 N the high modulus graphite fiber-reinforced composite qualifies for many industrial bearing applications.

8. The Wear Surface of High Modulus, Graphite-Reinforced Composites

The most striking aspect of wear of high modulus graphite fiber-reinforced material was the complete dissimilarity of the wear surface from that found on low modulus fiber-reinforced material. Figure 10 shows a

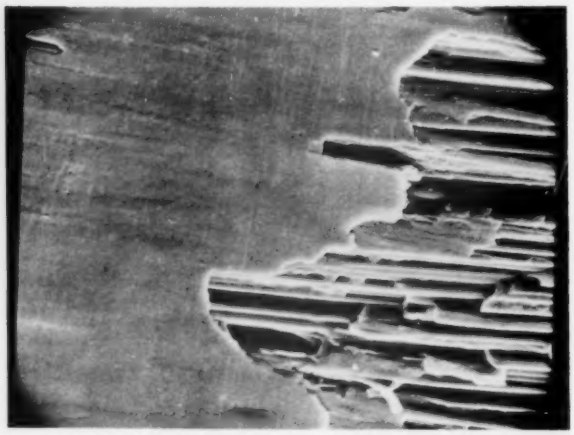

FIGURE 10. *Electron micrograph of wear surface on composite reinforced with noncircular high-modulus (GY 70) fiber, after approximately 5 km sliding. Note buildup of film.*

[9] The spectrographic data necessary to confirm the presence of a graphite film are not yet available.

[10] The reasons for the absence of wear on the steel rider, subject to sliding on the high modulus fiber reinforced surface are revealed through examination of the composite surface itself, and will be discussed below.

scanning electron micrograph of the wear surface of high modulus fiber-reinforced material during the early stages of wearing (5 km total sliding distance) at 9.8 N. As the micrograph indicates, a pasty, smooth film forms early in the wear process and covers the wear surface. This film is presently believed to be comprised of small graphite platelets which are broken off of the fibers during the wear process. Figure 11 shows the wear track of a specimen of high modulus fiber-reinforced material which was subjected to 10 km sliding under 19.6 N load. The individual fibers are only barely distinguishable, and the apparently smooth pasty film, typical of wear surfaces on this material, has completely covered the surface. Comparison of figures 11 and 4 provides an indication of the degree of dissimilarity of wear surfaces found on high modulus and low modulus graphite fiber-reinforced material. The smooth, pasty (apparently graphite) film is apparently responsible for preventing wear of the steel rider on material reinforced with the high modulus noncircular fiber studied here. If, as is presently supposed, the film does consist of small flakes of graphite, it is conceivable that the film itself could sustain large (average) shearing deformation by the sliding of graphite platelets over each other. In this case, the film would serve as a solid lubricant. The coefficient of friction measured on wear surfaces of high modulus graphite fiber-reinforced material are sufficiently small (see table 2) to be consistent with the presence of a solid lubricant film. If the film-like wear surface of high modulus material is comprised of graphite platelets, broken off of individual fibers, then the capacity of the high modulus fibers to produce this film may be related to the cross-sectional shape of the fiber and the implied intimate structure. As a general rule, those few investigations of fiber intimate structure which have been reported (e.g., Johnson and Tyson; [8] Hugo and Philips, [9]) indicate that in most fibers the graphite basal plane tends to lie tangent to the surface of the fiber. One might assume that this general observation applies to both the Modmor II and the Celanese GY70 fibers. With the graphite basal plane lying tangent to the surface of the "dog bone" shaped Celanese GY70 fiber, the basal planes must be sharply bent around the ends of the dog bone, producing high energy sites where microfracture, and production of graphite microplatelets by contact loading with the wear rider, would be facilitated. The graphite basal plane might terminate at the ends of the dog bone, as is suggested in figure 12. Since approximately half of the fibers in the wear surface are oriented so that the wear rider will strike the end of the dog bone, the proposed high energy sites or basal plane terminations in these ends should provide ample sources for production of graphite microplatelets via local exfoliation of graphite crystals. On the other hand, the low modulus fibers, having circular cross sections, would not offer such sites for film production.

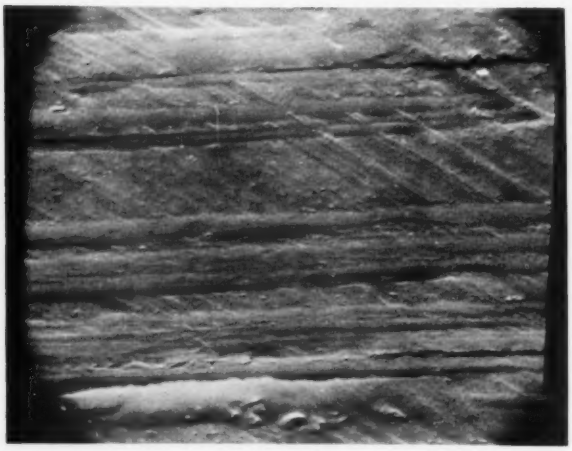

FIGURE 11. *Electron micrograph of wear surface on GY 70 reinforced composite after more than 10 km sliding. Note complete film cover.*

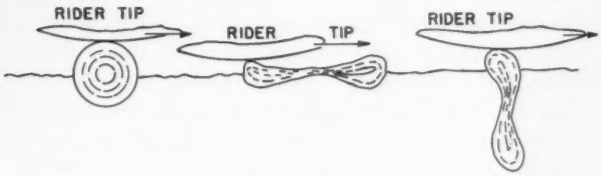

FIGURE 12. *Circular fiber at left, with basal planes (— — —) wrapped around fiber axis, is relatively impervious to wearing by the Rider tip. "Dog bone" shaped fiber, center and right, has high-energy sites at ends which provide sources of graphite flakes for film formation.*

The principal reason for the different cross-sectional geometry of the fibers studied here seems to be the nature of the precursor fiber, rather than the heat treatment which determines the modulus, strength, and extent of graphitization. As was pointed out above, the fibers studied here were chosen because they represent the extremes available in fiber modulus and cross section. However, high modulus fibers of circular cross section are available (e.g., Modmor I), and if the cross-sectional geometry and related intimate structure of the fiber are responsible for film production, then composites made of these fibers should not yield lubricating films. In fact, in a survey experiment using a specimen of Modmor I (circular cross section) fiber-reinforced epoxy, subject to a wearing load of 19.6 N for a total sliding distance of 10 km, the wear constant was found

468-108 OL - 72 - 4

to be approximately $5 \cdot 10^{-7}$, high wear was observed on the 52100 steel rider, and no evidence of individual fiber destruction was found. The worn surface of the composite was essentially the same as that of the low modulus fiber composite. Thus, the fiber cross section, and the associated intimate structure, do appear to determine whether a surface lubricating film may develop during wear.

We have proposed that the surface film found on worn, high modulus, graphite fiber-reinforced material is comprised of graphite platelets, but we must add that at present there is no experimental evidence of the precise chemical nature of this film, and the proposal given here must be viewed as an hypothesis in need of testing. One aspect of film formation which must be considered is the mechanism by which the film attaches to the surface of the composite. There is, apparently, a rather strong bond between the compo ite substrate and the film, for the material removal rate during wear after the development of the film is extremely small, much smaller in fact than would occur were he wear surface merely covered with powdered graphite. Scanning electron micrographs employing backscattered primary electrons which provide somewhat greater surface detail on polymeric composite specimens, indicate that the surface film which appears smooth when viewed via conventional secondary electron emission may, in fact, be rather porous (fig. 13). It has been suggested that with the coefficient of friction observed in these experiments local heating may play a part in the film formation seen on the GY70-R 350A composite; it has further been suggested that different effects of local heating on the different epoxy resins used in the two composites may be partly responsible for the different characters of the wear surfaces observed n these experiments. Further work is required to determine the nature and precise source of the film. With present evidence one can only offer the mechanism of film formation given above as a tentative proposal. However, one can say with certainty that the formation of the surface film on high modulus dog-bone shaped graphite fiber composites is accompanied by cessation of wear of the counterface, and this fact may bear importantly on future application of the high modulus material.

9. The Wearing-In Phenomenon with High Modulus Noncircular Fibers

An experiment with a total length of slide of 100 km was carried out using a specimen of the high modulus composite under contact with a 52100 steel rider carrying a load of 19.6 N. The incremental wear determined via periodic weighing of the specimen was used to calculate an incremental wear constant K_{inc}. Figure 14 gives the measured incremental wear constant as a function of the total length of slide *(L)* during the experiment. The wear rate is extremely high at the outset of sliding ($\sim 10^{-4}$), but within the first 5 km of sliding ($\sim 10^5$ passes over the surface) the wear rate decreases rapidly to the level of practical interest for bearing ap-

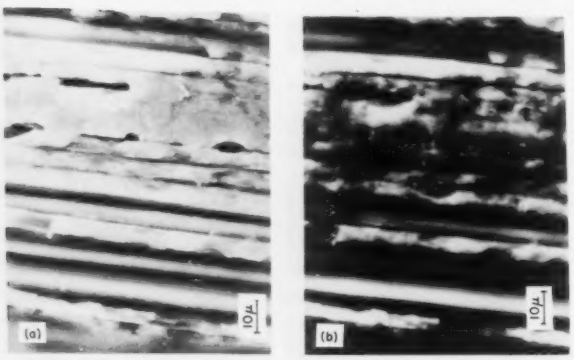

FIGURE 13. *(a) Scanning electron micrograph, via secondary electrons of GY 70 worn surface. Surface appears smooth; (b) scanning electron micrograph, via back scattered primary electrons, of GY 70 worn surface. Surface shows porosity.*

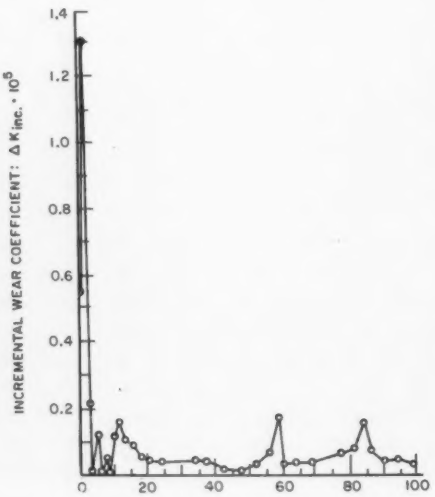

FIGURE 14. *Incremental wear coefficient measured in long duration (100 km) experiment with high-modulus fiber-reinforced material.*

plication ($\sim 10^{-6}$). Thereafter, the wear rate oscillates regularly ($10^{-7} < K_{\text{inc}} < 10^{-6}$), with a period of approximately 25 km sliding distance per cycle. The mechanism responsible for the cyclic wear rate indicated by the data of figure 14 is not presently understood. However, the total volume of material worn off of the surface (the area under each cycle in fig. 14) is approximately the same. This suggests that some basic structural unit on the surface (perhaps one layer of fiber) is destroyed during each cycle. The source of oscillating wear is yet another open question in the present state of understanding of wear of composite.

The data of figure 14 show a very strong "wearing-in" phenomenon, similar to that found in cast-iron bearings. Surface "preparation" occurs during the first 10^4 passes of the rider over the high modulus fiber-reinforced surface. Thus, in design of bearing parts from this material, one must provide for an adequate "wearing-in" period to obtain optimum performance in service. Also, one must take the removal of material during the wearing-in procedure into account, both with respect to the production of wear particles and with respect to the alteration of tolerances of bearing. Moreover, wear testing procedures employed to evaluate this material for long-life service must be sufficiently long to pass through the initial domain of high wear rate.

10. Characterization of Wear Via the Wear Constant

The definition of the wear constant (2) implies that the rate of removal of material by wear is independent of the length of slide and is proportional to the applied load. According to the data upon which this report is based (e.g., fig. 14) the wear rate may be treated as if it were independent of the length of slide, provided that one considers sufficiently long periods to include several of the "cycles" shown in figure 14, and provided that one recognizes the "wearing-in" phenomenon seen with high modulus noncircular fiber. Moreover, the data of table 2 show that the wear rate, as represented by the wear constant, is a rather weak function of applied load in the domain between the threshold wear load and the maximum bearing capacity (19.6 to 49.0 N for circular low modulus fiber, 4.90 to 19.6 N for the noncircular high modulus fiber). Thus, the use of the wear constant to characterize wear rates of the composites studied here appears justifiable. For those who prefer to express the wear rate in (say) cm^3/m, the fiber properties given above along with the reported wear constant may be inserted into (2).

11. Potential Applications

The possibility of using graphite fiber-reinforced epoxy as a bearing material in a number of industrial applications suggests itself. For example, journal bearings where sliding contact may occur upon the breakdown of a lubricating system, and bearings in which dry frictional sliding must be contemplated (e.g., engine seals, air bearings and other seals subject to vibration, machine ways) appear as promising areas of application for this material. In such applications the high modulus, noncircular fiber reinforcement would have the advantage of producing low or vanishing wear on a steel counterface, while both of the graphite fiber materials surveyed here would have the advantage of being highly wear resistant themselves and being capable of supporting substantial bearing loads. Of course, if one were able to replace steel bearing counterfaces with material of sufficient hardness (e.g., boron carbide) for use with the low modulus, circular fiber-reinforced material, one could also obtain low or vanishing counterface wear rates, but at substantially greater expense.

A possibly outstanding advantage of using graphite fiber-reinforced materials in bearing applications is the low cost of fabrication and repair. For example, one might provide an extremely wear resistant machine way by cementing a tape of graphite fiber-reinforced material on the machine. Such an operation can be completed at ordinary room conditions. The wear resistant surface of the way could be ground to provide the desired flatness. But since the tape would be applied on an already prepared metal surface, only minimal grinding of the composite surface would be required to complete preparation of the way. Grinding operations with alumina or silica wheels provide a means of preparing such a surface.[11] Once the surface were installed, it would provide an extremely wear resistant bearing surface without embrittling the machine way. If the composite surface were to be accidentally damaged (by, say, a sharp heavy object being dropped on it) the composite could be stripped off and replaced easily and cheaply. These same considerations would, of course, apply to the manufacture and maintenance of many other types of bearing surfaces. Finally, although the subject is not discussed here, it is appropriate to note that the extreme insusceptibility of graphite fiber-reinforced epoxy to environmental attack in atmospheres which are normally hostile to metals

[11] Studies of grinding and machining both types of GFRP reported on here have been conducted and will be reported in a later writing. These extremely wear resistant composites are surprisingly easy to grind.

(e.g., hot acids, salt water) suggests the possibility of using these materials to circumvent problems of corrosion wear, corrosion fretting, etc.

The extreme hardness of the low modulus, circular fiber reinforcement, and the severe wear it produces upon 52100 steel, suggest that this composite may be useful in polishing or cutting of hard metals. The use of graphite fiber-reinforced cutting and polishing wheels appears to merit further investigation.

12. Conclusion

Friction and wear of two different types of graphite fiber-reinforced epoxy were studied. Specimens with low modulus, circular fiber reinforcement and high modulus noncircular reinforcement were used. It was found that both materials, when worn against fully hardened 52100 steel, exhibited low coefficients of friction (~ 0.1 to 0.2) and very high resistance to wear. A wear constant, defined in such a way that the tensile strength of the fiber serves as a measure of surface hardness, was found to provide a useful characterization of composite wear. Epoxy reinforced with low modulus, circular, graphite fiber exhibited a threshold wear load of 19.6 N, a maximum bearing capacity of 49.0 N and between these load limits, a wear coefficient of approximately 0.23×10^{-6}. The 52100 steel rider, when used against the noncircular fiber reinforcement, exhibited no wear at all. The surface of the noncircular fiber-reinforced material developed a film, presumably of graphite platelets, which was tightly adhered to the composite substrate. The film inhibited further wear of the composite and prevented wear of the steel counterface. A very strong "wearing-in" phenomenon occurred with the high modulus, noncircular, fiber reinforcement, approximately 10^4 passes over the surface, at 19.6 N applied load on the rider, were required to pass through the initial transient period of high wear rate and reach the steady state condition in which the wear coefficient oscillated between 10^{-6} and 10^{-7}.

Certain bearing applications of these materials appear promising, including antifriction bearings, machine ways, safety liners for journal bearings in which loss of lubrication might occur, and anticorrosion bearings. Cutting tool applications of the low modulus circular fiber are also discussed. Further investigation of the mechanisms of film generation and attachment with the noncircular fiber, the mechanism of wear with this material, and the behavior of both materials as anticorrosion bearings are recommended.

The authors are pleased to acknowledge the assistance provided by Mr. Wm. Corwin and Mr. David Davis in conducting experiments. In addition, data provided by Mr. S. Smith (in particular, data of fig. 14) and by Mr. Wm. Hauser (in particular, fig. 6) are most gratefully acknowledged. The financial support of the MIT Center for Materials Science and Engineering and the Celanese Research Company of Summit, N.J. made the work reported here possible; in addition, preparation of this paper was supported in part by the National Bureau of Standards. This support is most gratefully acknowledged.

13. References

[1] Lancaster, J. K., The Effect of Carbon Fiber Reinforcement on the Friction and Wear of Polymers, Brit. J. Appl. Phys. (J. Phys. D), Ser. 3, **1**, 549 (1968).

[2] Giltrow, J. P., and Lancaster, J. K., Carbon Fiber Reinforced Polymers as Self-Lubricating Materials, 6th Tribology Group Convention 1968, Inst. of Mech. Engineers, Proceedings Vol. 182, part 3N, Paper 18, (1967-68).

[3] Giltrow, J. P., and Lancaster, J. K., The Probe of the Counterface in the Friction and Wear of Carbon Fiber Reinforced Thermosetting Resins, Wear **16**, 359-374 (1970).

[4] Harris, C. L., and Wyn-Roberts, D., Wear of Carbon Fiber Reinforced Polymers in a High Vacuum Environment, Nature, Vol. 217, 981 (Mar. 9, 1968).

[5] Scott, D., Blackwell, J., McCullough, P. S., and Mills, G. H., Composite Material for Rolling Bearing Cages, Wear **15**, 257-269 (1970).

[6] ASTM **A295**, Specifications for Carbon Chromium Ball and Roller Bearing Steel, ASTM, Phila., Pa., (1972).

[7] Rabinowicz, E., Friction and Wear of Materials, John Wiley and Sons, Inc., N.Y., N.Y., (1965).

[8] Johnson, D. J., and Tyson, C. N., Low Angle X-ray Diffraction and Structure and Physical Properties of Carbon Fibers, J. Phys. (Brit.); D:Appl. Phys. **3**, 526 (1970).

[9] Hugo, J. A., Phillips, V. A., and Roberts, B. W., Intimate Structure of High Modulus Carbon Fibers, Nature, Vol. 226, 144 (April 1970).

(Paper 76C1&2–331)

JOURNAL OF RESEARCH of the National Bureau of Standards—C. Engineering and Instrumentation
Vol. 76C, Nos. 1 and 2, January–June 1972

A Note on Construction of the Equivalent Plastic Strain Increment

C. A. Berg*

Institute for Basic Standards, National Bureau of Standards, Washington, D.C. 20234

(May 18, 1972)

Strain hardening plastic deformation of a material possessing a yield locus which may be written as a homogeneous function of the stress components, and which obeys the classical associated flow rule for metals is considered. The material may be anisotropic and may display plastic dilatation. A method is given for constructing the equivalent plastic strain increment in such a way that the increment of plastic work is always equal to the product of the equivalent plastic strain increment and the equivalent yield stress. The method is implied in classical treatments of hardening but seems not to have been given explicitly heretofore.

Key words: Equivalent strain; hardening; plasticity; strain hardening; work hardening.

1. Introduction

From time to time one encounters the need to employ an equivalent plastic strain increment in plasticity. Most frequently this need arises in the construction of mathematical descriptions of strain hardening [1, 2].[1] Several different forms of equivalent plastic strain increment have been suggested, and often the physical basis for the suggestion is not made clear. The purpose of this note is to offer a physically based rule for the determination of the equivalent plastic strain increment. The rule is implied in classical treatments of the subject, but appears not to have been given explicitly.

2. Plastic Deformation With Hardening

We assume, as is conventional in plasticity theory, that the yield condition may be given in the form

$$f(\sigma_{ij}) - Y(\text{history}) = 0, \tag{1}$$

where Y is the "equivalent yield stress" and depends upon the history of deformation so as to represent the hardening of the material. In this paper, Y is numerically equal to the yield stress in uniaxial tension. The function $f(\sigma_{ij})$ must, of course, have the physical dimensions of stress. We assume that $f(\sigma_{ij})$ is a homogeneous function of degree unity in the stress components σ_{ij}. These assumptions imply that the yield locus merely expands without changing shape as the material hardens, with the magnitude of Y determining the current size of the yield locus.

If one assumes (as in [3]) that hardening is determined by the plastic work (δw^p) done on the material during each increment of plastic strain ($\delta\epsilon_{ij}^p$), then one may construct an equivalent plastic strain increment to use in a theory of hardening as follows. The increment of plastic work (δw^p) for each increment of plastic strain ($\delta\epsilon_{ij}^p$) is

$$\delta w^p = \sigma_{ij}\delta\epsilon_{ij}^p, \tag{2}$$

where the σ_{ij} are the stress components which satisfy the yield condition and produce the required strain increment $\delta\epsilon_{ij}^p$. Now, the associated flow rule of plasticity theory requires that the plastic strain increment lie normal to the yield surface [4] (in the appropriate space) so that

$$\delta\epsilon_{ij}^p = \delta\lambda \left(\frac{\partial f}{\partial \sigma_{ij}}\right)_{f-Y=0}, \tag{3}$$

where $\delta\lambda$ is a nonnegative scalar multiplier. In attempting to identify an equivalent plastic strain ($\delta\epsilon^p$) one seeks a function of the plastic strain components ($\delta\epsilon_{ij}^p$) with the property that the product of the equivalent plastic strain increment and the equivalent yield stress is always equal to the increment of plastic work.

$$\delta\epsilon^p \cdot Y = \delta w^p = \sigma_{ij}\delta\epsilon_{ij}^p. \tag{4}$$

*Professor and Chairman, Department of Mechanical Engineering, The University of Pittsburgh. Presently Visiting Scientist, National Bureau of Standards, Washington, D.C.

[1] Figures in brackets indicate the literature references at the end of the paper.

From eq (3)

$$\delta w^p = \sigma_{ij}\delta\epsilon_{ij}^p = \delta\lambda\sigma_{ij}\frac{\partial f}{\partial\sigma_{ij}}, \tag{5}$$

and since $f(\sigma_{ij})$ has been assumed to be a homogeneous function of degree one, Euler's theorem for homogeneous functions requires

$$\sigma_{ij}\delta\epsilon_{ij}^p = \delta\lambda f = \delta\lambda Y, \tag{6}$$

the last step coming from eq (1). The desired relationship

$$Y\delta\epsilon^p = \delta w^p = \delta\lambda Y, \tag{7}$$

is satisfied by setting

$$\delta\epsilon^p = \delta\lambda. \tag{8}$$

That is, the equivalent plastic strain increment is just the nonnegative scalar multiplier $\delta\lambda$ which provides the generalized length of the plastic strain increment eq (3).

If one uses the quantity

$$||\,\delta\epsilon\,|| = (\delta\epsilon_{ij}^p\delta\epsilon_{ij}^p)^{1/2} = (\delta\epsilon_1^2 + \delta\epsilon_2^2 + \delta\epsilon_3^2)^{1/2}$$

as a measure of the magnitude of the plastic strain increment, where $\delta\epsilon_1$, $\delta\epsilon_2$, and $\delta\epsilon_3$ are the principal value of plastic strain increment, then from eq (3)

$$||\,\delta\epsilon\,|| = \delta\lambda\left(\frac{\partial f}{\partial\sigma_{ij}}\frac{\partial f}{\partial\sigma_{ij}}\right)^{1/2}. \tag{9}$$

Thus the equivalent plastic strain increment can be given as

$$\delta\lambda = \delta\epsilon^p = \frac{\sqrt{\delta\epsilon_1^2 + \delta\epsilon_2^2 + \delta\epsilon_3^2}}{\sqrt{\partial f/\partial\sigma_{ij}\partial f/\partial\sigma_{ij}}}, \tag{10}$$

for any yield locus $(f(\sigma_{ij}))$ with which one happens to be concerned. For example, in the case of the von Mises yield locus, eq (1) becomes

$$(3/2\; s_{ij}\, s_{ij})^{1/2} - Y = 0, \tag{11}$$

where $s_{ij} = \sigma_{ij} - 1/3\;\sigma_{kk}\delta_{ij}$, is the stress deviator. For this case, $\sqrt{\partial f/\partial\sigma_{ij}\partial f/\partial\sigma_{ij}} = \sqrt{3/2}$, and the equivalent plastic strain is given by

$$\delta\epsilon^p = \sqrt{2/3\;\delta\epsilon_{ij}^p\delta\epsilon_{ij}^p}, \tag{12}$$

which is the classical result. The use of eq (10) above as a rule for choosing the equivalent plastic strain increment may, at times, be complicated, because the quantity $(\partial f/\partial\sigma_{ij}\;\partial f/\partial\sigma_{ij})$ must be evaluated point by point along the yield locus. However, despite such complications one hopes that the rule offered in eq (10) will be useful as a basis for constructing measures of equivalent plastic strain.

Once the equivalent plastic strain increment has been constructed it may be used as a variable to describe the history of deformation upon which hardening depends. With the net equivalent plastic strain ϵ^p given by

$$\epsilon^p = \int \delta\epsilon^p, \tag{13}$$

(note: $\delta\epsilon^p > 0$ so that ϵ^p increases monotonically in any deformation process), one may rewrite eq (1) as

$$f(\sigma_{ij}) - Y(\epsilon^p) = 0. \tag{14}$$

Equation (14) can now be tested by comparing experimental data from various deformation histories as in [1]. Furthermore, the rate of hardening determines the magnitude of plastic strain increment where the material is at yield, under the stresses σ_{ij}, and then is subjected to an increment of stress $d\sigma_{ij}$. One may rewrite eq (3) to give the components of plastic strain increment $\delta\epsilon_{ij}^p$ in terms of the hardening rate Y' and the increase in yield stress dY required by the stress increment $d\sigma_{ij}$;

$$\delta\epsilon_{ij}^p = \frac{dY}{Y'}\frac{\partial f}{\partial\sigma_{ij}}. \tag{15}$$

The convenient formula (15) is the classical result of plasticity theory, but its derivation in the present note appears somewhat simpler than those usually found in the literature.

3. References

[1] Sidebottom, O. M. (1971), Note on effective plastic strain for a Tresca material, J. Appl Mech (Dec. 1971).

[2] Sato, Y., and Shegunice, S. (1971), Yielding of mild steel under biaxial state of uniform stress, Bul Japan Soc M.E. **14**, 72.

[3] Hill, R. (1950), The Mathematical Theory of Plasticity (Clarendon Press, Oxford, England).

[4] Bishop, J., and Hill, R. (1951), A theory of the "Plastic distortion of a polycrystalline aggregate under combined stress," Phil Mag **42**, 414–427.

(Paper 76C1&2–332)

JOURNAL OF RESEARCH of the National Bureau of Standards—C. Engineering and Instrumentation
Vol. 76C, Nos. 1 and 2, January–June 1972

Publications of the National Bureau of Standards*

Citations With Selected Abstracts

Argentar, H., **Determination of the degree of polymerization of a polymeric amine from NMR data using a "least-squares" approach,** *J. Polymer Sci.* **9,** *Part B, 657–659 (1971).*

Key words: Aromatic amine; multiple regression analysis; nuclear magnetic resonance; polymer; proton magnetic resonance; spectroscopy.

A polymeric amine, the reaction product of 3,5-xylidine and the diglycidyl ether of bisphenol A, which had been synthesized and reported elsewhere, was analyzed by nuclear magnetic resonance spectroscopy (NMR). A statistical method was derived to estimate the degree of polymerization based on linear multiple regression analysis of the intensity of the NMR absorption peaks.

Baker, M. A., **1939 Exposure test of porcelain enamels on steel 30-year inspection,** *Nat. Bur. Stand. (U.S.), Bldg. Sci. Ser. 38, 9 pages (Aug. 1971) 25 cents, SD Catalog No. C13.29/2:38.*

Key words: Acid resistance; color; gloss; porcelain enamel; weather resistance.

The weather resistance of 192 porcelain enameled panels representing 14 enamel types was evaluated after being exposed for 30 years at Washington, D.C. A direct correlation was found between the acid resistance and weather resistance of the enamels tested. The porcelain enamel protected the base metal from corrosion if the initial coverage was complete.
Similar evaluations and findings were made on 58 panels representing 13 enamel types that were added to this test in 1947.

Ballantyne, J. P., Yakowitz, H., Munro, E., Nixon, W. C., **Analysis of a variable geometry cylindrical detector for the scanning electron microscope,** *Proc. 25th Anniversary Meeting of the Electronmicroscopy and Analysis Institute Physics Group Conference, Cambridge, England, June 29–July 1, 1971, pp. 194–197 (1971).*

Key words: Electron detector; image contrast; magnetic domains; scanning electron microscope.

The cylindrical detector described by Banbury and Nixon (1969) provides enhanced contrast and directional information from many SEM specimens. This paper describes an initial theoretical analysis of such a detector.

Barbrow, L. E., Coordinator, **U.S. Metric Study Interim Report. The manufacturing industry,** *Nat. Bur. Stand. (U.S.), Spec. Publ. 345–4, 172 pages (July 1971) $1.25, SD Catalog No. C13.10:345–4.*

Key words: International System of Units; manufacturing industry; metric conversion; metric system; metric usage; metrication; metrication, attitudes toward; metrication, costs and benefits of; metrication, impact of; SI; U.S. Metric Study.

This publication reports the results of a study to assess the impacts of increasing metric usage—past, present and future—on U.S. manufacturing industry. The study, conducted pursuant to the U.S. Metric Study Act, is based on responses from more than 2,000 manufacturing companies. Information was obtained on: past and present experience with use of the metric system, including advantages and disadvantages thereof, and the views of the firms with regard to future U.S. policy—whether the country should continue its laissez faire approach to metric usage, or should undertake some sort of national program to encourage more widespread use of metric weights and measures. A separate survey of a smaller number of selected firms obtained detailed information as to estimated cost impact of a national metrication effort.

Barbrow, L. E., Coordinator, **U.S. Metric Study Interim Report. Department of Defense,** *Nat. Bur. Stand. (U.S.), Publ. 345–9, 132 pages (June 1971) $1.25, SD Catalog No. C13.10:345–9.*

Key words: Department of Defense; International System of Units; metric conversion; metric system; metrication; metrication, costs and benefits of; metrication, impact of; SI; U.S. Metric Study.

This publication reports the results of a Department of Defense study, conducted pursuant to the U.S. Metric Study Act, to determine and evaluate the advantages and disadvantages, including impact on operational capability, that would attend adoption of the International System of units of weights and measures (otherwise known as the Modernized Metric System) for use in the Department (DoD). The report includes estimates for each of the major components of the DoD of the costs of a transition to metric system usage. In addition to discussing the specific advantages and disadvantages that would be expected within the Department, the report describes the dependence of the DoD on the National Industrial Base, and discusses how this interaction would be involved in a national metrication effort.

Barnes, J. A., **A non-mathematical discussion of some basic concepts of precise time measurement,** *Frequency* **2,** *No. 2, 1–6 (Tracor, Inc., Austin, Texas, May 1971).*

Key words: Atomic time; standards; time; time standards, universal time.

A non-mathematical discussion of some of the basic concepts which must be understood by scientists and engineers who need to use precise time. It distinguishes between the concepts of date and time interval, describes the various scales used to measure astronomical and atomic time, and compares some major characteristics of astronomical and atomic time.

Barnes, J. A., Chi, A. R., Cutler, L. S., Healey, D. J., Leeson, D. B., McGunigal, T. E., Mullen, J. A., Jr., Smith, W. L., Sydnor, R. L., Vessot, R. F. C., Winkler, G. M. R., **Characterization of frequency stability,** *IEEE Trans. Instr. Meas.* **IM-20,** *No. 2, 105–120 (May 1971).*

Key words: Allan variance; frequency; frequency stability; sample variance; spectral density; variance.

Consider a signal generator whose instantaneous output voltage $V(t)$ may be written as $V(t) = [V_0 + \epsilon(t)] \sin [2\pi\nu_0 t + \psi(t)]$ where V_0 and ν_0 are the nominal amplitude and frequency respectively of the output. Provided that $\epsilon(t)$ and $\psi(t) = \frac{d\psi}{dt}$ are sufficiently small for all time t, one may define the fractional instantaneous frequency deviation from nominal by the relation $y(t) \equiv$

$\frac{\psi(t)}{2\pi\nu_0}$. A proposed definition for the measure of frequency stability is the spectral density $S_y(f)$ of the function $y(t)$ where the spectrum is considered to be one-sided on a per hertz basis.
An alternative definition for the measure of stability is the infinite time average of the sample variance of two adjacent averages of $y(t)$; that is, if

$$\bar{y}_k = \frac{1}{\tau}\int_{t_k}^{t_k+\tau} y(t)\,dt,$$

where τ is the averaging period, $t_{k+1} = t_k + T$, $k = 0, 1, 2 \ldots$, t_0 is arbitrary, and T is the time interval between the beginnings of two successive measurements of average frequency; then the second measure of stability is

$$\sigma_y^2(\tau) \equiv \left\langle \frac{(\bar{y}k+1 - y_k)^2}{2} \right\rangle,$$

where $\langle\ \rangle$ denotes infinite time average and where $T = \tau$.
In practice, data records are of finite length and the infinite time averages implied in the definitions are normally not available; thus estimates for the two measures must be used. Estimates of $S_y(f)$ would be obtained from suitable averages either in the time domain or the frequency domain. An obvious estimate for $\sigma_y^2(\tau)$ is

$$\sigma_y^2(\tau) \approx \frac{1}{m}\sum_{k=1}^{m} \frac{(\bar{y}_{k+1} - \bar{y}_k)^2}{2}.$$

Parameters of the measuring system and estimating procedure are of critical importance in the specification of frequency stability. In practice, one should experimentally establish confidence limits for an estimate of frequency stability by repeated trials.

Barnes, I. L., Sappenfield, K. M., Shields, W. R., **The mass spectrometric analysis of subpicogram quantities of lead,** *(Proc. Int. Conf. Mass Spectroscopy, Kyoto, Japan, 1970), Chapter in Recent Developments in Mass Spectroscopy, K. Ogata and T. Hayakawa, Ed., pp. 682–687 (University of Tokyo Press, Tokyo, Japan, 1970).*

Key words: Lead; mass spectrometer; microsample.

An analytical method has been developed which gives stable measurable ion beams from samples containing 10^{-8} to 10^{-14} grams of lead.
Using a two stage twelve inch radius mass spectrometer equipped with an ion multiplier and electronics for fast pulse counting, a series of chemical microstandards loaded with known quantities of NBS standard lead samples (as small as 10^{-14} grams of lead) were analyzed. These analyses showed that accuracy and precision of better than 0.5 percent (95% L. E. for a single analyses) could be obtained and that usually, the accuracy and precision were limited only by random counting statistics.
A series of quantitative analyses were done with two microgram or smaller samples taken from a single wafer of a silicate glass of known composition by the method of isotopic dilution. The required "spiking" of the sample was done utilizing an NBS Microstandard Ion Exchange Bead loaded with lead of known weight and composition.
The results obtained show severe cross-sectional variations of lead in the sample and demonstrate the importance of careful handling of samples for trace element analysis.
The use of the technique for the direct analyses of small crystals and/or particles is described. In this use only minimal chemical treatment is necessary thus eliminating most, if not all, of the usual sources of contamination and all chemical treatment may be performed directly on the mass spectrometer filament.

Beatty, R. W., Fentress, G. H., **A simple tuning circuit for waveguide and transmission line systems,** *IEEE Trans. Microwave Theory Tech.* **MTT-19,** *No. 3, 337–338 (March 1971).*

Key words: Impedance measurement; microwaves; null adjustments; reflection coefficient measurement; tuners; tuning circuit.

A simple tuning circuit for source or load matching is described that makes possible smooth and sensitive adjustments with no "holes" in frequency coverage over a complete waveguide band. Energy is coupled out of the mainline, the phase and magnitude adjusted with phase shifter and attenuator and fed back into the mainline to cancel the reflected signal. A simple analysis of the circuit is presented, and a graph given for estimating the maximum voltage standing-wave (VSWR) that can be "tuned out". Application to measurement of reflection coefficient or to impedance is proposed.

Beers, J. S., **Testing of cover glasses for hemacytometer chambers,** *Nat. Bur. Stand. (U.S.), Tech. Note 579, 7 pages (Sept. 1971) 20 cents, SD Catalog No. C13.46:579.*

Key words: Cover glass, test method for; hemacytometer; interferometry, planarity.

If cover glasses used with hemacytometer chambers are not sufficiently flat, a volume error, causing erroneous blood cel counts, may be introduced in the chamber. This document describes a method of testing cover glasses for conformity to a planarity specification.

Benjamin, I. A., **Research needs in fire and smoke control,** *Proc. Symp. Fire Hazards in Buildings, Semiannual Meeting, American Society of Heating, Refrigerating and Air-Conditioning Engineers, San Francisco, Calif., Jan. 19–22, 1970, pp. 35–38 (1971).*

Key words: Building design; dampers; ducts; fire control; fire spread; smoke movement.

The author discusses problems associated with the movement of smoke and fire in buildings and reviews some of the current design requirements. Selected areas of needed research are pointed out and mention is made of some of the work being conducted by the Fire Research Section of the National Bureau of Standards.

Bennett, L. H., Carter, G. C., **Enhanced lever rule for high-precision phase diagram determination,** *Met. Trans.* **2,** *3079–3081 (Nov. 1971).*

Key words: Alloys; high-precision; lever rule; nuclear magnetic resonance; phase diagrams.

A description is given of the conditions under which high-precision phase boundary determinations result from the application of the lever rule. This high precision results from a multiplication factor to the lever rule ratio, which is present only for experiments sampling one elemental site at a time. The multiplication factor is larger for smaller solubility limits. Precision of tenths of a percent can be readily attained under the indicated conditions. An example involving the ^{115} in nuclear magnetic resonance for the determination of the solubility of $AuIn_2$ in $AuAl_2$ is presented.

Blaine, R. L., Arni, H. T., **Interrelations between cement and concrete properties, Part 5,** *Nat. Bur. Stand. (U.S.), Bldg. Sci. Ser. 35, 129 pages (Nov. 1971) $1.25, SD Catalog No. C13.29/2:35.*

Key words: Absorption; autogenous healing; durability factor; dynamic modulus of elasticity; saturation coefficient.

The concretes described in earlier parts of this series were subjected to laboratory freezing and thawing tests, and measurements were made of the weight loss, dynamic modulus, durability factor, and number of cycles required to reach 40 percent reduction in dynamic modulus. Companion specimens were subjected to drying and subsequent soaking in the laboratory and to dynamic modulus tests at various ages and moisture conditions. The effect on these properties of a large number of variables connected with chemical and physical properties of the cements and with properties of the concretes was studied by multivariable regression techniques. Air content of the concretes and degree of saturation generally had the greatest effect on the measurements. In gen-

eral, minor constituents and trace elements did not show significant relationships with the measured properties, but there was evidence that some of the variables, such as alkali content, water cement ratio, slump, and possibly setting time might have influenced durability through an effect on the air-void system. Specimens stored in the fog room after the freezing-and-thawing tests generally regained most or all of their original dynamic modulus. There were significant differences between cements with respect to regain of dynamic modulus (autogenous healing), with the non-air-entrained cements gaining more than the air-entraining cements, on the average.

Blair, B. E., **Time and Frequency: A bibliography of NBS literature,** *Published July 1955–December 1970, Nat. Bur. Stand. (U.S.), Spec. Publ. 350, 52 pages (June 1971) 55 cents, SD Catalog No. C13.10:350.*

Key words: Atomic clocks; atomic standards; clock dissemination; crystal oscillators; definition of second; flicker noise; frequency; frequency stability; lasers; length standards; measurement standards; spectral density; standard frequency broadcasts; speed of light; statistics of time/frequency measurements; time; time/frequency dissemination; time scales; timing (HF, LF, satellite, TV, VLF); wavelengths standards; WWV; WWVB; WWVH; WWVL.

This publication gives bibliographic references to NBS time and frequency papers (principally those of the Time and Frequency Division or its predecessor sections) published over the past 15 years. The NBS material is classified under five general sections: Time and Frequency Standards; Time Scales, Time; Distribution/Reception of Time and Frequency Signals; Statistics of Time and Frequency Analyses, Frequency Stability; and General, Summary, and Status Reports. An additional section lists outside publications which describe the use of NBS time and frequency services or illustrate their varied use in seismic research, industrial practice, navigation, and propagation studies, among others. The bibliography documents past progress, will aid access to available literature, and gives an indication of the present direction, scope, and status of NBS time and frequency research.

Blandford, J. M., Baker, H. A., **Sewing threads for the apparel industry,** *Apparel Research Foundation, Inc., Washington, D.C., pp. 1–153 (May 15, 1971).*

Key words: Apparel Industry; Industry, apparel; performance, sewing thread; properties, sewing thread; quality control, sewing threads; sewing threads; Testing Programs, Sewing Thread; Tests, Sewing Thread; Thread Properties; Threads, Sewing.

The objectives, development, and achievements of the National Bureau of Standards (NBS) Sewing Thread Project, carried out in collaboration with The Apparel Research Foundation, Inc. (ARF) are discussed.
The results of two questionnaire surveys conducted among thread and apparel companies are summarized, as are the opinions expressed by thread and apparel manufacturers on industry-wide adoption of a uniform thread-sizing system.
Included are tabulations, graphs, and a statistical analysis of NBS tests of threads representative of those currently used by the apparel industry: soft and mercerized cotton; core and spun polyester; and nylon.
Testing programs for evaluating 1) the quality of threads purchased by the apparel manufacturer, and 2) the performance of threads in the apparel product, are discussed in detail. The following information is tabulated: testing procedures and evaluation materials employed; and sources of supply and approximate prices of the equipment and evaluation materials. Supplementing the text are reprints of the 21 referenced test methods.

Blandford, J. M., Bensing, P. L., **Testing programs for the apparel industry. Evaluation of material and components—Parts I and II,** *Part I, 35 pages (2nd ed. May 15, 1971); Part II, 249 pages (May 15, 1971).*

Key words: Apparel industry; equipment, textile testing; industry, apparel; performance, apparel materials; properties, apparel; quality control, apparel industry; testing programs, apparel industry; test methods, textile; textile testing, apparel materials.

This publication presents the details of minimum, intermediate, and advanced textile testing programs for evaluating the appearance and performance of materials and components used by the apparel industries. Tabulations give testing equipment, properties its use may determine, testing procedures and evaluation materials employed, and sources of supply and approximate prices of the equipment and evaluation materials.
Included are: 1) sections on the significance of a textile testing program, conditioning for testing textiles, performance requirements for textile fabrics, (American National Standard L22), evaluation of fabric defects, and the availability of short laboratory training courses for apparel company employees; 2) bibliography; 3) reprints of the 68 referenced test methods.

Blunt, R. F., Candela, G. A., Forman, R. A., Kahn, A. H., Mangum, B. W., **Magnetic susceptibility and optical studies of Cr^{3+} in Al_2O_3 (Ruby): Magnetic method for determining concentration,** *J. Appl. Phys.* **42,** *No. 8, 3058–3062 (July 1971).*

Key words: Concentration determination; magnetic susceptibility; optical absorption coefficient; radiation damage; ruby.

Magnetic susceptibility and optical absorption measurements were performed on ruby samples of varying chromium concentration. Susceptibilities were measured by the Faraday method, both with and without selective microwave saturation of the Cr^{3+} susceptibility at resonance. The susceptibility values were used to calculate the Cr^{3+} concentrations, and these together with the optical absorption used to obtain the "molar" absorption coefficients. The absorption coefficien of 56.8 ± 0.2 cm^{-1} per wt% equivalent Cr_2O_3, for both the 0.40 and 0.56 μm band maxima ($E \perp c$) resulted. A Co^{60} γ-irradiation was performed and the susceptibility was unchanged within experimental error.

Bowen, R. L., Argentar, H., **Amine accelerators for methacrylate resin systems,** *J. Dental Res.* **50,** *No. 4, 923–928 (July/August 1971).*

Key words: Amine accelerators; aromatic amines; color stability; methacrylate esters; polymerization; synthesis.

Tertiary aromatic amines were synthesized with various nitrogen and ring substituents. They were compared with commerical homologues using composites based on dimethacrylate monomer formulations containing benzoyl peroxide. Equimolar amounts of the different amines were the only variables. Although accelerating ability was a function of both ring and nitrogen substitution, color stability was influenced more by the substituents on the ring than by the substituents on the nitrogen.

Brandenberger, H., Hadron, F., Halford, D., Shoaf, J. H., **High quality quartz crystal oscillators: Frequency domain and time domain stability,** *Proc. 25th Frequency Control Annual Symp. Atlantic City, N.J., April 26–28, 1971. pp. 226–234 (Electronic Industries Association, Washington, D.C., April 1971).*

Key words: Allan variance; flicker of phase noise; frequency stability; oscillator noise models; phase noise spectral density; quartz crystal oscillator; time domain stability.

We measured the frequency stability of a pair of commercial 5-MHz quartz crystal oscillators which incorporate improved electronic design for enhanced short-term stability. The spectral density (frequency domain) of the phase noise, per oscillator, measured by each of our two laboratories, is

$$S_{\delta\phi} = +(10^{-11.8}\ \text{radians}^2\ \text{Hz}^2)\frac{1}{f^3} + (10^{-12.5}\ \text{radians}^2)\frac{1}{f} + (10^{-14.4}\ \text{radians}^2\ \text{Hz}^{-1})f^0,$$

over the range of about 10^{-2} Hz to 10^{+3} Hz.

Brauer, G. M., **A review of recent studies of *In Vitro* reactivity of surfaces of calcified tissues,** (*Proc. Int. Symp. Calcified Tissues, Dental and Surgical Materials and Tissue Material Interactions, University of Nijmegen, Nijmegen, The Netherlands, 1970*), *Dent. Tissues Mater. pp. 193–231 (1971).*

Key words: Adhesion to tooth surfaces; adsorption on calcified tissues; bone; calcified tissues; dentin; enamel; modification of tooth surfaces; reactivity of calcified tissues.

Studies of the reactivity and modification of the surfaces of calcified tissues offer an attractive approach for obtaining useful information to reduce dental caries and improve adhesion between tooth structure and restoratives. Investigation of the interaction of gases on such surfaces provides considerable insight into the structural details of surfaces of hard tissues. Effectiveness of potential conditioning agents can be demonstrated from alterations of the surface properties of teeth or bone as indicated by changes in: critical surface tension, oil-wettability, adsorption isotherms and adhesion-ability. Measurement and evaluation of heats of immersion and heats of reaction are useful for observing modifications and determining those groups that bond to tooth structure in aqueous environments. Application of dilute polyfunctional acids removes debris, etches enamel and increases surface wettability. Etching creates an increased surface area and opens pores into which resin can flow. Excellent adhesion is obtained after hardening because of mechanical interlocking of resin at the enamel-resin interphase. Long side chains have been grafted to collagenous surfaces (collagen powder or film, bone). Grafting monomers containing additional functional groups that are potential reactive centers for further modification is feasible. Surfaces with the desired degree of hydrophil-lipophil balance to suit specific applications can be prepared.

Braun, W., Peterson, N. C., Bass, A. M., Kurylo, M. J., **A vacuum ultraviolet atomic emission detector: Quantitative and qualitative chromatographic analysis of typical C, N, and S containing compounds,** *J. Chromatog.* **55,** *237–248 (1971).*

Key words: Analytical; atomic emission; detector; gas chromatography; spectroscopy; vacuum ultraviolet.

Vacuum ultraviolet atomic emission detection of effluent gases from a chromatographic column is a very sensitive and selective method for qualitative and quantitative elemental analysis of carbon, nitrogen and sulfur compounds. A low pressure microwave discharge through helium, with added trace amounts of molecular oxygen produced complete fragmentation of all compounds used and generated intense atomic emissions in the vacuum ultraviolet. Photometric measurement of these monochromator-isolated atomic emissions was successfully used to establish absolute concentration calibrations for the elements carbon, sulfur and nitrogen in various compounds. This detection method is sensitive, highly selective and has a range of linearity greater than four decades.

Breden, L. H., Technical Standards Coordinator, **Fluorinated ethylene-propylene (FEP) plastic tubing,** *Nat. Bur. Stand. (U.S.), Prod. Stand. 43–71, 12 pages (Sept. 1971) 10 cents, SD Catalog No. C13.20/2:43–71.*

Key words: Chemical, mechanical, and electrical tubing; FEP tubing; fluorocarbon plastic tubing; plastic tubing, fluorinated ethylene-propylene; tubing, FEP-fluorocarbon.

This Voluntary Product Standard covers plastic tubing made from fluorinated ethylene-propylene (FEP) resin intended for chemical, mechanical, or electrical use. It provides requirements and methods of test for materials, dimensions, and physical and chemical properties of FEP tubing. A method for identifying products which comply with this standard is provided.

Breden, L. H., Technical Standards Coordinator, **Heat-shrinkable fluorocarbon plastic tubing,** *Nat. Bur. Stand. (U.S.), Prod. Stand. 47–71, 14 pages (Sept. 1971) 20 cents, SD Catalog No. C13.20/2:47–71.*

Key words: FEP heat-shrinkable tubing; fluorocarbon plastic heat-shrinkable tubing; plastic tubing fluorocarbon; PTFE heat-shrinkable tubing; tubing, heat-shrinkable fluorocarbon plastic.

This Voluntary Product Standard covers commercially available PTFE and FEP plastic tubing which can be reduced to a predetermined inside diameter by the application of heat. Included are requirements and methods of test for materials, dimensions, and physical and electrical properties. A method for identifying products which comply with this standard is provided.

Breden, L. H., Editor, **World index of plastics standards,** *Nat. Bur. Stand. (U.S.), Spec. Publ. 352, 458 pages (Dec. 1971)* ***$5.50, SD Catalog No. C13.10:352.***

Key words: Index of plastics standards; plastics standards, world index; standards, plastics.

This computer-produced Index contains the printed titles of more than 9,000 national and international standards on plastics and related materials which were in effect as of December 31, 1970. These standards are published by technical societies, trade associations, government agencies and military organizations. The title of each standard can be found under all the significant key words which it contains. These key words are arranged alphabetically down the center of each page together with their surrounding context. The date of publication or last revision, the standard number, and an acronym designating the standard-issuing organization appear as part of each entry. A list of these acronyms and the names and addresses of the organizations which they represent are found at the beginning of the World Index.

Brenner, A., Sligh, J. L., **Electrodeposition of magnesium and beryllium from organic baths,** *Trans. Inst. Metal Finishing* **49,** *71–78 (May 1971).*

Key words: Beryllium; beryllium azide; beryllium thiocyanate; decaborane; dimethyl beryllium; electrodeposition of; Grignard reagents; magnesium; non-aqueous plating baths; organic plating baths; triethylboron.

Solutions that are feasible for electrodepositing magnesium were prepared from Grignard reagents with the addition of boranes in ether solutions. A typical bath consisted of methylmagnesium chloride, 3-molar, (dissolved in tetrahydrofuran) and 1-molar in triethylboron. The deposits were white, ductile, and contained at least 99% of Mg. Cathode and anode current efficiences were 100%. A similar beryllium plating solution, prepared with beryllium dimethyl and decaborane, yielded dark grey, coherent deposits containing 85% to 90% beryllium.

Brenner, D. J., **A technique for measuring the surface temperature of transistors by means of fluorescent phosphor,** *Nat. Bur. Stand. (U.S.), Tech. Note 591, 49 pages (July 1971) 50 cents, SD Catalog No. C13.46:591.*

Key words: Surface temperature; temperature measurement; temperature-sensitive phosphor; thermographic phosphor; transistor-chip temperature.

A technique that uses temperature-sensitive phosphor (TSP) to make quantitative measurements of transistor-chip surface temperatures over the range of 170–210 °C is described. The experimental procedure consisted of depositing a thin coating of phosphor on uncapped power transistors, and then photographing the visible fluorescence generated under near-ultraviolet (uv) excitation. The cooler regions produced a brighter fluorescence than the hotter areas. The surface temperatures of operating transistors were determined by comparing, on a point-by-point basis, the photographic density of operating photographs to the density of a family of calibration photographs. Repeated temperature measurements always fell within a 4 °C overall error range when the phosphor surface was scanned with a 25 x 25 μm aperture. The error band dropped to less than 2 °C when a 50 x 50 μm aperture was used. Coarseness of the phosphor coating seemed to limit spacial resolution to about 20 μm. Any narrow temperature range between 20 and 400 °C can probably be measured by selecting a suitable level of uv irradiation and/or a suitable phosphor.

Broadhurst, M. G., Mopsik, F. I., **Normal mode calculation of Grüneisen thermal expansion in *n*-alkanes,** *J. Chem. Phys.* **54,** *No. 104239–4246 (May 15, 1971).*

Key words: Entropy; Grüneisen relation; quasiharmonic; semirigid; specific heat; thermodynamic.

The normal mode problem is solved for a semirigid chain of beads in a quasiharmonic potential in order to separate the inter- and intrachain parts of the specific heat. The effects of lattice vibrations are included in an approximate way. The usual Grüneisen relation. $\alpha B_T = \gamma C_v / V$, valid only for acoustical modes, is generalized for optical modes to give $\alpha B_p = \Sigma_j (\gamma_j / V)\ (\partial S_j / \partial\ ln\ \omega_{jmax})$, where S_j and ω_{jmax} are the entropy and frequency cutoff of mode j. The predicted thermodynamic properties of the system are unusually sensitive to chain length because of interchain thermal energy effects. The parameters are given values from independent solid n-alkane data, and the calculated results are shown to predict quite well experimental C_p and V–T behavior of the n-alkanes.

Brown, D. W., Lowry, R. E., Wall, L. O., **Radiation-induced polymerization at high pressure of 2,3,3,3-tetrafluoropropene in bulk and with tetrafluoroethylene,** *J. Polymer Sci. Part* **A-1,** *9, 1999–2007 (1971).*

Key words: High pressure; polymerization; radiation; tetrafluoroethylene; tetrafluoropropene.

The radiation-induced polymerization of 2,3,3,3-tetrafluoropropene was studied as a function of temperature (22–100° C) and pressure (autogenous to 10^4 atm). Rates have varied 100 fold for the same reaction conditions probably because of trace impurities. The most rapidly polymerizing material has a rate of 4.5%/h at 6000 atm, 22 °C, and 1500rad/h. The activation enthalpy and volume are 4kcal/mole and 13cm^3/mole, respectively. Rates are proportional to the square root of the radiation intensity. Degrees of polymerization varied between 2×10^3 and 2×10^6. In copolymerization with tetrafluoroethylene the reactivity ratios at 22 °C and 5000 atm are 0.37 (the ratio for addition to the tetrafluoroethylene-ended radical) and 5.4 (the ratio for addition to the tetrafluoropropene-ended radical). Comparison of ratios for the copolymerization of other fluorine-containing monomers with tetrafluoroethylene shows that they generally disfavor incorporation of the latter.

Brown, W. E., **Physicochemical aspects of decay and decalcification,** *(Proc. Int. Symp. Calcified Tissues, Dental and Surgical Materials and Tissue Material Interactions, University of Nijmegen, Nijmegen, The Netherlands, 1970), Dent. Tissues Mater. pp. 69–97 (1971).*

Key words: Calcium phosphate; caries; caries mechanism; enamel; hydroxyapatite.

Standard thermodynamic concepts (chemical components, chemical potential of the acid responsible for dissolution is a variable that and steady-state models for the caries mechanism. The chemical potential of the acid responsible for dissolution is a variable that ranks in importance with pH and needs to be given far greater consideration. Another variable of great value is $\bar{U}(\pm)$ which is a measure of excess base over acid in the solution, and is defined by $\bar{U}(\pm)\ \Sigma_j c_j z_j = -\Sigma_i c_i z_i$, where i is summed over the ions present in the system $Ca(OH)_2 - H_3PO_4 - H_2O$ and j is summed over the ions foreign to this system.
Variability in the solubility of tooth mineral is a major factor in causing the extended form of the caries lesion. A possibly very important factor in determining the speed with which the lesion develops is the relative rate of transport of calcium ions relative to that of the phosphate ions. An unequivocal interpretation of the Donnan-membrane effect, described by von Bartheld, is not possible because even though the pH within the tooth may be tooth mineral, solubility.

Bullis, W. M., Editor, **Methods of measurement for semiconductor materials, process control, and devices,** *Quarterly Report October 1 to December 31, 1970, Nat. Bur. Stand. (U.S.), Tech. Note 592, 72 pages (Aug. 1971) 70 cents, SD Catalog No. C13.46:592.*

Key words: Alpha-particle detectors; aluminum wire; base transit time; carrier lifetime; die attachment; electrical properties; epitaxial silicon; gamma-ray detectors; germanium; gold-doped silicon; metallization; methods of measurement; microelectronics; microwave devices; nuclear radiation detectors; probe techniques (a-c); resistivity; semiconductor devices; semiconductor materials; semiconductor process control; silicon; thermal resistance; thermographic measurements; ultrasonic bonder; wire bonds.

This quarterly progress report, tenth of a series, describes NBS activities directed toward the development of methods of measurement for semiconductor materials, process control, and devices. Significant accomplishments during this reporting period include successful application of the surface photovoltage technique, a non-contacting method, to the measurement of carrier diffusion length in silicon epitaxial layers and development of a novel, but simple, method for measurement of acceleration and terminal angular velocity of a photoresist spinner. Work is continuing on measurement of resistivity, carrier lifetime, and electrical inhomogeneities in semiconductor crystals; specification of germanium for gamma-ray detectors; evaluation of wire bonds, metallization adhesion, and die attachment; measurement of thermal properties of semiconductor devices, transit-time and related carrier transport properties in junction devices, and electrical properties of microwave devices; and characterization of silicon nuclear radiation detectors. Supplementary data concerning staff, standards committee activities, technical services, and publications are included as appendixes.

Bullis, W. M., **Methods of measurement for semiconductor materials, process control, and devices.** *Quarterly Report January 1 to March 31, 1971, Nat. Bur. Stand. (U.S.), Tech. Note 598, 54 pages (October 1971) 55 cents, SD Catalog No. C13.46:598.*

Key words: Alpha-particle detectors; aluminum wire; base transit time; carrier lifetime; die attachment; electrical properties; epitaxial silicon; gamma-ray detectors; germanium; gold-doped silicon; methods of measurement; microelectronics; microwave devices; nuclear radiation detectors; probe techniques (a-c); resistivity; semiconductor devices; semiconductor materials; semiconductor process control; silicon; thermal resistance; thermographic measurements; ultrasonic bonder; wire bonds.

This quarterly progress report, eleventh of a series, describes NBS activities directed toward the development of methods of measurement for semiconductor materials, process control, and devices. Significant accomplishments during this reporting period include application of tuning and other related procedures for ultrasonic wire bonders in an industrial environment with a reported reduction of rejection rate at visual inspection by more than a factor of two, more complete evaluation of the photovoltaic method for determining radial resistivity profiles of circular semiconductor wafers, and identification of test conditions in which a d-c calibration curve may properly be used in measurements of thermal resistance. Work is continuing on measurement of resistivity, carrier lifetime, and electrical inhomogeneities in semiconductor crystals; specification of germanium for gamma-ray detectors; evaluation of wire bonds and die attachment; measurement of thermal properties of semiconductor devices, transit-time and related carrier transport properties in junction devices, and electrical properties of microwave devices; and characterization of silicon nuclear radiation detectors. Supplementary data concerning staff, standards committee activities, technical services, and publications are included as appendixes.

Bullis, W. M., Editor, **Methods of measurement for semiconductor materials, process control, and devices,** *Quarterly Report—April 1 to June 30, 1971, Nat. Bur. Stand. (U.S.), Tech. Note 702, 45 pages (Dec. 1971) 50 cents, SD Catalog No. C13.46:702.*

Key words: Alpha-particle detectors; aluminum wire; base transit time; carrier lifetime; die attachment; electrical properties; epitaxial silicon; gamma-ray detectors; germanium; gold-doped silicon; methods of measurement; microelectronics; microwave devices; nuclear radiation detectors; probe techniques (a-c); resistivity; semiconductor devices; semiconductor materials; semiconductor process control; silicon; thermal resistance; thermographic measurements; ultrasonic bonder; wire bonds.

This quarterly progress report, twelfth of a series, describes NBS activities directed toward the development of methods of measurement for semiconductor materials, process control, and devices.

Significant accomplishments during this reporting period include a demonstration of the high sensitivity of the infrared response technique by the identification of gold in a germanium diode doped to a level of 10^{11} gold atoms per cubic centimeter, verification that transient thermal response is significantly more sensitive to the presence of voids in die attachment than steady-state thermal resistance, and development of a simplified circuit for screening transistors for susceptibility to hot-spot formation by the current-gain technique. Work is continuing on measurement of resistivity of semiconductor crystals; study of gold-doped silicon; specification of germanium for gamma-ray detectors; evaluation of wire bonds and die attachment; measurement of thermal properties of semiconductor devices, transit time and related carrier transport properties in junction devices, and electrical properties of microwave devices; and characterization of silicon nuclear radiation detectors. Supplementary data concerning staff, standards committee activities, technical services, and publications are included as appendixes.

Burdick, M. D., **A test for the cleanability of surface finishes,** *Porcelain Enamel Inst. Bull.* **T-28,** *pp. 1–17 (1971).*

Key words: Cleanability; cleanability index; fluorescence; porcelain enamel; standard reference surface.

A detailed procedure is given to permit a numerical evaluation of the cleanability of surfaces. The method employs a fluorescent, water soluble soiling agent, a mechanized procedure for its application and partial removal, the water extraction of the retained soil and the calculation of a cleanability index through the use of a standard reference surface.

Carpenter, B. S., **The use of the nuclear track technique for boron and uranium analyses in botanical material,** (*Proc. American Nuclear Society Meeting, Boston, Mass., June 17, 1971*), *Trans. Am. Nucl. Soc.* **14,** *No. 1, 130–131 (1971).*

Key words: Alpha tracks; boron; botanical material; fission tracks; kale; orchard leaves; uranium.

The Nuclear Track Technique is used to determine trace quantities of boron and uranium in botanical materials. This technique uses both method of standard additions and the absolute method in its determinations.

Carpenter, R. J., Forman, R. A., **Zeeman modulator for nuclear quadrupole resonance spectroscopy,** *J. Phys. E: Sci. Instr.* **3,** *922–924 (November 1970).*

Key words: Current; modulator; nuclear; pulse; quadrupole; resonance; spectroscopy; transistor; Zeeman.

An instrument has been developed to drive modulation coils to produce Zeeman modulation in nuclear quadrupole resonance spectroscopy. A sequence of alternately negative and positive current pulses of up to 4A, spaced by no-current intervals, is produced. The frequency may be as high as 500 Hz, since no electromechanical components are employed. The instrument is described in detail and sample resonance curves are presented.

Carter, R. S., **The NBS reactor as a source of neutrons,** *Proc. American Nuclear Society Topical Meeting on Neutron Sources and Applications, April 19-21, 1971 Augusta, Ga.,* **2,** *1-10-1-17 (April 1971).*

Key words: High flux; irradiation facilities; neutron source; and reactor.

The NBS Reactor (NBSR) is a 10 Mx D_20 moderated and reflected reactor. The fuel elements are located 7 inches apart in hexagonal arrays around experimental irradiation facilities. In order to support the broad range of research programs typical of a laboratory like the NBS the reactor has extensive in-core, beam tube, and pneumatic tube facilities. Thermal neutron fluxes in the beam tubes and higher-flux irradiation facilities are about 10^{14}n/cm^2-s. Several unique features of the NBSR contribute to its versatility. They include a thermal column with cadmium ratios for gold foils as high as 30,000 to 1, a split core to minimize the intensity of very high energy neutrons in the beam tubes, and a cold neutron source to enhance the intensity of very low energy neutrons available for certain inelastic scattering experiments. Extensive, automated experimental facilities have been developed to fully utilize the neutron beams and irradiations provided by the NBSR.

Cassidy, E. C., Cones, H. N., Booker, S. R., **Development and evaluation of electrooptical high-voltage pulse measurement techniques,** *IEEE Trans, Instr. Meas.* **IM-19,** *No. 4, 395–402 (Nov. 1970).*

Key words: Electro-optical measurements; high voltage measurements; Kerr cell; pulse measurements.

Use of the Kerr electrooptical effect for time-resolved pulse measurements is extended to the 300-kV level. Pulse durations are as short as 5 μs. The performance of systems equipped with Kerr cells of various designs is investigated under a variety of operating conditions. Calibrations are achieved using both pulse-divider and high direct-voltage techniques. Methods are devised for measurement and correction of errors resulting from the fringing electric field at the ends of the Kerr-cell electrodes. Measurements of the temperature coefficient of the Kerr-cell constant are also included. The pulse waveform is reconstructed from typical Kerr-system results by automatic computation and compared with simultaneous time-resolved pulse-divider measurements. Comparisons at the peak of the pulse, where a "slideback" technique is used to enhance the resolution of the divider measurement, demonstrate agreement to better than 1 percent.
In addition, a novel technique is developed for measurement of the pulse magnitude from photographs of the Kerr-effect fringe patterns produced by passing an expanded, pulsed laser beam through the system. By this approach, voltage is measured optically without use of sophisticated electrical metering instrumentation.

Cezairliyan, A., **Measurement of the variation of normal spectral emittance of tantalum during melting by a pulse heating method,** *High temperatures-High Pressures* **2,** *501–506 (1970).*

Key words: Emittance; high-speed measurements; melting; normal spectral emittance; tantalum; thermal radiation properties.

A pulse heating method was used to measure the change in normal spectral emittance (at 650 nm) of tantalum as a function of the change in electrical resistance during the initial melting period. Duration of an individual experiment in which the specimen was heated from room temperature to its melting point was approximately 400 ms. The partial melting period was approximately 100 ms. A millisecond resolution photoelectric pyrometer was used for temperature measurements. The recordings of experimental quantities were made with a digital data acquisition system which has a full-scale signal resolution of approximately one part in 8000 and a time resolution of 0.4 ms. It was found that normal spectral emittance decreased by approximately 3.5 percent during the initial one third of the melting period.

Chandler, H. H., Bowen, R. L., Paffenbarger, G. C., **Method for finishing composite restorative materials,** *J. Am. Dental Assoc.* **83,** *No. 2, 344–348 (August 1971).*

Key words: Composite restorative materials; finishing; operative dentistry; polishing; surface finish.

An instrument, designed to finish the surface of composite restorative materials, was made by bonding 1u to 5u diamond particles to flexible paper disks. The surface finish produced by this instrument was superior to that obtained by fine cuttlefish disks and inferior to surfaces obtained by the hardening of the material in contact with polished glass. Results are presented with use of scanning electron photomicrographs.

Chandler, H. H., Bowen, R. L., Paffenbarger, G. C., **Physical properties of a radiopaque denture base material,** *J. Biomed. Mater. Res.* **5,** *335–357 (July 1971).*

Key words: Composite materials; denture base materials; physical properties; prosthetic materials; radiopacity-radiopaque.

Physical properties were determined for radiopaque composite denture base materials consisting of poly(methyl methacrylate) as the matrix and 30, 40, and 50% by weight of a silane-treated barium fluoride-containing glass powder as the reinforcing filler. Specimens without glass were included for comparison.
All of the materials met the requirements of ADA Spec. No. 12 for Denture Base Polymer except that the material containing 50% glass had less deflection than the minimum required at the 5000-gm load in transverse testing.
There was little or no difference among the materials with respect to hardness, indentation resistance, water sorption, color stability, and resistance to drop impact.
Addition of glass to the 30% level decreased the transverse strength while 50% glass specimens had slightly greater transverse strengths as compared to specimens with no glass. In general, the addition of glass increased the time to reach the packing stage, densities, and Young's bulk, shear, and flexural moduli, had only slight effect on solubility and decreased the cold-cure repairability and the coefficient of linear thermal expansion.
The solubility of the glass powder was about four times that of powdered porcelain teeth after 24 h, and totaled 0.55% after 5 days.

Chandler, H. H., Bowen, R. L., Paffenbarger, G. C., **Radiopaque denture base materials technic dentures,** *J. Biomed. Mater. Res.* **5,** *359–371 (July 1971).*

Key words: Composites; dentures; denture base materials; dimensional stability; foreign bodies; prosthetics; radiopacity silane bonding.

Technic dentures were made using composite base materials containing 30, 40, and 50 wt% of a silane-treated, radiopaque, powdered glass as the reinforcing filler and poly(methyl methacrylate) as the matrix. Dentures containing no glass were included for comparison. Molar-to-molar dimensional changes, effects of silane treatment of the porcelain teeth and handling and finishing characteristics were determined.
Dentures containing glass had less dimensional change during curing and subsequent water storage than those without glass. Thick upper dentures exhibited the least change and thin lowers, the most. The differences in the magnitudes of the changes would not be clinically noticeable.
Silane treatment of the porcelain teeth in thick upper dentures resulted in breakage of the posterior teeth in almost all instances. Posterior teeth also fractured in thick upper dentures containing 40 and 50% of the silane-treated glass even though the teeth were not treated with silane.
Mixing and molding properties of the composite materials, while accepting characteristics were definitely inferior in that it was more difficult and time-consuming to attain the final surfaces and these surfaces were not as smooth as those in dentures without glass.

Clark, G., Standards Coordinator, **Bit sequencing of the code for information interchange in serial-by-bit data transmission,** *Nat. Bur. Stand. (U.S.), Fed. Info. Process. Stand. Publ. (FIPS Pub.) 16, 4 pages (1971) 10 cents, SD Catalog No. C13.52:16.*

Key words: American Standard Code for Information Interchange; ASCII; communications; data communications equipment; data processing terminal equipment; data transmission; Federal information processing standards; serial-by-bit; serial-by-character; telecommunications; teleprocessing.

This publication prescribes the method for transmitting the American Standard Code for Information Interchange (ASCII) in systems employing serial-by-bit, serial-by-character data transmission. The least significant bit (b1) is transmitted first, the most significant bit (b7) last, followed by the character parity bit (if transmitted). (See also FIPS 17, CHARACTER STRUCTURE AND CHARACTER PARITY SENSE FOR SERIAL-BY-BIT DATA COMMUNICATION IN THE CODE FOR INFORMATION INTERCHANGE.)

Clark, G., Standards Coordinator, **Character structure and character parity sense for parallel-by-bit data communication in the code for information interchange,** *Nat. Bur. Stand. (U.S.), Fed. Info. Process. Stand. Publ. (FIPS Pub.) 18, 4 pages (1971) 10 cents, SD Catalog No. C13.52:18.*

Key words: American Standard Code for Information Interchange; ASCII; character structure; communications; data transmission; Federal information processing standards; parallel-by-bit; parity sense; serial-by-character; telecommunications; teleprocessing.

This publication specifies the character structure and character parity sense for transmitting the American Standard Code for Information Interchange (ASCII) in systems employing parallel-by-bit data transmission. The seven ASCII bits (b1 through b7) plus the character parity bit (P) are assigned to an ordered series of channel designators. The most significant bit (b1) is assigned to the lowest designator and (P) to the highest designator.

Clark, G., Standards Coordinator, **Character structure and character parity sense for serial-by-bit data communication in the code for information interchange,** *Nat. Bur. Stand. (U.S.), Fed. Info. Process. Stand. Publ. (FIPS Pub.) 17, 4 pages (1971) 10 cents, SD Catalog No. C13.52:17.*

Key words: American Standard Code for Information Interchange; ASCII; character structure; character parity sense; communications; data transmission; Federal information processing standards; serial-by-bit; telecommunications; teleprocessing.

This publication specifies the character structure and character parity sense for transmitting the American Standard Code for Information Interchange (ASCII) in systems employing serial-by-bit data transmission. Characters are to be transmitted as eight bits (seven ASCII bits plus one character parity bit). The parity sense shall be odd for synchronous transmissions and even for asynchronous transmission. (See also FIPS 16, BIT SEQUENCING OF THE CODE FOR INFORMATION INTERCHANGE IN SERIAL-BY-BIT TRANSMISSION.)

Clark, R. E., Tascher, J. M., **U.S. Metric Study Interim Report. Federal Government: Civilian agencies,** *Nat. Bur. Stand. (U.S.), Spec. Publ. 345–2, 328 pages (July 1971) $2.25, SD Catalog No. C13.10:345–2.*

Key words: Federal Government; International System of Units; metric conversion; metric system; metric usage; metrication; metrication, attitudes toward; metrication, costs and benefits of; metrication, impact of; SI; U.S. Metric Study.

This publication reports the findings of a survey to ascertain the views of the civilian agencies of the Federal Government on the issues raised by the U.S. Metric Study Act. With regard to internal operations of the Federal agencies, the report covers present metric (International System of Units, or SI) usage and its advantages and disadvantages, expectations of future changes in measurement usage if the U.S. continues its laissez faire policy toward the SI, and attitudes toward a possible nationally coordinated metrication program. In the latter connection, the report contains estimates of added cost or savings impacts on agency internal operating budgets to be expected from a nominally 10-year plan ed metrication program, both during the transition and thereafter. The survey also assessed the impacts of metric usage and of its increase on the areas of responsibility of the Federal agencies in the society at large (e.g., communications, science and technology, health, labor affairs, international affairs and trade), and on the agencies' interfaces therewith.

Clifton, J. R., Mathey, R. G., **Interrelations between cement and concrete properties, part 6,** *Nat. Bur. Stand. (U.S.), Bldg. Sci. Ser. 36, 118 pages (Aug. 1971) $1.25, SD Catalog No. C13.29/36.*

Key words: Cement; chemical composition; concrete; durability; material properties; physical properties.

Data are presented on the properties of Portland cements, mortars and concretes from a long term study reported principally by Blaine and Arni.
These data are from laboratory studies and cover a wide range of cements and concretes. A total of 199 different cements were included in the study.

Cohen, J., Edelman, S., **Piezoelectric effect in oriented poly-**

vinylchloride and polyvinylfluoride, *J. Appl. Phys.* **42,** *No. 8, 3072–3047 (July 1971).*

Key words: G moduli, piezoelectricity, polyvinylchloride, polyvinylfluoride.

The direct piezoelectric effect has been observed in roll-elongated films of polyvinylchloride and polyvinylfluoride. The effect was produced by applying tensile stress to a clamped specimen at a fixed frequency of 20 Hz. The piezoelectric modulus, g_{31} was determined to be 0.2 to 0.7 V m^{-1}/N m^{-2} in polyvinylchloride; in polyvinylfluoride $g_{31} \simeq 0.2$ V m^{-1}/N m^{-2} and $g_{32} \simeq 1$ V m^{-1}/N m^{-2}. The piezoelectric effect in these films is believed to be due to mechanical distortion of oriented dipoles, resulting from the tensile stress, and the orientation appears to differ in the two materials.

Cohen, J., Edelman, S., Vezzetti, C. F., **Pyroelectric effect in polyvinylfluoride,** *Nature (London), Phys. Sci.* **233,** *12 (Sept. 6, 1971).*

Key words: Infrared; piezoelectricity; polyvinylfluoride; pyroelectricity.

Significant infra-red sensitivity has been obtained in oriented polyvinylfluoride, apparently due to pyroelectricity.

Cooper, M. J., **Generalized scaling and the parametric equation of state in the critical region,** *Chapter in Critical Phenomena in Alloys, Magnets, and Superconductors, pp. 77–87 (McGraw-Hill Book Co., Inc., New York, N.Y., 1971).*

Key words: Critical phenomena; equation of state; parametric equation of state; scaling laws.

A description of the critical region is developed using a local parametric characterization of the thermodynamic potential surface. The physical consequences of the formalism are presented and its predictions compared with some of the experimental data. Results indicate an extended description of the thermodynamic properties over a much enlarged region about the critical point.

Corliss, E. L. R., **Estimate of the inherent channel capacity of the ear,** *J. Acoust. Soc. Am.* **50,** *No. 2, 671–677 (1971).*

Key words: Articulation function of ear; "bit" capacity of ear; channel capacity of ear; distinctive features of ear and hearing; intelligibility vs word lengths as block codes; speech; speech intelligibility as channel capacity; word capacity lengths as block codes.

The growth of intelligibility of speech stimuli as a function of level above threshold can be computed from the "circuit parameters" of the hearing mechanism by applying Shannon's concepts of channel capacity, equivocation and "bits". The calculation starts from the "least count" of the ear, derived from data on the hearing process for a model resembling a frequency-selective circuit (Corliss, 1967). By considering the rate at which phonemes are produced in speaking and the number of "distinctive features" characterizing the phonemes, intelligibility functions can be predicted that agree fairly closely with random-word and random-syllable intelligibility data obtained experimentally. This agreement shows that the listener need recognize no more than a single distinctive feature of each phoneme to display the recognition functions that have been observed. The duration of correlated utterance may be considered the "code length" that has the effect of lowering the channel capacity required for polysyllabic utterances as opposed to monosyllables (Shannon, 1957). Evidently, contextual effects are not prominent in the intelligibility of random-word lists; the hearing process involved is primarily recognition of groups of sounds; meaning is secondary. The results also lead to the inference that a direct relation may exist between channel capacity and loudness perception in broadband speech transmission, and suggest that loudness functions for impaired ears might be correlated with intelligibility functions.

Corliss, Edith L. R., **Facts about hearing and hearing aids,** *Nat. Bur. Stand. (U.S.), Consumer Info. Series 4, 31 pages, (Nov. 1971) 60 cents, Stock Number 0303–0920.*

Key words: Audition; communications; hearing; hearing aids; selection of hearing aids; speech communication.

A consumers informatio publication containing information on hearing aids including selection, use, and maintenance.

Cornog, J. R., Bunten, E. D., **U.S. Metric Study Interim Report: Nonmanufacturing businesses,** *Nat. Bur. Stand. (U.S.), Spec. Publ. 345–5, 200 pages (July 1971) $1.50, SD Catalog No. C13.10:345–5.*

Key words: International System of Units; metric conversion; metric system; metric usage; metrication; metrication, attitudes toward; metrication, costs and benefits of; metrication, impact of; nonmanufacturing businesses; SI; U.S. Metric Study.

This publication, prepared pursuant to the U.S. Metric Study Act, reports on the experiences and views of nonmanufacturing businesses with regard to metric usage and its increase. The study is based on a survey of more than 2500 companies and firms primarily involved in: agriculture, forestry, fisheries, mining, construction, transportation, communications, utilities, wholesale/retail trade (including exporters/importers), finance, insurance, real estate or services. Information was obtained on: past or present experience with use of the metric system (including perceived advantages and disadvantages thereof), attitudes toward future metrication in a world of increasing metric usage (including preferred U.S. policy regarding), and estimated cost impacts and benefits which would be attendant to a national metrication program.

Coxon, B., **Application of internuclear, double-resonance techniques to carbohydrates. Detection of small coupling-constants,** *Carbohydrate Res.* **18,** *No. 3, 427–442 (1971).*

Key words: 6-Deoxy-α-D-glucofuranose derivative; General Overhauser effect; Internuclear double resonance; Magnetic equivalence factoring; spin-tickling; transient nutations.

6-Deoxy-1,2:3,5-di-*O*-isopropylidene-α-D-glucofuranose-d_{12} (**1**-d_{12}) has been synthesized by exchange of its non-deuterated analog (**1**) with acetone-d_6. The p.m.r. spectrum of **1**-d_{12} at 90 MHz has been analyzed iteratively by means of a computer program for magnetic-equivalence factoring. Confirmation of the assignments of lines in the analysis has been investigated by proton–proton, internuclear, double-resonance (i.n.d.o.r.) techniques, which served also for the detection of a small long-range coupling-constant.
Examples of i.n.d.o.r. spectra containing genera Overhauser effects, spin-tickling effects, or transient nutations are shown, and are discussed in relation to the experimental power-levels of the observing and double-resonance frequencies, and their sweep-rates.

Coxon, B., Schaffer, R., **Characterization and quantitative analysis of D-glucose for use in clinical analysis,** *Anal. Chem.* **43,** *No. 12, 1565–1570 (Oct. 1971).*

Key words: α-D-glucose, anomerization, β-D-glucose; calorimetry, clinical analysis, differential scanning calorimetry; equilibration; gas chromatography; polarimetry; proton magnetic.

The results from analysis of α-D-glucose and β-D-glucose by a variety of spectroscopic, chromatographic, and polarimetric techniques are presented and discussed. The apparent values of purity obtained for α-D-glucose by differential scanning calorimetry are discussed in relation to the content of β anomer as determined by gas chromatography and proton magnetic resonance spectroscopy. It is shown that, during melting, both α-D-glucose and β-D-glucose anomerize rapidly to give an equilibrated mixture of these anomers.

Davis, D. D., **Frequency standard hides in every color TV set,** *Electronics pp. 96–98 (May 10, 1971).*

Key words: Dissemination; frequency; frequency synthesizers; linear phase comparators; television color subcarrier; time.

In color television broadcasting, a color "subcarrier" is transmitted at about 3.58 MHz. It is used as a reference signal in the color television receiver to demodulate the chrominance sidebands. The major U.S. networks use rubidium frequency standards to generate

the color subcarrier. This paper describes a method for making use of the color subcarrier as a frequency standard. The output of a 1 or 5 MHz local standard synthesized to 3.58 MHz is used as one input to a phase comparator and is adjusted to agree with the received subcarrier signal. Results of actual network measurements are given.

Davis, J. E., **The dry and wet bulb psychrometer,** (*Proc. ASHRAE Symp. Humidity Measurement, Columbus, Ohio, Feb. 5–8, 1968*), *Chapter in ASHRAE (Amer. Soc. Heat Refrig. Air-Cond. Eng.) Bull. Humidity Measurement pp. 6–17 (May 1970).*

Key words: Aspirating psychrometers; errors in psychrometric measurements; psychrometric formulas; thermocouple psychrometers, thermodynamic wet; wet-bulb psychrometers.

A paper describing the state of the art of dry and wet bulb psychrometry is presented. Mathematical relationships applicable to a sling psychrometer (or a dry and wet bulb thermometer in a test duct) are given. Short discussions of the universal psychrometric formula and three equations for use with the sling psychrometer are presented. Two of these equations consider effects which cause the reading of the wet-bulb to deviate from the true thermodynamic wet bulb temperature, but they have limitations which are described. The aspirating psychrometer is discussed and the performance of a simple thermocouple psychrometer devised at the National Bureau of Standards is described. Accuracy, precision, and laboratory fabrication techniques are also discussed. Results of tests at NBS using techniques published by earlier investigators at temperatures at 32 °F (0 °C) or below are given. Reference is made to instruments developed which measure true thermodynamic wet bulb temperature, but in their present stage of development are too large to be used in a test duct.

Dean, J. W., Brennan, J. A., Mann, D. B., Kneebone, C. H., **Cryogenic flow research facility provisional accuracy statement,** *Nat. Bur. Stand. (U.S.), Tech. Note 606, 40 pages (July 1971) 45 cents, SD Catalog No. C13.46:606.*

Key words: Accuracy statement; cryogenic; flow facility; liquid nitrogen; measurement.

The National Bureau of Standards and the Compressed Gas Association have jointly sponsored a research program on cryogenic flow measurement. A cryogenic flow research facility was constructed and was first used to evaluate commercially available cryogenic flowmeters operating with liquid nitrogen on a positive displacement principle.
The performance of the flow facility was simultaneously being evaluated during the meter tests. This is a summary report of the performance evaluation of the flow facility. An accuracy statement is given for both totalized mass and volumetric flow.

DeSimone, D. V., **A Metric America: A decision whose time has come,** *Nat. Bur. Stand. (U.S.), Spec. Publ. 345, 184 pages (July 1971) $2.25, SD Catalog No. C13.10:345.*

Key words: Metric conversion; metric system; metric usage; metrication; Public Law 90–472; U.S. Metric Study.

This publication is the comprehensive report on the U.S. Metric Study undertaken by the National Bureau of Standards pursuant to Public Law 90–472. The report evaluates and istills the information contained in the 12 interim reports of the study series and also covers what has been learned from Great Britain and other countries that are now in or have been involved in a metric changeover. Data in the report show that America is already metric in some respects and that the great majority of businessmen, educators and other informed participants in the study reported that increased use of the metric system is in the best interests of America. Included in the publication are the recommendations of the Secretary of Commerce to Congress that the United States change to the metric system through a coordinated national program over a 10-year period.

Devereux, C. W., II, Technical Standards Coordinator, **Body measurements for the sizing of boys' apparel,** *Nat. Bur. Stand. (U.S.), Prod. Stand. 36–70, 24 pages (Dec. 1971) 35 cents, SD Catalog No. C13.20/2:36–70.*

Key words: Apparel, boys'; body measurements, boys'; pattern sizes, boys'; size designations, boys'; span charts, boys' sizing.

This Voluntary Product Standard covers standard size designations, size classifications, and body measurements for the sizing of boys' apparel. The standard includes sections on applications of the system, recommended methods of identification, methods of measuring, and clothing allowances. The measurements given in this standard are body, not garment, measurements.

Devereux, C. W., Technical Standards Coordinator, **Body measurements for the sizing of women's patterns and apparel,** *Nat. Bur. Stand. (U.S.), Prod. Stand. 42–70, 29 pages (Sept. 1971) 40 cents, SD Catalog No. C13.20/42–70.*

Key words: Apparel, women's; body measurements, women's; classifications, women's size; grading charts, women's size; pattern size, women's; size designations, women's; span charts, women's sizing.

This Voluntary Product Standard covers standard size classifications, size designations, and body measurements to aid in the consistency of sizing of women's apparel and, by doing so, provides a means for the consumer to identify her body type and size for proper fit. This standard also covers applications of the system, definitions, methods of measurement, adjustments to compensate for the effect of foundation garments, spanning charts, and a recommended method of identification. The measurements given in this standard are body, not garment, measurements.

deWit, R., **Relation between dislocations and disclinations,** *J. Appl. Phys.* **42,** *No. 9, 3304–3308 (Aug. 1971).*

Key words: Burgers vector; crystal; disclination; dislocation; distant parallelism; hexagonal; wedge.

The theory of disclinations contains the equation $\partial_i \alpha_{ij} + e_{jmn}\theta_{mn} = 0$, where α and θ are the dislocation and disclination density tensors, respectively. This expression is interpreted to mean that dislocations can end on twist disclinations. A concrete example in a hexagonal crystal is discussed to illustrate this concept. It contains a 60° wedge disclination normal to the basal plane. By basic geometrical construction it is shown how a dislocation can be made to end on a jog in the wedge disclination. This jog is a small segment of twist disclination. Several ramifications of this concept are that disclinations can act as sources and sinks of dislocations, that dislocations change their Burgers vectors as they glide around disclinations, that a dislocation which crosses a disclination remains connected to it by a dislocation, that dislocations encircling a disclination must have a node, and that the local Burgers vector is not conserved on following a dislocation around a disclination.

Douglas, C. A., **A survey of the use of flashing lights in aviation,** *Proc. Intern. Symp. on Perception and Application of Flashing Lights, London, England, April 1971, pp. 251–270 (Adam Hilger Ltd., London, England, April 1971).*

Key words: Aerodrome lighting; aircraft lighting; anti-collision lights; beacons; effective intensity; flashing lights.

Flashing lights have been used as beacons since the first days of night flying. They are also used as identification lights in approach and runway light systems. They have been used for many years to mark obstructions and other hazards by night and are now being introduced as daytime markers. Flashing lights have been used since the 1940's to supplement the navigation lights on aircraft. Photometric performance of these lights is usually specified in terms of steady state intensity and minimum flash duration or in terms of the candela seconds in the flash. Use of the integral form of the Blondel-Rey relation was introduced in the 1950's and use of this relation is increasing.

Douglas, T. B., **Summary of recent thermodynamic measurements by calorimetric, transpiration, mass spectrometric microwave, and infrared techniques,** *Proc. Conf. Interagency Chemical Rocket Propulsion Group, Thermochemistry Working Group, Huntington Beach, Calif., March 25–27, 1968, 6th Meeting Bulletin 173, I, 93–104, (Chemical Propulsion Information Agency,*

The Johns Hopkins University, Applied Physics Laboratory, Silver Spring, Md., August 1968).

Key words: Calorimetry; infrared spectroscopy; mass spectrometry; microwave spectroscopy; thermodynamics; vaporization.

This paper summarizes recent precise thermodynamic measurements, completed or in progress, by several research groups at the National Bureau of Standards ("NBS"). The heats of formation of ClF_3(g) and BeO(c) are being measured by reaction calorimetry. "Heat-capacity calorimetry" has been completed at low temperatures on Be_3N_2(c) and on BeO(c) (larger crystals than usual), and at high temperatures on tungsten (to 2600 K) and on $BeO \cdot Al_2O_3$(c, l) (to 2350 K). A new technique of fast dynamic calorimetry at high temperature has become operational for millisecond heating, with preliminary measurements on molybdenum and other electrically conducting refractories. Transpiration data on the AlF_3-$AlCl_3$ system have been analyzed to give the heats of formation of AlF_2Cl(g) and $AlFCl_2$(g). High-temperature mass spectrometry is underway on the BeF_2-$BeCl_2$ and the BeO-H_2O systems. In the high-temperature microwave and the matrix-isolation infrared investigations of the alkali-hydroxide molecules, spectra have recently been observed and analyzed for RbOH (microwave and infrared) and for NaOH (infrared).

Driscoll, R. L., Olsen, P. T., **Compensation of earth's field variations by field controlled rubidium oscillator,** *Rev. Sci. Instr.* **42,** *No. 10, 1427–1431 (Oct. 1(71).*

Key words: Absorption cell; earth's magnetic field; helmoltz coil; magnetometer; optical pumping; resonance line; rubidium oscillator; solenoid.

The east-west variations of the earth's magnetic field over the working volume of the NBS precision solenoid are being canceled out by a closed loop system featuring a field controlled rubidium oscillator. The rubidium oscillator and solenoid are sufficiently separated in distance and do not affect each other's operation. Each system is enclosed in three-dimensional Helmholtz coils. Vertical and north-south components of earth's field are canceled. An east-west bias field is provided for rubidium oscillator operation at 10kHz. The output of a phase sensitive detector locked to the 10kHz frequency standard provides current for the electrically series connected east-west Helmholtz coils at both locations. The magnitude of this current is proportional to the phase difference of oscillator and reference. The full range of compensation is 100 nT. The rate of compensation is limited by a time constant of 0.002 s, an adequate rate for most disturbances. To the extent that the two separated components of the closed loop system can be oriented directionally the same at any given time, the earth's field east-west variation is compensated exactly.

Durst, R. A., **Ion-selective electrodes in science, medicine, and technology,** *Am. Sci.* **59,** *No. 3, 353–361 (May–June 1971).*

Key words: Electrodes; ion-selective electrode review; ion-selective electrodes, membrane electrodes; potentiometry.

The state of the art of the newer, non-glass types of ion-selective electrodes is reviewed. This brief survey includes discussions of the characteristics of the solid-state, liquid ion-exchange, and heterogeneous membrane electrodes. Applications of these sensors to a wide variety of scientific disciplines is presented, including biomedical research and industrial monitoring and control systems.

Durst, R. A., Duhart, B. T., **Ion-selective electrode study of trace silver ion adsorption on selected surfaces,** *Anal. Chem.* **42,** *No. 9, 1002–1004 (1970).*

Key words: Electrometric study of silver adsorption; silver adsorption; silver ion-selective electrode; trace silver determination.

This study demonstrates the feasibility of using a silver ion-selective electrode for monitoring silver ion losses in long-term investigations of trace silver adsorption on various container surfaces. The electrometric technique offers the advantages of less complex and costly equipment, simplified procedure, and improved precision over the radiometric method. Nernstian electrode response was observed down to 4×10^{-7} M silver. For maximum sensitivity, 2×10^{-6} M (0.2 ppm) silver was selected as the concentration for the test solution which was placed in Pyrex, Desicoted Pyrex, Polyethylene, Vycor, and Teflon containers. At various intervals up to 46 days, duplicate EMF readings were made on each of the five solutions with periodic restandardization of the electrode to permit drift corrections. Adsorption levels at the end of 30 days increased in the order: Vycor < polyethylene ≈ Teflon < Desicoted Pyrex < Pyrex; ranging from 28% adsorption for Vycor to 48% for Pyrex. Although for periods of up to a day, silver losses on Teflon were less than 2%, this study indicates that none of the above materia s is suitable for long-term storage of solutions containing low levels of silver.

Edelman, S., Grisham, L. R., Roth, S. C., Cohen, J., **Improved piezoelectric effect in polymers,** *J. Acoust. Soc. Am.* **48,** *No. 5, Part 1, 1040–1043 (November 970).*

Key words: Piezoelectricity; polymers; polyvinylchloride; strain modulus; underwater sound receiver.

Improved poling techniques have led to improvement in the piezoelectric activity of bulk polymers. Results now achieved approach the activity of conventional piezoelectric materials such as quartz, and further improvement is anticipated. The measured value of the piezoelectric strain modulus d_{31} of a length expander bar of polyvinylchloride was 0.6×10^{-12} m V^{-1} and the electromechanical coupling factor k_{31} was 0.6%. The response of a sample as an underwater sound receiver was −112 dB *re* 1 V/μbar.

Edsinger, R. E., Guildner, L. A., Anderson, R. L., **Precision measurement of internal diameters of long, small bore metal tubing,** *Rev. Sci. Instr.* **42,** *No. 7, 945–950 (July 1971).*

Key words: Capacitance probe; cylindrical gauge blocks; inside diameters; small-bore tubes; standard hole; wringing.

Internal diameters of a long, small-bore metal tube were calculated from the measured capacitances between it and a cylindrical coaxial probe of known characteristics. The tube and the probe were used as the electrodes of a three-lead capacitor, measurable with high accuracy in a transformer ratio-arm bridge. For tubes of 0.1 cm bore or less, average diameters as a function of position can be determined by this method with an overall uncertainty of $\pm 6 \times 10^{-5}$ cm over lengths of 1 meter. The method can readily be extended to larger bores and greater lengths.

Eisele, J. W., Technical Standards Coordinator, **Flame-resistant paper and paperboard,** *Nat. Bur. Stand. (U.S.), Prod. Stand. 46–71, 10 pages (Oct. 1971), 10 cents, SD Catalog No. C13.20/2:46–71.*

Key words: Flame-resistant, paper and paperboard; paper, paperboard, flame-resistant; paperboard, paper, flame-resistant.

This Voluntary Product Standard covers requirements and test methods for flame-resistant paper and paperboard which are 0.060 inch or less thick. Definitions are provided, and a method for identifying products conforming to the standard is given. Two classifications of flame-resistant paper and paperboard are covered: Type I, which is flame-resistant only before water leaching and Type II, which is flame-resistant both before and after water leaching.

Ekstrom, M. P., McCaa, W. D., Jr., Nahman, N. S., **The measured time and frequency response of a miniature superconducting coaxial line,** *IEEE Trans. Nucl. Sci.* **NS-18,** *No. 5, 18–25 (Oct. 1971).*

Key words: Attenuation measurement; picosecond; rise-time measurement; superconducting; transmission lines; two fluid theory.

A miniature superconducting 52 ohm coaxial transmission line 278 meters long, having a lead outer conductor (0.129 cm id), a teflon dielectric, and a niobium center conductor (0.038 cm), has been measured in both the time and frequency domains. The observed system step response (10%–90%) times were 1.5 μs at room temperature, 375 ns at 77K, and 255 ps at 4.2K. The system step response data for 4.2K was processed by a numerical system identification routine to determine the step response of the miniature superconducting line; the processed data gave a 220 ps risetime. Although the observed step responses at 4.2K were smooth transitions, the

observed swept frequency (0.1 GHz–12 GHz) attenuation at 4.2K was a quasi-periodic function of frequency, which indicated that the nonuniformity of the superconducting line was significant. For example, near 5 GHz and at 4.2K, the attenuation minimum was 1.1 dB while about 0.5 MHz away the attenuation was 5 dB. By making normal conductivity measurements of the Nb conductor and incorporating he results into the two fluid model, the uniform line attenuation for 5 and 10 GHz was calculated with the classical and anomalous limits. The lowest observed attenuation values in the vicinity of 5 and 10 GHz fell between the computed classical and anomalous limit attenuation values.

Engen, G. F., Power equations: **A new concept in the description and evaluation of microwave systems,** *IEEE Trans. Instr. Meas.* **IM-20,** *No. 1, 49–57 (Feb. 1971).*

Key words: Attenuation; impedance; microwave; mismatch; power; power equation; terminal invariant.

In the existing art, the description and evaluation of microwave systems is usually in terms of the complex wave amplitudes in the (assumed) uniform waveguide by which the components are interconnected. The interrelationships among these amplitudes are given by the scattering equations or indirectly by impedance parameters. This paper introduces an alternative description, based on power equations, where the basic parameter is the net power in the waveguide of interest. Compated with the circuit description, there is a substantial suppression of detail and the remaining parameters are placed in better perspective. In particular, the technique provides a simplified method of describing and evaluating mismatch corrections, in which the precision connector and uniform waveguide requirements have been eliminated.

Evans, J. P., Wood, S. D., **An intercomparison of high temperature platinum resistance thermometers and standard thermocouples.** *Metrologia* **7,** *No. 3, 108–130 (July 1971).*

Key words: Calibration; fixed point; freezing point; furnaces; high temperature; IPTS–68; platinum resistance thermometer; temperature scale; thermocouple; triple point.

To obtain some of the information necessary for redefining a practical temperature scale in terms of resistance thermometry up to the gold point, we have intercompared nine high temperature platinum resistance thermometers and eight standard thermocouples at 50 degree intervals over the range 630.74 to 1064.43 °C. Values of temperature were derived from "before and after" calibrations of the instruments at the freezing points of gold, silver, antimony, zinc, and tin, and at the triple point of water.—Analysis of the data showed that the standard deviation of temperatures measured with thermometers was about 4 mK, while with thermocouples it ranged from 25 to 30 mK. When systematic errors were accounted for, we found that values of temperature on IPTS–68 could be determined with a single thermometer, using an interpolation formula analogous to that used below 630.74 °C, with about one-third the uncertainty usually attributed to a single thermocouple determination (±200 mK). The data also revealed that there is a lack of "smoothness" in the scale at 630.74 °C—first derivatives with respect to t_{68} are discontinuous by about 0.1% at this temperature.—We conclude from the results of this work that if a practical temperature scale were redefined in terms of presently available high temperature platinum resistance thermometers, it could be realized with significantly less uncertainty (±12 mK for a single determination) than IPTS–68, as it is now realized with thermocouples (±200 mK for a single determination). We recommend, however, that the adoption of such a scale be deferred until indicated improvements in thermometers have been made, and until current researchers in gas thermometry have provided new values of thermodynamic temperatures for calibrating fixed points.

Fickett, F. R., **Magnetoresistance of very pure polycrystalline aluminum,** *Phys. Rev.* **B. 3,** *No. 6, 1941–1952 (March 15, 1971).*

Key words: Aluminum; electron scattering; magnetoresistance; resistance.

The behavior of the resistance of polycrystalline aluminum wires as a function of magnetic field and purity at temperatures of 4, 15, and 19.6 K is reported. Both longitudinal and transverse configurations were measured. The residual resistance ratios of the specimens varied from 1600 to 31000. The measured magnetoresistance ($\Delta R/R_0$) is separated into a saturating and a linear part. The value of the saturating component is high at 19.6 K but is shown to be less than 6, even in the limit of infinite specimen purity. The linear component varies with both temperature and purity. Possible sources for the large saturating magnetoresistance values and for the variations observed in the linear portion are discussed. An analysis scheme is presented which allows prediction of the saturating component from zero-field resistance values. A deviation from Matthiessen's rule observed here, and by several other experimenters, is presented and discussed.

Fickett, F. R., **Martensite transformation detection in cryogenic steels (magnetometer development),** *Nat. Bur. Stand. (U.S.), Tech. Note 613, 31 pages (Dec. 1971) 40 cents, SD Catalog No. C13.46:613.*

Key words: Fatigue monitor; low temperature; magnetometer; martensite; nondestructive.

This report presents design criteria for a magnetometer device developed to determine the martensite concentration in 304 stainless steel. Specifically, the device is designed to monitor the cold tank of an airborne liquid oxygen container which is subject to periodic stress pulses. The amount of martensite is relatable to the plastic strain and thus provides a mechanism for the prediction of impending failure.

The magnetometer, developed after a critical review of the constraints, is an excitation coil-Hall effect system. The system is very versatile is design and is easily adapted to particular problems. It is relatively insensitive to thermal and mechanical shock and easily capable of detecting martensite at the 1% level.

Flynn, T. M., Smith, C. N., **Trends in cryogenic fluid production in the United States,** *(Proc. Int. Institute of Refrigeration, Tokyo, Japan, 1970), Int. Inst. Refrig. Bull. Suppl. Commission I, pp. 241–247 (Annex 1970–2).*

Key words: Argon; cryogenics; forecasts; helium; hydrogen; liquefied natural gas; nitrogen; oxygen; trends.

The cryogenic industry in the U.S. has changed dramatically in both scope and character during the last decade. It has progressed from a liquid hydrogen technology to a liquid helium technology to developing new technologies dependent upon both the upper and lower extremes of the cryogenic scale. Among these are practical applications of superconductivity and the use of liquefied natural gas as a major world energy source. This change in the nature of the industry, and some of its implications for the future, is seen in this paper which traces the production of the economically significant cryogens over the last decade and gives the present status of cryogen production in the U.S.

Fong, E., **A survey of selected document processing systems,** *Nat. Bur. Stand (U.S.), Tech. Note 599, 67 pages (October 1971), 65 cents, SD Catalog No. C13.46:599.*

Key words: Bibliographic system; computer package; data base; document processing; information retrieval; document storage and retrieval; text; text processing.

There are many document processing systems that are commercially available or Government-owned. These systems emerged in the evolution from early efforts in library automation to current on-line systems. Due to the diverse nature of the facilities provided in the document processing systems, it is difficult to evaluate them. The purpose of this paper is to present a list of features as a set of dimensions along which to compare the surveyed systems. The feature list is also developed to serve as a common basis for describing document processing systems. Another purpose of this paper is to provide a reference tool for the eight systems surveyed. They are CIRCOL, DDC, ITIRC, The Mead Data Central, MEDLARS II, New York Times Information Bank, ORBIT II, and RECON/STIM.

This paper first explored the characteristics of available, large document processing systems in general. An overview of the eight systems surveyed is presented. The paper then defines the feature list. The description of the eight systems surveyed according to the feature list outline is included as an Appendix.

Forthofer, R. J., **Developing standards technology for automotive braking systems,** *Proc. 1969 18th Annual Meeting, Standards Engineers Society, Washington, D.C., Sept. 15–17, 1969, pp. 27–42 (Sept. 1969).*

Key words: Automotive; brake; brake fluid; brake lining; standards; testing.

The Office of Vehicle Systems Research (OVSR) of the National Bureau of Standards (NBS), U.S. Department of Commerce, is concerned with the research, development, testing and evaluation necessary to provide the technical basis for recommended safety performance standards of motor vehicle systems issued by the National Highway Safety Bureau in the Department of Transportation. This paper discusses briefly the history of the Government's interest in automotive braking safety standards. Problems associated with the collection of research data for the performance of brake systems, brake linings, and brake fluid in more detail. The author comments on the direction that research is expected to take in the 1970's.

Fraker, A. C., Ruff, A. W., Jr., **Observations of hot saline water corrosion of aluminum alloys,** *Corrosion* **27,** *No. 4, 151–156 (April 1971).*

Key words: Aluminum alloys; hot saline; oxide films; precipitates; transmission microscopy; water corrosion.

Corrosion films formed on aluminum in hot salt water (100 to 177 °C) after short time tests of 30 seconds to one hour were studied by transmission electron microscopy and diffraction. It was concluded from observation of 6061, 5454, 2024, Al–1.52Mn and Al–1.66Ni alloys that one controlling factor in the initiation and growth of the outer film of the duplex oxide film is the alloy composition. The outer film formed earlier on alloys containing copper and the film growth was also more rapid on these alloys. Additions of magnesium, manganese and nickel retarded this outer film formation but with nickel additions, pitting attack was more severe and deposition of copper from solution was increased. The formation and growth of the outer film was slowest on the 5454 alloy which was also the most resistant alloy tested.

Franklin, A. D., **Theory of linear dielectrics,** *Proc. Conf. Electronic Phenomena in Ceramics, University of Florida, Gainesville, Fla., Nov. 10–14, 1969, Chapt. 17, 451–489 (1971).*

Key words: Ceramics; dielectric constant; electronic polarization; interfacial polarization; lattice polarization; orientation polarization; theory.

A cursory review is given of the theory of the linear response of a dielectric to an impressed electric field, including the electronic, lattice, dipole orientation, and linear interfacial polarizations. Most emphasis is given to the crystalline ionic, insulating models appropriate for the more ionic ceramics. Modifications to the theory for semiconducting and vitreous materials are briefly touched upon.

Franklin, A. D., Bennett, H. S., Editors, **ARPA–NBS program of research on high temperature materials and laser materials, Reporting Period–January 1 to June 30, 1971,** *Nat. Bur. Stand. (U.S.), Tech. Note 703, 39 pages (Dec. 1971) 50 cents, SD Catalog No. C13.46:703.*

Key words: Al_2O_3; crystal growth; damage threshold; glass; high temperature materials; laser; oxides; oxygen diffusion; pure materials; sapphire.

Progress reports are given for projects on the growth of ultra-pure Al_2O_3 crystals, the development of a mass spectrometer-based sectioning technique for measuring oxygen diffusion in oxides and the development of a precision facility for measuring the threshold energy in a laser beam producing damage in a transparent substance.

Freeman, D. H., Enagonio, D. P., **Interactive gel networks for organic separations, Nature (London),** *Phys. Sci.* **230,** *135–136 (April 1971).*
Key words; Chromatography; interactive gel networks; liquid chromatogrqphy; organic separations.

Conventional organic networks, such as crosslinked polyvinylpyridine, can be used or modified so that chemical interactions of various specific types are obtained. They show excellent resolution and high capacity. The chromatographic properties are related to complexative interactions whose understanding in liquid media is independently established.

French, J. L., **Discussion of "Are individual current-meter ratings necessary,"** *J. Hydraulics Div. Proc. Am. Soc. Civil Engrs.* **HY 1,** *507–511 (Jan. 1969).*

Key words: Calibration; current meters (fluids); hydraulics; measurement; open-channel flow; standards.

This is a discussion of the paper "Are Individual Current-Meter Ratings Necessary?" by George F. Smoot and Rolland W. Carter, Journal of the Hydraulics Division, American Society of Civil Engineers, March 1968. Experimental data relating to the performance of a Price current meter are presented. The data were obtained in a simulated working section of a water tunnel. It is concluded that the precision with which a Price meter responds to a given water flow is greater than might be expected from the data listed in the authors' tables 1 and 2.

French, J. L., **Nonenlarged box culvert inlets,** *J. Hydraulics Div. Proc. Am. Soc. Civil Engrs.* **HY 6,** *2115–2137 (Nov. 1969).*

Key words: Culverts; entrance control; hydraulics; inlets.

The effect of variation in the dimensions of beveled leading edges on the discharge capacity of box culvert inlets of rectangular cross section is investigated. It is demonstrated that the effective control surface of a beveled edge may be either the face of the headwall or the beveled surface of the edge geometry, depending on the relative dimensions of the beveled edge. The bevel dimensions required to ensure bevel surface control are determined. The dependence of the discharge coefficient on the dimensions of the beveled leading edge and on the cross-sectional shape of the barrel is demonstrated. Methods for estimating the capacity in submerged entrance flow of box culvert inlets operating in entrance control are developed for various beveled leading edge geometries.

Frenkiel, F. N., Klebanoff, P. S., **Statistical properties of velocity derivatives in a turbulent field,** *J. Fluid Mech.* **48,** *Part 1, 183–208 (July 13, 1971).*

Key words: Computer; correlations; grid; intermittency; isotropy moments; probability-distributions; turbulence; velocity-gradients.

High-speed digital computing methods are applied to the study of the statistical behavior of turbulent velocity derivatives in a nearly isotropic turbulent field downstream of a grid. Higher-order correlations of turbulent velocity gradients, up to the eighth order, are measured. Contrary to the case of *velocities*, the higher even-order correlations of *velocity gradients* more clearly evidence the departure from a two-dimensional Gaussian probability distribution. Using non-Gaussian probability distribution laws the relations between different odd- and even-order correlations are obtained and compared with the experimental measurements. The conditions of similarity and isotropy are evaluated for the small-scale structure as evidenced by the behavior of the turbulent velocity gradients. The concept of intermittency of the small-scale structure is also discussed.

Fussell, W. B., **Effect of ceramic spectral emissivity variations on the computed luminous emissivity of the NBS standard of light,** *Nat. Bur. Stand. (U.S.), Tech. Note 595, 58 pages (Sept. 1971) 65 cents, SD Catalog No. C13.46:595.*

Key words: Ceramic; light; photometry; radiometry; spectral emissivity; standard.

A simplified model of the National Bureau of Standards (NBS) 1970 design for the standard of light (platinum point blackbody) is introduced. This model is used to calculate the apparent luminous emissivity of the base of the sighttube of the standard of light, and of the wall near the base, by two different methods. The first method includes the effect of variations with wavelength in the spectral emissivity of the ceramic composing the sighttube; the second method does *not* include the effect of ceramic spectral emissivity variations. The results of the two methods are compared and their difference (about 6×10^{-6}) is found to be negligible for the NBS 1970 design when the sighttube is made of alumina, compared with other uncertainties and the precision of measurement.
A formula is derived for estimating the apparent luminous emissivity of a standard of light, given: a., the length-to-diameter ratio of the sighttube; b., the half-angle of the conical base; c., the wall thickness of the sighttube; d., the thermal conductivity of the sighttube ceramic; e., the average thermal and luminous emissivities of the sighttube ceramic.

Gebbie, K. B., Thomas, R. N., **The temperature control bracket,** *Astrophys. J.* **168,** *No. 3, 461–479 (Sept. 15, 1971).*

Key words: Boundary temperature; collosional-control; radiative-control; temperature-control-bracket.

The factors determining the temperature distribution in a stellar atmosphere are divided into transfer effects and population effects. As a measure of the latter, we introduce the Temperature Control Bracket, which, in radiative equilibrium, describes the control of T_e by the quantity and spectral distribution of the radiation field. Algebraic expressions for the [TCB] are given in terms of the microscopic rate processes for a pure hydrogen atmosphere. A caricatured computation is presented to demonstrate the influence of the various physical effects on the distribution of T_e in radiative equilibrium.

Geist, J., **Note on the quality of freezing point blackbodies,** *Appl. Opt.* **10,** *No. 9, 2188–2190 (Sept. 1971).*

Key words: Apparent emissivity; freezing point blackbodies; quality.

For freezing point blackbodies a quantity which satisfies the intuitive ideas suggested by the word quality, and which is the solution to a Fredholm integral equation of the second kind, can be defined. The integral equation provides significant physical insight into the interaction of the reflectance and thermal resistance of the wall material in reducing the quality of freezing point blackbodies. In the case where the walls of the cavity reflect diffusely, the integral equation for the quality of a freezing point blackbody reduces to an equation of the same form as the integral equation for the apparent emissivity of an isothermal cavity of the same geometry. Thus the previously published results for the apparent emissivity of cavities with diffusely reflecting walls can be modified to yield the quality of freezing point blackbodies with diffusely reflecting walls.

Geist, J. C., Richmond, J. C., **On the absorptance of cavity-type receivers,** *Nat. Bur. Stand. (U.S.), Tech. Note 575, 38 pages (July 1971) 45 cents, SD Catalog No. C13.46:575.*

Key words: Absorptance; black coatings; cavity absorptance; cavity reflectance; laser-source reflectometer; Parsons black; retro-reflectance.

The directional-hemispherical reflectance of a number of flat samples that had been coated with Parsons Optical Black Lacquer procured from Thos. Parsons and Sons and The Eppley Laboratory, respectively, was measured at 0.6328 and 1.15 μm with a laser-source integrating sphere reflectometer. The reflectance varied significantly with method of application, and was significantly higher for the Eppley lacquer than for the Parsons lacquer. The reflectance of two cavity receivers, one coated with each lacquer, was also measured. At 0.6328 μm the reflectance of the Parsons cavity was higher, but at 1.15 μm it was lower. The measured reflectance of the Parsons cavity was appreciably higher than that computed from the measured reflectance of the lacquer and the geometry of the cavity, assuming the coating to be a perfectly diffuse reflector. Retro-reflectance measurements revealed that both lacquers reflected more radiant energy back into directions near the direction of incidence than would a perfect diffuser of the same directional-hemispherical reflectance, but the Parsons lacquer was by far the more pronounced retro-reflector. The principal conclusion is that the diffuse assumption can lead to significant errors in computing the absorptance of cavity-type receivers, when the cavity coating is in fact not diffuse.

Geller, S. B., **Standard reference materials: Calibration of NBS secondary standard magnetic tape (computer amplitude reference) SRM 3200 using the reference tape amplitude measurement "Process A" Model II,** *Nat. Bur. Stand. (U.S.), Spec. Publ. 260–29, 57 pages (June 1971) 60 cents, SD Catalog No. C13.10:260–29.*

Key words: Average signal peak level; computer amplitude reference; magnetic tape; master standard; saturation curves; secondary standard; signal level calibration; standard reference materials; unrecorded reference.

This publication describes the design, operation and calibration of the NBS signal amplitude measuring system (Process A – Model II) that is used for calibrating unrecorded Secondary Standard Magnetic Tapes (Computer Amplitude Reference) SRM 3200. This system supersedes the measurement system that was described in the NBS Special Publication 260–18 (November 1969). The signal level calibration is made with respect to a reference signal level derived from the NBS Master Standard Magnetic Tape (Computer Amplitude Reference) that is kept in repositiory at NBS. The techniques for measuring and recording the data that accompany each Secondary Standard magnetic Tape in the form of strip chart recordings and saturation curves are described.

Gordon, G. F., U.S. **Metric Study Interim Report: International trade,** *Nat. Bur. Stand. (U.S.), Spec. Publ. 315–8, 188 pages (July 1971) $1.50, SD Catalog No. C13.10:345–8.*

Key words: Foreign trade; International System of Units; metric conversion; metric conversion, effect on foreign trade; metric system; metric usage; metric usage, effect on foreign trade; metrication; metrication, impact of on foreign trade; SI; U.S. Metric Study.

This publication, one of a series prepared pursuant to the U.S. Metric Study Act, evaluates the potential effects that a U.S. conversion to the metric system may have on the Nation's foreign trade. The report is based on a survey of exporters and importers trading in measurement-sensitive products, which was conducted by the Bureau of Domestic Commerce of the Department of Commerce.

Grabner, L., Stokowski, S. E., **Photoluminescence of Cr-doped $CaTiO_3$,** *Phys. Rev.* **B. 2,** *No. 11, 4351–4353 (Dec. 1, 1970).*

Key words: Cr^{3+}; energy transfer; excitation; lifetime; photoluminescence.

At 4 K and 77 K photoluminescence from nominally undoped and $CaTiO_3$: 0.0025% Cr show identical spectra in the infrared with an intensity ratio of 1:2. The emission is attributed to the $^2E \rightarrow {}^4A_2$ transition of the Cr^{3+} ion at a Ti^{4+} site. At 4 K it consists of a single no-phonon line at 1.744 eV of half-width 1.5 meV and a complex vibronic spectrum which is anomalously intense. Data at 77 K shows a splitting of the ^2E state of 2 meV. The absorption spectrum of $CaTiO_3$: Cr is dominated by a "background absorption" by unknown defects. From the coincidence of the excitation spectrum with the absorption spectrum, we conclude that the excitation is dominated by absorption by unknown defects which transfer energy into Cr^{3+}, presumably by resonant energy transfer. In undoped $CaTiO_3$ a single exponential decay of the emission of 700 μs is reported. In $CaTiO_3$:0.0025% Cr, on the other hand, two exponentials of 700 μs and 11 ms were observed. The former is assigned to CR^{3+}, the latter to the time of energy transfer from defects responsible for the background absorption to the Cr^{3+}.

Grabner, L., Stokowski, S. E., Bro er, W. S., Jr., **No-phonon $^4T_{2g}$–$^4A_{2g}$ transitions of Cr^{3+} in TiO_2,** *Phys. Rev.* **B. 2,** *No. 3, 590–598 (August 1, 1970).*

Key words: Absorption; defect phonon; emission; excitation; lifetime; $^4T_2$ state.

Absorption and emission at 4 K and 77 K are observed in Cr-doped TiO_2 consisting of two sharp no-phonon lines at 12685 cm^{-1} and 12732 cm^{-1} and vibronic side bands with an integrated intensity 10^4 that of the no-phonon lines. In undoped TiO_2, identical spectra are observed but are a factor of 100 less intense. The center responsible for these spectra is identified as substitutional Cr^{3+} by observing, in emission, a splittering of the 12685 cm^{-1} line of 1.4 cm^{-1}, a value previously determined by EPR measurements. The vibronic side bands have some structure superposed on a broad band. The vibronics are different in emission and absorption and have a lifetime of 45 μs, equal to that of the no-phonon line. They are shown to be principally due to defect induced phonons arising from the Cr^{3+} defect. We argue that the spectra observed are not characteristic of the usual ^2E_g–$^4A_{2g}$ transition and propose that the $^4T_2$ lies lower in energy than the ^2E_g state. If so, the new results of this work are: (1) no-phonon line emission for the $^4T_2$–$^4A_2$ transition, and (2) defect phonon states which are different for the $^4A_2$ and $^4T_2$ states. The excitation spectrum is also presented. It shows that the excitation of the Cr^{3+} emission occurs mainly by the transfer of energy from excited trapping centers rather than by direct excitation.

Gravatt, C. C., **The application of light scattering,** *Appl. Spectry.* **25,** *No. 5, 509–516 (Sept.–Oct. 1971).*

Key words: Air pollution; lasers; light scattering; macromolecules; optical mixing spectroscopy; review.

Light scattering provides information concerning the size, shape, number, and time dependence of the physical nonuniformities of a system. Measurements of the scattered intensity as a function of both scattering angle and wavelength describe static properties, whereas the spectral distribution of the scattered radiation is related to time dependent phenomena. The applications of light scattering are discussed, including critical phenomena, molecular weight determination, air pollution analysis, and diffusion phenomena.

Grimes, D. N., **Imaging of tri-bar targets and the theoretical resolution limit in partially coherent illumination,** *J. Opt. Soc. Am.* **61,** *No. 7, 870–876 (July 1971).*

Key words: Coherence; diffraction; resolution.

In viewing systems that employ critical, Kohler, or collimated illumination, the illumination may frequently be characterized by the complex degree of coherence in the form of a first-order Bessel function divided by its argument. The anomalies that occur in the image of tri-bar target viewed in partially coherent illumination of this form are discussed for a two-dimensional circular diffraction-limited imaging system. The Sparrow criterion, which in this case correlates with experimental measurements of resolving power, is applied to determine the resolution limit. The computed resolution-limit curve for a tri-bar target is shown and compared to the previously published two-point resolution-limit curve for a one-dimensional system and to the limiting values obtained in a two-dimensional system for coherent and incoherent illumination. In the latter case, the full curve is shown as a special case of the application of the Sparrow criterion to the partially coherent imaging equations for a circular two-dimensional system. Experimental confirmation of the calculations is given.

Grimes, D. N., **Linear microdensitometry,** *J. Opt. Soc. Am.* **61,** *No. 9, 1263 (Sept. 1971).*

Key words: Diffuse density measurement; linear microdensitometer; microdensitometry.

A linear microdensitometer is proposed whose operation is independent of the coherence of the source used and which measures diffuse density. A theoretical analysis is given.

Grimes, D. N., **Measurement of the second-order degree of coherence by means of a wavefront shearing interferometer,** *Appl. Opt.* **10,** *No. 7, 1567–1570 (July 1971).*

Key words: Coherence; coherence measurement; interferometry; wavefront shearing interferometer.

A method of measuring the second order degree of coherence in an arbitrary plane by means of a compact wavefront shearing interferometer is described. The prism interferometer previously described by Saunders produces two sheared images which interfere allowing measurement of the degree of spatial coherence. If the degree of coherence is a function of co-ordinate differences only, the visibility is constant over the field. Otherwise it varies point-to-point. Experimental results are given.

Haar, L., Shenker, S. H., **Equation of state for dense gases,** *J. Chem. Phys.* **55,** *No. 10, 4951–4958 (Nov. 15, 1971).*

Key words: Argon; compressibility factor; dense fluids; equation of state; molecular dynamics; molecular interactions; nitrogen; pair potentials; temperature perturbation theory.

A simple quantitative equation of state of the van der Waals type is proposed for dense fluids. The equation yields compressibility factors with a precision comparable to those from the more complicated temperature perturbation theory when tested against "computer experiments", including isotherms as low as 0.8 liquid-vapor critical temperature. The equation is capable of predicting compressibility factors for real gases as illustrated by calculations for argon and nitrogen at pressures up to 10 000 atm. The derivation of the equation is based on a rearrangement of the terms in the Ursell-Mayer density expansion of the configuration integral. The equation contains two temperature-dependent parameters, to be determined from the dilute gas second virial coefficients. A principal feature of our approach is that it does not require explicit knowledge of the details of the pair interaction.

Hall, J. L., Barger, R. L., Bender, P. L., Boyne, H. S., Faller, J. E., Ward, J., **Precisions long path interferometry and the velocity of light,** *A. Smolinski, and S. Hahn, Ed., (Proc. URSE Conf. Laser Measurements, Warsaw, Poland, Sept. 24–26, 1968), Electron Technol.* **2,** *No. 2/3, 53–66 (Panstwowe Wydawnictwo Naukowe Polish Scientific Publ., Warsaw, Poland, 1969).*

Key words: Interferometry; laser; optical heterodyne; velocity of light.

We report on several aspects of the JILA/NASA/NBS velocity of light experiment. We discuss first the theory of the experiment and illustrate numerically that signal-to-noise ratio is not of primary concern. Considerable thought has gone into planning the experiment to be as free as possible from systematic error and these considerations will be briefly reviewed. We discuss a promising pair of laser transitions in pure neon and report two technological developments related to them. We will give a few illustrations of the kind of geophysical information that can be obtained from long-baseline interferometry of the type developed in this work. Finally we briefly report a useful laser transfer standard and a new wavelength reference based on laser saturation of a methane absorption line. A reproducibility of 3 parts in 10^{11} has already been demonstrated by optical heterodyne techniques in preliminary experiments.

Hammond, H. K., III, Mason, H. L., Editors, **Precision measurement and calibration. Selected NBS papers on radiometry and photometry,** *Nat. Bur. Stand. (U.S.), Spec. Publ. 300,* **V. 7,** *685 pages (Nov. 1971) $7.00, SD Catalog No. C13.10:300/v.7.*

Key words: Emissivity; flashing light; flux measurement; irradiance; material properties; photometry; projectors; radiance; radiometry; reflectometry.

This volume is one of an extended series which brings together some of the previously published papers, monographs, abstracts and bibliographies by NBS authors dealing with the precision measurement of specific physical quantities and the calibration of the related metrology equipment. The contents have been selected as being useful to the standards laboratories of the United States in tracing to NBS standards the accuracies of measurement needed for research work, factory production, or field evaluation.
Volume 7 contains reprints of more than 60 items on radiometry and photometry published between 1957 and 1970. The material has been placed in groups according to the following subjects:

general radiometry, emissivity standards, emissivity measurements and techniques, material properties, irradiance standards, radiometric measurement techniques, radiance standards, flux measurement, reflectometry, general photometry, projectors, flashing lights, and chronological bibliography of publications by NBS staff.

Hatos, S. L., **U.S. Metric Study Interim Report. Commercial weights and measures,** *Nat. Bur. Stand. (U.S.), Spec. Publ. 345–3, 116 pages (July 1971) $1.0 , SD Catalog No. C13.10:345–3.*

Key words: Commercial weights and measures, International System of Units; metric conversion; metric system; metric usage; metrication; metrication, attitudes toward; metrication, costs and benefits of; metrication, impact of; SI; U.S. Metric Study.

This publication, one of a series prepared pursuant to the U.S. Metric Study Act, explores the impacts metrication would have on commercial weights and measures activities. More specifically, the report, concerns: (1) the cost of adapting or changing commercial weighing and measuring devices to record and/or indicate in metric units, and (2) the effects of metrication on state and local weights and measures jurisdictions.

Haupt, G. W., **Glass limit standards deposited at NBS for railway, highway and airways traffic signal colors—history, permanence and colorimetric properties,** *Nat. Bur. Stand. (U.S.), Tech. Note 564, 121 pages (June 971) $1.00, SD Catalog No. C13.46:564.*

Key words: Aircraft signals; color standards; filter permanence; limit filters; railroad signals; signal colors; signal standards; spectral transmittance of glass filters; traffic signals.

Signal glass limit standards for railway, highway, and aviation colors, selected by user-organizations, are on deposit at the National Bureau of Standards. Many duplicates of these standards have been issued by NBS.
The first standards were selected in 1931 for railway use. Highway standards were adopted in 1940, and selection of aviation standards began in 1942. At the present time the NBS is custodian of 63 standards for these signal colors.
Permanence of the filters is examined, based on colorimetric conversions for CIE standard illuminant. A derived from spectrophotometric measurements made on different instruments over periods of years.
Spectral transmittance data and the resulting colorimetric data are given for 9 illuminants ranging in distribution temperature from 1500 to 3250 kelvins and for CIE standard illuminants B and C. Figures show, for several filters of each color, the shifts occurring both in chromaticity (x, y) and in redness and brightness index (u, W^*) with changes in illuminant.

Heinrich, K. F. J., Myklebust, R. L., Rasberry, S. D., Michaelis, R. E., **Standard Reference Materials: Preparation and evaluation of SRM's 481 and 482 gold-silver and gold-copper alloys for microanalysis,** *Nat. Bur. Stand. (U.S.), Spec. Publ. 260–28, 100 pages (Aug. 1971) $1.00, SD Catalog No. C13.10:260–28.*

Key words: Alloys; corrections; electron probe; homogeneity; matrix scanner; microanalysis; quantitative analysis; standard reference materials; x-ray emission.

The reasoning behind the choice of the systems Au-Ag and Au-Cu for SRM's, and their suggested uses are described. We also report on the preparations of the materials, their chemical analysis, the tests performed to ascertain macroscopic and microscopic homogeneity, and on relative x-ray intensity measurements at various x-ray lines and voltages. A description of the instrumentation (matrix scanner), techniques, and programs employed in the homogeneity studies, as well as tables and graphs of the x-ray intensity measurements, are appended.

Hellwig, H., Barnes, J. A., Glaze, D. J., **Frequency biases in a beam tube caused by Ramsey excitation phase differences,** *Proc. 25th Annual Symp. on Frequency Control, Atlantic City, N.J., April 26–28, 1971, pp. 309–312. (Electronic Industries Association, Washington, D.C., April 1971).*

Key words: Cavity phase shift; cesium beam tube; frequency accuracy; frequency standard; power shift; resonance line shape.

A phase difference between the two interaction regions of a Ramsey excitation resonance structure results in a frequency bias in the measured beam resonance. A simple mathematical model is discussed which describes the dependence of this bias on the phase difference, the microwave power level, the modulation amplitude, and the resonance linewidth. This dependence results from the interaction of the modulated microwave excitation frequency with the asymmetric shape of the slightly shifted resonance line. In a first order approximation, no dependency on the frequency modulation amplitude is expected. Near-linear dependencies on the linewidth and microwave power level which are quite pronounced even at relatively small cavity phase differences are predicted. The theoretical results are compared with one set of experimental data on the microwave power dependence as measured in 1969 with the primary cesium beam standard NBS–III. After a correction is applied to the power dependence due to spectral impurity of the microwave excitation, the remaining measured power dependence agrees quantitatively with that calculated using a cavity phase difference of about 3 milliradians.

Hermach, F. L., **Testing hospital electric equipment for safe performance,** *Proc. National Research Council Workshop on Electric Hazards in Hospitals, Washington, D.C., April 4–5, 1968, pp. 175–177 (National Academy of Sciences, Washington, D.C., 1970).*

Key words: Electric equipment; hospitals; safety; testing.

The importance of testing hospital electric equipment to determine the extent of the conformance with accepted performance standards is emphasized. The need for test sets to make measurements of leakage currents from electric equipment to ground is paramount. Standardizing bodies can help by outlining performance requirements for such test sets.

Heuer, A. H., Hockey, B. J., Wiederhorn, S. M., **Discussion of "Observation of plastic deformation in sapphire base ceramics,"** *Metallurgical Trans.* **2,** *1475–1476 (May 1971).*

Key words: Alumina; fracture; mechanical properties; plastic deformation; sapphire; strength.

A paper presented in Metallurgical Abstracts by George F. Hurley is discussed. It is concluded that the observations concerning plastic deformation in sapphire-based ceramics are incorrect and that there is no evidence at present to link plastic deformation and fracture to alumina ceramics.

Heydemann, P. L. M., **A fringe-counting pulsed ultrasonic interferometer,** *Rev. Sci. Instr.* **42,** *No. 7, 983–986 (July 1971).*

Key words: Phase sensitive detection; speed of sound; ultrasonic interferometer; ultrasonics.

A new ultrasonic interferometer for the automatic measurement of transit times is described. Its main advantage is its ability to follow very large changes of the transit time (1–20) and still maintain a resolution of typically 2.5×10^{-10} s. The method is based on the phase sensitive detection of multiple echoes, counting of the output signal at the rate of four counts per full cycle, and an additional interpolation.

Hogben, D., Peavy, S. T., Varner, R. N., **OMNITAB II—User's reference manual,** *Nat. Bur. Stand. (U.S.), Tech. Note 552, 264 pages (Oct. 1971) $2, Stock Number 0303–0918.*

Key words: Automatic printing; Bessel functions; data analysis; data manipulation; easy and effective programming in English; list of instructions; matrix operations; numerical analysis; OMNITAB II user oriented computing system; self-teaching; statistical analysis.

OMNITAB II, a highly user-oriented system for a large computer, is designed to make computing easy, accurate and effective, particularly for persons who are not programmers. It is a general-purpose program, which can be learned quickly, for both simple and complex numerical, statistical and data analysis. OMNITAB

executes instructions written in the form of simple English sentences. Problem-solving is further enhanced by the natural structure of the system and its many features. OMNITAB has been used successfully in government, industry and universities across the country and in several centers abroad. The system has been implemented on large computers of at least seven different manufacturers.

The original version of OMNITAB has been completely rewritten to make it as machine independent as possible and to implement many improvements. This manual describes Version 5.0. Details are presented so that the user can easily find the specific information needed in any particular instance. PART A is a simple, compact introduction to OMNITAB for people who have had no experience using a large computer. PART B describes the general and special features of the OMNITAB system. PART C gives explanations, with short examples, for the use of specific instructions. PART D is a complete list of the instructions which are in the system.

Hudson, P. A., Saulsbery, L. F., **An adjustable-slot-length UHF coaxial coupler with decade bandwidth,** *IEEE Trans. Micro. Theory Tech.* **MTT-19,** *No. 9, 781–783 (Sept. 1971).*

Key words: Attenuator; directional coupler, coaxial; power measurement, rf.

A coaxial directional coupler has been developed which allows adjustment of the length of the coupling slot to λ/4 or 3λ/4 throughout the frequency range 0.3 to 8.5 GHz. Coupling is flat to within 0.05 dB from 0.3 to 3 GHz (λ/4 mode) and 0.1 dB from 0.9 to 8.5 GHz (3λ/4 mode). The coupler has 50 dB coupling, 30 to 40 dB directivity and was designed primarily for high power measurement (1–1000 W) using a low-power meter on the sidearm. The VSWR for the two modes of operation is 1.02 to 1.05. Five octave bandwidth type couplers would be required to cover this same frequency range.

Hudson, R. D., **Critical review of ultraviolet photoabsorption cross sections for molecules of astrophysical and aeronomic interest,** *Nat. Stand. Ref. Data Ser., Nat. Bur. Stand. (U.S.), 38, 106 pages (Aug. 1971) $1.00, SD Catalog No. C13.48:38.*

Key words: Aeronomic; astrophysical; partial; photoabsorption cross sections; photodissociation; photoexcitation; photoionization; photon-scattering; total; ultraviolet cross sections.

This paper is devoted to a critical review of photoabsorption cross sections for molecules of aeronomic and astrophysical interest at wavelengths less than 3000 Å. A discussion of the relative merits of various experimental techniques is given along with possible systematic and random errors that may be associated with them. The problems in data analysis associated with finite spectral bandwidths are reviewed, with special emphasis on the interpretation of published absorption cross sections. This review does not contain a complete set of cross-section-versus-wavelength values for each molecule; the prepared figures are used to compare the results of several determinations or to point out where difficulties of interpretation might arise. However, references to all papers believed to contain the more reliable data are given.

Hussmann, E. K., McLaughlin, W. L., **Dose-distribution measurement of high-intensity pulsed radiation by means of holographic interferometry,** *Radiation Res.* **47,** *No. 1, 1–14 (July 1971).*

Key words: Calorimetry; depth dose; dosimetry; holography; interferometry; isodose.

A novel calorimetric method has been developed for evaluating the spatial distribution of radiation absorbed dose in transparent liquids, particularly for dosimetry of pulsed, high-intensity electron beams. Local temperature change is determined without the introduction of temperature sensors that may disturb the radiation field. The change in a liquid's refractive index, which is a function of temperature, is measured by an interferometric method employing holographic wavefront reconstruction. For radiation beams essentially symmetric to the direction of propagation, the three dimensional dose distribution can be derived from the information given by the interferogram. Dose distributions in water have been evaluated for short electron pulses of different energy spectra.

Hussmann, E. K., McLaughlin, W. L., **Dye films and gels for megarad dosimetry,** *Proc. United Kingdom Panel on Gamma and Electron Irradiation, The National Physical Laboratory, Teddington, England, July 1970, pp. 35–60 (April 1971).*

Key words: Dosimetry; dyes; films; gels; pulsed beams.

The liquid, gel, and thin-film radiochromic dye system developed by McLaughlin and Chalkley for dosimetry have been shown to be useful for measuring large doses from electron and x and gamma irradiations. The thin films are particularly suited to imaging and measuring radiation field profiles and dose distributions in various materials, even across interfaces of media with different stopping powers and absorption coefficients.

Hust, J. G., Sparks, L. L., **Standard reference materials: Thermal conductivity of electrolytic iron, SRM 734, from 4 to 300 K,** *Nat. Bur. Stand. (U.S.), Spec. Publ. 260–31, 19 pages (Nov. 1971) 35 cents, SD Catalog No. C13.10:260–31.*

Key words: Cryogenics; electrical resistivity; electrolytic iron; Lorenz ratio; Seebeck effect; thermal conductivity; transport properties.

Thermal conductivity data are reported for a specimen of electrolytic iron, SRM 734, for temperatures from 4 to 300 K. Variability of this iron was studied by means of electrical residual resistivity ratio measurements on 63 specimens. This study showed that with a 2-hour anneal at 1000 °C one can obtain a thermal conductivity Standard Reference Material that has variability of less than 1% in thermal conductivity.

Jennings, D. A., Baldwin, D. L., **Construction of a flashlamp-pumped dye laser and an acousto-optic modulator for mode-locking,** *Nat. Bur. Stand. (U.S.), Tech. Note 603, 33 pages (July 1971) $1.00, SD Catalog No. C13.46:603.*

Key words: Acousto-optic modulator; flashlamp-pumped dye laser; mode-locking; subnanosecond pulses.

In this paper is presented the design of a flashlamp-pumped dye laser capable of emitting light pulses 500 ns wide (FWHM) with a risetime of 300 ns. The energy output in the visible region of light is 1 to 10mJ with an energy conversion efficiency of about 0.01% at a repetition rate of 30 pps. The design of an acousto-optic modulator used to mode-lock the dye laser by intracavity loss modulation is presented. The laser output for a given cavity length depends on the frequency and voltage applied to the modulator; a 10%–100% modulated output can be obtained with 1 V rms–20 V rms, whereas a train of light pulses narrower than 0.8 ns (FWHM) can be obtained with 80 V rms.

Kao, R., Perrone, N., Capps, W., **Large-deflection solution of the coaxial-ring-circular-glass-plate flexure problem,** *J. Am. Ceramic Soc.,* **54,** *No. 11, 566–571 (Nov. 1971).*

Key words: Coaxial ring; flexure; glass; non linear elastic theory; strength.

Nonlinear deflections and radial surface stresses in thin elastic circular plates laterally deformed into symmetrical concave shapes are analyzed. The deformations are induced by loading each plate with a small center ring while the plate is resting on a ring of nearly the same diameter as the plate. The rings and plate are coaxial, i.e. concentric. Center deflections up to 3 and 4.5 times the plate thickness were predicted for ring-diameter ratios of 0.5 and 0.2, respectively. The predicted deflection profiles at various loads agreed quite well with those which were determined experimentally on a chemically strengthened glass plate. This analysis provides a new criterion for using the coaxial-ring loading method for flexural strength testing of brittle materials.

King, D. A., Madey, T. E., Yates, J. T., Jr., **Interaction of oxygen with polycrystalline tungsten II. Corrosive oxidation,** *J. Chem. Phys.* **55,** *No. 7, 3247–3253 (Oct. 1, 1971).*

Key words: Adsorption; chemisorption; corrosion; flash desorption; oxidation; oxygen; tungsten; tungsten oxides.

The kinetics of formation of a corrosive oxide layer of apparently unlimited thickness during the interaction of oxygen with a polycrystalline tungsten filament at temperatures between 500 and 1000 K has been investigated by line-of-sight flash desorption mass spectrometry. The major desorption product from this multilayer oxide film is WO_2, which desorbs over the temperature range 1000–1300 K. The rate of formation of the oxide film was shown to be directly proportional to the oxygen gas phase pressure at pressures $\leq 10^{-4}$ torr. A study of the temperature dependence of the oxidation rate revealed that the formation of the WO_2-producing oxide layer proceeds through two distinct steps; these occur subsequent to the first three stages in the interaction of oxygen with W characterized in Paper I. In the final state of oxidation, the rate is shown to be independent of the thickness of the oxide film. The results are in qualitative accord with the theoretical model of Mott. Desorption of the oxide film is a zero order process, with a desorption activation energy of 420 kJ mol^{-1}.

Kirsch, R. A., **Computer determination of the constituent structure of biological images,** *Comput. Biomed. Res.* **4,** *315–328 (1971).*

Key words: Artificial intelligence; image processing; pattern recognition.

A class of algorithms is described which enables computer quantized images to be decomposed into constituent parts reflecting the structure of the images. This decomposition is viewed as the morphological precursor to a higher level syntactic analysis. Numerical results for a typical biological image are presented.

Kirstein, A. F., **Universal testing machine of 12-million-lbf capacity at the National Bureau of Standards,** *Nat. Bur. Stand. (U.S.), Spec. Publ. 355, 18 pages (Sept. 1971) 30 cents, SD Catalog No. C13.10:355.*

Key words: Force calibration; large test facilities; structural testing; universal testing machine.

A 12-million pounds-force capacity universal testing machine, which is believed to be the largest of its kind in the world, has been put into operation in the Engineering Mechanics Laboratory of the National Bureau of Standards in Gaithersburg, Maryland. This hydraulically operated machine, which has an overall height of over 100 feet, was designed to test full scale structural components and to apply the forces needed to calibrate large capacity force measuring devices. The testing machine is capable of applying axial forces of 12,000,000 lbf in compression, 6,000,000 lbf in tension, and a transverse force of 4,000,000 lbf to a flexural specimen.

Kranbuehl, D. E., **Atomic, molecular, and ionic interactions,** *Dig. Lit. Dielectrics* **33,** *No. 2, 84–118 (1969).*

Key words: Dielectric, ionic polarizability, relaxation.

A review of those papers in the 1969 literature on dielectrics which make a significant contribution toward understanding the fundamental dielectric properties of atoms, molecules and ions.

Kranbuehl, D. E., Verdier, P. H., **Stochastic molecular model studies of the relaxation of vector end-to-end length in polymer chains,** *Am. Chem. Soc. Polymer Preprints* **12,** *No. 2, 625–628 (1971).*

Key words: End-to-end length; excluded volume; Monte Carlo; polymer chain dynamics; relaxation.

The effects of excluded volume interactions upon the dynamical behavior of random-coil polymer chains are studied by obtaining autocorrelation functions for the vector end-to-end length of lattice model chains of 9, 15, 33, and 63 beads by a Monte Carlo simulation technique. The configuration of the polymer chain, N–1 units long, is represented by a string of N connected points on a 3-dimensional cubic lattice. Excluded volume is accounted for by not allowing two beads to occupy the same lattice site. It is found that the relaxation of vector end-to-end length for a lattice chain with excluded volume varies substantially from that of a lattice chain without excluded volume. Relaxation of the vector end-to-end length requires from four to seven times as long as relaxation of its square, contrary to the predictions of simple models without excluded volume effects. This behavior suggest that the ratio of the relaxation time of vector end-to-end length to that of its square is a measure of the presence or absence of excluded volume effects.

Kulin, G., **Discussion of the paper "Triangular broad-crested weir,"** *by C. D. Smith and W. S. Liang, Proc. American Society Civil Engineers, Irrigation Drainage Div. 96,* **IR4,** *494–497 (Dec. 1970).*

Key words: Broad-crested; flow measurement; weirs.

Published data on discharge coefficients for triangular broad-crested weirs are analyzed using a boundary layer model. Effects of changing the critical Reynolds number for boundary layer transition and possible scale effects are pointed out.

Kuriyama, M., **On the principle of x-ray interferometry,** *Acta Cryst.* **A27,** *273–280 (1971).*

Key words: Diffraction theory; lattice constants; measurements; X-Ray interferometry; wave optics.

The scattering amplitude of an x-ray interferometer is calculated using a general theory of x-ray diffraction. Analytic expressions are given for the intensities of diffracted beams in interferometry; these expressions include the effect of the positions of each crystal lattice in addition to ordinary dynamical effects. It is concluded that the fringes observed in x-ray interferometry of a lattice spacing are accounted for by an optical effect rather than by dynamical effects of x-ray diffraction.

Langenberg, D. N., Taylor, B. N., **Precision measurement and fundamental constants, Proceedings of the International Conference held at the National Bureau of Standards, Gaithersburg, Maryland, August 3–7, 1970,** *Nat. Bur. Stand. (U.S.), Spec. Publ. 343, 543 pages (Aug. 1971) $6.00, SD Catalog No. C13.10:343.*

Key words: Fundamental constants; least squares adjustments; precision measurements.

This volume presents the Proceedings of the International Conference on Precision Measurement and Fundamental Constants, held at the National Bureau of Standards in Gaithersburg, Maryland, from August 3 through August 7, 1970. The conference brought together theoretical, experimental, and applied scientists for the purpose of discussing modern techniques of precision physical measurement and their application, along with modern theoretical developments, to the determination of the fundamental constants. The topics covered were: frequency and time standards; length standards; the velocity of light; the Rydberg constant; electrical standards; the proton gyromagnetic ratio; the Faraday constant; atomic masses; the proton magnetic moment; Josephson effects; x-rays; fine and hyperfine structure in simple atoms; lepton *g*-factor anomalies; the gravitational constants; least squares adjustments of the constants. These Proceedings contain the invited tutorial talks as well as the contributed papers presented at the Conference. Also included are the post-paper discussions and a panel discussion entitled "Should Least Squares Adjustments of the Fundamental Constants Be Abolished?"

Lawless, W. N., Radebaugh, R., Soulen, R. J., **Studies of a glass-ceramic capacitance thermometer between 0.025 and 2.4 K,** *Rev. Sci. Instr.* **42,** *No. 5, 567–570 (May 1971).*

Key words: Capacitance thermometer; refrigeration; $SrTiO_3$; thermometer.

Capacitance measurements from 0.025 to 2.4 K are reported for capacitance thermometers (made from an $SrTiO_3$ glass-ceramic crystallized at 1100 and 1203 °C) two of which were the ones reported in the previous article. It was found that the 1200 type thermometer has a useful thermometric range down to 0.06 K and a linear C–T region down to 0.5 K. The 1100-type thermometer has a useful range down to 0.110 K and a linear region down to 1.1 K. The measured data do not appear to be influenced by self-hearing or adiabatic correction effects. Both thermometers display an un-

expected increase in capacitance with decreasing temperature below their monotonically decreasing ranges. The 1100-type thermometer displays the more pronounced increase, with $C \propto T^{-1}$ from 0.100 to 0.025 K. It is argued that this T^{-1} behavior is due to the onset of an ultralow temperature phase transition in the glass crystallized $SrTiO_3$ and the possibility of using this effect to achieve adiabatic depolarization cooling is discussed.

Leasure, W. A., Jr., **Truck tire noise—preliminary results of a field measurement program,** *Proc. Purdue Noise Control Conference, Purdue University, West Lafayette, Indiana, July 14–16, 1971, pp. 41–48 (July 1971).*

Key words: Acoustics; noise measurement; noise pollution; noise (sound); sound transmission; tires; transportation noise.

This paper presents an inventory of peak A-weighted sound levels measured during an extensive parametric study conducted to characterize the noise generated by typical rib, cross-bar, and retread type truck tires in actual use. A test sample of nine tread designs, estimated to represent 70–80% (these exact designs) of the truck tire population on the road today, was investigated considering the following variables: wear, loading, speed, pavement surface, and tire location. Test vehicles included both single-chassis vehicles and a tractor-trailer.
The results show that the A-weighted sound level increased with either an increase in load or speed. The pocket retread design always produced the highest level followed by the cross-bar tires and then the rib tires. This ranking held for both new and half-worn tires. The influence of wear and pavement surface is more comple . For all of the tread designs except one there was an increase in noise level between the new and half-worn states. The results for different pavement surfaces are much the same as with wear. The generated noise appears to depend on both the specific tread design and the surface roughness. Individual tires do contribute differently to the overall level depending on their location on the vehicle. In some cases, significant reductions in the noise level were observed when "noisy" tires were mounted inboard of "quieter" tires.
The paper includes a discussion of the measurement and analysis techniques utilized for the establishment of this data base.

Lee, T. G., **Interlaboratory evaluation of smoke density chamber,** *Nat. Bur. Stand. (U.S.), Tech. Note 708, 80 pages (Dec. 1971) 75 cents, SD Catalog No. C13.46:708.*

Key words: Building materials; fire tests; interlaboratory tests; optical density; round robin; smoke; smoke density chamber; statistical analysis.

Results are reported of an interlaboratory (round-robin) evaluation of the smoke density chamber method for measuring the smoke generated by solid materials in fire. A statistical analysis of the results from 10 material-conditioned combinations and 18 laboratories is presented. For the materials tested, the median coefficient of variation of reproducibility was 7.2% under non-flaming exposure conditions and 13% under flaming exposure conditions. A discussion of errors and recommendations for improved procedures based on user experience is given. A tentative test method description is included as an appendix.

Little, J. L., Standards Coordinator, **Hollerith punched card code,** *Nat. Bur. Stand. (U.S.), Fed. Info. Process. Stand. Publ. (FIPS Pub.) 14, 4 pages (1971) 10 cents, SD Catalog No. C13.52:14.*

Key words: American Standard Code for Information Interchange; ASCII; card punch; card reader; data communications; data interchange; data processing; electric accounting machine; EAM cards; Federal Information Processing Standard; Hollerith punched card code; Hollerith punched cards; information interchange; information processing; punched cards.

This publication provides a standard set of 128 hole patterns which represent the 128 characters of the Federal Standard Code for Information Interchange (ASCII) FIPS 1, in 12-row, 80 column, rectangular hole, "Hollerith" punched cards, or the subsets of ASCII as specified in FIPS 15, Subsets of the Standard Code for Information Interchange. It adopts one-half of the 256 hole patterns given in the American National Standard X3.26–1969, Hollerith Punched Card Code.

Little, J. L., Standards Coordinator, **Subsets of the Standard Code for Information Interchange,** *Nat. Bur. Stand. (U.S.), Fed. Info. Process. Stand. Publ. (FIPS Pub.) 15, 10 pages (1971) 25 cents, SD Catalog No. C13.52:15.*

Key words: American Standard Code for Information Interchange; ASCII; coded character subsets; codes; data communication; data interchange; data processing; Federal Information Processing Standards; graphic character subsets; graphic subsets; information interchange; information processing; standards; subsets.

This publication provides three subsets of 95, 64 and 16 graphic characters derived from the Federal Standard Code for Information Interchange (FIPS 1), which was adopted from the American Standard Code for Information Interchange (ASCII) X3.4–1968. These subsets are for use in Federal printers, display devices, punched card equipment, and other data processing or communication equipments which utilize a character subset less than the full 128-character set of FIPS 1.

Little, J. L., Standards Coordinator, **Rectangular Holes in Twelve-Row Punched Cards,** *Nat. Bur. Stand. (U.S.), Fed. Info. Process. Stand. Publ. (FIPS Pub.) 13, 4 pages (1971) 10 cents, SD Catalog No. C13.52:13.*

Key words: American Standard Code for Information Interchange; ASCII; card punch; card reader; data communications; data interchange; data processing; electric accounting machine; EAM cards; Federal Information Processing Standard; Hollerith punched cards; information interchange; information processing; punched cards; rectangular holes.

This publication provides information on the size, location and dimensional tolerances of rectangular holes in 12-row, $3^1/_4$ inch wide punched cards. It applies to card reading and punching equipment used in data processing, communications and similar operations in the Federal government. This Federal standard adopts in whole a revised version of American National Standard X3.21–1967, Rectangular Holes in 12-Row Punched Cards.

Loebenstein, W. V., **Calculations and comparisons of nonideal gas corrections for use in gas adsorption,** *J. Colloid Interface Sci.* **36,** *No. 3, 397–400 (July 1971).*

Key words: Adsorption; correction for gas; gas; gas law correction; imperfect gas; nonideal gas; second virial coefficient.

Volumetric gas adsorption measurements have become increasingly popular in recent years. The techniques for determination of surface area and pore size distribution have become so commonplace that they can almost be termed routine. At the temperature of the adsorption experiment, it is necessary at each equilibrium pressure to correct for the nonideal behavior of the gas surrounding the sample in order to obtain by difference an accurate evaluation of the amount of gas actually adsorbed. The correction factors that are continually used by most adsorption chemists have not been critically reexamined by these ultimate users since they were originally recommended more than 30 years ago. Indeed, textbooks published more than 25 years later continue to perpetuate the same correction factors. It is the purpose of this paper, by comparing correction factors derived from various sources, to avoid gross inaccuracies and to suggest a procedure whereby the investigator may estimate his own factor in instances where tabulated values are not readily available to him.

Mandel, J., **Repeatability and reproducibility,** *Mater. Res. Stand.* **11,** *No. 8, 8–16 (August 1971).*

Key words: Evaluation of; interlaboratory testing; precision, repeatability; reproducibility; test methods.

A simple method is presented for the evaluation of the repeatability and the reproducibility of test methods. The method obviates such difficulties as transformations of scale or weighted analysis of variance.
It is shown, furthermore, that the concepts of repeatability and

reproducibility are, by themselves, insufficient to answer the major questions related to interlaboratory testing. Alternative procedures are mentioned. Finally, the paper presents a rationale for a proper choice of the number of laboratories and the number of replicate determinations required for an adequate interlaboratory study.

Marlow, W. F., LaFleur, P. D., **Standard reference materials for analysis of environmental samples,** *Proc. Symp. Nuclear Techniques in Measurement and Control of Environmental Pollution, Salzburg, Austria, Oct. 26–30, 1970, pp. 91–94 (International Atomic Energy Agency, Vienna, Austria, March 1971).*

Key words: Activation analysis; biological; botanical; environment; Standard Reference Material.

As is evidenced by the large number of publications on the subject, especially at this Symposium, many groups are engaged in the analysis of environmental samples of all kinds for their trace element content, as well as for their major constituent content. Perhaps the most versatile and popular method for the rapid, economical analysis of environmental samples for a large number of elements is neutron activation analysis. Also extensively used are x-ray fluorescence analysis, atomic absorption spectroscopy, spark-source mass spectrometry, and emission spectrometry. In many cases, meaningful results for multi-element analysis have been difficult to obtain because of the lack of adequate standard materials, despite the limited efforts by some investigators to produce them. Particularly, in the cases of neutron activation analysis and spark-source mass spectrometry the matrix of the sample can have a pronounced effect upon the analysis. It is extremely important that the standard material have a matrix as similar as possible to that of the sample. At present, such suitable standard materials are not widely available. Therefore, the US Atomic Energy Commission and the US National Bureau of Standards have instituted a program for the production of a series of special Standard Reference Materials, fully characterized for at least 22 and possibly 30 elements, suitable for use in the analysis of environmental samples, particularly biological samples. These Standard Reference Materials will be available for purchase by all laboratories. Multi-laboratory intercomparisons of these Standard Reference Materials will be encouraged.
Details of the nature of these materials, elements for which they will be characterized and analytical techniques used in standardizing them will be discussed.

Marsden, C. P., **Tabulation of data on semiconductor amplifiers and oscillators at microwave frequencies,** *Nat. Bur. Stand. (U.S.), Tech. Note 597, 48 pages (Dec. 1971) 50 cents, SD Catalog No. C13.46:597.*

Key words: Amplifiers; basic characteristics; microwave; oscillators; semiconductor; solid state.

This tabulation includes some of the basic characteristics of semiconductor microwave devices, specifically amplifiers and oscillators of foreign and domestic origin.

Marshall, R. D., **Surface pressure fluctuations near an axisymmetric stagnation point,** *Nat. Bur. Stand. (U.S.), Tech. Note 563, 67 pages (Aug. 1971) 70 cents, SD Catalog No. C13.46:563.*

Key words: Disk; pressure fluctuations; stagnation point; turbulence.

Surface pressure fluctuations on a circular disk placed normal to a turbulent air stream have been investigated. Turbulence intensities of approximately 10% were produced by a coarse grid installed at the test-section entrance. The turbulent field in the neighborhood of the disk was homogeneous and nearly isotropic.
Experimental results indicate that existing linear theories which do not consider distortion of the flow fail to predict the nature of surface pressure fluctuations on a bluff body. Only for wavelengths which are large compared to the body do these theories yield satisfactory results. A strong attenuation of the high frequency components occurs as the flow stagnates. This is accompanied by a transfer of energy from short to long wavelengths. The opposite effect is observed as the flow attains a radial direction and approaches the edge of the disk. A neutral wavelength which undergoes little change in energy was observed. Integral scales of surface pressure fluctuations are much larger than the lateral integral scale of the free-stream turbulence.

Marzetta, L., **A high-performance phase-sensitive detector,** *IEEE trans. Instr. Meas.* **IM–20,** *No. 4, 296–301 (Nov. 1971).*

Key words: Operational amplifier, op amp., operational rectifier, phase-sensitive detector, signal extraction ratio.

A phase-sensitive detector is described that enables the retrieval of signals submerged 90 dB (voltage) below the noise level. Operation over four decades of signal amplitude (a full scale linearity error of 0.01%) is possible for a frequency range of 0 to 150 Hz. Design features are offered allowing an experimenter to construct the device from inexpensive components and be assured a predictable performance.

McBee, C. L., Kruger, J., **Optical changes in oxide films on iron prior to breakdown,** *Nature Phys. Sci.* **230,** *No. 17, 194–195 (April 26, 1971).*

Key words: Chloride; ellipsometry; passive film; spectroscopy.

Evidence for optical changes in the passive film on iron prior to complete breakdown by chloride is presented. The technique of ellipsometric-spectroscopy is used to locate a wavelength affected by the chloride addition. The recovery of the passive film by removal of the chloride ion is also reported.

McCarty, R. D., Weber, L. A., **Thermophysical properties of oxygen from the freezing liquid line to 600 R for pressures to 5000 psia,** *Nat. Bur. Stand. (U.S.), Tech. Note 384, 189 pages (July 1971) $1.50, SD Catalog No. C13.46:384.*

Key words: Density; dielectric constant; enthalpy; entropy; equation of state; fixed points; heat transfer coefficients; index of refraction; Joule-Thomson; latent heat; melting point; Prandtl number; oxygen; specific heat.

Tables of thermophysical properties of oxygen are presented for temperatures from the melting line to 600 R for pressures to 5000 psia. The tables include, entropy, enthalpy, internal energy, density, volume, speed of sound, specific heat, thermal conductivity, viscosity, thermal diffusivity, Prandtl number and the dielectric constant for 79 isobars. Also included in the isobaric tables are quantities of special utility in heat transfer calculations: $(\partial P/\partial V)_T$, $(\partial P/\partial T)_p$, $V(\partial H/\partial V)_P$, $V(\partial P/\partial U)_V$, $V(\partial P/\partial V)_T$, $1/V(\partial V/\partial T)_P$.
In addition to the isobaric tables, tables for the saturated vapor and liquid are given which include all of the above properties, plus the surface tension. Tables for the $P-T$ of the freezing liquid, index of refraction and the derived Joule-Thomson inversion curve are also presented. The specific heat of the saturated liquid is given in graphical form. A temperature-entropy chart and a Mollier diagram are also included.

McDowell, H., Brown, W. E., Sutter, J. R., **Solubility study of calcium hydrogen phosphate. Ion-pair formation,** *Inorg. Chem.* **10,** *1638–1643 (Aug. 1971).*

Key words: Calcium-phosphate ion pairs; solubility of anhydrous dicalcium phosphate; solubility of calcium monohydrogen phosphate; solubility of dibasic calcium phosphate.

The solubility of $CaHPO_4$ has been determined in the ternary system, $Ca(OH)_2$-H_3PO_4-H_2O, at 5, 15, 25 and 37 °C. The same results are obtained when equilibrium is approached from super- and undersaturation. Solubility product constant, $K_{sp}=(Ca^{2+})(HPO_4^{2-})$, varies with pH unless formation of ion pairs $CaHPO_4^\circ$ and $CaH_2PO_4^+$ is taken into account. Solubility product constants and standard errors for $CaHPO_4$ are $1.97\pm0.03\times10^{-7}$, $1.64\pm0.01\times10^{-7}$, $1.25\pm0.01\times10^{-7}$ and $0.94\pm0.01\times10^{-7}$ at 5, 15, 25 and 37 °C, respectively. Association constants and standard errors are 243 ± 32, 187 ± 24, 377 ± 37 and 355 ± 62 for $CaHPO_4^\circ$ and 5.2 ± 0.7, 9.6 ± 0.6, 9.6 ± 0.7 and 8.1 ± 0.6 for $CaH_2PO_4^+$ at the same respective temperatures. Thermodynamic functions for the dissolution reaction for $CaHPO_4$ and the association reactions for $CaHPO_4^\circ$ and $CaH_2PO_4^+$ are also presented.

Menis, O., Iyer, C. S. P., **Spectrophotometric determination of vanadium and iron with β-isopropyltropolone,** *Anal. Chim. Acta* **55,** *89–95 (1971).*

Key words: Analysis of steel samples; extraction with β-isopropyltropolone; simultaneous determination of vanadium and iron; spectrophotometric determination of vanadium.

A spectrophotometric procedure is described for the determination of vanadium and for the simultaneous determination of iron and vanadium using two wavelength measurements, at 470 and 540 nm or 418 and 470 nm. It is based on the formation of chelate complex with β-isopropyltropolone. The complex is extracted with chloroform and in the presence of alcohol the color develops rapidly and is stable for at least 24 hours. The precision of the calibration curve is 1 percent relative standard deviation. The application and results of the analysis of NBS Standard Reference Material steel samples are presented.

Mighell, A. D., Santoro, A., Donnay, J. D. H., **Reduced cells, Chapter in International Tables for X-ray Crystallography,** *Norman F. Henry, and Kathleen Lonsdale, Ed., II, 530–535 (The Kynoch Press, Birmingham, England, 1969).*

Key words: Bravais lattice, identification, reduced cells, transformation matrix.

Tables and text are given that make it possible to determine the reduced cell for any lattice. Finally, a detailed table is presented which establishes the relationship of each of the 44 reduced cell types to one of the Bravais lattice.

Moore, G. A., **Design of a practical scanner unit for precision analysis of micrographs,** *Pattern Recognition* **3,** *91–122 (Oct. 1971).*

Key words: Analysis of Microstructures; Automatic Scanning (of micrographs); Precision Scanning (of micrographs); Quantitative Microscopy.

A precision mechanical scanner has been constructed for the purpose of preparing digital transcriptions of micrographs for computer analysis, and of performing elementary analysis without resort to a computer. Design criteria include convenience of operation and precision sufficient to correctly record all of the real information in one micrographic field.
Performance data are included. An analysis is given of the precision which may be expected in estimating area and volume percentage of a phase under various conditions. The attained precision is at least an order of magnitude greater than is normally obtained by manual methods.

Moore, R. T., **Determination of performance of digital data communication systems,** *(Proc. IEEE, ICC 71 CIC Intern. Conf. Communications, Montreal, Canada, June 14–16, 1971), IEEE, ICC 71 CIC Conf. Record VII, Session 12A, VIII, 12–1—12–3 (1971).*

Key words: Digital data communication; digital system performance; draft standard ANSI X3; RER; TOT; RER.

An overview is presented of the work of American National Standards Institute Task Group X3S3.5 in the development of a standard for the determination of the performance of data communication systems.
Four performance criteria are identified. These are: (1) Transfer Rate of Information Bits (TRIB), a measure of information throughput; (2) Transfer Overhead Time (TOT), a measure of delays associated with the communications process; (3) Residual Error Rate (RER); and (4) System Availability (A). These criteria, as defined, are independent and are both necessary and sufficient to express the performance of any Information Path operated in accordance with the applicability limitations of the document.
Data communications system description is developed on a functional rather than a physical basis, and only to the extent necessary for performance determination.
The five possible phases of data communications are identified as: (1) Connection Establishment, (2) Link Establishment, (3) Information Transfer, (4) Link Termination, and (5) Connection Disestablishment. The beginning and end of each of these phases is rigorously defined and these definitions support the methodology for determining values for the performance criteria TRIB and TOT.

Myklebust, R. L., Heinrich, K. F. J., **Rapid quantitative electron probe microanalysis with a nondiffractive detector system,** *Am. Soc. Testing Mater. Spec. Tech. Publ. 485, pp. 232–424 (1971).*

Key words: Electron diffraction; electron probes; evaluation; gas flow; lithium; microanalysis; multichannel analyzer; proportional counters; quantitative analysis; silicon; solid state counters; tests; x-ray spectra; x-ray spectrometers.

Nondiffractive detector systems on electron probe microanalyzers have decreased the time required for a qualitative analysis from 30 or 40 min to 1 or 2 min. The nondiffractive technique may be extended to the quantitative determination of an element by comparing either the peak height or the area beneath the peak of the signal from the specimen with that from the pure chemical element or a standard of known composition run under identical conditions. Results are given for quantitative analyses of several materials with a lithium-drifted silicon detector, used for x-ray lines above 1 keV, and a gas flow proportional detector, for x-ray lines from 0.16 to 1.5 keV. Quantitative analyses can be accomplished only when the experimental conditions are carefully selected and maintained throughout the measurement. They are then sufficiently precise to warrant the use of a "matrix" correction procedure to obtain concentrations. An analog curve analyzer is useful for resolving overlapping peaks and for integrating the areas beneath the peaks.

Oberholtzer, B. L., **Publications of the National Bureau of Standards 1970,** *Nat. Bur. Stand. (U.S.), Spec. Publ. 305 Suppl. 2, 378 pages (July 1971) $3.25, SD Catalog No. C13.10:305 Suppl 2.*

Key words: Abstracts; key words; NBS publications; publications.

This Supplement to Special Publication 305 Supplement 1 of the National Bureau of Standards lists the publications of the Bureau issued between January 1, 1970 and December 31, 1970. It includes an abstract of each publication (plus some earlier papers omitted from Special Publication 305 Supplement 1), key-word and author indexes; and general information and instructions about NBS publications. Previous catalogs of NBS publications referenced in Special Publication 305, Supplement I remain in effect.

Odom, J. V., Editor, **U.S. Metric Study Interim Report. Testimony of nationally representative groups,** *Nat. Bur. Stand. (U.S.), Spec. Publ. 345–12, 180 pages (July 1971) $1.50, SD Catalog No. C13.10:345–12.*

Key words: International System of Units; metric conversion; metric system; metric usage; metrication; metrication, attitudes toward; metrication, costs and benefits of; metrication, impact of, National Metric Study Conferences; SI; U.S. Metric Study.

This publication, a part of the U.S. Metric Study series, summarizes the inputs received from the more than 700 associations, societies, unions and other groups which were invited to submit their opinions and viewpoints on the issues raised by the U.S. Metric Study Act. Most of these submissions were publicly presented at hearings held during the course of the Study.

Page, C. H., **External field of an ideal toroid,** *Am. J. Phys.* **39,** *No. 9, 1039–1043 (Sept. 1971).*

Key words: Leakage flux; magnetic field; toroid; transformer; vector potential.

The external magnetic field of an ideal toroid vanishes for dc excitation but not for ac excitation. The external static field has a nonvanishing vector potential; the emf in a transformer winding is due to the time variation of this vector potential. An expression for the external flux density is a negligible fraction of the flux density in the core.

Page, C. H., **On the external magnetic field of a closed-loop core,** *Am. J. Phys.* **39,** *No. 10, 1206–1209 October 1971.*

Key words: Magnetic field; solenoid; toroid; transformer; vector potential.

An infinite solenoid, or a toroidal coil, has no external magnetic field for dc excitation but has a nonvanishing vector potential field. The development of the steady-state condition from the transient response to step excitation is discussed. Under ac excitation, an external magnetic field must be present, but in practical cases its magnitude is negligible.

Parker, V. B., Wagman, D. D., Evans, W. H., **Selected values of chemical thermodynamic properties—Tables for the alkaline earth elements (Elements 92 through 97 in the standard order of arrangement),** *Nat. Bur. Stand. (U.S.), Tech. Note 270–6, 119 pages (Nov. 1971) $1.25, SD Catalog No. C13.46:270–6.*

Key words: Enthalpy; entropy; Gibbs energy of formation; beryllium compounds; magnesium compounds; calcium compounds; strontium compounds; barium compounds; radium compounds.

Contains tables of values for the standard heats and Gibbs (free) energies of formation, entropies and enthalpies at 298.15 K and heats of formation at 0 K for compounds of beryllium, magnesium, calcium, strontium, barium, and radium (elements 92–97 in the Standard Order of Arrangement). These tables are a continuation of the comprehensive revision of NBS Circular 500.

Persson, K–B, Johnson, E. G., Jr., **The errors in plasma measurements by the microwave cavity techniques.** *Nat. Bur. Stand. (U.S.), Tech. Note 607, 64 pages (Oct. 1971) 65 cents, SD Catalog No. C13.46:607.*

Key words: Collision frequency; helium negative glow discharge; microwave cavity; plasma density.

This report presents the results of a theoretical and experimental study of the microwave cavity techniques used in measuring electron density and collision frequency in transient plasmas. Sources of errors are discussed and certain calibration procedures are recommended to minimize the error. In particular, the abnormal negative glow discharge in helium is presented as an inexpensive reference plasma for calibration purposes.

Phucas, C. B., Technical Standards Coordinator, **Package quantities of cubed, sized, crushed and block ice,** *Nat. Bur. Stand. (U.S.), Prod. Stand. 48–71, 10 pages (Nov. 1971) 15 cents, SD Catalog No. C13.20/2:48–71.*

Key words: Block ice, package quantities of; crushed ice, package quantities of; cubed ice, package quantities of; ice, package quantities of; package quantities of ice; sized ice, package quantities of.

This Voluntary Product Standard covers the net weights of the package quantities recommended for cubed, sized, crushed, and block ice. Definitions of terms and methods for identifying products packaged in accordance with this Standard are included.

Phucas, C. B., Technical Standards Coordinator, **Paper ice bag sizes,** *Nat. Bur. Stand. (U.S.), Prod. Stand. 44–71, 12 pages (Sept. 1971) 15 cents, SD Catalog No. C13.20/2:44–71.*

Key words: Bag sizes, ice; ice bag sizes; paper ice bag sizes.

This Voluntary Product Standard covers the dimensions and the capacities of paper ice bags intended for use in the packaging of cubed, sized, crushed, and block ice. Methods of measuring and for identifying bags that conform to this standard are provided.

Phucas, C. B., Technical Standards Coordinator, **Portable picnic coolers,** *Nat. Bur. Stand. (U.S.), Prod. Stand. 49–71, 9 pages (October 1971) 15 cents, SD Catalog No. C13.20/2:49–71.*

Key words: Coolers, portable picnic; picnic coolers, portable; portable picnic coolers.

This Voluntary Product Standard covers portable picnic coolers in which the smallest of the internal dimensions exceeds 6 inches and the total continuous volume exceeds 1.1 cubic feet. Included in the Standard are requirements relating to the construction of coolers and to the closures, release devices, and handles of picnic coolers. A test for determining the force required to release the closure is included also. Methods of identifying products which conform to the Standard are provided.
For the purposes of this Standard, the term "picnic cooler" shall be used to include "beverage coolers," "ice chests," portable "food chests," and the like, which are designed to be carried by an individual.

Plitt, K. F., Utech, H. P., **Flammability of turnout coats tested,** *Fire Eng.* **124,** *No. 10, 60 (Nov. 1971).*

Key words: Bunker coats; fabric flammability; firefighter clothing; fireman; flame resistance; turnout coats.

Flame resistance tests (vertical burn method) were conducted on four commercially purchased firefighters' turnout coats. Each coat had three fabric layers: outer shell, inter lining, and inner lining. The results show that two of three fabric layers in each coat produced a char length of 12 inches.

Post, M. A., **Copolymer determination in surface filler,** *Paint Varnish Prod.* **61,** *No. 9, 31–38 (Sept. 1971).*

Key words: Absorbance ratio method; infrared spectroscopy; resins; styrene-butadiene; surface fillers, vinyl toluene-acrylate; vinyl toluene-butadiene.

Styrene-butadiene, vinyl toluene-butadiene and vinyl toluene-acrylate copolymers in surface fillers are quantitatively determined by two methods. In one, a dual extraction method, which should be useful in acceptance testing of solvent type fillers, the resin is determined as the difference between the total benzene and *n*-pentane extractables. The second method, a combination of single extraction and infrared analysis, involves determination of the total benzene extractables and the resin content therein. The latter is determined by measuring the $3.3\mu m/3.5\mu m$ absorbance ratio of cast films from the benzene extract, using the baseline method, and reading the weight percent resin from the appropriate standard curve. This method depends on a constant ratio of styrene to butadiene, vinyl toluene to butadiene or vinyl toluene to acrylate. Its use is restricted to resins of a particular monomer ratio for which a standard curve has been made. These methods were developed and confirmed using commercially prepared fillers of known resin content.

Powell, F. J., **Research needs in thermal insulation,** *(Proc. Symp. Thermal Insulation, Columbus, Ohio, Feb. 5–8, 1968), ASHRAE (Amer. Soc. Heat Refrig. Air-Cond. Eng.) Bull. Thermal Insulation, pp. 14–17 (1971).*

Key words: Computers; load calculation; thermal insulation; transient heat flow.

The role that research in respect to thermal insulation can play will be examined in this paper. Efforts to develop better insulation materials through research and to search for better methods of application need to be continued, and, in addition, the need to develop methods of measurement, performance coefficients, load calculations and applications based on transient or dynamic conditions of heat flow rather than steady-state concepts will be discussed. With the advent of computers, the sophistication required for treating the complex transient heat flow problems becomes feasible and the time has arrived for research to enable accurate estimation of transient loads that are indicative of actual performance.

Powell, F. J., Robinson, H. E., **The effect of moisture on the heat transfer performance of insulated flat-roof constructions,** *Nat. Bur. Stand. (U.S.), Bldg. Sci. Ser. 37, 81 pages (Oct. 1971) 75 cents, SD Catalog No. C13.29/2:37.*

Key words: Flat roofs; heat transfer; moisture transfer; thermal insulation.

A solution to the problem of unwanted moisture in the thermal insulation of flat roofs was found during a recently completed laboratory investigation of the effects of moisture on heat transfer through these constructions. The objective of the research was to ascertain how much the insulating performance of conventional constructions, having insulation over concrete decks, was affected by moisture. This is presented as Part I. Also, the objective was to investigate properties of materials, their arrangement and dimensions which would yield a construction having an adequate degree of self-drying ability, combined with low winter moisture regain rate. This is presented as Part II. The results show that the best insulating and moisture performance was obtained by utilizing the heat of the summer sun on the roof to vaporize and transfer to the room beneath any free moisture contained within the construction. Roof specimens made from moderately vapor-permeable materials without conventional vapor barriers were, in winter, able to accommodate the small quantity of slowly accumulated condensation without dripping or severe loss of insulating value. During the nine-year investigation, the performance characteristics of 73 insulated roof deck specimens were obtained and two new methods of measurement were developed. Criteria for the design of self-drying insulated flat roofs were developed and limits of the parameters containing the main variables that affect performance were suggested.
This paper presents complete results of the research which was sponsored jointly by the National Bureau of Standards, the Army, the Navy, and the Air Force.

Rasberry, S. D., **Applications of x-ray analysis,** *20th annual Denver x-ray conference, Denver, 11–13, August 1971, Appl. Opt.* **10,** *No. 12, 2795 (Dec. 1971).*

Key words: Applied x-ray analysis; conference report; material analysis; x-ray diffraction; x-ray fluorescence.

In this meeting report of the 20th Annual Denver X-ray Conference, the general nature of this series of meetings is outlined. Some details specific to the papers presented this year are reported.

Reed, R. P., Durcholz, R. L., Schramm, R. E., Patrician, T. J., **Study of cryogenic storage tank fatigue life,** *Nat. Bur. Stand. (U.S.), Tech. Note 609, 86 pages (Aug. 1971) 75 cents, SD Catalog No. C13.46:609.*

Key words: Fatigue; fracture; impact; low temperature; mechanical property equipment; stainless steel.

Two 300 series stainless steels were tested for impact-fatigue life and tensile properties as a function of temperature, percent transformed phase (martensite), stress level, and specimen geometry. These alloys were studied to predict the fracture characteristics of parent material and weld joints in large cryogenic dewars which are subjected to periodic stresses. Normally, AISI 304 is employed in the construction of such dewars. Under fatigue loading conditions at cryogenic temperatures, the behavior of AISI 304 is complicated by the gradual transformation to a martensitic structure. The influence of this transformation on the fracture characteristics was studied. For this purpose, a new impact-fatigue test and necessary equipment were developed.
The fatigue strength of AISI 304 and 310 exhibit similar trends, but at a given fatigue life and temperature, the fatigue strength of AISI 304 is slightly superior. AISI 310 displays an endurance limit of about 20,000 psi; the 304 limit is 25–30,000 psi. However, the lowest endurance limit (weakest) specimens appear to be the triaxially-loaded AISI 304 weld specimens which have an endurance limit near 10,000 psi. Little temperature-dependence of the impact-fatigue properties was observed.

Robinson, B. D., **U.S. Metric Study Interim Report. Education,** *Nat. Bur. Stand. (U.S.), Spec. Publ. 345–6, 216 pages (July 1971) $1.75, SD Catalog No. C13.10:345–6.*

Key words: Education; International System of Units; metric conversion; metric system; metric usage; metrication; metrication, attitudes toward; metrication, costs and benefits of; metrication, impact of; SI; U.S. Metric Study.

This publication concerns the effects of increasing worldwide use of the metric system on education in the United States. The study was carried out and the report prepared for the U.S. Metric Study by the Education Development Center in Newton, Massachusetts. The aims of this education study were fourfold: (1) to assess the educational advantages and disadvantages of both the metric and the customary systems of units, (2) to determine the current usage of metric measures in U.S. schools and trends in that usage, (3) to find the ways in which education would have to change as the U.S. accommodates to increased worldwide use of the metric system, under a laissez faire or a planned approach, and estimate the costs of the changes, and (4) to make recommendations of ways in which to take best advantage of said changes. The report also discusses and suggests ways of achieving curriculum changes needed in view of increasing metric usage. The publication includes the program of the Education Conference, held in October, 1970, as one of a series of National Metric Study Conferences, and the texts of the key papers presented at that conference by the National Education Association and the National Science Teachers Association.

Robinson, D. C., **Determination of dynamic loads in a high-frequency direct-stress fatigue machine,** *Nat. Bur. Stand. (U.S.), Tech. Note 578, 24 pages (June 1971) 35 cents, SD Catalog No. C13.46:578.*

Key words: Dynamic loads; dynamometer; fatigue machine.

A refined test procedure is given for accurately recording the dynamic signals from instrumented test bars used to measure loads during simulated fatigue tests. Loads indicated by the load transducer of a direct-stress fatigue machine are compared with those determined from these instrumented test bar specimens which have been calibrated under static conditions. An application of this procedure is described for a resonant, electromagnetic, direct-stress fatigue machine having an optical dynamometer for indicating programmed loads. The variables investigated were the operating speed, cyclic load and specimen stiffness. In addition, the influence of test fixture mass on the load measurements was determined at one test frequency. The mean loads indicated by the instrumented test bars are compared with those indicated by the dynamometer to determine the errors in load measurements under various test conditions.

Rothrock, B. D., Editor, **U.S. Metric Study Interim Report. The consumer,** *Nat. Bur. Stand. (U.S.), Spec. Publ. 345–7, 152 pages (July 1971) $1.25, SD Catalog No. C13.10:345–7.*

Key words: Consumers; International System of Units; metric conversion; metric system; metric usage; metrication; metrication, attitudes toward; metrication, costs and benefits of; metrication, impact of; National Metric Study Conferences; SI; U.S. Metric Study.

This report, one of a series prepared pursuant to the U.S. Metric Study Act, presents information on U.S. consumers' knowledge of the metric system and attitudes and opinions regarding metrication in the U.S., and discusses the effects of increasing worldwide metric usage on selected areas of consumer concern. This study is based on 1) an extensive survey conducted by the Survey Research Center of the University of Michigan and (2) prepared expert papers on selected areas of consumer interest. The survey data permitted an analysis of the receptivity of consumers to metrication, and of the need and possible effecitveness of a program to educate citizens should planned metrication be undertaken.

Rubin, S., Oettinger, F. F., **Thermal hysteresis and its possible effect in restricting the hot-spot-free operating range of some power transistors,** *IEEE Trans. Electron Devices* **ED–18,** *No. 6, 393–394 (June 1971).*

Key words: Current constriction; d-c current gain; hot spots; thermal hysteresis; therographic measurements; transistors.

Studies conducted on a number of silicon power transistors indicate that for some devices a hot spot, once formed, will remain even though the power dissipation is reduced to a level at which operation was previously free of hot spots. The hot spot can be

eliminated only by a significant reduction in power dissipation from the level at which the hot spot first appeared. The effect of the hot spot on reliable device operation is discussed.

Rukwied, A., Ruff, A. W., Willard, W. A., **Study of the cellular solidification structure in a continuously cast high purity copper,** *Metallurgical Trans.* **2,** *2105–2114 (August 1971).*

Key words: Cavities; cellular solidification; constitutional supercooling, copper (99.999%); dislocation arrangements; distribution of impurities; precipitate particles; thermomechanical treatment.

The aim of this paper is to characterize the principal microstructural features of continuously cast high purity copper (99.999 pct Cu), particularly those which might influence high temperature creep. This material contains a cellular solidification structure resulting from impurity segregation due to constitutional supercooling of the melt during solidification. This structure could not be eliminated from the solid copper by thermomechanical treatment. The grown-in structure was studied using optical and electron metallography as well as etch-pitting techniques. In the as-cast material a loose network of dislocation tangles was observed, and in certain locations, preferential etching attack. In addition, small voids were found within the dislocation tangles. Thermomechanical treatment eliminated the dislocation tangles almost entirely, but left locations susceptible to preferential etching attack. At those locations impurities were probably concentrated into zones of a size of a few 1000Å. From solubility and concentration considerations, small precipitates (less than 80Å in size) or clusters of carbon are suspected.

Rupp, N. W., Bowen, R. L., Paffenbarger, G. C., **Bonding cold-curing denture base acrylic resin to acrylic resin teeth,** *J. Am. Dental Assoc.* **83,** *601–606 (Sept. 1971).*

Key words: Acrylic teeth; adhesion; autoadhesion; bonding cold-curing methyl methacrylate; dentures; tensile strength.

Bonding of cold-curing acrylic resin to acrylic resin teeth increases tooth retention and strengthens denture bases because the plastic teeth become an integral part of the denture base. Bonding was effected in this manner; the necks of the teeth were coated with a solution of equal parts by bolume of methylene chloride and cold-curing methyl methacrylate monomer. This treatment combines a solvent attack on the teeth with polymerization bonding and develops tensile strengths of more than 80% of those of the acrylic resin denture base materials. The bonding was verified in experimental dentures made of a compression molded and a pour type poly(methyl methacrylate). The resin teeth became integral parts of the denture as evidenced by their retention in the base. On application of stresses, the fracture lines went through the teeth rather than through the tooth-denture base interfaces as before. The technique adds neither time nor equipment to currently used laboratory procedures.

Ryan, J. V., Editor, **The flammable fabrics program 1970,** *Nat. Bur. Stand. (U.S.), Tech. Note 596, 68 pages (Sept. 1971) 65 cents, SD Catalog No. C13.46:596.*

Key words: Annual report to Congress; blankets; carpets and rugs; children's sleepwear; cooperation; flammability; flammability reduction; mattresses; research; small carpets and rugs; standards; test development.

This Annual Report to the Congress, required by the Flammable Fabrics Act, covers calendar year 1970. Specific flammability standards outputs were standards for carpets and rugs and for small carpets and rugs, a proposed standard for children's sleepwear, and notices of possible need and institution of proceedings for standards for certain items of children's apparel, all blankets, and all mattresses. Research included studies, in-house and by contract, on subjects such as full scale carpet burn experiments and heat transfer from burning fabrics. Studies of the feasibility of reducing flammability included pyrolysis of textile materials and chemical aspects of fire retardancy. Test development was completely related to the standards outputs, and training ranged from the preparation of bibliographies through Congressional and public presentations to full time Research Associateship participation in the program. Cooperation was carried out with HEW, the public, industry, and voluntary standards groups.

Sanchez, I. C., DiMarzio, E. A., **Dilute solution theory of polymer crystal growth: A kinetic theory of chain folding,** *J. Chem. Phys.* **55,** *No. 2, 893–908 (July 15, 1971).*

Key words: Chain folding; cilia; localization free energy; nucleation; rate constants.

A kinetic theory of polymer crystallization from dilute solution is formulated for linear chain modules of finite molecular weight (monodisperse). Two models of crystal growth are considered; both are essentially "regular" chain folding type models. Formulas for the crystal growth rates are derived as a function of the fundamental rate constants associated with the various states of molecular crystallization. These rate constants are evaluated as a function of polymer concentration, molecular weight, crystallization temperature, and crystal thickness. Consideration of finite molecular weight molecules requires an understanding of how these molecules are incorporated into the crystal and what happens to chain ends. Attention is focused on these problems and a description of how "cilia" are formed in polymer crystals is given. A remarkable aspect of cilia formation is that the uncrystallized portion of a chain molecule which dangles in the solution can participate in nucleating a new growth strip (fold plane) on the crystal face—a kind of "self-nucleating" mechanism.

Saylor, C. P., **Refractive index, Chapter in The Characterization of Chemical Purity of Organic Compounds,** *L. A. K. Staveley, Ed., pp. 67–79 (July 1971).*

Key words: Crystals; liquids; purity; refractive index.

Usually measurement of refractive index on liquids has limited usefulness in the evaluation of purity. The tendency of materials and their contaminants to have similar values is demonstrated. The methods of refractive index measurement are described and evaluated. The dissimilar conditions that occur with solid substances are pointed out. Instances of application of refractive index measurement to solids are appraised.

Schade, P. A., **Signal decoder eliminates jitter,** *Electron. Design* **19,** *No. 24, 1 (Nov. 25, 1971).*

Key words: False counts, incremental encoder; jitter; 90° phase decoder; up-down counter.

The two main types of decoders used with incremental shaft encoders are discussed. Emphasis is given to the problem of decoding signals which result from an oscillating shaft. A particular decoder circuit designed and tested by the author is presented.

Schafft, H. A., **Wire-bond electrical connections: Testing, fabrication and degradation–A bibliography 1957–1971,** *Nat. Bur. Stand. (U.S.), Tech. Note 593, 58 pages (Jan. 1972) 60 cents, SD Catalog No. C13.46:593.*

Key words: Bibliography; degradation (wire-bond); discrete devices; electrical interconnection; fabrication (wire-bond); failure (wire-bond); hybrid circuits; integrated circuits; microelectronics; reliability; testing; (wire-bond); wire-bond.

More than 245 papers relevant to wire-bond type electrical interconnections used in microelectronic and low-power discrete and hybrid devices are listed together with key words. The bibliographic search concentrated on compiling papers which appeared in the period from 1965 to 1970, inclusive. The selection of papers was generally limited to those that were pertinent to wire-bonds where the wire diameter is less than about 50μm (2 mils) and where the wire is bonded by either thermocompressive or ultrasonic means. Two indexes are provided: (1) an Author Index and (2) a Key Word Index. The latter includes a tabulation of the literature citations.

Schwartz, R. B., Heaton, H. T., II, Schrack, R. A., **High-accuracy total-cross-section measurements with the NBS Linac,** (*Proc. Symp. Neutron Standards and Flux Normalization, Argonne Na-*

tional Laboratory, Argonne, Ill., Oct. 21–23, 1970), AEC Symp. Series Neutron Standards and Flux Normalization **23**, *377–384 (Aug. 1971).*

Key words: Cross section; MeV; neutron; time-of-flight.

A high-accuracy fast-neutron time-of-flight spectrometer used for neutron energies between 0.5 and 20 MeV is described. The neutrons are produced by a 2-ns-wide electron-beam pulse from the National Bureau of Standards Linac. The resolution, with a 40-m flight path, is approximately 0.1 ns/m, and the accuracy of the measurements is estimated to be 1%.

Sher, A. H., Croll, W. K., Thurber, W. R., **Determination of oxygen in germanium below 20 parts per billion by measurements of lithium mobility and precipitation,** *Anal. Chem.* **43**, *No. 13, 1831–1834 (Nov. 1971).*

Key words: Germanium; infrared absorption; lithium mobility; lithium precipitation; oxygen.

The range of sensitivity and the expected degree of precision for the analysis of oxygen concentration in germanium by measurements of lithium-ion drift mobility and lithium precipitation have been determined. The relative sample standard deviations have been found to be ±10% and ±15%, respectively, in the range of oxygen concentration from 20 ppb (atomic) to 0.2 ppb (atomic). However, the lithium precipitation method alone cannot be used ambiguously in the determination of oxygen concentration in germanium. The sole previously-published value for the dissociation constant of the LiO^+ complex in germanium at 295 K has been confirmed. A newly-observed feature in the lithium precipitation curve is shown to give semiquantitative information about oxygen concentration.

Sher, A. H., Thurber, W. R., **Minority carrier and lithium-ion drift mobilities and oxygen concentration in *p*-type germanium,** *J. Appl. Phys.* **42**, *No. 11, 4508–4509 (Oct. 1971).*

Key words: Electron mobility; germanium; lithium mobility; oxygen concentration.

No correlations have been experimentally observed between electron dirft mobility and lithium drift mobility nor between electron drift mobility and oxygen concentration in *p*-type germanium single crystals, as had been previously suggested.

Simmons, J. H., Macedo, P. B., Napolitano, A., Haller, W. K., **Investigation of liquid-liquid phase transitions in oxide melts by viscosity measurements,** *Discussions Faraday Soc., Bristol, England, September 1970, No. 50, 155–165 (1970).*

Key words: Composition fluctuations; glass; immiscibility; phase separation; viscosity; viscous flow.

Results from viscosity measurements conducted above and below the liquid-liquid phase transition of a series of molten oxide glasses are reported in order to analyze the effect of supercritical composition fluctuations on viscous flow, and to investigate the mechanisms of phase separation. Measurements of four oxide mixtures with similar high temperature structures and widely different critical temperatures, revealed an anomalous increase in viscosity at temperatures above the critical point. The anomalous increase occurs when large composition fluctuations characterizing the critical point are present. The effect is explained in terms of an interaction between viscous flow and the supercritical fluctuations through the structural relaxation process. An analysis of this interaction is presented.
Measurements conducted at temperatures slightly below the critical point of one of these glasses indicate that the microstructure resulting from the phase separation is highly sensitive to the preceding heat-treatment. Phase separation by the formation of isolated spheres of the silica-rich component is identified a few degrees below the critical point. Further measurements of viscosity by a fibre elongation method, conducted far below the critical temperature, are reported in order to analyze the growth mechanisms occurring in the separated phases. In this case, the rearrangement stage of phase separation is characterized by a growing interconnected structure.

Simpson, J. A., **Use of a microscope as a noncontacting microdisplacement measurement device,** *Rev. Sci. Instr.* **42**, *No. 9, 1378–1380 (Sept. 1971).*

Key words: Dimensional metrology, displacement measurement, microscope, noncontact sensing, optical surface probe, surface detection.

It is shown that a common research microscope with vertical illuminator can be easily converted to a noncontacting measuring device of submicroinch resolution.

Simpson, P. A., Ondrejka, A. R., **Improvements to the NBS rf peak-pulse power standard,** *Instrument Society of America Silver Jubilee International Conference and Exhibit, October 26–29, 1970, Philadelphia, Pa., Paper 709–70, 1–7 (Oct. 26–29, 1970).*

Key words: Peak pulse power measurement; sampling power measurement; solid state switch.

The National Bureau of Standards maintains a standard for measuring rf peak-pulse power. This standard employs a sampling-comparison method in which a solid state diode switch is used to intercompare equal time-interval samples of cw and pulsed rf power. Recently a new type diode switch has been developed which, when coupled with a sensitive peak detection system, has greatly improved the performance of the standard in two general areas.
The first major improvement is in the frequency coverage. The earlier version of the standard used two separate diode switches to cover the frequency bands 300 to 500 MHz and 950 to 1200 MHZ. The new diode switch permits measurements to be made over the frequency range 0.1 to 4.4 GHz because of its low VSWR (typically 1.1 or less).
The other major improvement is in the dynamic power range of the system. The basic range of the earlier version was 0.1 to 1.2 watts. The new version operates over a power range of 5 mW to 2 W.
This paper reviews the history of the system, describes its performance characteristics, and gives some of its more important constructional details.

Smith, J. C., Kermish, G. A., Fenstermaker, C. A., **Separation of filler particles from the matrix in a particulate-loaded composite subjected to tensile stress,** *Proc. 162nd Meeting American Chemical Society, Organic Coatings and Plastics Chemistry, Washington, D.C., Sept. 13–15, 1971,* **31**, *No. 2, 149–155 (Sept. 1971).*

Key words: Composite materials; coupling agents; epoxy polymer; parting agents; poisson's ratio; release agents; stress-strain curve; volume dilation.

Simultaneous measurements of tensile stress, longitudinal strain, and transverse strain were obtained on particulate-filled composites. The matrix was a flexible epoxy polymer. Small glass spheres were used as filler in various volume ratios up to .35. The spheres were pretreated as follows: clean, coated with a parting agent, coated with either of two silane coupling agents. The volume expansion behavior of composites containing parting agent treated spheres could readily be distinguished from that of composites containing clean glass spheres, but differences caused by coating the spheres with coupling agents could not be distinguished. Stress-strain behaviors for the various composite systems also showed differences. These differences in both kinds of data are taken as indicative of matrix-filler separation and subsequent vacuole formation.

Smith, R. V., **Steam-water, critical flow in a venturi,** *Nat. Bur. Stand. (U.S.), Tech. Note 608, 25 pages (July 1971) 35 cents, SD Catalog No. C13.46:608.*

Key words: Critical flow; pressure profile; steam; venturi; water.

This paper is the second part of an analytical and experimental investigation in which the primary object was to test the hypothesis that the flow of the gas phase controls critical and near critical two-phase flow for cases where the gas and liquid flow essentially in separate streams. In the first part of the investigation, a two-component system (air-water) was used. The results presented here

substantiate the hypothesis. The analytical results also indicate the use of one dimensional flow equations with reasonably accurate estimates for droplet size and for the drag and heat transfer coefficients (without consideration of mass transfer—vaporization or condensation) describe critical and near-critical flow reasonably well. This indicates that mass transfer may be a secondary effect for these flow conditions.

Smith, S. J., **Lasers and lengths, Comments** *At. Mol. Phys.* **2,** *No. 3, 92–97 (August 1970).*

Key words: Coherence; laser stabilization; length; methane; saturated absorption.

We review here developments which strongly suggest that laser stabilization techniques fully complementary to the amazing coherence properties of the laser will ultimately be found. Indeed progress in hand assures an advance more revolutionary than evolutionary, and discussions of a possible redefinition of the standard of length are now beginning to be taken seriously.

Souders, T. M., **A wide range current comparator system for calibrating current transformers,** *IEEE Trans. Power Appar. Syst. PAS–90,* **1,** *318–324 (January/February 1971).*

Key words: Calibration; current comparator; current transformer; overload testing; self-balancing current comparator; transformer; wide-range.

This paper describes a new measurement system for the calibration of current transformers at 60 Hz for ratios up to 10,000/5 and higher at four times rated current. An accuracy of 5 parts per million (ppm) can be achieved for ratios up to 1200/5, above which the accuracy of a standard must be included. Also, it includes an example of how a laboratory could use such a system with minimum recourse to the facilities of a national laboratory.

Stiehler, R. D., **U.S. Metric Study Interim Report. Engineering standards,** *Nat. Bur. Stand. (U.S.), Spec. Publ. 345–11, 264 pages (July 1971) $2.00, SD Catalog No. C13.10:345–11.*

Key words: Engineering standards; international standards; International System of Units; metric conversion; metric system; metrication; metrication and engineering standards; SI; standards; U.S. Metric Study.

This report, one of a series prepared pursuant to the U.S. Metric Study Act, is concerned with (1) the relationship between measurement language and engineering standards, and (2) the compatibility of U.S. Standards with corresponding international standards. Incompatibilities between corresponding standards result from differences of engineering practice. Measurement units contribute to the incompatibilities among many dimensional specifications which comprise about 25% of engineering standards. In the remaining standards, measurement units are either not involved or serve merely as a language. The study compares U.S. standards with other national and international standards.

Stull, D. R., Prophet, H., **JANAF thermochemical tables second edition,** *Nat. Stand. Ref. Data Ser., Nat. Bur. Stand. (U.S.),* **37,** *1141 pages (June 1971) $9.75, SD Catalog No. C13.48:37.*

Key words: Evaluated data; thermal functions; thermodynamic properties of materials; thermodynamics.

This monograph is the second edition of the JANAF Thermochemical Tables. It contains thermodynamic properties for some 1,099 chemical species. The following properties are tabulated as functions of temperatures: C_p°, S°, $(F^\circ - H_{298}^\circ)/T$, $H_{298}^\circ - H^\circ$, ΔH_f° and Log Kp.

Treat, C. F., **A history of the metric system controversy in the United States,** *Nat. Bur. Stand. (U.S.), Spec. Publ. 345–10, 312 pages (August 1971) $2.25, SD Catalog No. C13.10:345–10.*

Key words: Metric system; weights and measures.

A review of the debate between 1790 and 1968 on the question of whether or not the United States should adopt the metric system of weights and measures. Legislative activities with respect to weights and measures and campaigns for and against adoption of the metric system are reviewed. Significant investigations of the question by both public and private bodies are highlighted. An extensive bibliography is included.

Swanson, H. E., McMurdie, H. F., Morris, M. C., Evans, E. H., Paretzkin, B., DeGroot, J. H., Carmel, S. J., **Standard x-ray diffraction powder patterns,** *Nat. Bur. Stand. (U.S.), Monogr. 25-Section 9, 128 pages (Dec. 1971) $1.25, SD catalog No. C13.44:25/sec. 9.*

Key words: Crystal structure; integrated intensities; lattice constants; peak intensities; powder patterns; reference intensities; standard; x-ray diffraction.

Standard x-ray diffraction patterns are presented for 63 substances. Forty of these patterns represent experimental data and 23 are calculated. The experimental x-ray powder diffraction patterns were obtained with an x-ray diffractometer. All d-values were assigned Miller indices determined by comparison with computer interplanar spacings consistent with space group extinctions. The densities and lattice constants were calculated, and the refractive indices were measured whenever possible. The calculated x-ray powder diffraction patterns were computed from published crystal structure data. Both peak height and integrated intensities are reported for the calculated patterns.

Swartzendruber, L. J., Bennett, L. H., **Use of ultrasonics in laboratory development tests of cupro-nickel alloys for desalination,** *Desalination* **9,** *387–389 (June 1971).*

Key words: Alloys; corrosion; Cupro-Nickel; high velocity; sea water; ultrasonics.

Ultrasonic agitation of the salt water bath is suggested as a simple laboratory corrosion test method for evaluating the relative performance of alloys intended for use at moderate or high sea water velocities.

Thomas, D. B., **Some studies on the reproducibility of tungsten-rhenium type thermocouples,** *Proc. 26th Intern. Instrument Society of America Conf. and Exhibit on Advances in Instrumentation, Chicago, Ill., Oct. 4–7, 1971, 26, Part II, Paper 71–611 (Oct. 1971).*

Key words: Anneal; beryllium-oxide; calibrations; electromotive force; thermal-cycling; thermocouple; tungsten-rhenium.

Representative samples of commercially available tungsten-rhenium type thermocouples were obtained from American manufacturers and calibrated in an argon atmosphere up to 2100 °C. After the initial calibrations were performed, the thermocouples were subjected to thermal-cycling between 1000 °C and 2100 °C and were also annealed for periods up to 420 hours at 2300 °C in argon. A comparison is made between the emfs of the thermocouples before and after the thermal-cycling and annealing periods. In general, the tungsten versus tungsten-26% rhenium thermocouples indicated the largest changes in emf after the thermal cycling and annealing periods while the tungsten–3% rhenium versus tungsten–25% rhenium thermocouples indicated the least change in emf. Some of the thermocouples were calibrated with and without beryllium-oxide insulation in argon, helium, and vacuum and a comparison is made between the thermocouple emfs under these conditions.

Tsang, W., Wasik, S. P., **The application of the isotope dilution GLC technique to air pollution analysis,** *J. Chromatog. Sci.* **9,** *567–569 (Sept. 1971).*

Key words: Air pollution; benzene; benzene-d_6; gas analysis; gas chromatography; isotope dilution; isotope effect.

It is shown that the isotope dilution technique provides a simple means of accurately determining air pollutant concentrations under adverse conditions. This is demonstrated in various simu-

lated situations with a sample of approximately 20 ppm benzene in argon.

Viezbicke, P. P., Editor, **NBS frequency and time broadcast services. Radio stations WWV, WWVH, WWVB, and WWVL,** *Nat. Bur. Stand. (U.S.), Spec. Publ. 236, 15 pages (July 1971) 25 cents, SD Catalog No. C13.11:236. Supersedes NBS Special Publication 236, 1970 and Previous Editions.*

Key words: Broadcast of standard frequencies; high frequency; low frequency; standard frequencies; time signals; very low frequency.

Detailed descriptions are given of the technical services provided by the NBS radio stations WWV, WWVH, WWVB, and WWVL. These services are: 1. Standard radio frequencies; 2. Standard audio frequencies; 3. Standard musical pitch; 4. Standard time intervals; 5. Time signals; 6. UT corrections; and 7. Official announcements. In order to provide users with the best possible services, occasional changes in broadcasting schedules are required. This publication shows the schedules in effect on July 1, 1971.

Wagner, H. L., Hoeve, C. A. J., **Effect of molecular weight on the refractive increment of polyethylene and *n*-alkanes,** *J. Polymer Sci. Part A-2,* **9,** *1763–1776 (1971).*

Key words: Differential refractive index, differential refractometer, Lorenz-Lorenz, molecular weight, *n*-Alkanes, polyethylene, polystyrene.

As in the case with other polymers previously reported, the values of the refractive index increment dn/dc of polyethylene and the *n*-alkanes change with molecular weight. Most of the variation may be understood by examination of the role of density in the Lorenz-Lorenz mixing equation for specific refractivity, $R_{12}=P_1R_1+P_2R_2$ used to calculate dn/dc. It may also be shown that as the absolute refractive index difference between solute and solvent becomes smaller, dn/dc becomes more sensitive to density change of the solute.

Weir, C. E., **Concerning the maximum melting point,** *Jap. J. Appl. Phys.* **10,** *No. 6, 714–716 (June 1971).*

Key words: High pressure, melting point.

The theory of Kawai and Inokuti of the behavior of the melting point of solids as a function of pressure is discussed. The general theory is not considered applicable to the vast majority of materials known to date.

Weissler, P. G., **ANSI-1969 Standard reference threshold sound-pressure levels for Audiometers: Some comments,** *J. Acoust. Soc. Am.* **49,** *No. 4, Part 2, 1319–1320 (April 1971).*

Key words: Audiometry; earphones; NBS 9-A Coupler; reference threshold sound pressure levels; standards for audiometers; threshold of hearing.

New standard reference threshold sound-pressure levels for four audiometric earphones are given in Appendix F of ANS "Specification for Audiometers" S3.6 (1969) effective 1 September 1970. The change in reference level for ASA (1951) to ANSI (1969) is shown to be different for each earphone type. The sources of data for these new reference levels and the relationship of these new levels to ISO standards is discussed.

Wexler, A., **Book review on "modern hygrometry"** *by A. Pande, Bull. Am. Meteorol. Soc.* **52,** *No. 9, 897–898 (September 1971).*

Key words: Humidity; hygrometry; moisture; water vapor.

Book review on a monograph on the subject of hygrometry.

Yokel, F. Y., **Stability and load capacity of members with no tensile strength,** *J. Struct. Div. Am. Soc. Civil Engineers* **97,** *No. ST7, 1913–1926 (July 1, 1971).*

Key words: Buckling; compression members; concrete; deflection; equilibrium; load eccentricity; masonry; section cracking; stability; stress distribution; unreinforced concrete.

A mathematical solution is derived, which permits the computation of critical load, deflection and stresses for eccentrically loaded slender prismatic compression members, made of materials that have compressive strength but no tensile strength. A graphical presentation of the solution facilitates its application. In an example of application the solution is used to compute the strength of masonry walls which were tested by the Structural Clay Products Institute. Even though there are limitations to our ability to predict the behavior of a complex material such as masonry by a mathematical solution based on a simplified model, there is good agreement between computed and measured strength.

Yule, H. P., **Computer data reduction in activation analysis,** *Proc. NATO Advanced Study Institute on Activation Analysis in Geochemistry and Cosmochemistry, Kjeller, Norway, Sept. 7–12, 1970, pp. 145–166 (1971).*

Key words: Activation analysis; component identification; result computation; spectral resolution.

Methods of result computation with activation analysis gamma-ray spectra are reviewed, emphasizing recent developments. For NaI(Tl) detector spectra, the multiple linear regression technique is reported. For Ge(Li) detector, methods of peak location, net peak area computation and complex peak resolution are indicated. Each technique is discussed for applicability and difficulties in utilization. General features of result computation and of various numerical analytic techniques are discussed.

Other NBS Publications

J. Res. Nat. Bur. Stand. (U.S.), 75A (Physics & Chemistry), No. 6 (November–December 1971), SD Catalog No. C13.22/sec.A:75/6, $1.75.

The accuracy of measurements of viscosity of liquids. R. S. Marvin.
An absolute determination of viscosity using a torsional pendulum. H. S. White and E. A. Kearsley.
An absolute determination of viscosity using channel flow. R. W. Penn and E. A. Kearsley.
A new determination of the atomic weight of zinc. G. Marinenko and R. T. Foley.
High-speed (subsecond) measurement of heat capacity, electrical resistivity, and thermal radiation properties of niobium in the range 1500 to 2700 K. A. Cezairliyan.
Stable radical-anions derived from glyoxal bis(phenylhydrazones). A. J. Fatiadi.
Temperature dependence of photocurrents produced by x and gamma rays in silicon radiation detectors. K. Scharf and R. K. Mohr.
Isomerization processes in ions of the empirical formula $C_4H_8^+$. S. G. Lias and P. Ausloos.
The photochemistry of propane at high photon energies (8.4–21. 2 eV). R. E. Rebbert, S. G. Lias, and P. Ausloos.

J. Res. Nat. Bur. Stand. (U.S.), 76A (Physics & Chemistry), No. 1 (Jan.–Feb. 1972), SD Catalog No. C13.22/sec.A76/1, $1.25.

The absorption spectra of krypton and xenon in the wavelength range 330–600 Å. K. Codling and R. P. Madden.
A reference calorimeter for laser energy measurements. E. D. West, W. E. Case, A. L. Rasmussen, and L. B. Schmidt.
Accurate calculations of properties of the two-tube electrostatic lens. I. Improved digital methods for the precise calculation of electric fields and trajectories. S. Natali, D. Di Chio, and C. E. Kuyatt.
Dielectric constant of compressed gaseous and liquid oxygen. B. A. Younglove.
Thermal analysis of calcium sulfate dihydrate and supposed α and β forms of calcium sulfate hemihydrates from 25 to 500 °C. J. R. Clifton.

Modulus of natural rubber cross-linked by dicumyl peroxide. I. Experimental observations. L. A. Wood, G. W. Bullman, and G. E. Decker.

J. Res. Nat. Bur. Stand. (U.S.), 76A (Physics & Chemistry), No. 2 (Mar.–Apr. 1972), SD Catalog No. C13.22/sec.A76/2, $1.50.

Guidelines for the reporting of numerical data and experimental procedures. D. Garvin.

A study of equilibrium in argon arcs. J. B. Shumaker and C. H. Popenoe.

Rates of reaction of atomic oxygen III. Spiropentane, cyclopentane, cyclohexane, and cycloheptane. R. E. Huie and J. T. Herron.

Densities of compressed liquid methane, and the equation of state. R. D. Goodwin and R. Prydz.

Spin-relaxation effects on the EPR spectrum of gaseous hydrogen atoms. R. L. Brown.

Photoionization of C_4H_8 isomers. Unimolecular and bimolecular reaction of the $C_4H_8^+$ ions. L. W. Sieck, S. G. Lias, L. Hellner and P. Ausloos.

Theoretical investigation of the odd configurations of Ni II. Y. Shadmi and E. Caspi.

The characterization of linear polyethylene SRM 1475.

I. Introduction. C. A. J. Hoeve, Herman L. Wagner, and P. Verdier.

II. Determination of total methyl content by infrared spectrophotometry. J. E. Brown.

III. Density determination. J. E. Brown.

IV. Melt flow rate. J. R. Maurey.

V. Solution viscosity measurements. R. G. Christensen.

VI. Preparation of calibrating fractions. R. G. Christensen.

VII. Differential refractive index of polyethylene solutions. H. L. Wagner.

VIII. Light scattering studies on polyethylenes in 1-chloronaphthalene. L. J. Frolen, G. S. Ross, A. M. Wims, and P. Verdier.

IX. Number average molecular weight of fractions by membrane osmometry. J. E. Brown and P. H. Verdier.

X. Gel permeation chromatography. G. Ross and L. Frolen.

J. Res. Nat. Bur. Stand. (U.S.), 75 B (Mathematical Sciences), Nos. 3 & 4 (July–December 1971), SD Catalog No. C13.22/sec.B75/3&4, $1.25.

Some elementary formulas in "matrix calculus" and their applications. J. T. Fong.

Linear transformations on matrices. M. Marcus.

Eigenvalues of sums of hermitian matrices. III. R. C. Thompson and L. F. Garbanti.

A new type of boundary value coupling for second order Sturm-Liouville systems. J. Geist.

An ergodic source which is not a function of any finite Markov process. R. D. Traub.

On entire functions of exponential type. S. M. Shah and W. C. Sisarcick.

A table of integrals of the error function. II. Additions and corrections. M. Geller and E. W. Ng.

A note on the time dependence of the effective axis and angle of a rotation. H. Gelman.

A numerical solution of integral equation of the first kind applied to slit correction in small-angle x-ray scattering. J. Mazur.

Abramowitz, S., Acquista, N., Thompson, K. R., The infrared spectrum of matrix-isolated uranium monoxide, J. Phys. Chem. **75,** No. 15, 2283–2285 (1971).

Abramowitz, S., Levin, I. W., Raman spectra of the hexahalogenated benzenes in the solid phase, Spectrochim. Acta **26A,** 2261–2268 (1970).

Alexandropoulos, N. G., Parks, S. H., Kuriyama, M., Polarization of the x-ray Compton-Raman radiation, Physics Letters **35A,** No. 5, 369–370 (June 28, 1971).

Allpress, J. G., Roth, R. S., The effect of annealing on the concentration of Wadsley defects in the Nb_2O_5–WO_3 system, J. Solid State Chem. **3,** 209–216 (1971).

Ambler, E., Measurement standards, physical constants, and science teaching, Sci. Teacher **38,** No. 8 63–71 (Nov. 1971).

Bardos, D. I., Waterstrat, R. M., Rowland, T. J., Darby, J. B., Jr., The magnetic susceptibility of transition-metal A15-type phases, J. Low Temp. Phys. **3,** No. 5, 509–518 (1970).

Bederson, B., Kieffer, L. J., Total electron-atom collision cross sections at low energies—A critical review, Rev. Mod. Phys. **43,** No. 4, 601–641 (Oct. 1971).

Bennett, H. S., Acoustic phonons in Heisenberg paramagnets, J. Phys. **32,** No. C1, 526–527 (Feb./Mar. 1971).

Bennett, H. S., Two-electron F^- centers in the alkaline-earth fluorides, Phys. Rev. **B. 4,** No. 4, 1327–1335 (Aug. 15, 1971).

Bloom, D. W., Finegold, L., Lye, R. G., Radebaugh, R., Siegwarth, J. D., Upper limit on electron-photon interaction in vanadium carbide, Physics Letters **33A,** No. 3, 137–138 (Oct. 19, 1970).

Boyd, M. E., Larsen, S. Y., First quantum-mechanical correction to the classical viscosity cross section of hard spheres, Phys. Rev. **A. 4,** No. 3, 1155–1163 (Sept. 1971).

Brady, R. F., Jr., Enolization of hexodiulose acetals. Synthesis of derivatives of D-psicose by reduction of a hex-3-enulopyranose, Carbohydrate Res. **20,** 170–175 (Nov. 1971).

Brauer, G. M., Huget, E. F., Heats of immersion of the components of tooth structure, J. Dental Res. **50,** No. 3, 776 (May–June 1971).

Brennen, J. A., Dean, J. W., Mann, D. B., Kneebone, C. H., An evaluation of positive displacement cryogenic volumetric flowmeters, Nat. Bur. Stand. (U.S.), Tech. Note 605, 134 pages (July 1971) $1.25, SD Catalog No. C13.46:605.

Byerly, R., Jr., Beaty, E. C., Sunlight photodetachment of O_3^-, J. Geophys. Res. **76,** No. 19, 4596–4601 (July 1, 1971).

Cali, J. P., Seward, R. W., The challenge of the 70's NBS standard reference materials program, Am. Lab. **3,** No. 6, 10–14 (June 1971).

Carroll, J. J., Melmed, A. J., Optical constants of (011) tungsten in the visible region, J. Opt. Soc. Am. **61,** No. 4, 470–473 (Apr. 1971).

Casella, R. C., The reversal symmetry and its breaking in physics, Phys. Teacher **8,** No. 3, 114–123 (Mar. 1970).

Cezairliyan, A., Morse, M. S., Beckett, C. W., Measurement of melting point and electrical resistivity (above 2,840 K) of molybdenum by a pulse heating method, (Proc. Conf. Thermophysical Properties, Manchester, England, April 7–10, 1970), Rev. Int. Hautes Tempér. Réfract t. **7,** 382–388 (1970).

Chandler, H. H., Bowen, R. L., Paffenbarger, G. C., Development of a radiopaque denture base material, J. Biomed. Mater. Res. **5,** 253–265 (Mar. 1971).

Chandler, H. H., Bowen, R. L., Paffenbarger, G. C., The need for radiopaque denture base materials: A review of the literature, J. Biomed. Mater. Res. **5,** 245–252 (Mar. 1971).

Chang, S. S., Bestul, A. B., Heat capacities of cubic monoclinic, and vitreous arsenious oxide from 5 to 360 K, J. Chem. Phys. **55,** No. 2, 933–946 (July 15, 1971).

Chang, T-T, Cohen, M. I., Hosler, W. R., Superhyperfine interactions in CdF_2: Yb, J. Chem. Phys. **54,** No. 10, 4278–4280 (May 15, 1971).

Clifton, J. R., The infrared spectra of supposed α and β forms of calcium sulphate hemihydrate, Nature (London), Phys. Sci. **232,** No. 32, 125–126 (Aug. 9, 1971).

Coriell, S. R., Hardy, S. C., Sekerka, R. F., A non-linear analysis of experiments on the morphological stability of ice cylinders freezing from aqueous solutions, J. Crystal Growth **11,** 53–67 (May 1971).

Coxon, B., Studies of ^{15}N-labeled amino sugars. The synthesis and mass spectrometry of derivatives of 6-amino-6-deoxy-D-glucose-6-^{15}N, Carbohydrate Res. **19,** 197–210 (1971).

Coxon, B., Johnson, L. F., The N.M.R. spectroscopy of derivatives 6-amino-6-deoxy-D-glucose-6-^{15}N. ^{13}C Fourier-transform and internuclear, double- and triple-resonance studies, Carbohydrates Res. **20,** 105–122 (Nov. 1971).

Creutzberg, F., Hougen, J. T., Rotational line intensities for singlet-triplet transitions in molecules belonging to the point groups D_{2h}, C_{2v}, and D_2, J. Mol. Spectry. **38,** No. 2, 257–272 (1971).

Danos, M., One physicist's view of special functions (Proc. SIAM National Meeting, Washington, D.C., June 10–12, 1969), Chapter in Studies in Applied Mathematics 6, pp. 18–29 (1970).

Dehmer, J. L., Starace, A. F., Fano, U., Sugar, J., Cooper, J. W., Raising of discrete levels into the far continuum, Phys. Rev. Letters **26,** No. 25, 1521–1525 (June 21, 1971).

Devereux, C. W., Technical Standards Coordinator, Steel bi-fold closet door units, frames, and trim, Nat. Bur. Stand. (U.S.), Prod.

Stand. 38–70, 12 pages (May 1971) 15 cents, SD Catalog No. C13.20/2:38–70.

Dibeler, V. H., Photoionization studies and thermodynamic properties of some halogen molecules (Proc. Intern. Conf. on Mass Spectroscopy, Kyoto, Japan, Sept. 6–13, 1969), Chapter in Recent Development in Mass Spectroscopy, K. Ogata and T. Hayakawa, Ed., pp. 781–790 (University of Tokyo Press, Tokyo, Japan, 1970).

Dibeler, V. H., Walker, J. A., McCulloh, K. E., Dissociation energy of fluorine, J. Chem. Phys. Letters to Editor **50**, No. 10, 4592–4593 (May 15, 1969).

Dibeler, V. H., Walker, J. A., McCulloh, K. E., Photoionization study of the dissociation energy of fluorine and the heat of formation of hydrogen fluoride, J. Chem. Phys. **51**, No. 10, 4230–4235 (Nov. 15, 1969).

Dibeler, V. H., Walker, J. A., McCulloh, K. E., Threshold for molecular photoionization of bromine, J. Chem. Phys. **53**, No. 12, 4715–4716 (Dec. 15, 1970).

Dibeler, V. H., Walker, J. A., McCulloh, K. E., Rosenstock, H. M., Effect of hot bands on the ionization threshold of some diatomic halogen molecules, Intern. J. Mass Spectrom. Ion Phys. **7**, 209–219 (1971).

Dickens, B., Brown, W. E., The crystal structure of $Ca_5(PO_4)_2SiO_4$ (silico-carnotite), Tschermaks Mineral. Petrog. Mitt. **16**, 1–27 (June 1971).

Dickens, B., Brown, W. E., The crystal structure of $Ca_7Mg_3(Ca, Mg)_2(PO_4)_{12}$, Tschermaks Mineral. Petrog. Mitt. **16**, 79–104 (June 1971).

DiMarzio, E. A., Rubin, R. J., Adsorption of a chain polymer between two plates, J. Chem. Phys. **55**, No. 9, 4318–4336 (Nov. 1, 1971).

Distefano, G., Dibeler, V. H., Photoionization study of the dimethyl compounds of zinc, cadmium, and mercury, Intern. J. Mass Spectrom. Ion Phys. **4**, 59–68 1970).

Dove, R. B., Marshak, H., Shaft seal for mechanical pump, J. Vacuum Sci. Technol. **8**, No. 3, 519 (May–June 1971).

Eisele, J. W., Technical Standards Coordinator, School Chalk. Nat. Bur. Stand. (U.S.), Prod. Stand. 30–70, 14 pages (May 1971) 15 cents, SD Catalog No. C13.20/2:30–70.

Fatiadi, A. J., Evidence for adsorption as the first step in the solid-state oxidation of benzenehexol with active manganese dioxide, J. Chem. Soc. Section B. 889–894 (1971).

Fatiadi, A. J. (*p*-Bromophenyl)osotriazoles from inositols, Carbohydrate Res. **20**, 179–184 (Nov. 1971).

Fetters, L. J., Yu, H., Equilibrium conformation and "worm-like coil" configuration of poly(*n*-alkyl isocyanates), Macromolecules **4**, No. 4, 385–389 (July–Aug. 1971).

Flynn, J. H., The historical development of applied nonisothermal kinetics (Proc. 2nd Intern. Conf. on Thermal Analysis, Holy Cross College, Worcester, Mass., Aug. 19–23, 1969), Thermal Analysis **2**, 1111–1126 (Academic Press, Inc., New York, N.Y., 1969).

Fong, E., A preliminary design of a data retrieval language to handle a generalized data base: DRL, Nat. Bur. Stand. (U.S.), Tech. Note 590, 26 pages (July 1971) 35 cents, SD Catalog No. C13.46:590.

Franklin, A. D., Marzullo, S., 9.—EPR study of point-defect equilibria in CaF_2 containing GdF_3, Proc. No. 19 British Ceramic Society, "Role of Point Defects in Solid State Mass," Mass Transport Proc. Non-Metallic Solids, London, England, Dec. 17–18, 1969, pp. 135–150 (British Ceramic Society, Stoke-on-Trent, England, 1971).

Franklin, A. D., Crissman, J., Reorientation of trivalent cation-interstitial fluorine pair in CaF_2, Letters to the Editor, J. Phys. C: Solid State Phys. **4**, L239–L242 (July 12, 1971).

Freeman, D. H., Zielinski, W. L., Jr., Editors, Separation and Purification Section: Summary of Activities—July 1970 to June 1971, Nat. Bur. Stand. (U.S.), Tech. Note 589, 64 pages (Oct. 1971) 60 cents, SD Catalog C13.46:589.

Fuhr, J. R., Wiese, W. L., Bibliography on atomic transition probabilities, July 1969 through June 1971, Nat. Bur. Stand. (U.S.), Spec. Publ. 320 Suppl. 1, 67 pages (Sept. 1971) 65 cents, SD Catalog No. C13.10:320 Suppl. 1.

Gadzuk, J. W., Hartman, J. K., Rhodin, T. N., Approach to alkali-metal chemisorption within the Anderson model, Phys. Rev. **B. 4**, No. 2, 251–255 (July 15, 1971).

Gebbie, K. B., The Menzel symposium on solar physics, atomic spectra, and gaseous nebulae, Nat. Bur. Stand. (U.S.), Spec. Publ. 353, 213 pages (Aug. 1971) $1.75, SD Catalog No. C13.10:353.

Gibson, B. F., Williams, H. T., Virtual photon cross sections for two-body electrodisintegration, Nucl. Phys. **A163**, 193–202 (1971).

Godfrey, J. T., Vidal, C. R., Smith, E. W., Cooper, J., The effect of time ordering on the Lyman α profile, Nat. Bur. Stand. (U.S.), Monogr. 121, 14 pages (June 1971) 30 cents, SD Catalog No. C13.44:121.

Grundl, J. A., Fission-neutron spectra: macroscopic and integral results, Proc. Neutron Standards and Flux Normalization, Symp. Argonne National Laboratory, Argonne, Ill., Oct. 21–23, 1970. Sponsored by the European American Nuclear Data Committee, pp. 417–451 (Aug. 1971).

Hall, J. T., Dixon, R. G., Getting it all together the cybernetic way, Management Rev. pp. 16–22 (American Management Association, Inc., New York, N.Y., July 1971).

Haller, W., Simmons, J. H., Napolitano, A., Viscosity-drift technique for determination of critical liquid-liquid immiscibility temperature of glasses, J. Am. Ceram. Soc. **54**, No. 6, 299–302 (1971).

Haller, W., Winogradoff, N. N., Explosive vapor release as cause of laser-induced surface damage of glass, J. Am. Ceram. Soc. **54**, No. 6, 314–315 (1971).

Hastie, J. W., Thermodynamic studies, by mass spectrometry, of molten mixed halide systems, Chapter 5 in Advances in Molten Salt Chemistry 1, 225–257 (Plenum Press, Inc., New York, N.Y., 1971).

Hastie, J. W., Hauge, R. H., Margrave, J. L., Infrared spectra and geometries for the dichlorides of Ca, Sc, Ti, V, Cr, Mn, Fe, and Ni, High Temp. Sci. **3**, No. 3, 257–274 (May 1971).

Herron, J. T., Mass spectrometric studies of atomic and free radical reactions, Advan. Mass Spectrometry 5, 453–461 (1971).

Hoeve, C. A. J., On the general theory of polymer absorption at a surface, J. Polymer Sci. Symposia, Part C, No. 30, 361–367 (1970).

Hugen, J. T., Interpretation of molecular-beam radiofrequency orthopara transitions in methane, J. Chem. Phys. **55**, No. 3, 1122–1127 (Aug. 1, 1971).

Hudson, R. P., Mangum, B. W., Effects of applied magnetic fields on cooperative Jahn-Teller transition temperatures of $DyAsO_4$ and $DyVO_4$, Physics Letters **36A** No. 3, 157–158 (Aug. 30, 1971).

Hummer, D. G., Rybicki, G. B., Radiative transfer in spherically symmetric systems. The conservative grey case, Monthly Notices Roy Astron. Soc. **152**, No. 1, 1–19 (1971).

Jacox, M. E., Milligan, D. E., Matrix-isolation study of the vacuum-ultraviolet photolysis of chloroform. Infrared spectra of the CCl_3^+ $HCCl_2^+$, and $HCCl_2$ molecular ions, J. Chem. Phys. **54**, No. 9, 3935–3950 (May 1, 1971).

Johannesen, R. B., Duerst, R. W., Nuclear magnetic resonance studies of inorganic fluorides VI. Magnetic nonequivalence in *bis* (perfluorovinyl) mercury, J. Magn. Resonance **5**, No. 3, 355–366 (Dec. 1971).

Johnson, D. R., Powell, F. X., Kirchhoff, W. H., Microwave spectrum, ground state structure, and dipole moment of thioformaldehyde, J. Mol. Spectry. **39**, No. 1, 136–145 (July 1971).

Julienne, P. S., Krauss, M., Donn, B., Formation of OH through inverse predissociation, Astrophys. J. **170**, 65–70 (Nov. 15, 1971).

Julienne, P. S., Neumann, D., Krauss, M., Calculation of the temperature dependence for absorption in CO_2 in the 1750–1200 Å region, J. Atmospheric Sci. **28**, No. 6, 833–837 (Sept. 1971).

Kaldor, A., Absorption spectrum of borazine in the vacuum ultraviolet, J. Chem. Phys. **55**, No. 9, 4641–4643 (Nov. 1, 1971).

Karp, S. S., Matteson, T. T., The integrated team concept of simulation model development, Proc. 1971 Summer Computer Simulation Conf., Boston, Mass., July 19–21, 1971, pp. 1301–1307 (July 1971).

Kaufman, V., Sugar, J., One-electron spectrum of doubly ionized lutetium (Lu III) and nuclear magnetic dipole moment of ^{175}Lu, J. Opt. Soc. Am. **61**, No. 12, 1693–1698 (Dec. 1971).

Kieffer, L. J., Low-energy electron-collision cross-section data Part III: Total scattering; differential elastic scattering, Atomic Data **2**, No. 4, 293–391 (June 1971).

Klein, M., Practical treatment of coupled gas equilibrium, Chapter in Physical Chemistry, Vol **1**, Thermodynamics, Chapter 7, 489–544 (Academic Press, Inc., New York, N.Y., 1971).

Koonce, C. S., Mangum, B. W., Thornton, D. D., Low temperature properties of $DyPO_4$ in a magnetic field, Proc. 12th Intern. Conf. on Low Temperature Physics, Kyoto, Japan, Sept. 4–10, 1970, pp. 705–707 (Keigaku Publishing Co., Japan, Mar. 1971).

Krauss, M., Maldonado, P., Wahl, A. C., Interaction energy curves of LiHe and NaHe ($X\ ^2\Sigma^+$, $A\ ^2\Pi$, $B\ ^2\Sigma^+$) and $X\ ^1\Sigma^+$ ions, J. Chem. Phys. **54**, No. 11, 4944–4953 (June 1, 1971).

Krauss, M., Mielczarek, S. R., Neumann, D., Kuyatt, C. E., Mechanism for production of the fourth positive band system of CO by electron impact on CO_2, J. Geophys. Res. **76**, No. 16, 3733–3737 (June 1, 1971).

Kuriyama, M., Alexandropoulos, N. G., On the relationship between X-ray inelastic scattering and absorption spectra, J. Phys. Soc. Japan **31**, No. 2, 561–562 (Aug. 1971).

Kushner, L. M., Welcoming address, Proc. Footwear Manufacturing Executives Conf. held at the King's Grant Motor Inn, Danvers, Mass., Dec. 1, 1970, pp. 7–11 (Sponsored by the COMTECH, American Footwear Manufacturers Association, and the New England Footwear Association, Dec. 1970).

Lafferty, W. J., Ritter, J. J., Microwave spectrum, dipole moment, and structure of ethynyldifluoroborane, J. Mol. Spectry. **38**, No. 1, 181–194 (Apr. 1971).

Larson, W., Hunter, R. D., A broadband noncontacting sliding short, Nat. Bur. Stand. (U.S.), Tech. Note 602, 18 pages (June 1971) 30 cents, SD Catalog No. C13.46:602.

Laufer, A. H., Okabe, H., Heat of formation and bond dissociation energy of diazomethane by a photodissociation method, J. Am. Chem. Soc. **93**, 4137–4140 (1971).

LaVilla, R. E., Neon K emission spectrum, Phys. Rev. A. **4**, No. 2, 476–480 (Aug. 1971).

Lee, J. N., Moos, H. W., Mangum, B. W., Magnetic properties of $TbPO_4$, a canted antiferromagnet, Solid State Commun. **9**, No. 13, 1139–1141 (1971).

Linsky, J. L., Can the Ion H_3^+ account for missing opacity in the solar ultraviolet? Solar Physics **11**, No. 2, 198–207 (Feb. 1970).

Linsky, J. L., On the relative residual intensities of the calcium H and K lines, Solid Physics **11**, No. 3, 355–373 (Mar. 1970).

Linsky, J. L., Teske, R. G., Wilkinson, C. W., Observations of the infrared triplet of singly ionized calcium, Solar Physics **11**, No. 3, 374–383 (Mar. 1970).

Loebenstein, W. V., The exchange of ^{45}Ca and ^{32}P with hydroxyapatite as interpreted by adsorption from solution, J. Colloid Interface Sci. **36**, No. 2, 234–246 (June 1971).

Lutz, G. J., Boreni, R. J., Maddock, R. S., Meinke, W. W., Editors, Activation analysis: A bibliography, Nat. Bur. Stand. (U.S.), Tech. Note 467, Part 1, 477 pages and Part 2, Appendices, 202 pages (May 1971). Supersedes publication issued September 1968 and December 1969. Price $5.25 per set of 2 volumes, sold in sets only, SD Stock No. 0303–0852.

Madey, T. E., Yates, J. T., Jr., Electron-stimulated desorption as a tool for studies of chemisorption: A review, J. Vacuum Sci. Technol. **8**, No. 4, 525–555 (July/Aug. 1971).

Manning, J. R., Correlation factors for diffusion in nondilute alloys, Phys. Rev. **B. 4**, No. 4, 1111–1121 (Aug. 15, 1971).

Martin, W. C., Energy differences between two spectroscopic systems in neutral, singly ionized and doubly ionized lanthanide atoms, J. Opt. Soc. Am. **61**, No. 12, 1682–1686 (Dec. 1971).

Mason, H. L., Pounds, atoms, papers, and laws, Instrument Society of America Silver Jubilee International Conference and Exhibit, Oct. 26–29, 1970, Philadelphia, Pa., 25, Part II, Paper 70–662, 1–5 (1970).

Masters, L. W., Lutz, G. J., Determination of thaillium by photon activation analysis, Anal. Chim. Acta **56**, 365–370 (1971).

McNesby, J. R., Kelly, R. V., Abstraction of hydrogen by methylene, Intern. J. Chem. Kinetics **3**, 293–305 (1971).

Means, C. R., Rupp, N. W., Paffenbarger, G. C., Clinical evaluation of two types of resilient liners on dentures, J. Am. Dental Assoc. **82**, 1375–1380 (June 1971).

Menis, O., Shultz, J. I., Editors, Analytical Coordination Chemistry Section: Summary of Activities July 1970 to June 1971, Nat. Bur. Stand. (U.S.), Tech. Note 584, 175 pages (Dec. 1971) $1.50, SD Catalog No. C13.46:584.

Milligan, D. E., Jacox, M. E., Infrared spectrum of the $BrHBr^-$ Ion isolated in an argon matrix, J. Chem. Phys. **55**, No. 5, 2550–2560 (Sept. 1, 1971).

Milligan, D. E., Jacox, M. E., Infrared spectrum and structure of the SO_2^- radical ion, J. Chem. Phys. **55**, No. 3, 1003–1012 (Aug. 1, 1971).

Milligan, D. E., Jacox, M. E., Matrix-isolation study of the interaction of electrons and alkali metal atoms with various nitrogen oxides. Infrared spectra of the species NO^-, NO_2^-, and $N_2O_2^-$, J. Chem. Phys. **55**, No. 7, 3404–3418 (Oct. 1, 1971).

Ming, T-K, Tauber, S. J., Chemical structure and substructure search by set reduction, J. Chem. Doc. **11**, No. 1, 47–51 (Feb. 1971).

Mohan, R., Danos, M., Biedenharn, L. C., Three-fluid hydrodynamical model of nuclei, Phys. Rev. C. **3**, No. 5, 1740–1749 (May 1971).

Moore, C. E., Selected tables of atomic spectra, atomic energy levels and multiplet tables, N IV, N V, N VI, N VII, Nat. Stand. Ref. Data Ser., Nat. Bur. Stand. (U.S.), 3, sec. 4, 46 pages (Aug. 1971) 55 cents, SD Catalog No. C13.48:3/sec. 4.

Moore-Sitterly, C., The periodic table interpreted from atomic spectra, Proc. Mendeleev Conf., Torino-Rome, Italy, September 15–21, 1969, pp. 163–188 (1969).

Mountain, R. D., Raveché, H. J., Entropy and molecular correlation functions in open systems. II. Two- and three-body correlations, J. Chem. Phys. **55**, No. 5, 2250–2255 (Sept. 1, 1971).

Nagasawa, T., Kobayashi, K., Paracrystalline structure of polymer-crystal lattice distortion induced by electron irradiation, J. Appl. Phys. **41**, No. 11, 4276–4284 (Oct. 1970).

Negas, T., Roth, R. S., Phase equilibria and structural relations in the system $BaMnO_{3-x}$, J. Solid State Chem. **3**, 323–339 (1971).

Newman, M., Invariant factors of combinatorial matrices, Israel J. Math. **10**, No. 1, 126–130 (1971).

Newman, M., Units in cyclotomic number fields, J. Reine Angew. Math. **250**, 1–11 (1971).

Nuttall, R. L., Laufer, A. H., Kilday, M. V., The enthalpy of formation of ketene, J. Chem. Thermodynamics No. 3, 167–174 (1971).

Okabe, H., Laufer, A. H., Ball, J. J., Photodissociation of $OCCl_2$ in the vacuum ultraviolet: Production and electronic energy of excited Cl_2, J. Chem. Phys. **55**, No. 1, 373–378 (July 1, 1971).

Peterson, N. C., Kurylo, M. J., Braun, W., Bass, A. M., Keller, R. A., Enhancement of absorption spectra by dye-laser quenching, J. Opt. Soc. Am. **61**, No. 6, 746–750 (June 1971).

Phucas, C. B., Technical Standards Coordinator, Package quantities of toothpaste, Nat. Bur. Stand. (U.S.), Prod. Stand. 50–71, 8 pages (July 1971) 25 cents, SD Catalog No. C13.20/2:50–71.

Pilling, M. J., Bass, A. M., Braun, W., Oscillator strengths of CH_2 and CH_3 in the vacuum ultraviolet, Chem. Phys. Letters **9**, No. 2, 147–148 (Apr. 15, 1971).

Prince, E., Refinement of the crystal structure of apophyllite II. Determination of the hydrogen positions by neutron diffraction, Am. Mineralogist **56**, 1243–1251 (July–Aug. 1971).

Raveché, H. J., Entropy and molecular correlation functions in open systems I. Derivation. J. Chem. Phys. **55**, No. 5, 2242–2250 (Sept. 1, 1971).

Reimann, C. W., Zocchi, M., The crystal structure of Bis-[μ-(tri-1,2,4-triazolo-N^1,N^2)-triaquonickel]nickel hexanitrate dihydrate, $[(H_2O)_3(C_2H_3N_3)_3Ni]_2Ni(NO_3)_6(H_2O)_2$, Acta Cryst. **B27**, Part 3, 682–691 (Mar. 1971).

Ritter, J. J., Coyle, T. D., B llama, J. M., Reactions of diboron tetrahalides with haloolefins. Formation of poly(dihaloboryl)ethanes, J. Organometal. Chem. **29**, 175–184 (1971).

Rosenstock, H. M., Harmonic oscillator Franck-Condon factors for the ionization of N_2O, Intern. J. Mass Spectrom. Ion Phys. **7**, 33–39 (1971).

Rubin, R. J., Comment on "Conformation of adsorbed polymeric chain. II". J. Chem. Phys. **51**, No. 10, 4681 (Nov. 15, 1969).

Rubin, R. J., Transmission properties of an isotopically disordered one-dimensional harmonic crystal. II. Solution of a functional equation J. Math. Phys. **11**, No. 6, 1857–1867 (June 1970).

Rubin, R. J., Greer, W. L., Abnormal lattice thermal conducitivity of a one-dimensional, harmonic, isotopically disordered crystal, J. Math. Phys. **12**, No. 8, 1686–1701 (Aug. 1971).

Rupp, N. W., Paffenbarger, G. C., Significance to health of mercury used in dental practice: A review, J. Am. Dental Assoc. **82**, 1401–1407 (June 1971).

Saylor, C. P., Return of the prodigal, Capital Chem. 21, No. 6, 95–99 (Sept. 1971).

Scheer, M. D., Klein, R., McKinley, J. D., Surface lifetimes of alkali metals on molybdenum, J. Chem. Phys. **55**, No. 7, 3577–3584 (Oct. 1, 1971).

Schwartz, R. B., Schrack, R. A., Heaton, H. T., II, A search for structure in the N–P total cross section, Proc. Neutron Standards and Flux Normalization Symp. Argonne National Laboratory, Argonne, Ill., Oct. 21–23, 1970. Sponsored by the European American Nuclear Data Committee, AEC Symposium Series 23, pp. 57–62 (Aug. 1971).

Selby, M. C., Translator, Standard reference materials: Standard samples issued in the USSR, by R. S. Gorozhanina, A. Y. Freedman, and A. B. Shaievitch, All-Union Scientific Research Institute of Metrology Sverdlovsk Branch, All-Union Scientific Research Center of the State Service for Standard Samples, USSR, Nat. Bur. Stand. (U.S.), Spec. Publ. 260-30, 86 pages (June 1971) $1.00, SD Catalog No. C13.10:260-30.

Sengers, J. M. H. L., Straub, J., Vicentini-Missoni, M., Coexistence curves of CO_2, N_2O, and $CClF_3$ in the critical region, J. Chem. Phys. **54,** No. 12, 5034-5050 (June 15, 1971).

Sher, A. H., Carrier trapping in ge(li) detectors, IEEE Trans. Nucl. Sci. **NS-18,** No. 1, 175-183 (Feb. 1971).

Shirk, J. S., Laser excited fluorescence of CCl_2, J. Chem. Phys. **55,** No. 7, 3608-3609 (Oct. 1, 1971).

Shoup, R. R., VanderHart, D. L., Effect of CH scaler coupling on ^{13}C transverse relaxation times, J. Am. Chem. Soc. **93,** 2053-2054 (1971).

Simmons, J. A., deWit, R., Bullough, R., Editors, Fundamental aspects of dislocation theory. Proceedings of a Conference held at the National Bureau of Standards, Gaithersburg, Maryland, April 21-25, 1969, Nat. Bur. Stand. (U.S.), Spec. Publ. 317, Vol. **1,** 752 pages and Vol. **2,** 624 pages (Dec. 1970). Price $8.25 per set of 2 volumes, sold in sets only, SD Catalog No. C13.10:317.

Smith, S. J., Molecular negative ion structure, Comments At. Mol. Phys. **2,** No. 6, 175-180 (Feb.-Mar. 1971).

Spencer, L. V., Remarks on the theory of energy deposition in cavities, Acta Radiol. **10,** No. 1, 1-20 (February 1971).

Sugar, J., New energy levels of triply ionized praseodymium, J. Opt. Soc. Am. **61,** No. 6, 727-732 (June 1971).

Tech, J. L., Ward, J. F., Accurate wavelength measurement of he $1s2p\ ^3p^0 - 2p^2\ ^3P$ transition in ^{4}He I, Phys. Rev. Letters **27,** No. 7, 367-370 (Aug. 16, 1971).

Tsai, D. H., MacDonald, R. A., Molecular dynamical studies of the phase transformation of iron under pressure, (Proc. Symp. Mechanisms of the Phase Transitions, University of South Carolina, Columbia, S. C., Feb. 1, 1971), Trans. Am. Crystallogr. Assoc. **7,** 107-129 (Feb. 1, 1971).

Utton, D. B., Temperature dependence of ^{35}Cl NQR in sodium chlorate, J. Chem. Phys. **54,** No. 12, 5441-5442 (June 15, 1971).

Vadelund, E. A., The role of the Department of Commerce under the fair packaging and labeling act, (Proc. Conf. 11th Annual Meeting—Food Distribution Research Society, St. Louis, Mo., Oct. 25-28, 1970), J. Food Distribution Res. 2, No. 1, 103-106 (The Food Distribution Research Society, Inc., Hyattsville, Md., Feb. 1971).

West, E. D., Data analysis for isoperibol laser calorimetry, Nat. Bur. Stand. (U.S.), Tech. Note 396, 34 pages (Feb. 1971) 40 cents, SD Catalog No. C13.46:396.

White, H. S., Jr., Metropolitan Statistical Areas, Nat. Bur. Stand. (U.S.), Fed. Info. Process Stand. Publ. (FIPS Pub.) 8-1, 7 pages (1971) 10 cents, SD Catalog No. C13.52:8-1. Supersedes FIPS PUB 8, June 9, 1969.

Winnewisser, G., Maki, A. G., Johnson, D. R., Rotational constants for HCN and DCN, J. Mol. Spectry. **39,** No. 1, 149-158 (1971).

Winogradoff, N. N., Osinsky, V. I., Density-of-states tails associated with the <100> conduction band minima in heavily doped *n*-type GaAs, Solid State Commun. **8,** No. 23, 2001-2003 (Dec. 1, 1970).

Wright, J. R., Editor, Industrialized building in the Soviet Union. A report of the U.S. delegation to the U.S.S.R., Nat. Bur. Stand. (U.S.), Spec. Publ. 334, 81 pages (Dec. 1970) 75 cents, SD Catalog No. C13.10:334.

Yates, J. T., Jr., Madey, T. E., Interactions between chemisorbed species: H_2 and CO on (100) tungsten, J. Chem. Phys. **54,** No. 12, 4969-4978 (June 15, 1971).

**Publications for which a price is indicated are available by purchase from the Superintendent of Documents, U.S. Government Printing Office, Washington, D.C. 20402 (foreign postage, one-fourth additional). The NBS non-periodical series are also available from the National Technical Information Service (NTIS), Springfield, Va. 22151, which was formerly the Clearinghouse. Reprints from outside journals and the NBS Journal of Research may often be obtained directly from the authors.*

U. S. GOVERNMENT PRINTING OFFICE : 1972 OL - 468-108

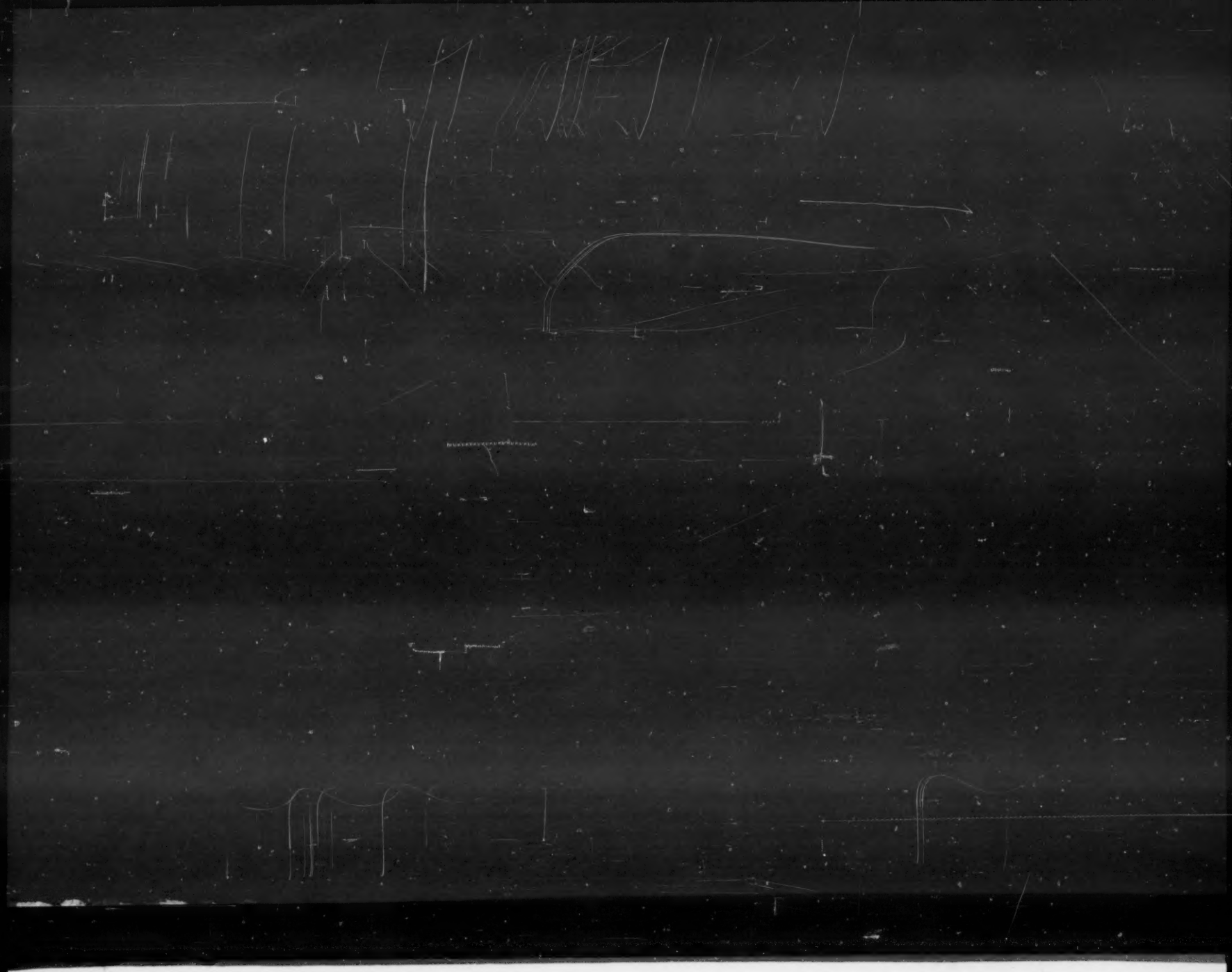

UNIVERSITY MICROFILMS
JOY
ROOM
ANN ARBOR MI 48106

UNITED STATES
GOVERNMENT PRINTING OFFICE
PUBLIC DOCUMENTS DEPARTMENT
WASHINGTON, D.C. 20402

OFFICIAL BUSINESS

PENALTY FOR PRIVATE USE, $300

POSTAGE AND FEES PAID
U.S. GOVERNMENT PRINTING OFFICE
375

U.S.MAIL

JOURNAL OF RESEARCH of the National Bureau of Standards
C. Engineering and Instrumentation

Vol. 76C, Nos. 1 & 2 January–June 1972

Contents

Page

National Bureau of Standards one kilogram balance NBS No. 2. H. E. Almer. 1

Ball and cylinder interferometer. J. B. Saunders, Sr. 11

Precision reference specimens of surface roughness: Some characteristics of the Cali-block. Russell D. Young and Frederic E. Scire. 21

Absorption of sound in liquids by the resonator-decay technique: A critique. Martin Greenspan. 25

Ductile fracture by development of surfaces of unstable cavity expansion. C. A. Berg. 33

Friction and wear of graphite fiber composites. C. A. Berg, S. Batra, and J. Tirosh. 41

A note on construction of the equivalent plastic strain increment. C. A. Berg. 53

Publications of the National Bureau of Standards. 55

Important Notice

With this issue, the National Bureau of Standards is ceasing publication of Section C: Engineering and Instrumentation of the National Bureau of Standards Journal of Research.

Section C was initiated in 1959 to meet a then–existing need for a publications medium suitable for the reporting of study results chiefly of interest to the engineer or applied scientist. Since that time, other publications media suitable for this purpose have come into being. With their existence, Section C ceases to serve the unique function that led to its creation. It is therefore appropriate that it be discontinued at this time.

Library of Congress Catalog Card Number: 62–3900

For sale by the Superintendent of Documents, U.S. Government Printing Office, Washington, D.C. 20402. (Order by SD Catalog No. C 13.22/sec. C: 76 (1 & 2). Price $1.25 (single copy). Subscription price: $5.00 a year; $1.25 additional for foreign mailing.
UNITED STATES GOVERNMENT PRINTING OFFICE, WASHINGTON : 1972